

# PHOTON SCIENCE 2021.

Highlights and Annual Report

Deutsches Elektronen-Synchrotron DESY  
A Research Centre of the Helmholtz Association





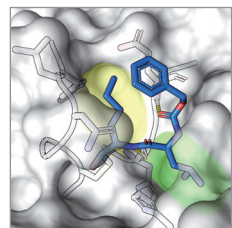
# PHOTON SCIENCE 2021.

Highlights and Annual Report

## Cover

While vaccines offer great relief to the burden that the SARS-CoV-2 virus has put on global health and economics, the appearance of more resistant coronavirus mutants has demonstrated that additional treatment options with drugs are desperately needed. Among other screening techniques, X-ray crystallography is a powerful tool in modern drug discovery as it sheds light on how exactly a drug acts on its target protein — with atomic resolution. In a massive screening campaign at PETRA III one promising drug compound was identified and is being further evaluated.

The cover picture displays a promising candidate for a drug against SARS-CoV-2. The potent inhibitor calpeptin (blue sticks) shows antiviral activity and binds tightly to the active site of the key enzyme ( $M^{pro}$ ) of SARS-CoV-2 (grey surface). The X-ray structure of  $M^{pro}$  and calpeptin reveals that the inhibitor uses important pockets (green and yellow) in the active site of the protein for binding. Further amino acids that interact with calpeptin are shown as grey sticks (details see page 18).



(Reprint from original publication in 'Science' licensed under CC BY 4.0)

# Contents

> Introduction	4
> News and Events	8
> Science Highlights	16
• Life sciences	18
• Nano and materials science	30
• Electronic and magnetic structure	40
• Structure and structural dynamics	54
• Quantum optics, atomic and molecular dynamics	62
• Science of laser and X-ray sources – methods and developments	70
> Light Sources and User Infrastructures	82
> Campus and Collaborations	102
> Facts and Numbers	112

## Publications

The list of publications based on work done at DESY Photon Science is accessible online:

[http://photon-science.desy.de/research/publications/list\\_of\\_publications/index\\_eng.html](http://photon-science.desy.de/research/publications/list_of_publications/index_eng.html)

DESY tries to keep this list complete and up-to-date and relies on the support by all users, who are kindly requested to register their publications via DOOR ([door.desy.de](http://door.desy.de)).

# The year 2021 at DESY

## Chairman's foreword

*Dear Colleagues and Friends of DESY,*

German Nobel Prizes in physics and chemistry in 2021 as well as in 2020 and the rapid development of a Covid-19 vaccine through the outstanding research and development work in the BioNTech company: These are spectacular scientific breakthroughs that impressively show the strong German role in worldwide fundamental and applied research.

To open up completely new possibilities of knowledge generation, DESY has a highly ambitious future plan at its two sites to shape the research campus of the 21st century. Here, applied research leveraging the potential of cutting-edge research infrastructures and rapid transfer to industry and society will be promoted and shaped in a smart 'ecosystem'.

In order to implement this plan in a highly competitive environment, we need to get important construction projects underway quickly in the current funding period so as not to fall behind internationally. This applies to the various con-

struction projects in the areas of research, transfer and knowledge communication at the DESY sites in Hamburg and Zeuthen. But it applies especially to the PETRA IV project, the world-leading lighthouse in research with synchrotron radiation. With the newly developed revolutionary storage ring technology, the hybrid 6-bend achromat (H6BA) lattice, we are placing the performance of German and European light sources ahead of those in the USA and China.

The lessons learned from the Corona pandemic and the acute climate crisis are forcing us to leave comfort zones. For us at DESY this means that we are questioning our daily life we have become used to. How will we work and research at DESY in the future? How and how much will we travel in the future? How will we organise a sustainable research campus in the future? How do we coordinate a climate-friendly operation for users at our large-scale research facilities that does not allow any compromises in quality? Will it then be possible to be still appealing to new

The newly opened Start-up Labs Bahrenfeld building close to the PETRA III experimental hall 'Max von Laue'.



user groups from academia and industry? If we find the right answers and smart solutions I am convinced that DESY will remain a future-oriented research centre, perhaps even more diverse and even more climate — and family — friendly and it will continue to attract the best talents from all over the world.

We were privileged to host the award ceremony for this year's Karl Heinz Beckurts Prize at DESY. The Helmholtz Association, together with the Siemens AG, established the Karl Heinz Beckurts foundation. In addition to the prize winner Vasilis Ntziachristos (Helmholtz Zentrum München and TU München), also Ingmar Hoerr (CureVac), Uğur Sahin and Özlem Terici (BioNTech) were honored with a special prize. Among the guests was Roland Busch, chief executive officer of Siemens who was very impressed by a tour of the DESY site. Personally, I was touched by the first names of the award winners: Vasilis, Ingmar, Uğur, Özlem. There is no shorter or better way to show where our future lies — DESY has lived this diversity since its foundation.

This year, DESY has signed the 'Diversity Charter' to be part of Germany's largest diversity network and is actively committed to a diverse as well as prejudice-free working environment and to a signal of appreciation of all employees regardless of their gender and gender identity, nationality, ethnic origin, religion or belief, disability, age, sexual orientation and identity. Here at DESY, great importance is attached to an appreciative working atmosphere, the equality of all employees and a better work-life balance.

Since September 2021 the Start-up Labs Bahrenfeld, a project jointly managed by DESY, the University of Hamburg and the City of Hamburg, is the new place for science

entrepreneurship on DESY's research campus. The variety of different fields covered by our young entrepreneurs is huge, ranging from synchronisation systems to individualised tests for diagnosing cancer.

DESY and the Hamburg University of Applied Sciences (HAW Hamburg) agreed on a new strategic Cooperation for Application and Innovation (KAI) with a focus on joint research and development programmes, dual education as well as innovation and technology transfer. KAI will help shape Hamburg's structural transformation to become a science and innovation place in the North of Germany.

Finally, I would like to mention our public outreach format 'Wissen vom Fass' (Science on tap) in which scientists from the University of Hamburg and DESY explain science topics and answer exciting questions from the world of research to the public. This year, the event was purely digital, but it was just as entertaining and enjoyable as before for all.

In these challenging times, I would like to thank the staff and all our national and international users and partners for their valuable contribution to DESY. Please remain very careful in this tricky winter period and beyond. I wish you all the best!

*Yours  
Helmut Dosch*

Helmut Dosch  
Chairman of the DESY Board of Directors



DESY tour during the Karl Heinz Beckurts Award ceremony in October 2021 (from left): Oliver Seeck, Wim Leemans, Roland Busch (Siemens), Helmut Dosch, Ingmar Hoerr (CureVac), Vasilis Ntziachristos (Helmholtz Zentrum München and TU München), Venetia Ntziachristos, Christian Stegmann, Arik Willner.

# Photon Science at DESY

## Introduction



The DESY site in Hamburg with the Center for Free-Electron Laser Science (CFEL) in front, the Max Planck Institute for the Structure and Dynamics of Matter (MPSD) on the left (with roof garden), the Centre for X-ray and Nano Science (CXNS) above the right end of the curved PETRA III experimental hall, as well as the adjacent FLASH experimental halls on the right side of the aerial view (September 2021).

Dear Colleagues and Friends of DESY Photon Science,

The year 2021 has already been the second one within the Covid-19 pandemic and since new mutations keep arising that seem to escape the trained or acquired capabilities of our immune system, no one can really predict when we will be able to go back to a normal situation — whatever that means after the pandemic. However, the restrictions within the pandemic have also forced us to accelerate a number of developments that probably would have taken much longer otherwise. We learned to use different video-conferencing tools to communicate quite efficiently and I dare predict that we will no longer travel for hours for brief meetings or workshops in the future. As soon as larger in-person meetings will be possible again, almost all conferences will likely be hybrid meetings just because one will be able to reach out to a much larger audience. This has been demonstrated by the 2021 DESY Photon Science Users' Meeting with more than 2000 registered participants from about 40 countries and by many on-line workshops and poster sessions organised during the last year at DESY.

The pandemic is also influencing the way we are organising our user operation in the future. Due to an increased fraction of mail-in and remote-access experiments, the number of user visits was reduced by about 30%, even though the scope of the experimental user programme was not reduced. To a large extent, this was only possible due to the exceptional effort the beamline staff at PETRA III and FLASH made to enable almost all scheduled experiments. However, such an operation mode is not sustainable without additional personnel and resources. The challenge for the future will be to organise an efficient user operation that also provides complex *in situ* or *operando* experiments in a sustainable fashion with a reduced travel CO<sub>2</sub> footprint and at the same time renders excellent communication between facility staff and users as well as training opportunities for young scientists.

Despite the pandemic, the user operation at PETRA III was very successful under the conditions mentioned above. Due to travel restrictions, the number of non-German on-site users was significantly reduced with a large fraction of

mail-in experiments for international users. With the start of user operation at the time-resolved luminescence spectroscopy beamline P66 the PETRA III extension project has officially been completed. Activities to fill up the remaining two undulator ports of beamline P25 and P63 are still ongoing.

So far user proposals for PETRA III were ranked according to their scientific excellence as the only criteria after a suitable feasibility check. After discussion in our advisory bodies, in future proposals for the DESY Photon Science facilities will in addition be ranked according to their socio-economic impact.

The preparatory work for DESY's main future project PETRA IV is progressing well. According to the present schedule the Technical Design Report (TDR) should be finished by the end of 2023 and if a funding decision will be made in same year the shutdown for the upgrade would be from 2026 to 2028. During 2021, important project milestones have been achieved. In collaboration with colleagues from ESRF, a new design of the magnetic lattice has been worked out that will enable a world-record low horizontal emittance in the 20 pmrad regime and at the same time operation conditions in terms of beam lifetime and injection schemes comparable to present 3<sup>rd</sup> generation facilities. The new lattice will enable 33-35 undulator ports. In close collaboration with the user community, the DESY Photon Science Committee (PSC) and external experts, a first portfolio of 27 PETRA IV beamlines has been selected from a much larger number of scientific instrument proposals. The remaining free ports will provide ample of opportunities for new ideas in future.

The user operation at FLASH was somehow stronger affected by the pandemic due to the often significantly more complex experiments that require enhanced user involvement. Also, at FLASH remote participation of users has been significantly increased. Presently, the first phase of the shutdown due to the FLASH2020+ project is ongoing. During this phase, mostly improvements of the superconducting linear accelerator towards a higher electron

beam energy and optimisations concerning the bunch compression will be carried out. In a second phase scheduled for the year 2024, new tuneable-gap undulators and schemes for external seeding will be implemented.

DESY Photon Science is involved in three larger user consortia (SFX, HiBEF, hRIXS) at European XFEL. In 2021 the hRIXS consortium was able to commission the new instrumentation and to take first data.

In 2021 there was also significant progress in the multi-disciplinary research centres on campus with DESY participation. Scientists from the Center for Free-Electron Laser Science (CFEL) continued to be among the most active experimental groups at European XFEL. After more than two years of construction, scientists from DESY, Hereon, CAU Kiel and IKZ Berlin were able to move into the new building for the Centre for X-ray and Nano Science (CXNS). As the 10<sup>th</sup> partner, the Forschungszentrum Borstel joined the Centre for Structural Systems Biology (CSSB), strengthening the centre's expertise in lung research. Within the frame of the Centre for Molecular Water Science (CMWS), a very successful 'Water Week' has been organised and a White Paper published, describing the aims of this centre.

The year 2021 was again a difficult one for all research groups and especially for the user operation at our facilities. I heartily thank all those involved for their commitment, so that we could continue to do excellent science under these challenging conditions. In addition, I sincerely hope that we can go back towards a more normal life at some point during the year 2022.

A handwritten signature in black ink, appearing to read 'E. Weckert'.

Edgar Weckert  
Director DESY Photon Science



## News and Events

# News and Events

A busy year 2021

## January

**25 January:**  
**Hamburg supports DESY's large-scale project PETRA IV**

Hamburg is supporting DESY for its planned large-scale project PETRA IV with 2.85 million Euro over the next two years. Funding is being provided for the detailed technical planning phase, the so-called Technical Design Report (TDR) of the unique facility, as a precondition for the inclusion of the project in the national roadmap for research infrastructures. PETRA IV is set to become the world's best 3D X-ray microscope, providing images of processes in new materials and in future medical agents that are hundreds of times more accurate than previously possible. PETRA IV will thus become the scientific beacon project in the future Science City Hamburg Bahrenfeld.



**29 January:**  
**Online DESY Photon Science Users' Meeting discusses Corona research and future facility developments**

Due to the Corona pandemic, the annual Users' Meeting for the Hamburg X-ray light sources took place completely online for the first time in 2021. The users of the DESY X-ray sources PETRA III and FLASH met from January 25 to 29 in conjunction with the European XFEL Users' Meeting. The interest was undiminished: In total, more than 2000 participants from about 40 countries had registered for the events. In about 30 lectures, more than a dozen satellite workshops, and with almost 370 scientific posters presented, the participants exchanged information about current research results, new developments and future perspectives in numerous disciplines. Among others, an important topic was the various research projects on the corona virus carried out soon after the pandemic had started. This was partially possible thanks to the fast-track access to DESY's X-ray sources for corona-related research and support from the DESY Strategy Fund DSF. The pandemic-proof operation of the light sources will be further expanded in the future. Furthermore, future developments of the DESY facilities were also discussed at the meeting.

## March

**15 March:**  
**DGK 2021 online conference at DESY attracted very high attendance**

The DGK conference is held annually by the German Crystallographic Society — the Deutsche Gesellschaft für Kristallographie. The very high number of more than 600 participants, mainly from Germany but also from 20 other countries, registered for this year's conference which took place online for the first time from 15–18 March 2021. The original plans were to welcome the participants by the organising institution DESY in Hamburg. However, due to the ongoing Covid-19 pandemic, a re-organisation of the whole event in close collaboration with the DGK 'Arbeitskreise' (AKs) as an online format was required. The online DGK 2021 conference featured a lively exchange within over 25 sessions presenting 80 talks across the many fields of science that are conducted in the research field of crystallography.



**26 March:**  
**More than 250 scientists met online for the CMWS DAYS 2021**

About 275 participants from 19 countries met online from 24–25 March 2021 for the CMWS DAYS 2021 to discuss the key challenges in molecular water research as well as the status and future of the Centre for Molecular Water Science (CMWS). Water is the most important liquid for our life and plays an important role in biology, chemistry, physics and geoscience with high relevance for many societal challenges such as climate, sustainability, energy, environment and health.

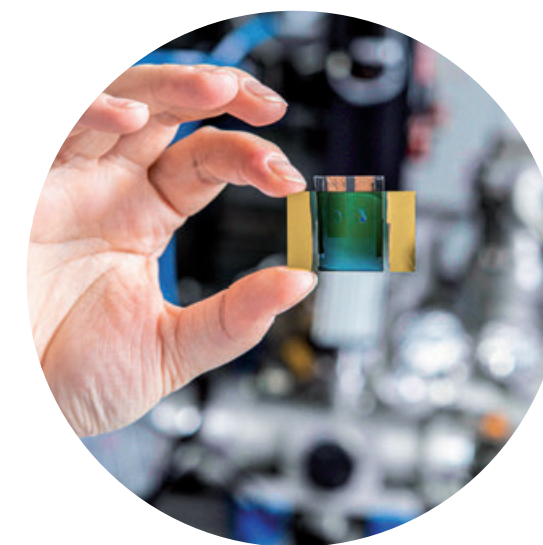


Despite its central role and numerous research efforts worldwide, we are still lacking a comprehensive molecular picture of the hydrogen bonding network believed to be responsible for the wealth of effects in water. The CMWS initiative brings together key experts to approach the understanding of the fundamental questions about molecular processes in water and at water interfaces systematically.

## April

**15 April:**  
**Clean ideas with hydrogen**

Representatives from Helmholtz centres, politics, business and NGOs met for the Helmholtz Sustainability Talk on 19 April 2021. They discussed how a hydrogen economy can be developed and built up in a sustainable and resource-saving way. Many developments in the field of energy research are not possible without basic research. Through research with the help of the X-ray light sources at DESY, for example, the group of Simone Techert has developed mini power plants that are smaller than a hair's thickness. These cells imitate nature and produce hydrogen from sunlight and water.



## May

### 7 May: Innovation for light sources in Europe

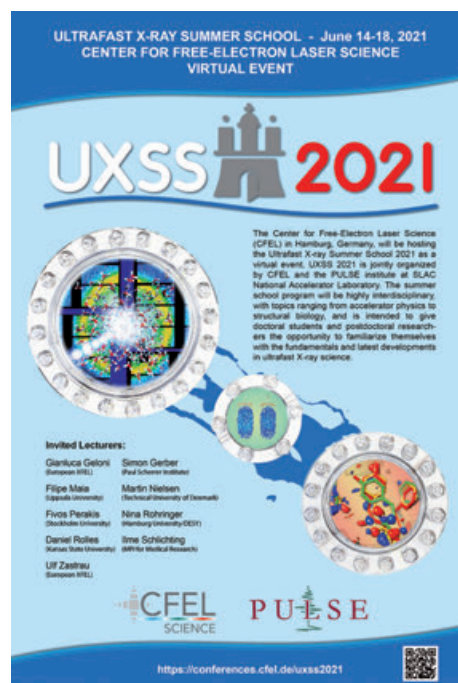
The LEAPS-INNOV kick-off meeting took place online on 20 and 21 April with over 140 participants. LEAPS-INNOV is a project under the European Commission's Horizon 2020 programme. It will implement the LEAPS technology roadmap and enhance partnership with industry by offering joint technological developments and advanced research capabilities for industry as collaborator, supplier and user. LEAPS, the League of Accelerator-Based Light Sources, is a European research consortium established in 2017 to foster synergies across Europe's accelerator-based light source facilities. The goal is to identify different approaches and actions for partnerships with industry in order to develop a strategy for long-term industry engagement for LEAPS on a European level. Elke Plönjes from DESY is the scientific coordinator of LEAPS-INNOV.



## June

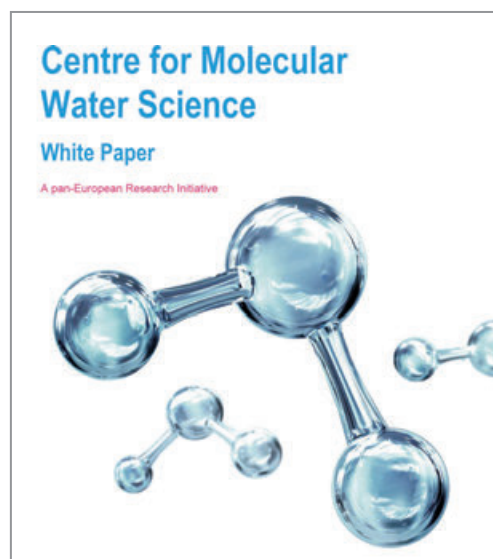
### 14 June: Ultrafast X-ray Summer School 2021

The Center for Free-Electron Laser Science (CFEL) virtually hosted the Ultrafast X-ray Summer School 2021 (UXSS 2021). UXSS is an annual school on X-ray science aimed at PhD students and postdocs and was jointly organised with the PULSE Institute at SLAC National Accelerator Laboratory. The programme of the school consisted of nine lectures given by distinguished scientists in the field and a virtual tour of the European XFEL with instrument presentations and guided hands-on project work in which the participants worked out a mock proposal for beamtime at the European XFEL.



### 15 June: White Paper of the Centre for Molecular Water Science published

More than 45 institutions from Europe and across the globe have joined in an initiative for a new research centre at DESY, unveiling the many secrets of a very common substance: water. Today, after three years of intense discussion and planning, the initiative has published a White Paper which describes the aims and tasks of the new Centre for Molecular Water Science (CMWS). Water is the key substance for life on our planet and plays a central role in numerous environmental and technological processes in our daily life. At the same time, it is one of the most fascinating chemical compounds showing many anomalies: It expands when cooled, is virtually incompressible, has an unusually high heat-storage capacity and, under certain conditions, it freezes when heated. In order to shed light on water's mysteries, more than 300 researchers from over 20 countries came together to discuss the research agenda of the CMWS in several workshops at DESY during the last years.



### 18 June: Marie Betker wins poster prize at the Bunsen Conference 2021

Marie Betker, a PhD student at PETRA III beamline P03, has won one of the highly-coveted poster prizes at the Bunsen Conference. The prestigious award was presented to her during the meeting of the German Bunsen Society which took place in May. Marie Betker is a nanoscientist at DESY and is doing her PhD at the Royal Institute of Technology (KTH) Stockholm. Her topic, which also won her the prize, is research into novel cellulose-based solar materials and their production in industry-compatible processes. Winning this year's poster prize includes an invitation for Marie Betker to give a talk on her research at next year's conference.



### 28 June: Tailwind for top research in Germany

Three research centres in the Helmholtz Association have developed a joint future plan for the research conducted at the light sources they operate in Hamburg, Berlin and Dresden. The upgrades proposed in the strategy for their world-class accelerator-based facilities will strengthen Germany as a research location and promote innovations in many different fields. The strategy paper was presented on 28 June at the Helmholtz Symposium 'Research Infrastructures of the Future' as a component of the Helmholtz Roadmap. The future light sources of DESY, Helmholtz-Zentrum Berlin (HZB) and Helmholtz-Zentrum Dresden-Rossendorf (HZDR) complement each other and are true multi-talents in terms of, e.g. drugs and novel materials development.

## July

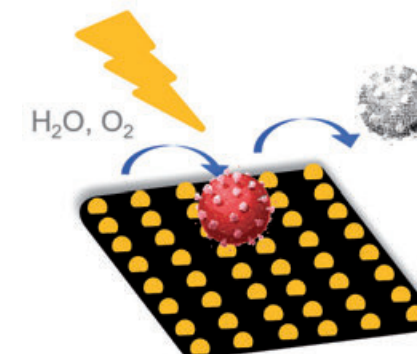
### 2 July: Making research data transparent and sustainably available

In its meeting on 2 July 2021, the Joint Science Conference of the Federal Government and the Länder (GWK) decided to fund the two DESY-led consortia, DAPHNE4NFDI and PUNCH-4NFDI, within the framework of the German National Research Data Infrastructure (NFDI). The user-driven DAPHNE4NFDI (DATA from PHoton and Neutron Experiments for NFDI) consortium, which is coordinated by Anton Barty, scientist at DESY Photon Science, aims at a sustainable utilisation of research data and the establishment of a FAIR data management for large-scale photon and neutron user facilities. It brings together several universities, including CAU and GAU, as well as research institutions to advance the state of data management in the photon and neutron science communities. The more than 5500 neutron and photon users in Germany come from a wide range of different disciplines — from biology and pharmacy, engineering, physics and chemistry to geology and archaeology. This community is facing the common challenge of coping with the increasing need for rapid analysis of large amounts of data and data transfer rates and of organising them according to the FAIR (Findable, Accessible, Interoperable and Reusable) principles. The project will be funded for the next five years. After an evaluation, five more years of funding may follow.



### 27 July: CORAERO project: stopping viruses spreading

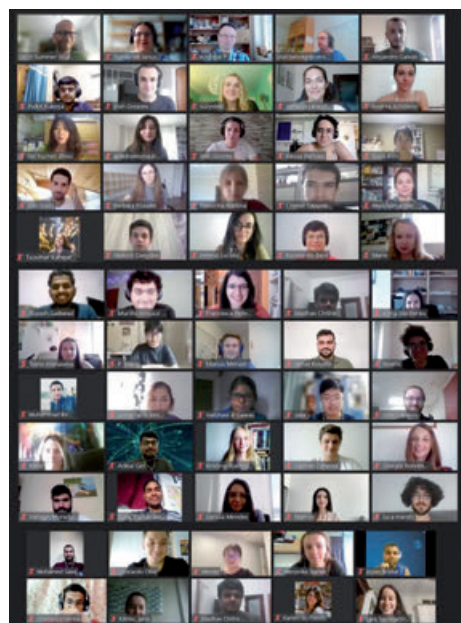
The Helmholtz Association is taking a holistic approach to overcome the Covid-19 pandemic. How do we get out of the current crisis, how can we prevent new pandemics? Interdisciplinary collaborative projects from Helmholtz research centres that address these questions are now being funded as part of the campaign 'The Corona Pandemic: Awareness, Management, Prevention'. The research consortia are funded through the Helmholtz Initiative and Networking Fund as part of a pilot project for campaign-like pioneering projects which is a new funding scheme of the Helmholtz Association. Scientists from the DESY NanoLab are also involved in one of the projects called CORAERO — 'Airborne Transmission of SARS Coronavirus — From Fundamental Science to Efficient Air Cleaning Systems'. Here, experts from medicine, biology, physics, chemistry, materials science, engineering and social sciences are working together to develop technologies that will stop the spread of viruses. The project will benefit from the expertise at the Centre for X-ray and Nano Science (CXNS) where the DESY NanoLab is located.



## August

**29 July:**  
**DESY welcomes summer students from 25 nations**

In July, almost 80 students of physics and related natural sciences started their journey through top-class research and practical experience in science at DESY. The majority of the students were participating remotely, using online tools due to the pandemic conditions while seven students had been integrated into the research groups on-site in Hamburg. The DESY summer student programme has been running for several decades and is one of the largest of its kind in Europe. The 'Summies' are integrated into research groups and gain invaluable experience, living the life of a scientist. Students are engaged in several fields of research, including particle physics, photon science, accelerator technology, computing and astroparticle physics. It was the first time that most of the programme was conducted in an online format, creating a new experience for everyone involved.



**31 August:**  
**Extreme conditions in the lab — HIBEF beamline at European XFEL inaugurated**



Under the leadership of the Helmholtz-Zentrum Dresden-Rossendorf (HZDR) in cooperation with DESY, HIBEF pools equipment and expertise from various research institutions to make them available to the international scientific community. Christian Luft, State Secretary at the Federal Ministry of Education and Research, the Minister of Science of Schleswig-Holstein, Karin Prien and the State Secretary for Science, Research, Equalities and District Authority of the Free and Hanseatic City of Hamburg, Dr. Eva Gümbel, inaugurated the Helmholtz International Beamline for Extreme Fields (HIBEF) at the European XFEL. The beamline is part of the High Energy Density (HED) experimental station at European XFEL, enabling deep insights into the structure of materials and ultra fast natural plasma-physical processes.

## September

**8 September:**  
**Barbara Mez-Starck Prize for Melanie Schnell**

DESY researcher Melanie Schnell received this year's International Dr. Barbara Mez-Starck Prize. The DESY Lead Scientist at Photon Science was honoured for her outstanding studies of structural changes in water complexes with increasing amounts of water molecules as well as for her pioneering investigations of enantiomers and the separation of these chirally different molecules, as the jury announced in Ulm. The award ceremony took place on 29 August during the 27th Colloquium on High-Resolution Molecular Spectroscopy in Cologne.



**20 September:**  
**Opening of Start-up Labs Bahrenfeld**

Start-ups and established companies in the field of physics and biophysics have found a new home in Western Hamburg. Start-up Labs Bahrenfeld, a project jointly managed by DESY, the University of Hamburg and the City of Hamburg, is the new place for science entrepreneurship on DESY's research campus. The innovation centre for deep-tech start-ups will also enhance the profile of the future Science City Bahrenfeld. The Start-up Labs were officially opened on 20 September with laboratories, workshops, offices and meeting rooms, covering an area of 2700 square metres. DESY Photon Science start-ups are among the first tenants.

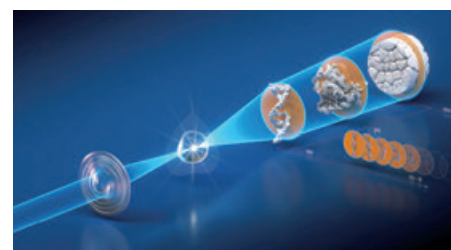
**27 September:**  
**'Wissen vom Fass': This year's event was launched purely digital**

In 'Wissen vom Fass' (Science on tap), scientists from the University of Hamburg and DESY answered exciting questions from the public about different research topics. Unlike previously, this year's popular lectures were not held in various Hamburg bars and pubs due to the pandemic. Instead, five videos were available for interested DESY followers.



**29 September:**  
**PETRA IV Workshops**

In a series of workshops, the science case and technical requirements for the ultralow emittance storage ring PETRA IV was discussed with experts and future users from many fields of science. The PETRA IV Scientific Instrumentation Proposal (SIP) submission process for the future PETRA IV instrumentation has been finalised at the end of 2020. Since then, there has been a technical and scientific review of the SIPs. The PETRA IV project team and DESY management have developed the future PETRA IV beamline portfolio based on the SIPs, their reviews and discussions with DESY partners and collaborators. In this workshop the current status of the PETRA IV beamline portfolio was presented and discussed with the user community and all SIP proposers.



## October

**13 October:**  
**AttoChem Workshop 2021**

The 2nd Annual Workshop of the European Cooperation in Science and Technology (COST) action, AttoChem was organised by CFEL/DESY online from 13–15 October 2021. The AttoChem network coordinates experimental and theoretical efforts to exploit the large potential of attosecond techniques in chemistry with the aim of designing new strategies for the control of charge migration in molecules by acting directly on the attosecond time scale. This ability will also be used to selectively break and form chemical bonds, thus opening new avenues for the control of chemical reactions. The results of the action are expected to have a significant impact in several areas of chemistry, such as photovoltaics, radiation damage, catalysis, photochemistry or structural determination.



## November

**1 November:**  
**DESY scientist Sadia Bari becomes professor at the University of Groningen**

DESY has sealed its first joint professorship agreement with a university outside of Germany: Research group leader Sadia Bari has been appointed associate professor equivalent to German 'W2' level at the University of Groningen in the Netherlands to work in the field of soft X-ray research on the dynamic structure of isolated and solvated single biomolecules. Bari returns to her academic roots: after studying and doing her PhD at the University of Groningen herself, she will now teach physics to undergraduate and graduate students there.

**21 November:**  
**DESY distinction for Albrecht Wagner and Jochen Schneider**

At this year's DESY Science Day, Albrecht Wagner and Jochen Schneider were honoured with DESY's Golden Pin of Honour. They had been DESY pioneers in a very special time for the centre: Albrecht Wagner was Chairman of the DESY Board of Directors from 1999 to 2009, Jochen Schneider was DESY Director for Research with Photons from 2000 to 2007. As head of the Hamburg Synchrotron Radiation Laboratory (HASYLAB) since 1993, Jochen Schneider shaped the strategic expansion of Photon Science at DESY. In addition to setting the course for PETRA III and the European XFEL, Jochen Schneider is also considered the spiritual father of the Center for Free-Electron Laser Science (CFEL) which was launched together with the University of Hamburg and the Max Planck Society.



# Science Highlights

## Life sciences

- > Massive X-ray screening identifies drug candidates against SARS-CoV-2 18
- > Hole in the wall 20
- > Unlocking the molecular mechanism of glycine reuptake inhibition 22
- > From microanatomy to spatial chemistry 24
- > Insights into pH-responsiveness of mRNA delivery systems 26
- > New opportunities to combat 28

## Nano and materials science

- > The new gold standard in single-particle X-ray imaging 30
- > Unravelling the non-classical emergence of CoO nanoassemblies 32
- > Fighting a greenhouse gas 34
- > What determines the elastic properties of teeth? 36
- > Unexpected twist of catalytic nanoparticles 38

## Electronic and magnetic structure

- > New pathway to harnessing the sun for a clean energy future 40
- > One zeptosecond for a quantum beat 42
- > Making monopoles visible 44
- > Ultrafast THz Ohmmeter at extreme temperatures 46
- > Spin fluctuations unfreeze on cooling 48
- > Imaging the electronic states of quantum materials 50
- > Twisting magnetisation with light 52

## Structure and structural dynamics

- > Dynamical heterogeneity in a cooked egg 54
- > Unusual melting in diamond 56
- > Structural dynamics of laser-induced shock waves 58
- > Probing the interior of water-rich planets 60

## Quantum optics, atomic and molecular dynamics

- > Zeptoseconds across the molecule 62
- > Exploring astrochemistry with ultrafast XUV pulses at FLASH 64
- > An ultrafast photoprotection mechanism against radiation damage 66
- > Attoseconds on a chip 68

## Science of laser and X-rays sources — methods and developments

- > Chirping FEL pulses 70
- > Towards ultimate time resolution in speckle correlation dynamics 72
- > New XFEL techniques to understand rapid synthesis at high-pressures and dynamics of planetary interiors 74
- > Automatic differentiation is capturing X-ray images 76
- > A microscope with soft X-ray spectroscopy eyes 78
- > First determination of the bulk spin polarisation of magnetite 80

# Massive X-ray screening identifies drug candidates against SARS-CoV-2

One promising drug compound is being further evaluated

While vaccines offer great relief to the burden that the SARS-CoV-2 virus has put on global health and economics, the appearance of more resistant coronavirus mutants has demonstrated that additional treatment options with drugs are desperately needed. Among other screening techniques, X-ray crystallography is a powerful tool in modern drug discovery as it sheds light on how exactly a drug acts on its target protein — with atomic resolution. As a response to the current Covid-19 pandemic, we combined drug-repurposing with high-throughput X-ray crystallography. The goal was to identify, from the pool of known active substances, suitable drugs that can inhibit a key enzyme of SARS-CoV-2, its main protease ( $M^{pro}$ ), and thus can stop the virus from replicating. 29 compounds were found unambiguously binding to  $M^{pro}$ , with two of them showing strong antiviral activity in cell-cultures.

The process of drug development usually starts with a compound screening where hundreds to hundreds of thousands of different molecules are tested for their interaction with a selected target protein. Most commonly, such screens are performed with high-throughput biochemical or cell-based assays. As an outcome of such a screening ideally several compounds are identified that bind to the target protein or can even inhibit its biological function. These hit compounds from the initial screening can then be chemically modified in order to improve their inhibitory properties. The commonly applied biochemical and cell-culture-based screening techniques provide extremely high-throughputs; however, they do not yield any 3D

information about the interaction and location of the compound binding to the target protein.

X-ray crystallography screening has a clear advantage over other techniques, since it does not only show whether a compound binds to the target protein but at the same time also provides detailed information how these molecules interact with the target protein on the atomic level. Because the effort of performing such an X-ray screening is quite high compared to other methods, it is typically conducted with a smaller number of so-called fragments. These molecules of lower chemical complexity are usually not able to bind to the target very specifically and tightly.

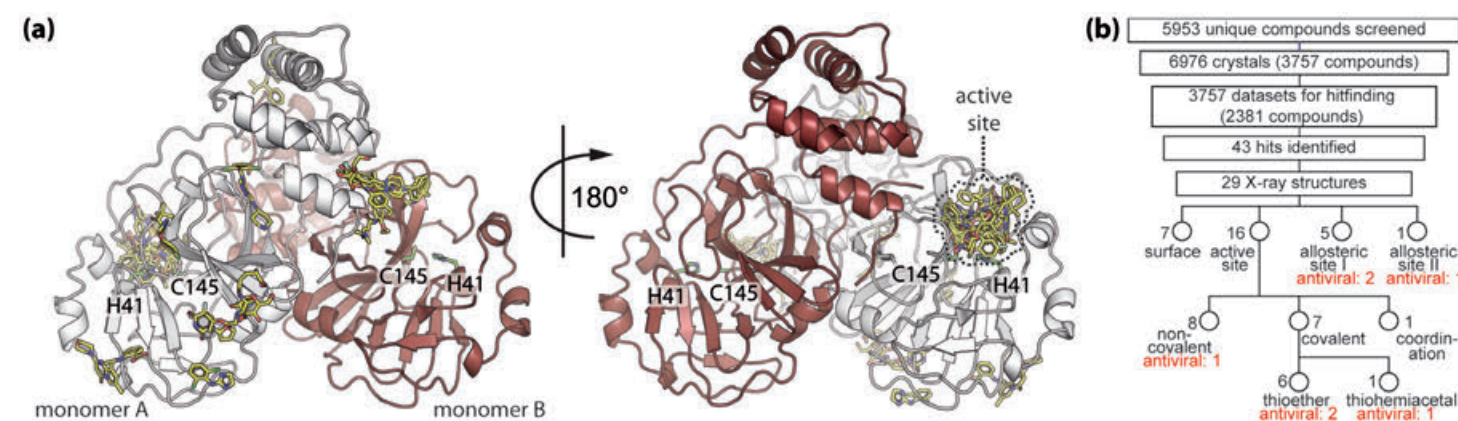
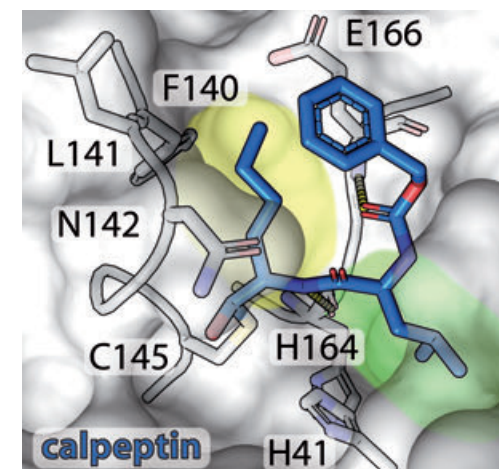


**Figure 1**  
X-ray screening identifies 29 drugs that bind to SARS-CoV-2  $M^{pro}$ . a) In its active form,  $M^{pro}$  is a dimer of two identical monomers, A and B (marked in white and red). The X-ray screening of substances listed in two drug-repurposing libraries identified compounds (yellow sticks) that bind at various locations of the protein. For clarity, the bound compounds are only shown on one of the two monomers. The majority of compounds bind at the active site of  $M^{pro}$  with the key amino acids cysteine 145 (C145) and histidine 41 (H41) (green sticks). b) Overview of the X-ray screening steps leading from 5953 tested compounds to the identification of seven compounds with antiviral activity. (Credit: Partly from original publication licensed under CC BY 4.0)

**Figure 2**  
The potent inhibitor Calpeptin (blue sticks) binds tightly to the active site of  $M^{pro}$  (grey surface). The X-ray structure of  $M^{pro}$  and calpeptin reveals that the inhibitor uses key pockets (green and yellow) in the active site of the protein for binding. Further amino acids that interact with calpeptin are shown as grey sticks and are labelled. (Credit: Partly from original publication licensed under CC BY 4.0)



If several fragments are identified to bind to the drug target, they may be linked or build the starting point for a more complex chemical synthesis.

For our study, we employed a different approach of X-ray screening. Instead of using only fragments, we tested 5953 unique compounds listed in two drug-repurposing libraries for binding to the important SARS-CoV-2 target protein. These libraries contain drugs that are either already approved for use or have been tested in clinical and preclinical studies. This approach offers the advantage that identified suitable compounds typically have high bio-availability at the site of drug action. Moreover, in the best cases, safety and other data are already available, potentially speeding up the path to an approved Covid-19 pharmaceutical.

Shortly after the SARS-CoV-2 outbreak became pandemic in 2020, we formed a consortium with specialists from several fields, including computational chemists, structural biologist and virologists all coming mainly from the Hamburg area. Our initial search focused on the main protease  $M^{pro}$ , a protein that is essential for the replication of the virus in the human host cell [1]. We co-crystallised this protease with 5939 individual compounds from the two drug-repurposing libraries. X-ray diffraction experiments of these crystals were performed at the macromolecular crystallography PETRA III beamlines P11 from DESY, as well as P13 and P14 from EMBL. Within a month we collected about 8000 datasets from almost 7000 crystals. In parallel we established a 'data analysis pipeline' to process all data and to identify all compounds that bind to the SARS-CoV-2  $M^{pro}$ . From this screening effort we identified 43 compounds binding to  $M^{pro}$  and could clearly describe the interaction between the compound and the target protein in 29 cases. These 29 molecules bound at various sites across the protein that functions as a dimer with two identical sub-units (Fig. 1a). The majority of molecules bind at the active site which the protein uses to fulfil its function. Moreover, we observed a variety of chemical interaction that were used by these molecules (Fig. 1b).

Subsequently, the compounds binding to  $M^{pro}$  were tested for their inhibition of the protein function. Cells infected with SARS-CoV-2 were treated with these compounds. Indeed, seven molecules showed antiviral activity and were not too toxic to the cells. In fact, one compound, calpeptin

(Fig. 2), showed antiviral activity in the nanomolar range. This compound is currently tested further in preclinical studies to evaluate its potential to treat SARS-CoV-2 infections.

The infrastructure and tools developed within this project are now available for X-ray screening activities related to other SARS-CoV-2 infection-relevant proteins and also for targeting further viruses that have the potential for epidemic outbreaks.

Author contact: Alke Meents, [alke.meents@desy.de](mailto:alke.meents@desy.de)  
Sebastian Günther, [sebastian.guenther@desy.de](mailto:sebastian.guenther@desy.de)

## References

1. L. Zhang, D. Lin, X. Sun, U. Curth, C. Drosten, L. Sauerhering, S. Becker, K. Rox and R. Hilgenfeld, 'Crystal structure of SARS-CoV-2 main protease provides a basis for design of improved  $\alpha$ -ketoamide inhibitors', *Science* 368, 409–412 (2020).

## Original publication

'X-ray screening identifies active site and allosteric inhibitors of SARS-CoV-2 main protease', *Science* 372, 642–646 (2021).  
DOI: 10.1126/science.abf7945



Sebastian Günther, Patrick Y. A. Reinke, Yaiza Fernández-García, Julia Lieske, Thomas J. Lane, Helen M. Ginn, Faisal H. M. Koua, Christiane Ehrhart, Wiebke Ewert, Dominik Oberthuer, Oleksandr Yefanov, Susanne Meier, Kristina Lorenzen, Boris Krichel, Janine-D. Kopicki, Luca Gelisio, Wolfgang Brehm, Ilona Dunkel, Brandon Seychell, Henry Gieseler, Brenna Norton-Baker, Beatriz Escudero-Pérez, Martin Domaracky, Sofiane Saouane, Alexandra Tolstikova, Thomas A. White, Anna Hänle, Michael Groessler, Holger Fleckenstein, Fabian Trost, Marina Galchenkova, Yaroslav Gevorkov, Chufeng Li, Salah Awel, Ariana Peck, Miriam Barthelmeß, Frank Schülzen, P. Lourdu Xavier, Nadine Werner, Hina Andaleeb, Najeeb Ullah, Sven Falke, Vasundara Srinivasan, Bruno Alves Franca, Martin Schwinzer, Hévila Brognaro, Cromarte Rogers, Diogo Melo, Joana J. Zaitseva-Doyle, Juraj Knoska, Gisel E. Peña Murillo, Aida Rahmani Mashhour, Vincent Henricke, Pontus Fischer, Johanna Hakanpää, Jan Meyer, Philip Gribbon, Bernhard Ellinger, Maria Kuzikov, Markus Wolf, Andrea R. Beccari, Gleb Bourenkov, David von Stetten, Guillaume Pompidor, Isabel Bento, Saravanan Panneerselvam, Ivars Karpics, Thomas R. Schneider, Maria M. Garcia-Alai, Stephan Niebling, Christian Günther, Christina Schmidt, Robin Schubert, Huijong Han, Juliane Boger, Diana C. F. Monteiro, Linlin Zhang, Xinyuan Sun, Jonathan Pletzer-Zelgert, Jan Wollenhaupt, Christian G. Feiler, Manfred S. Weiss, Eike-C. Schulz, Pedram Mehrabi, Katarina Karničar, Aleksandra Usenik, Jure Loboda, Henning Tidow, Ashwin Chari, Rolf Hilgenfeld, Charlotte Uetrecht, Russell Cox, Andrea Zaliani, Tobias Beck, Matthias Rarey, Stephan Günther, Dusan Turk, Winfried Hinrichs, Henry N. Chapman, Arwen R. Pearson, Christian Betzel and Alke Meents

For affiliation details refer to original publication.

# Hole in the wall

## Elucidating weak spots in the mycobacterial fortress

Over the past two years, all eyes have been focused on the SARS-CoV-2 pandemic. However, an often-overlooked infectious disease, tuberculosis, has stalked society for ages. Regarded as a disease that has co-evolved with humankind, tuberculosis still kills ~1.5 million people every year. *Mycobacterium tuberculosis*, the pathogen causing this deadly disease, is well protected by a cell envelope that surrounds it like the ramparts of a fortress. To transport various molecules across this cell envelope, the pathogen uses intricate nanomachineries called type VII secretion systems. Through a combination of genetics, biochemistry and cryo-electron microscopy, we unveiled the first intact structure of such a machinery from *Mycobacterium tuberculosis*. Unravelling these systems enables the identification of potential weak spots in the mycobacterial fortress and can aid in the development of better therapeutics.

In 2019 alone, tuberculosis (TB) caused ~1.4 million deaths. With the WHO's End TB strategy targets already falling well behind its objectives, 2020 has seen the situation worsen even more due to the Covid-19 pandemic. Not only has this year seen the first consistent raise in TB-related deaths in over a decade, but it has also witnessed a strong reduction in treatment options and funding made available for combating tuberculosis [1]. The TB epidemic has persevered due to an insufficiently protective vaccine for adults as well as long treatment plans that require a cocktail of 4 antibiotics for 6 months. The long treatment schedule often leads to loss of patient compliance, thus fuelling the global emergence of multi and extreme-drug resistant cases [1].

Bacteria can be roughly divided into two categories: Gram-positive bacteria which have a single membrane and Gram-negative which have two membranes. Mycobacteria, including the causative agent of TB, *Mycobacterium tuberculosis* (*Mtb*), are rod-shaped bacteria which, although ge-

netically classified as Gram-positive, are surrounded by two membranes. However, the composition of their second membrane, the mycobacterial outer membrane (MOM), is vastly different from the Gram-negative outer membrane with the main constituents being long-chain fatty acids called mycolic acids [2].

The MOM serves as an efficient permeability barrier, allowing *Mtb* to persist inside host cells for long periods of time while also conferring intrinsic resistance to many antibiotics. The MOM does, however, need to allow the transport of molecules, such as export of extracellular proteins or uptake of nutrients, across it. In mycobacteria, the majority of secreted proteins are transported by a group of unique protein transport machineries, called type VII secretion systems (T7SSs) with up to five different systems called ESX-1 to ESX-5 [2]. Research in the last decade has demonstrated that T7SSs are among the most important tools used by *Mtb* for both growth and disease propagation. The

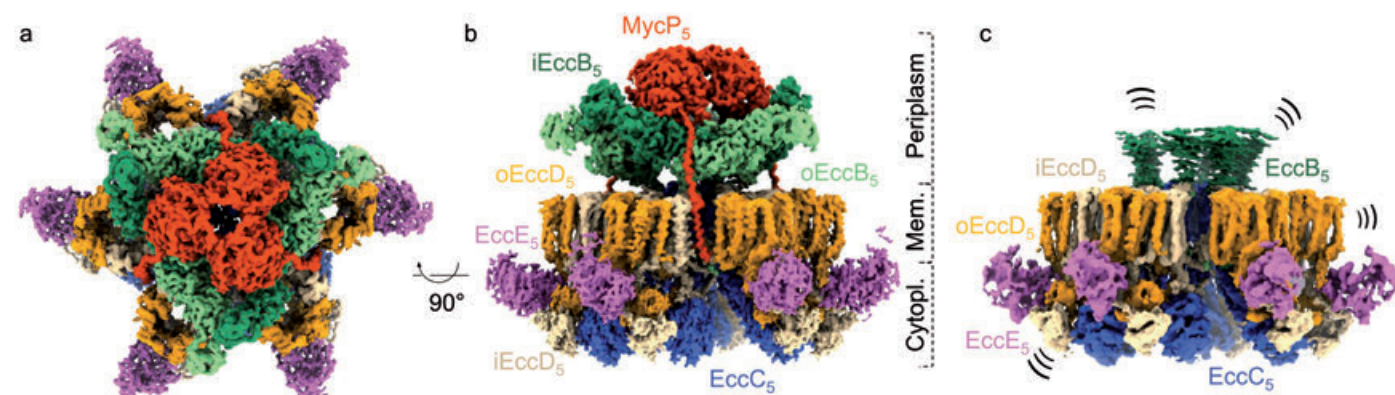
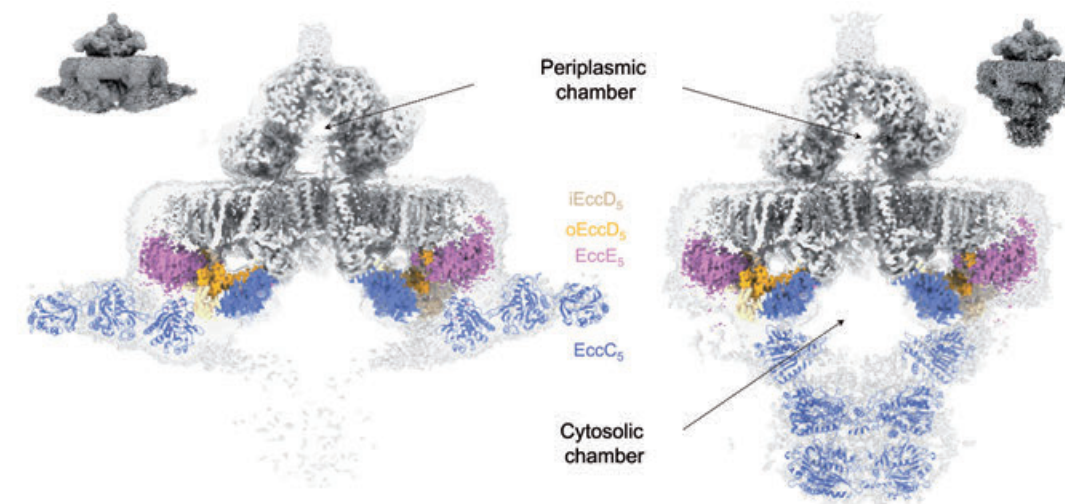


**Figure 1** Cryo-EM structure of an ESX-5 inner membrane complex from *Mtb* a) Top view and b) side view cryo-EM density of the intact ESX-5 inner-membrane complex of *Mtb*, zoned and coloured for every individual component. c) Side view of a membrane complex lacking the MycP protease, highlighting a completely disorganised periplasmic assembly and an overall increased flexibility of the entire complex. This figure is licensed under CC BY 4.0.

**Figure 2** Two conformational snapshots for the EccC motor protein. Side cross-section of the two conformational snapshots of EccC, highlighting the extended (left) and the contracted state (right). This figure is licensed under CC BY 4.0.



decisive mutation which leads to the attenuation of the current live vaccine strain, *M. bovis* BCG, is a (partial) deletion of the ESX-1 system, further underscoring its importance.

Although we previously demonstrated that four T7SS components form a six-sided star-shaped complex, high-resolution structural information and mechanistic insights could not be determined due to the inherent instability of the complex [3]. Building on our previous work, we succeeded in determining the high-resolution structure of the ESX-5 machinery from *Mtb*, a system that is essential for nutrient uptake and immunomodulation. Cryo-EM data were collected at the Cryo-EM Facility at CSSB.

This large 2.32 MDa inner membrane complex is assembled as a trimer of dimers with 5 components assembling into a 33-subunit machinery displaying a 6:6:12:6:3 stoichiometry (Fig. 1a,b). The machinery is anchored in the bacterial inner membrane via a staggering 165 domains. Whereas 4 of the components, i.e. EccB/EccC/EccD/EccE, have previously been shown to interact, our analysis is the first to show and structurally define a stable interaction of the fifth component, the MycP protease. A MycP trimer caps a central triangular chamber, formed by EccB subunits on the periplasmic side, with the transmembrane domains anchored towards the edge of the machinery. The proteolytic sites of MycP are directed towards the inside of this chamber, suggesting this to constitute the point where secreted substrates are being cleaved prior to their secretion through the MOM. Critically, in our analysis we were also able to solve the structure of T7SS machineries that lacked the protease. Without MycP, which anchors the central periplasmic assembly to the edges of the transmembrane area, the EccB assembly was completely disorganised while the whole complex displayed increased flexibility and heterogeneity, confirming previous biochemical evidence [4] (Fig. 1c).

As opposed to other specialised secretion systems, T7 secretes proteins in a folded state, suggesting that a rather large pore is required. Our work outlines this central secretion conduit to high resolution for the first time, highlighting an opening of ~45 Å in diameter. The translocation pore is sealed by the transmembrane domains of the EccC

component, an ATPase containing 4 separate hydrolysing domains. As the complex contains 6 copies of EccC, the entire machinery encodes a total of 24 domains capable of hydrolysing ATP which potentially create motion in the process. Furthermore, we have succeeded in characterising two distinct structural snapshots of the flexible EccC ATPase, likely representing separate secretion states (Fig. 2).

Our results are a huge step forward in understanding T7SSs and *Mtb* itself. The work suggests a previously undescribed mechanism of protein transport and provides a structural scaffold to aid in the development of novel drugs against this major disease-causing pathogen.

### Author contact:

Catalin Bunduc, [catalin.bunduc@cssb-hamburg.de](mailto:catalin.bunduc@cssb-hamburg.de)

Thomas Marlovits, [thomas.marlovits@cssb-hamburg.de](mailto:thomas.marlovits@cssb-hamburg.de)

### References

1. World Health Organization, Global Tuberculosis Report (2021).
2. C. M. Bunduc, W. Bitter and E. N. G. Houben, 'Structure and function of the mycobacterial type VII secretion systems', *Annu. Rev. Microbiol.* 73, 315–335 (2020).
3. K. S. Beckham, L. Ciccarelli, C. M. Bunduc, H. D. Mertens, R. Ummels, W. Lugmayr, J. Mayr, M. Rettel, M. M. Savitski, D. I. Svergun, W. Bitter, M. Wilmanns, T. C. Marlovits, A. H. Parret and E. N. G. Houben, 'Structure of the mycobacterial ESX-5 type VII secretion system membrane complex by single-particle analysis', *Nat. Microbiol.* 2, 17047 (2017).
4. V. J. C. van Winden, R. Ummels, S. R. Piersma, C. R. Jimenez, K. V. Korotkov, W. Bitter and E. N. G. Houben, 'Mycosins are required for the stabilization of the ESX-1 and ESX-5 type VII secretion membrane complexes', *mBio* 7, e01471-16 (2016).

### Original publication

'Structure and dynamics of a mycobacterial type VII secretion system', *Nature* 593, 445–448 (2021). DOI: 10.1038/s41586-021-03517-z



Catalin M. Bunduc<sup>1,2,3,4</sup>, Dirk Fahrenkamp<sup>1,2,3</sup>, Jiri Wald<sup>1,2,3</sup>, Roy Ummels<sup>5</sup>, Wilbert Bitter<sup>4,5</sup>, Edith N. G. Houben<sup>4</sup> and Thomas C. Marlovits<sup>1,2,3</sup>

1. Centre for Structural Systems Biology (CSSB) c/o DESY, Hamburg, Germany
2. Institute of Structural and Systems Biology, University Medical Centre Hamburg-Eppendorf, Hamburg, Germany
3. Deutsches Elektronen-Synchrotron DESY, Hamburg, Germany
4. Molecular Microbiology Section, Amsterdam Institute of Molecular and Life Sciences, Vrije Universiteit Amsterdam, Amsterdam, The Netherlands
5. Department of Medical Microbiology and Infection Control, Amsterdam Infection and Immunity Institute, Amsterdam UMC, Amsterdam, The Netherlands

# Unlocking the molecular mechanism of glycine reuptake inhibition

Unravelling the structure of glycine transporter paves the way for the development of novel psychiatric therapeutics

Crystal structure determination of human membrane proteins is usually limited by the availability of sufficiently sized crystals and by the fact that crystal quality deteriorates during data collection with X-rays. To overcome this limitation, we have devised a serial synchrotron crystallography (SSX) approach for collecting data from many micrometre-sized crystals and applied it to determine the structure of the glycine transporter 1 (GlyT1). GlyT1, a protein in the neuronal cell membranes, is responsible for the uptake of neurotransmitter glycine into neurons, thereby, terminating glycine-mediated signalling. Increasing glycine levels in synapses by inhibition of GlyT1 is a strategy to treat schizophrenia.

Schizophrenia is a debilitating psychiatric disorder with no cure. Over the past twenty years, many pharmaceutical companies and academic research groups have focused on glycinergic signalling to find a treatment. GlyT1 is a membrane transport protein that regulates neuronal activity in the brain mediated by the amino acid glycine as a neurotransmitter. Glycine can both be activating as a co-agonist of excitatory glutamate receptors and inactivating as the agonist of inhibitory glycine receptors. GlyT1 terminates glycinergic signalling by mediating glycine reuptake from the synapse back into the neurons. Selective inhibition of

GlyT1 prolongs glycinergic signalling, and it has been extensively studied in the search for an effective treatment for a broad range of central nervous system disorders, including schizophrenia [1]. Clinical studies have found several potent small-molecule inhibitors for GlyT1 that alleviate cognitive impairments in schizophrenia. However, a successful drug candidate has yet to come [2].

To elucidate the structure-based mechanism of inhibition, we set out to determine the GlyT1 structure with one of its most advanced inhibitors from a Roche phase III drug programme [3]. Investigating the transporter in a clinically relevant inhibition-state conformation helps to re-evaluate the efforts for developing selective inhibitors and devising new strategies to target the glycine reuptake transporter.

To enable crystallisation of GlyT1, we combined several approaches to stabilise this difficult membrane protein target; among others, we generated stabilising molecular chaperones as synthetic single-domain antibodies, so-called sybodies, against a unique cell surface-exposed

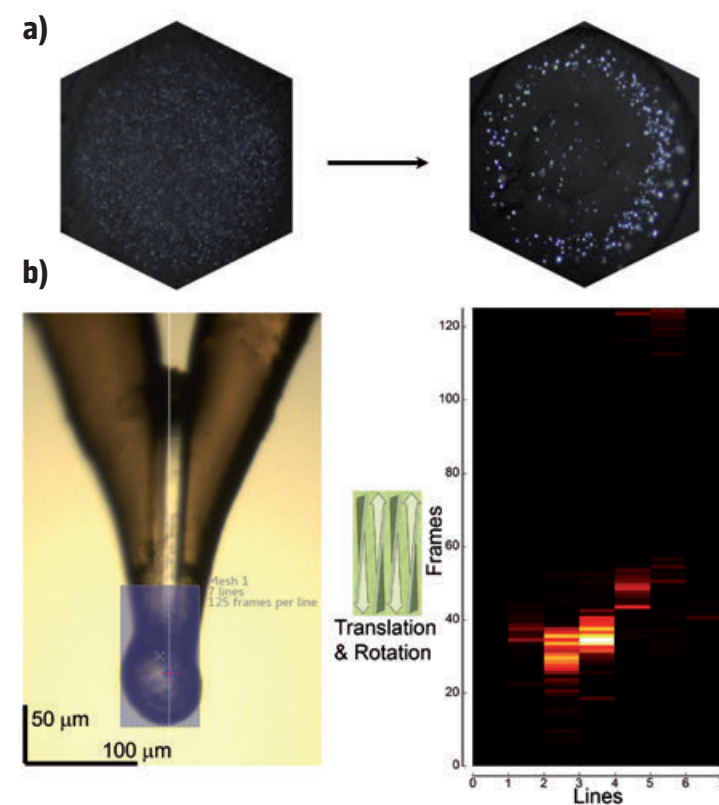


Figure 1

a) Microcrystals of GlyT1 (bright spots) in meso phase (black space) as initial hits (left) and optimised microcrystals (right) as shown by light microscopy. b) A cryogenically cooled loop carrying microcrystals embedded in meso phase, oriented perpendicularly to the incoming beam is shown on the left. We typically defined a region of interest of  $60 \times 14 \mu\text{m}^2$  up to  $290 \times 340 \mu\text{m}^2$  on such sample holders (indicated by the square) for subsequent diffraction data acquisition using serial helical line scans. The heat map for 7 lines of 125 frames covering an area of  $60 \times 14 \mu\text{m}^2$  generated from scoring for the presence of Bragg spots, indicating the location of crystals in the region of interest is shown on the right.

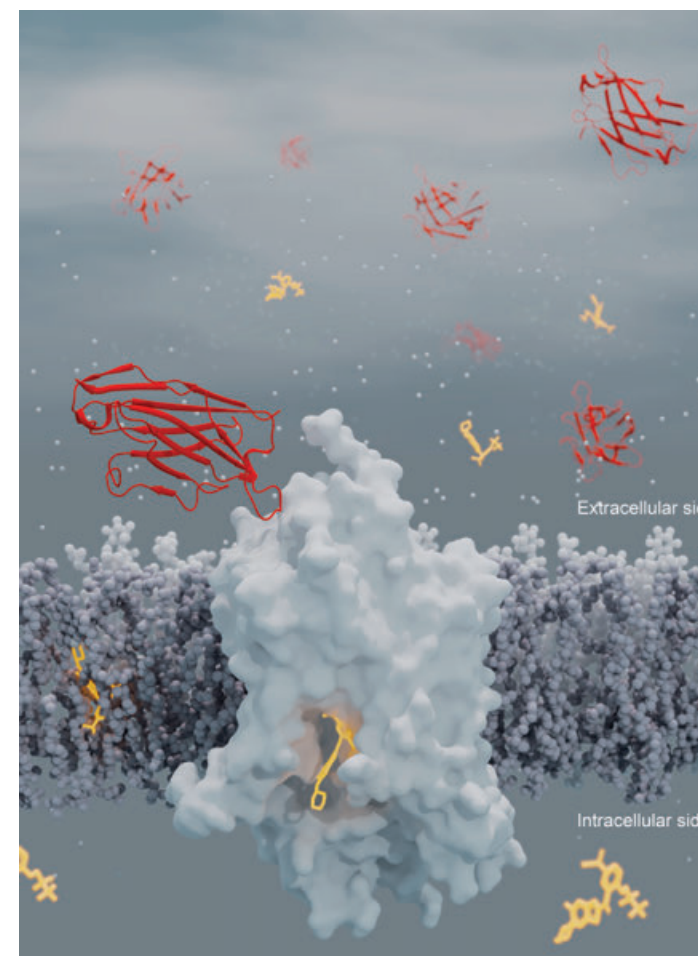
Figure 2  
GlyT1 (white) opens to the outside and inside of the cell alternately to transport substrate glycine. GlyT1 is inhibited by its small-molecule inhibitor (light orange) from the intracellular side. The sybody (red) also inhibits GlyT1 by binding to an extracellular site.

binding site of GlyT1 with the goal to address its inhibition state [4]. Employing lipid-based crystallisation methods, we obtained microcrystals ( $< 10 \mu\text{m}$ ) of GlyT1 in complex with the small-molecule inhibitor and the sybody (Fig. 1). The microcrystals would not individually suffice to acquire a complete diffraction data set. We therefore established an SSX approach that allowed us to determine the first structure of a human membrane protein from hundreds of microcrystals.

Diffraction data was collected using serial helical line scans [5] on the MD3 diffractometer (ARINAX, Moirans, France) installed on the EMBL P14 beamline at the PETRA III storage ring. A microfocus beam with a total photon flux of  $1.3 \times 10^{13}$  photons per second at the sample position (Fig. 1) was used. We carried out a total of 514 two-dimensional (2D) helical scans on 409 cryogenically cooled loops carrying microcrystals of GlyT1. This strategy resulted in the collection of partial 'mini datasets', comprising 3–20 consecutive diffraction images, extracted from a total of about 1.36 million frames acquired. We merged reflections from 207 mini datasets, corresponding to a total of 3400 oscillation patterns, whereby outliers were identified and rejected based on their correlation coefficient with the rest of data being lower than 0.7 — yielding a complete dataset with a resolution of  $3.4 \text{ \AA}$ , enabling us to determine the 3D structure of GlyT1 (Fig. 2).

The GlyT1 structure reveals the selective inhibitor-bound state, and importantly, we found it to adopt an inward-open conformation blocked by the inhibitor. The data unveil a dual nature of non-competitive inhibitors of functional transport also exhibiting competitive binding to the substrate binding site of glycine. The structure reveals a unique binding mode for the small-molecule inhibitor and depicts molecular determinants of the selectivity. The sybody is also highly selective for the inhibited, inward-open conformation of GlyT1. Recent efforts to engineer antibodies as 'brain shuttles' [6] crossing the blood-brain barrier and delivering an inhibition-state-specific sybody represent an alternative approach to small-molecule inhibitors of GlyT1. Our results define a mechanism of inhibition in neurotransmitter transporters in general that is elegant in its simplicity, and powerful in its explanatory properties. It provides blueprints for further development of small molecules and antibodies as selective inhibitors.

Author contact: Azadeh Shahsavari, [ash@mbg.au.dk](mailto:ash@mbg.au.dk)  
Thomas R. Schneider, [thomas.schneider@embl-hamburg.de](mailto:thomas.schneider@embl-hamburg.de)  
Roger J. P. Dawson, [rogerdawson@linkstertherapeutics.com](mailto:rogerdawson@linkstertherapeutics.com)  
Poul Nissen, [pn@mbg.au.dk](mailto:pn@mbg.au.dk)



## References

1. R. J. Harvey and B. K. Yee, 'Glycine transporters as novel therapeutic targets in schizophrenia, alcohol dependence and pain', *Nat. Rev. Drug Discov.* **12**, 866–885 (2013).
2. C. L. Cioffi, 'Glycine transporter-1 inhibitors: a patent review (2011–2016)', *Expert Opin. Ther. Pat.* **28**, 197–210 (2018).
3. E. Pinard et al., 'Discovery of benzoylisoindolines as a novel class of potent, selective and orally active GlyT1 inhibitors', *Bioorg. Med. Chem. Lett.* **20**, 6960–6965 (2010).
4. I. Zimmermann et al., 'Synthetic single domain antibodies for the conformational trapping of membrane proteins', *eLife* **7**, e34317 (2018).
5. C. Gatti et al., 'Serial crystallography on in vivo grown microcrystals using synchrotron radiation', *IUCr* **1**, 87–94 (2014).
6. F. Weber et al., 'Brain shuttle antibody for Alzheimer's disease with attenuated peripheral effector function due to an inverted binding mode', *Cell Rep.* **22**, 149–162 (2018).

## Original publication

'Structural insights into the inhibition of glycine reuptake', *Nature* **591**, 677–681 (2021). DOI: [10.1038/s41586-021-03274-z](https://doi.org/10.1038/s41586-021-03274-z)



Azadeh Shahsavari<sup>1,2</sup>, Peter Stohler<sup>3</sup>, Gleb Bourenkov<sup>2</sup>, Iwan Zimmermann<sup>4,5</sup>, Martin Siegrist<sup>3</sup>, Wolfgang Guba<sup>3</sup>, Emmanuel Pinard<sup>3</sup>, Steffen Sinning<sup>6</sup>, Markus A. Seeger<sup>4</sup>, Thomas R. Schneider<sup>2</sup>, Roger J. P. Dawson<sup>3,5</sup> and Poul Nissen<sup>1</sup>

1. Danish Research Institute of Translational Neuroscience (DANDRITE), Nordic EMBL Partnership for Molecular Medicine, Department of Molecular Biology and Genetics, Aarhus University, Aarhus, Denmark
2. European Molecular Biology Laboratory (EMBL) c/o DESY, Hamburg, Germany
3. Roche Pharma Research and Early Development, Therapeutic Modalities, Roche Innovation Center, Basel, Switzerland
4. Institute of Medical Microbiology, University of Zurich, Zurich, Switzerland
5. Linkster Therapeutics AG, Zurich, Switzerland
6. Department of Forensic Medicine, Aarhus University, Aarhus, Denmark

# From microanatomy to spatial chemistry

Visualising the tomography and chemistry of symbionts and parasites in an earthworm

Global ecosystems depend on small critters — decomposers that work the soil, pollinators that sustain the plants — just as much as they depend on their microbial partners. In our study we focused on earthworms, key organisms that substantially shape terrestrial ecosystems, from our backyards to tropical rainforests. Combining high-resolution tomography with metabolite imaging, we were able to resolve the metabolic interactions between the invertebrate host, the earthworm, its symbiotic bacteria and tissue parasites at unprecedented detail.

Integrating chemical imaging with unique synchrotron radiation-based microtomography (SR- $\mu$ CT) techniques developed at beamline P14 at PETRA III [1] increased the resolution almost 20-fold over previous approaches. Our correlative chemical and anatomical 3D data allowed us, for the first time, to describe ecological niches within the 'ecosystem earthworm' for microbes and nematodes.

Our cultivation-independent chemo-histo-tomography (CHEMHIST) approach advanced the study of *in situ* metabolic interactions among symbiotic/parasitic organisms in their natural settings. Key for imaging metabolites in specific niches within the earthworm was our integration of mass spectrometry imaging (MSI) with a detailed multi-scale microtomography ( $\mu$ CT) body atlas of the same worm (Fig. 1). MSI is a powerful tool for deciphering the chemical nature of microbial and eukaryotic metabolism and their interactions through the analysis of native tissues. Substantial technical advances over the last years have improved the spatial resolution and sensitivity of MSI, so that hundreds of metabolites can now be mapped at the microme-

tre scale [2,3]. However, despite its potential, MSI has yet to become a broadly applied tool for cellular biologists and microbiologists. The biggest challenge has been to link the imaged metabolome to the identity of the tissues and cells — for example parasites and microorganisms living in the tissues of host organisms.

Combining high-resolution metabolite imaging with fluorescence *in situ* hybridisation (FISH) and  $\mu$ CT allowed us to visualise and identify microorganisms and nematodes within the anatomical landscape of the earthworm (Fig. 2,3). This further enabled us to link phenotypes and phylotypes in an unculturable host-microbe symbiosis *in situ*; we visualised the phenotypic heterogeneity of the nematodes and the bacterial symbionts within the associated organs. Also, from the same data, we could observe their effects on the host metabolome (Fig. 3).

Among the hundreds of metabolite images, we saw certain metabolites that appeared as large blobs on the earthworm's posterior end. We could only explain these chemical signals by additionally analysing a sample by SR- $\mu$ CT. This revealed that the blobs were actually cross sections of cysts containing parasitic nematodes: worms within a worm! This surprising subtendency revealed the intricate interactions to be discovered in an animal collected directly from the field. In addition, our high-resolution MSI revealed that the nematode cysts had their own specific chemical composition — possibly related to an immune response by the earthworm against the intruders (Fig. 3). This is a vivid example of how metabolite measurements can take 3D imaging to a whole new level: While the latter is important for

Figure 1

A chemo-histo-tomography atlas of a worm. This multimodal 3D imaging atlas of the rear end of an earthworm was compiled from five  $\mu$ CT datasets and four tissue sections, each imaged with mass spectrometry imaging, fluorescence and bright-field microscopy.

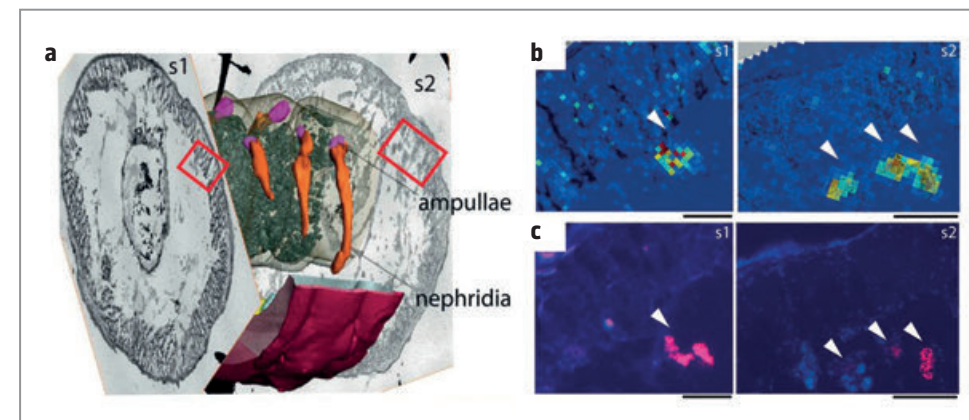
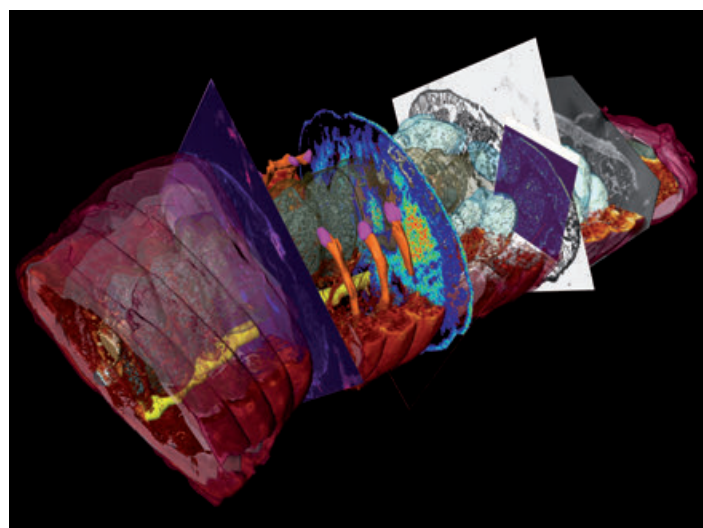
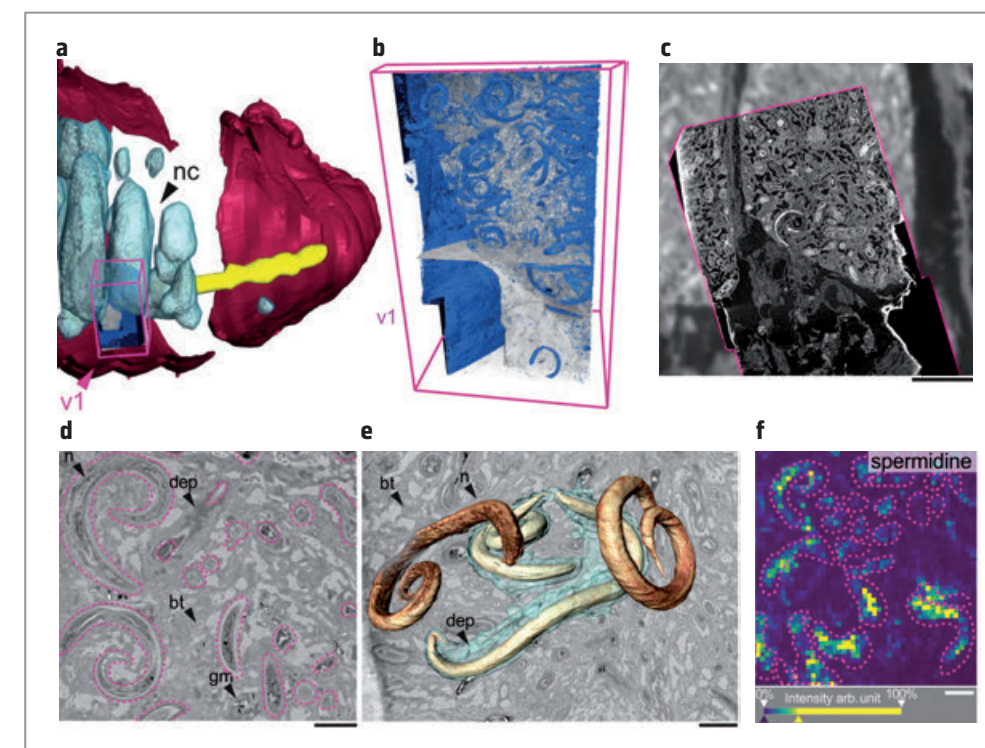


Figure 2

Bacterial cells within organs have unique molecular fingerprints. a) The 3D model shows the surface reconstruction of the nephridia, including the bacteria-containing ampullae of the tissue block between tissue sections s1 and s2. b) The ion images of whole tissue sections show an unidentified metabolite ( $m/z$  1,116.833 Da), with the highest co-localisation to MALDI-MSI. c) FISH microscopy signals showing the presence of bacteria. Scale bars in b) and c) 250  $\mu$ m.

Figure 3

Use of the 3D CHEMHIST atlas to guide high-resolution imaging of the interactions between earthworm and parasitic nematodes. a)  $\mu$ CT model with the tissue volume (v1) imaged with high-resolution SR- $\mu$ CT. b) Isosurface 3D rendering of the nematodes (blue) and a virtual sectioning plane (xy) through the SR- $\mu$ CT image stack (v1). c) Overlay of the  $\mu$ CT and SR- $\mu$ CT (magenta outline, xy plane) to show the increased resolution and detail gained with SR- $\mu$ CT. d) Virtual plane through the SR- $\mu$ CT data shows sections of nematodes in the cysts (magenta outlines). e) Three-dimensional renderings of four nematodes of which two were surrounded by a homogeneous deposit (cyan cloud). f) High-resolution MSI shows distribution of the metabolite spermidine ( $m/z$  146.1645,  $[C_7H_{19}N_3 + H]^+$ ). nc: nematode cyst; n: nematode; dep: deposit; bt: brown body tissue; gm: granular mass. Scale bars in c) 500  $\mu$ m and in d-f) 50  $\mu$ m.



understanding the anatomical and cellular features that might change within an animal, the former can reveal certain functions, from metabolic immune responses to digestive processes along the gut.

Extending common histo-tomography into CHEMHIST opens new avenues for label-free correlative imaging. Future technical developments of the presented workflow being developed in cooperation with beamline P05 could integrate phase-contrast SR- $\mu$ CT, allowing for quantitative 3D imaging of tissues without contrasting agents at nanometre scales. With continued improvements in MSI measurement speed, serial metabolite imaging in combination with phase-contrast SR- $\mu$ CT could facilitate a lossless anatomic and metabolic 3D model of the same organism in the near future.

Author contact: Manuel Liebeke, [mliebeke@mpi-bremen.de](mailto:mliebeke@mpi-bremen.de)  
Grace D'Angelo, [gdangelo@mpi-bremen.de](mailto:gdangelo@mpi-bremen.de)  
Benedikt Geier, [bgeier@mpi-bremen.de](mailto:bgeier@mpi-bremen.de)

## References

1. M. Polikarpov, G. Bourenkov, A. Snigirev and T. Schneider, 'High-throughput x-ray imaging, microscopy, and tomography for biological applications on EMBL beamline P14 at PETRA III (Conference Presentation)', Proc. SPIE 11113, Developments in X-Ray Tomography XII, 1111307 (2019).
2. J. Soltwisch, H. Kettling, S. Vens-Cappell, M. Wiegmann, J. Mützing and K. Dreisewerd, 'Mass spectrometry imaging with laser-induced postionization', Science 348, 211–215 (2015).
3. M. Kompauer, S. Heiles and B. Spengler, 'Atmospheric pressure MALDI mass spectrometry imaging of tissues and cells at 1.4- $\mu$ m lateral resolution', Nat. Methods 14, 90–96 (2017).

## Original publication

'Connecting structure and function from organisms to molecules in small-animal symbioses through chemo-histo-tomography', PNAS 118, e2023773118 (2021). DOI: 10.1073/pnas.2023773118



Benedikt Geier<sup>1</sup>, Janina Oetjen<sup>2</sup>, Bernhard Ruthensteiner<sup>3</sup>, Maxim Polikarpov<sup>4</sup>, Harald R. Gruber-Vodicka<sup>3</sup> and Manuel Liebeke<sup>1</sup>

1. Max Planck Institute for Marine Microbiology, Bremen, Germany
2. MALDI Imaging Lab, University of Bremen, Bremen, Germany
3. SNSB - The Bavarian State Collection of Zoology, Munich, Germany
4. European Molecular Biology Laboratory (EMBL) c/o DESY, Hamburg, Germany

# Insights into pH-responsiveness of mRNA delivery systems

A closer look to develop a model for the design of future mRNA drug products

RNA-based nanomedicines have proven to be a promising new class of drugs, with their broad field of potential applications ranging from protein substitution, over tumour immunotherapy, up to the recent success of being the first approved Covid-19 vaccines. The basic concept for all mRNA drugs is to deliver protein-encoding mRNA, like tumour or virus antigens, into target cells in order to be transfected into the protein and for example induce antitumoral responses. To make intravenous application of mRNA possible, formulations are required that protect the mRNA from degradation through the ubiquitous nucleases, deliver it to the target site and promote cellular uptake and translation. Non-viral lipid-based delivery vehicles have demonstrated to be suitable for this purpose.

While considerable effort has been spent on efficacy studies and general physicochemical characterisation of RNA nanomedicines, a lack of insight into the internal structures, their transformation in relation to environmental changes and the implications thereof still remains. To provide a successful therapy, mRNA nanomedicines need to overcome several hurdles. The mRNA needs to be protected from degradation and delivered into its target cells, followed by endosomal release and expression of the protein. The administration of pure mRNA does not fulfil this requirement. Therefore, lipoplexes, lipid-based nanoparticulate delivery systems for the mRNA, have been introduced which have been improved throughout the years.

Basically, all of these approaches are based on the interaction of mRNA with cationic or ionisable lipids, resulting in

complexation. Ionisable lipids are thought to be advantageous over their non-ionisable counterparts, as their pH-dependent charge can be used for reducing the toxicity of cationic lipids during systemic circulation while also facilitating a better release from the endosome [1,2]. For these ionisable lipids, the exact pH at which they change their charge has been recognised as essential for improved efficacy [3]. The classic tool to determine their pH-responsivity is fluorescence-based, where the quantum yield of the dye bound to the lipids sensitively changes with their charge. However, while straightforward, this approach has some limitations. It does not provide direct structural information from inside the lipoplexes or information on the binding state of the mRNA to the lipid matrix. Such information may be valuable for the optimisation of the systems for a given setting, though.

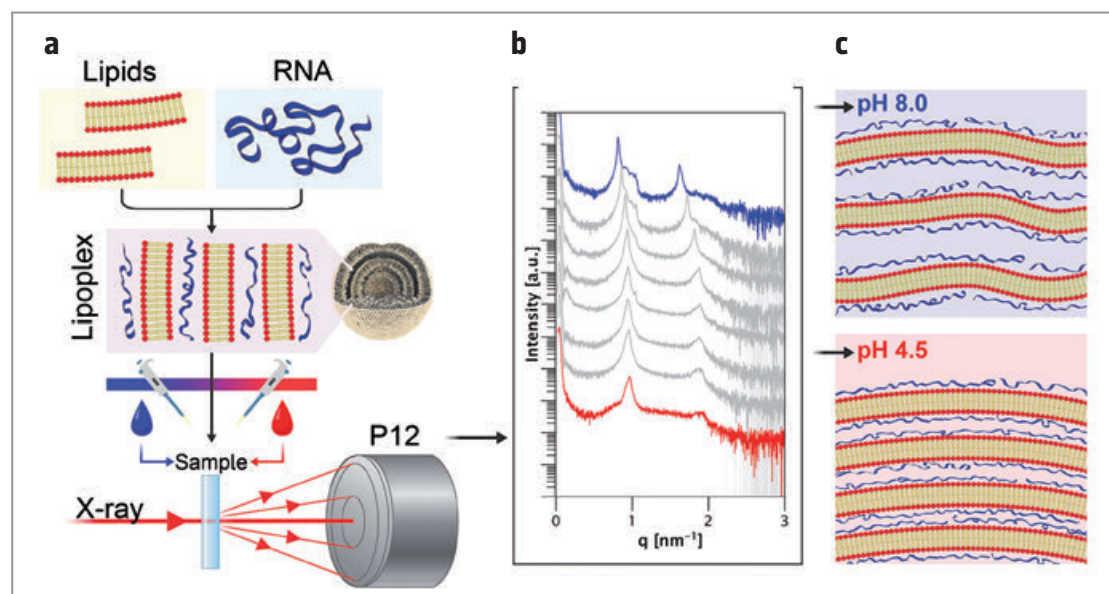


**Figure 1** SAXS measurements of pH-responsive lipoplexes. a) Sketch of the sample preparation for measurements at the EMBL beamline P12 at PETRA III. b) Scattering curves with characteristic Bragg peaks of a lipoplex system comprising the ionisable lipid DODMA over a pH range from pH 4.5 (bottom) to pH 8.0 (top). c) Illustration of the derived model describing the pH responsiveness of these systems concerning inter-bilayer spacing (d-spacing) and particle order (Copyright: 2020 American Chemical Society).

Previous research in our group has shown that small-angle X-ray scattering (SAXS) can be a useful tool to obtain direct and quantitative structural insight into lipoplexes [4]. Using model systems, we were able to determine the binding stoichiometry between the mRNA and the lipids and to reveal the balance of attractive and repulsive interactions between them. In this study, we utilised similar systems — comprising both ionisable and non-ionisable cationic lipids — in order to investigate the effect of pH variation on their internal organisation. The aim was to elucidate pH-dependent coherencies between structural and biological processes during delivery, endosomal uptake and release in pH-responsive lipoplexes.

SAXS curves of a variety of lipoplex systems were recorded over a pH range of 4.5–8.0 at the EMBL beamline P12 at PETRA III. Changes in the scattering curves were determined for different lipids present at various molar fractions and N/P ratios (ratio of ionisable lipid to RNA) inside the formulations. Careful analysis of these curves proved that the investigated systems have a lamellar organisation and allowed an accurate determination of pH-dependent structural changes concerning layer spacing and long-range particle order (Fig. 1). For further analysis, the layer spacing was investigated in relation to the pH level. The values for the systems comprising ionisable lipids changed in a sigmoidal manner, allowing the fitting of a mathematical model from which the pH level, around which the internal structure of each lipoplex changed, was determined. This ‘conformational pH’ could not only be affected by the selection of the ionisable lipid but also by the N/P ratio. For comparison, the systems were investigated by a well-established assay utilising the fluorescent dye TNS to measure the lipid ionisation constant  $pK_a$ . When comparing the pH-dependent structural changes observed in the SAXS measurements to the TNS assay, the calculated  $pK_a$  values showed a systematic shift to higher values for the fluorescence assay (Fig. 2). Therefore, the structural changes depend not only on the protonation state of the ionisable lipid, but rather the overall lipid assembly has to be considered. A further noteworthy information in this context — both measurements indicated that the conformational transition point also depends on the fraction of mRNA inside the membranes, where a monotonous change as a function of the N/P ratio was determined. Thus, the conformational transition points seem to be dependent on three factors: the type of the ionisable lipid, its molar fraction within the particles and the N/P ratio.

Overall, the results from this study provide a contribution to a better understanding of the structural and functional coherencies inside mRNA nanoparticles comprising ionisable lipids. Such understanding may help to assemble mRNA delivery systems with fine-tuned responsiveness to changes of pH in the local environment to obtain optimised expression in a given target.

Author contact: Peter Langguth, [langguth@uni-mainz.de](mailto:langguth@uni-mainz.de)

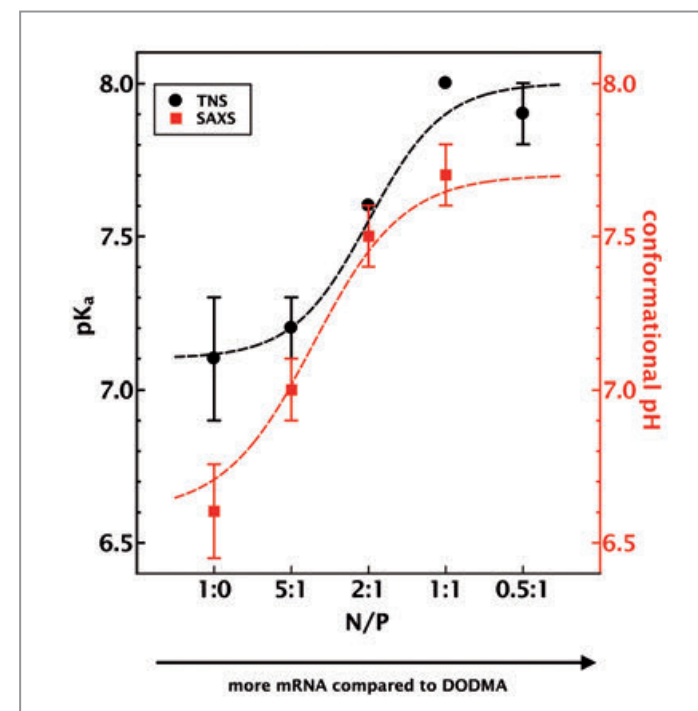


**Figure 2** Comparison of the formulations' conformational transition point and lipid  $pK_a$  for samples comprising the ionisable lipid DODMA as determined by SAXS (red) and TNS (black). Dashed lines are meant as a guide to the eye and do not represent fitting of a physical model (Copyright: 2020 American Chemical Society).

## References

1. M. Ramezanzpour, M. L. Schmidt, I. Bodnariuc, J. A. Kulkarni, S. S. W. Leung, P. R. Cullis, J. L. Thewalt and D. P. Tieleman, 'Ionizable amino lipid interactions with POPC: implications for lipid nanoparticle function', *Nanoscale* **11**, 14141 (2019).
2. R. Kedmi, N. Ben-Arie and D. Peer, 'The systemic toxicity of positively charged lipid nanoparticles and the role of Toll-like receptor 4 in immune activation', *Biomaterials* **31**, 6867–6875 (2010).
3. M. Jayaraman, S. M. Ansell, B. L. Mui, Y. K. Tam, J. Chen, X. Du, D. Butler, L. Eltepu, S. Matsuda, J. K. Narayanannair, K. G. Rajeev, I. M. Hafez, A. Akinc, M. A. Maier, M. A. Tracy, P. R. Cullis, T. D. Madden, M. Manoharan and M. J. Hope, 'Maximizing the potency of siRNA lipid nanoparticles for hepatic gene silencing in vivo', *Angew. Chem. Int. Ed.* **51**, 8529–8533 (2012).
4. A. Ziller, S. S. Nogueira, E. Huehn, S. S. Funari, G. Brezesinski, H. Hartmann, U. Sahin, H. Haas and P. Langguth, 'Incorporation of mRNA in lamellar lipid matrices for parenteral administration', *Mol. Pharm.* **15**, 642–651 (2018).

## Original publication

'Investigation of pH-responsiveness inside lipid nanoparticles for parenteral mRNA application using small-angle X-ray scattering', *Langmuir* **36**, 13331–13341 (2020). DOI: 10.1021/acs.langmuir.0c02446



Lukas Uebbing<sup>1</sup>, Antje Ziller<sup>2</sup>, Christian Siewert<sup>1</sup>, Martin A. Schroer<sup>2</sup>, Clement E. Blanchet<sup>2</sup>, Dmitri I. Svergun<sup>2</sup>, Srinivas Ramishetti<sup>3</sup>, Dan Peer<sup>2</sup>, Ugur Sahin<sup>4,5,6</sup>, Heinrich Haas<sup>4</sup> and Peter Langguth<sup>1</sup>

1. Department of Pharmaceutics and Biopharmaceutics, Institute of Pharmaceutical and Biomedical Sciences, J. Gutenberg University Mainz, Germany
2. European Molecular Biology Laboratory (EMBL) c/o DESY, Hamburg, Germany
3. Laboratory of Precision NanoMedicine, Shmunis School for Biomedicine and Cancer Research, Tel Aviv University, Tel Aviv, Israel
4. BioNTech RNA Pharmaceuticals GmbH, Mainz, Germany
5. TRON – Translational Oncology at the University Medical Center, J. Gutenberg University Mainz, Germany
6. Research Center for Immunotherapy (FZI), University Medical Center at the J. Gutenberg University Mainz, Germany

# New opportunities to combat tuberculosis

Detailed structure of a bacterial protein complex critical for tuberculosis infection determined

Tuberculosis, which remains one of the diseases killing the most people worldwide, is caused by infection with *Mycobacterium tuberculosis*. This research provides new insights into the biology of mycobacterial infections. In a joint effort we determined the high-resolution structure of a protein complex that enables mycobacteria to release molecules into its host and is therefore critical for the infection process. Our findings open new possibilities for studies on novel drugs and vaccines against tuberculosis.

Tuberculosis is one of the top ten causes of death worldwide, infecting about one-quarter of the world's population. Although it is treatable, the rise of multidrug-resistant tuberculosis poses a major threat to global health security and has been declared by the World Health Organisation as a global health emergency. In addition, reduced access to diagnosis and treatment during the Covid-19 pandemic is expected to dramatically increase the number of tuberculosis infections. This will set global efforts to tackle the disease back several years [1]. With this study, we pave the way to future research aimed at the development of novel drugs and vaccines against tuberculosis.

Tuberculosis is caused by infection with *Mycobacterium tuberculosis*: a bacterium that infects human lungs and other organs by using complex molecular machineries; these include protein complexes known as type VII secretion systems, which enable *M. tuberculosis* to release molecules into its host, disarming the immune system and ultimately inducing the disease [2]. Up to five such secretion systems, labelled ESX-1 to ESX-5, are found among *M. tuberculosis* and other closely related mycobacteria, many of which are pathogenic. The different ESX systems have

different functions and do not only play a role in virulence but are also important for the viability of mycobacteria [2].

Our group at European Molecular Biology Laboratory (EMBL) Hamburg is using high-resolution structural biology methods to study mycobacterial proteins, including ESX systems. In this study, we determined the molecular structure of the mycobacterial secretion system ESX-5 to a resolution of 3.4 Å (Fig. 1,2). Our structure of the ESX-5 secretion complex provides deep insight into the major sluice gate that separates the inner of these bacteria from the outer host environment. Opening this gate allows the pathogen to transport its proteins into the human cell and to establish an infection. Ultimately, we can use this structure as a toolbox with literally thousands of potential drug targets. This will open an entirely new field of studies on tuberculosis.

Determining the molecular structure of ESX-5 was particularly challenging because of its large size, complexity and dynamics. No single structural biology method could provide the full picture. While the resolution of the cryo-EM map allowed building a detailed model in the transmembrane region and in the cytoplasmic region close to the membrane, the resolution of the cryo-EM map alone was not sufficient in the periplasm and distal cytosolic side due to the dynamic nature of the complex. Therefore, we complemented the cryo-EM data with an X-ray crystallography structure of a single protein component obtained at the EMBL beamline P13 at PETRA III, homology models and crosslinking mass spectrometry results and combined the data by using the software 'Assemble', developed at

Figure 1

The mycobacterial ESX-5 secretion system is located in the bacterial inner membrane and consists of six units which assemble into a symmetrical structure with a pore at the centre. (Credit: Isabel Romero Calvo (EMBL)).

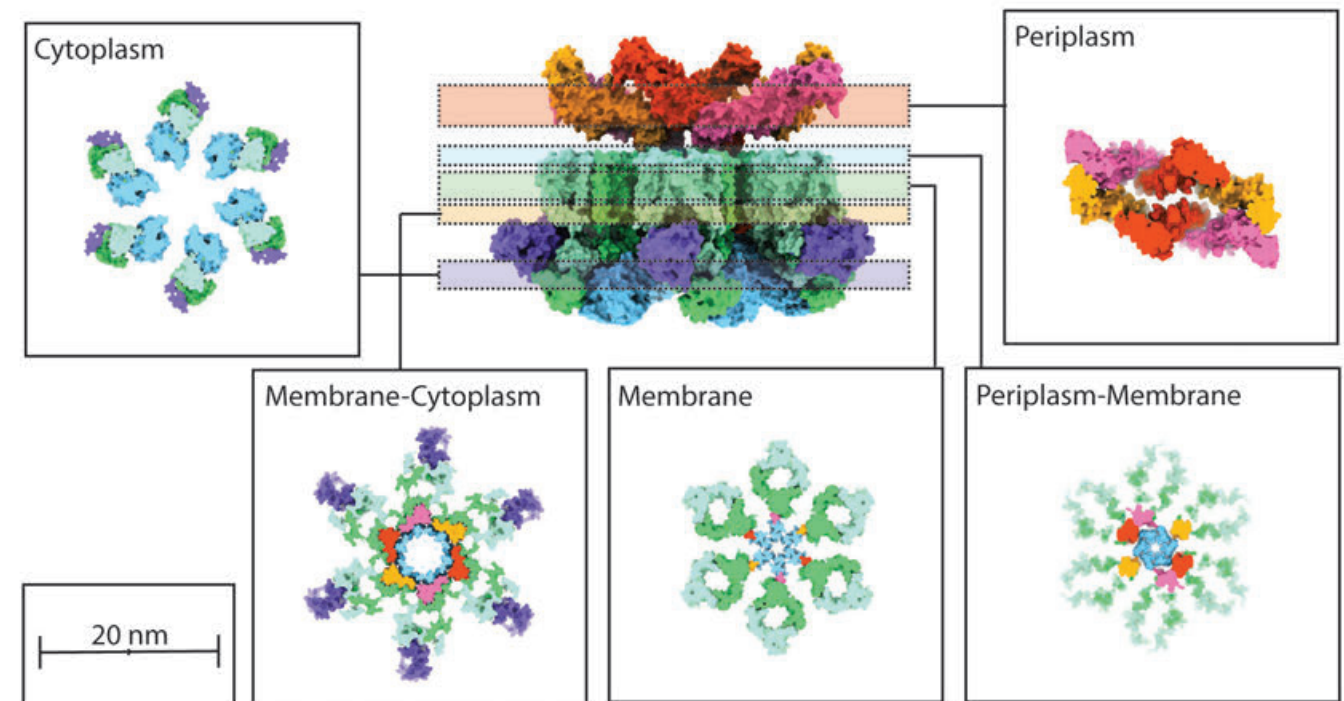
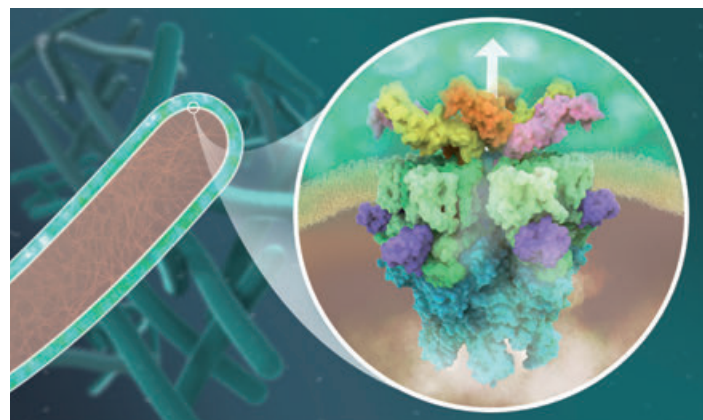


Figure 2

Cross-sections of the ESX-5 complex displayed as a surface representation of the atomic model shown as insets. Each inset highlights the subunit/subunit interactions occurring on the periplasmic, periplasmic-membrane, membrane, membrane-cytoplasmic and cytoplasmic level, demonstrating the highly dynamic nature of the complex at different sections within and next to the mycobacterial membrane. The five different subunits of the ESX-5 complex which due to its hexameric symmetry multiply to a total of 30 are shown in distinct colours. (Credit: adopted from original publication licensed under 4.0 (CC BY), Christiana Ritter (EMBL)).

EMBL Hamburg. This approach enabled us to create a coherent model of the ESX-5 complex.

The level of detail achieved exceeds by far the results of our previous study from 2017 in which we described the overall dimension, stoichiometry and shape of the ESX-5 secretion machinery based on negative stain electron microscopy, small-angle X-ray scattering (SAXS) and mass spectrometry data [3]. With the structural information we have obtained now, we can analyse in detail the architecture of the secretion machinery and understand the secretion mechanism and the role of specific protein residues for the secretion process.

In our final model, the big inner-membrane core complex of ESX-5 is built by four protein components that form six identical subcomplexes, symmetrically arranged around a central membrane pore. Interestingly, this central membrane pore was observed to be considerably more dynamic compared to the rest of the membrane-spanning protein domains. We suggest that these dynamics are crucial to contribute to the plasticity of the complex needed to transport a diverse set of 'weapons' and molecular machines across the mycobacterial membrane. Targeting this mechanism with small-molecule drugs could be one of many possible ways to develop new treatments based on our structure.

The study could also help scientists to develop new vaccines for tuberculosis. The widely used *Bacillus Calmette-Guérin* (BCG) vaccine, which has its 100th anniversary this year [4], is based on a strain of mycobacterium that has

lost its ability to cause diseases because of a defect in the ESX-1 system. However, as BCG vaccination offers insufficient protection and is most effective in infants, alternative vaccines are urgently needed. Due to its close structural and functional relation with ESX-1, targeting the ESX-5 secretion system might spur the development of new vaccines which could complement or replace those currently used.

Author contact:

Matthias Wilmanns, [matthias.wilmanns@embl-hamburg.de](mailto:matthias.wilmanns@embl-hamburg.de)

Jan Kosinski, [jan.kosinski@embl-hamburg.de](mailto:jan.kosinski@embl-hamburg.de)

## References

1. World Health Organization, 'Global Tuberculosis Report 2021' (2021).
2. M. I. Gröschel, F. Sayes, R. Simeone, L. Majlessi and R. Brosch, 'ESX secretion systems: mycobacterial evolution to counter host immunity', *Nat. Rev. Microbiol.* **14**, 677–691 (2016).
3. K. S. H. Beckham L. Ciccarelli, C. Bunduc, et al., 'Structure of the mycobacterial ESX-5 type VII secretion system membrane complex by single-particle analysis', *Nat. Microbiol.* **2**, 17047 (2017).
4. S. Luca and T. Mihaescu, 'History of BCG vaccine', *Mædica (Bucur.)* **8**, 53–58 (2013).

## Original publication

'Structure of the mycobacterial ESX-5 type VII secretion system pore complex', *Science advances* **7**, eabg9923 (2021). DOI: 10.1126/sciadv.abg9923



Katherine S. H. Beckham<sup>1</sup>, Christina Ritter<sup>1</sup>, Grzegorz Chojnowski<sup>1</sup>, Daniel Ziemianowicz<sup>2</sup>, Edukondalu Mullapudiv, Mandy Rettel<sup>2</sup>, Mikhail M. Savitski<sup>2</sup>, Simon A. Mortensen<sup>1</sup>, Jan Kosinski<sup>1,2,3</sup> and Matthias Wilmanns<sup>1</sup>

1. European Molecular Biology Laboratory (EMBL) c/o DESY, Hamburg, Germany
2. European Molecular Biology Laboratory (EMBL), Heidelberg, Germany
3. Centre for Structural Systems Biology (CSSB) c/o DESY, Hamburg, Germany

# The new gold standard in single-particle X-ray imaging

Millions of diffraction patterns are combined to produce 3D images of nanoparticles

An ambitious application considered for X-ray free-electron lasers is to obtain the 3D structures of macromolecules without having to crystallise or cryogenically cool them. Single-pulse diffraction patterns are measured from individual molecules in random orientations, and millions of these are combined into a 3D dataset that encodes the structure. Extremely high-quality data is required — nothing larger than a single molecule may contribute to the measurement! In experiments carried out at the European XFEL, over 10 million patterns from gold nanoparticle test objects were collected. Using new algorithms, it was possible to not only orient each pattern in 3D space, but to separate them according to particle heterogeneity. The results show the feasibility of imaging macromolecules.

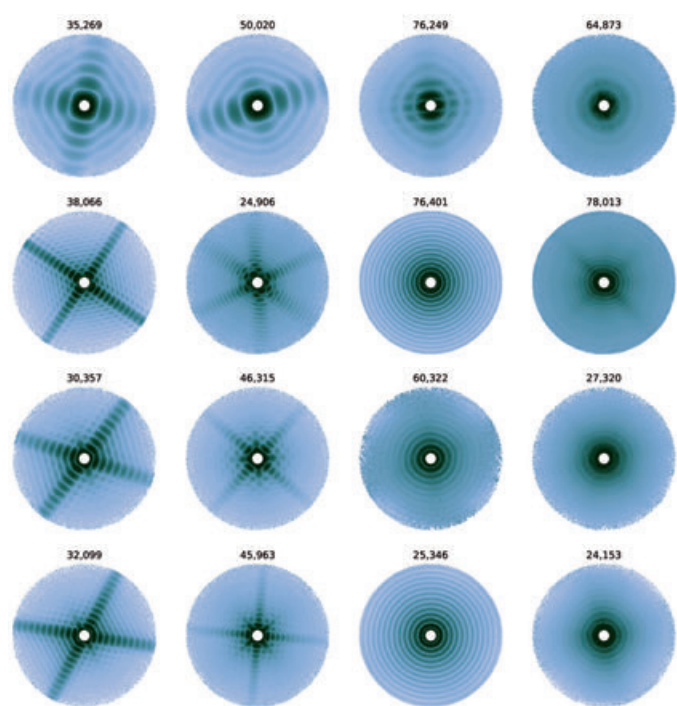
The determination of the structures of biomolecules at atomic resolution requires bright sources of short-wavelength radiation, which are so energetic that they degrade the very object under observation. Crystallography provides a work-around to this problem by distributing the deposited energy over billions of molecules, oriented and arranged in the regular lattice of the crystal to diffract constructively, giving strong diffraction that can be measured within a tolerable dose. Cooling to cryogenic temperatures extends this tolerable dose somewhat, and also enables electron microscopes — which suffer from similar damage restrictions — to record noisy images of reproducible single molecules. The femtosecond-duration pulses of X-ray

free-electron lasers offer yet another way to overcome radiation damage [1]. A femtosecond pulse outruns atomic motions triggered by the X-ray induced ionisation, the motions being limited by the inertia of atoms. In this way, the exposure to the molecule can be increased by thousands of times, to the point where every atom in the sample is ionised several times and the molecule vaporises as a tiny plasma. This destruction occurs after the diffraction. Of course, this also means that an object can only be imaged once. Three-dimensional information requires recording diffraction from a large number of views of the object, which in turn means that we need a large supply of identical (or near-identical) molecules.

This general paradigm of 'diffraction before destruction' also applies to non-biological materials, such as the metallic nanoparticles imaged here, and is used in the method of serial femtosecond crystallography — a technique that arose from initial research in single-particle imaging (SPI). An advantage of the approach is that it has an inherently high time resolution and there is no need to cryogenically cool the sample, so it is possible to capture diffraction at different time points during a reaction. The methods demonstrated here to sort heterogeneous structures may also be used to sort the structure of a protein folding into its equilibrium structure or to track a reaction [2].

Figure 1

A selection of summed diffraction patterns of single particles that have been separated into different classes for four different samples. The edge resolution is 3.3 nm and the numbers list the number of patterns summed in each class. The first two columns were used for 3D classification and image reconstruction shown in Fig. 2. The third and fourth columns show diffraction from spherical contaminants or other rare events.



While lacking the amplification of diffraction signals from molecules arranged in a crystal lattice, and hence giving very weak signals, single-particle diffractive imaging does have some advantages over crystallography. The diffraction from a compact object such as a single molecule is continuous and is usually described as a pattern of 'speckles' — constructive interference of waves scattered from the constituent atoms — surrounded by dark regions of destructive interference. The width of these speckles scales inversely with the size of the object. It has been known since the 1950s that it is not necessary to measure at more than two points across each speckle, since measurements at that spacing completely determine the entire pattern. This is easily achieved with a pixelated detector such as the AGIPD used here. Furthermore, this type of measurement fully encodes the structure of the diffracting object, such that the image can be recovered using an iterative algorithm which finds the most compact object in agreement with the measured diffraction pattern [3]. This is in contrast to the situation found in crystallography, where constructive interference is found only at half of the required points per spatial dimension.

Another advantage of measuring molecules one by one instead of together in a crystal is that variations in structures can potentially be separated from each other and a set of structures could be determined. This has even higher demands on the processing of the diffraction dataset. Not only do we need to figure out what the molecule orientation was from the noisy diffraction pattern, but we also need to decide which structure it belongs to. A diffraction pattern is a two-dimensional slice of a three-dimensional spectrum of spatial frequencies. Every pattern cuts through the origin of this space, so two patterns of the same object must intersect along a common line. Patterns of different objects will have no such common line. However, when working with patterns as weak as expected for single molecules, this common line is not enough to base decisions on. Here, instead, the entire collection of diffraction patterns was brought into a number of self-consistent 3D averages using the Expand-Maximize-Compress (EMC) algorithm [4].

Our experiments used gold nanoparticles, smaller than 50 nm, that were specifically synthesised to have a number of discrete shapes and sizes of cubes and octahedra with a narrow range of variability. These were aerosolised and entrained into a narrow beam directed at the X-ray focus of the SPB/SFX instrument at European XFEL using an aerodynamic lens stack. Benefitting from the high repetition rate of the European XFEL, we collected over 10 million diffraction patterns of these particles, overcoming a previous bottleneck in SPI experiments. From this huge dataset, four different structures were imaged in 3D at a resolution of 3 nm by considering the sample inhomogeneities. These results show that it is not only possible to record the numbers of high-quality patterns needed for single-particle imaging, but the algorithms are effective at sorting and classifying with a high degree of accuracy. The next step

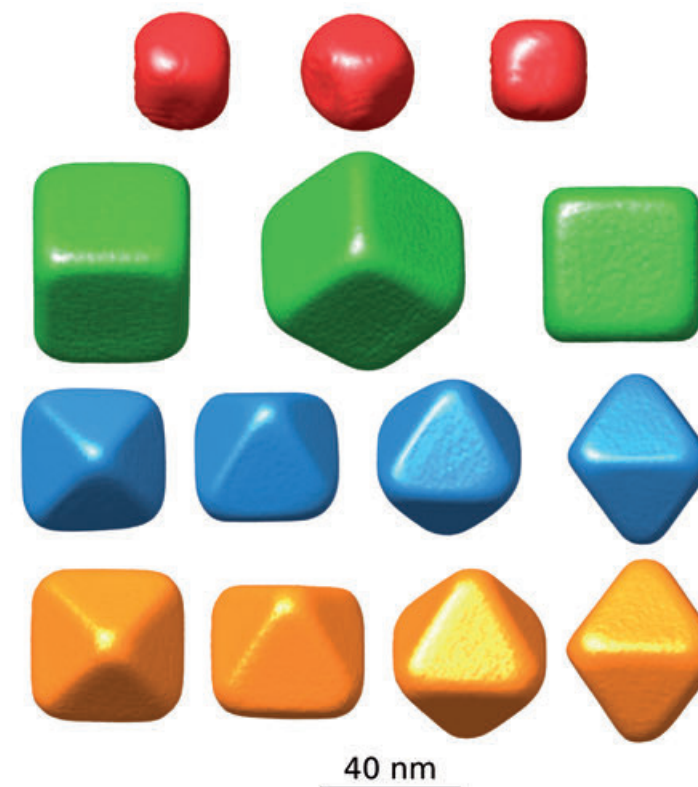


Figure 2

Isosurface plots of electron densities recovered using phase retrieval from the separate classes of data.

will be to repeat the experiment using an even finer-focused beam which should allow similar results with more weakly-scattering biological materials.

Author contact: Kartik Ayyer, [kartik.ayyer@mpsd.mpg.de](mailto:kartik.ayyer@mpsd.mpg.de)  
P. Lourdu Xavier, [lourdu.xavier.paulraj@desy.de](mailto:lourdu.xavier.paulraj@desy.de)  
Henry Chapman, [henry.chapman@desy.de](mailto:henry.chapman@desy.de)

## References

1. R. Neutze, R. Wouts, D. van der Spoel, E. Weckert and J. Hajdu, 'Potential for biomolecular imaging with femtosecond X-ray pulses', *Nature* 406, 753–757 (2000).
2. A. Hosseinizadeh, N. Breckwoldt, R. Fung, R. Sepehr, M. Schmidt, P. Schwander, R. Santra and A. Ourmazd, 'Few-fs resolution of a photoactive protein traversing a conical intersection', *Nature* 599, 697–701 (2021).
3. H. N. Chapman and K. A. Nugent, 'Coherent lensless X-ray imaging', *Nat. Photonics* 4, 833–839 (2010).
4. N.-T. D. Loh and V. Elser, 'Reconstruction algorithm for single-particle diffraction imaging experiments', *Phys. Rev. E* 80, 026705 (2009).

## Original publication

'3D diffractive imaging of nanoparticle ensembles using an X-ray laser', *Optica* 8, 15–23 (2021). DOI:10.1364/OPTICA.410851



Kartik Ayyer, P. Lourdu Xavier, Johan Bielecki, Zhou Shen, Benedikt J. Daurer, Amit K. Samanta, Salah Awel, Richard Bean, Anton Barty, Martin Bergemann, Tomas Ekeberg, Armando D. Estillore, Hans Fangohr, Klaus Giewekemeyer, Mark S. Hunter, Mikhail Karneviskiy, Richard A. Kirian, Henry Kirkwood, Yoonhee Kim, Jayanath Koliyadu, Holger Lange, Romain Letrun, Jannik Lübke, Thomas Michelat, Andrew J. Morgan, Nils Roth, Tokushi Sato, Marcin Sikorski, Florian Schulz, John C. H. Spence, Patrik Vagovic, Tamme Wollweber, Lena Worbs, Oleksandr Yefanov, Yulong Zhuang, Filipe R. N. C. Maia, Daniel A. Horke, Jochen Küpper, N. Duane Loh, Adrian P. Mancuso and Henry N. Chapman

For affiliation details refer to original publication.

# Unravelling the non-classical emergence of CoO nanoassemblies

X-ray *in situ* studies bridge the molecular and macro length scales

The fabrication of nanomaterials with well-defined size and shape requires the control of chemical reactions at various length scales. In this context, the classical model of nucleation and growth by monomer addition from a supersaturated solution continues to be the standard. However, recent studies suggest a much more versatile landscape of formation processes [1], including the evolution of small pre-crystalline particles and their assembly into distinct superstructures [2]. Although these non-classical routes have opened up new ways of nanomaterials design, little is yet known about the mechanisms involved. This situation, however, is changing with the development of advanced X-ray spectroscopic and scattering *in situ* methods bridging the length scales from molecular to macroscopic.

Recent advancements in X-ray spectroscopic and scattering techniques enabled studying the formation of nanomaterials *in situ* with an unprecedented level of detail. However, a single method is not enough to follow both, chemical and structural changes in solution. Here, using the example of CoO nanoassemblies [3], we illustrate how the combination of spectroscopy and scattering sheds light on all steps of the formation process. The monodisperse nanoassemblies are composed of small, individual crystallites with various edgy shapes (Fig. 1a). With high resolution transmission electron microscopy (HR-TEM), we find different crystallographic orientations within a single assembly (Fig. 1b). These observations suggest a multi-step pathway from the dissolved precursor molecule to the final assembled structure.

We use high energy-resolution fluorescence-detected X-ray absorption near edge structure (HERFD-XANES) measurements to elucidate the formation process from a chemical perspective. Following the concentration of the chemical species over time (Fig. 2a) indicates a fast reduction of the precursor cobalt(III) acetylacetonate ( $\text{Co}(\text{acac})_3$ ) to  $\text{Co}(\text{acac})_2$  in benzyl alcohol, which we identify as a stable intermediate. In a second step, the CoO phase forms. With its high energy resolution, HERFD-XANES is sensitive to

subtle changes in the local environment of the absorbing ion, and thus it allows to go beyond identifying chemical species and their oxidation states. In combination with simulated absorption spectra, we can directly read out the conformation of the molecular complex. The cobalt ion in the  $\text{Co}(\text{acac})_2$  intermediate keeps an octahedral coordination geometry by coordinating to two solvent molecules.

To complement the chemical information, we tracked structural changes during the nucleation and growth of CoO with *in situ* total X-ray scattering measured at beamline P21.1 at PETRA III. We transformed the data into atomic pair distribution functions (PDF), using both the Bragg scattering from crystalline and the diffuse scattering from amorphous phases. The resulting representation of interatomic distances allows to investigate the structure of all constituents in the reaction mixture. We observed a stepwise increase in the bond distance between the central cobalt ion and the surrounding oxygen ions (Fig. 2b). The steps match the three reaction stages identified earlier with spectroscopy (Fig. 2c). When the  $\text{Co}(\text{acac})_3$  complex rearranges to form  $\text{Co}(\text{acac})_2$  and coordinates to solvent molecules, the Co–O distance increases from 1.90 Å to 1.98 Å. The second increase to 2.12 Å matches the transition from the dissolved complex to crystalline CoO. Furthermore, we extract the sizes of the crystallites (Fig. 2d). Starting as small as 3.5 nm, they grow to a final size of 6.5 nm.

Figure 1

Electron microscopy images of CoO nanoassemblies. Different magnifications highlight their hierarchical structure. (a) SEM image of the spherical nanoassemblies composed of individual crystallites with various edgy shapes. (b) HR-TEM image revealing that different crystallite orientations are present within a single nanoassembly. The inset shows the corresponding Fourier transformation. (Adapted from a figure in the original publication licensed under CC BY 4.0)

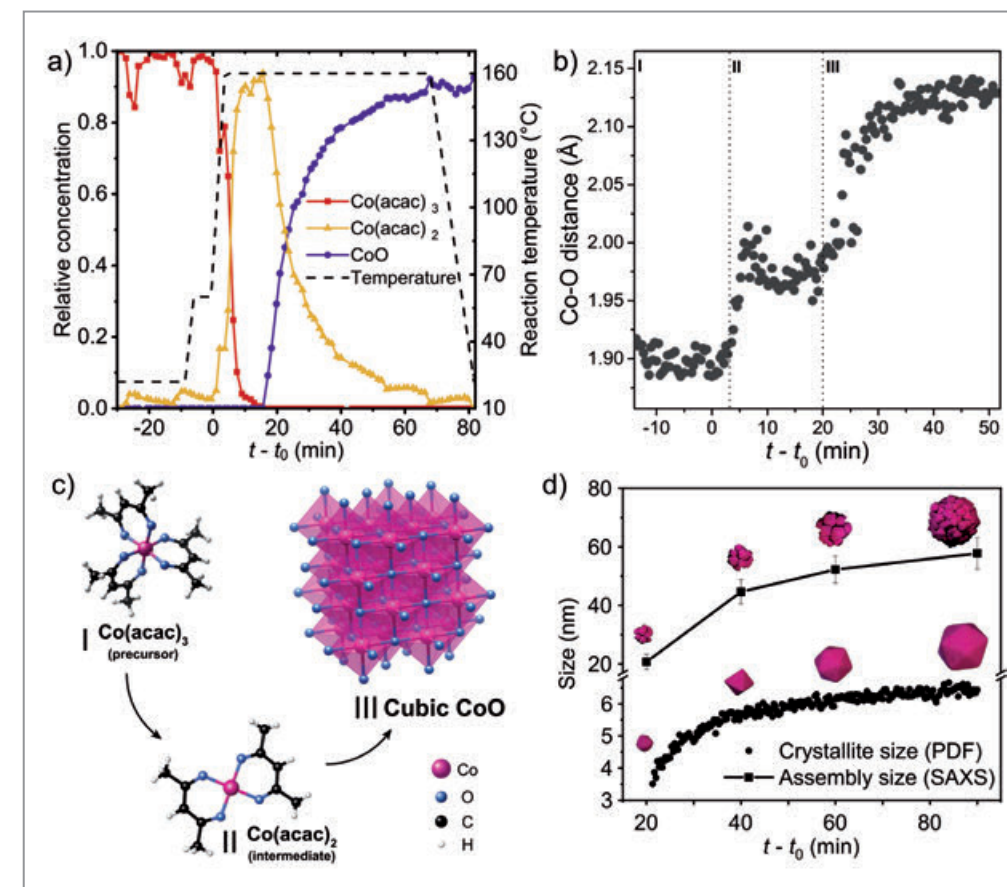
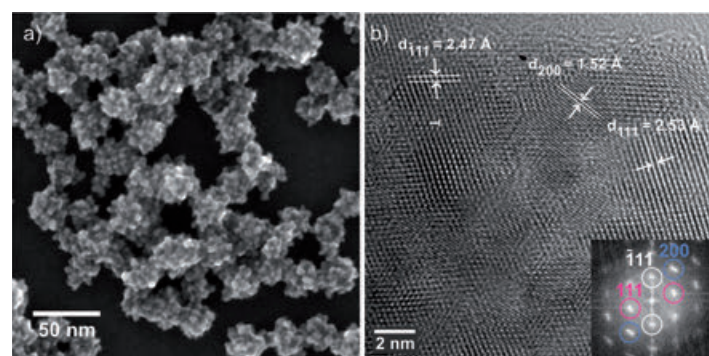


Figure 2

Determination of the chemical reaction steps and the rearrangement of the organometallic complex. (a) Relative concentrations of chemical constituents identified by the *in situ* HERFD-XANES study. The reaction proceeds over three stages from the precursor  $\text{Co}(\text{acac})_3$  via the intermediate  $\text{Co}(\text{acac})_2$  to the product CoO. (b) The shortest Co–O bond length obtained from PDF exhibits a stepwise increase corresponding to the three stages observed in (a). (c) Structural models for the proposed reaction stages. (d) Comparison of the growth rates of the individual crystallites obtained from PDF and of the assemblies obtained from SAXS. We find similar growth rates on both length scales. (Adapted from a figure in the original publication licensed under CC BY 4.0)

Ultimately, small-angle X-ray scattering (SAXS) partly measured at beamline P03 at PETRA III uncovered the assembly process of the crystallites into spherical superstructures. Using a model-based approach to fit the SAXS data, we find that the nanoassemblies grow at a similar pace as the individual crystallites (Fig. 2d), and also the number of crystallites in each assembly increases following the same trend. We conclude that the assembly starts as soon as the smallest crystallites have formed and continues till the end of the reaction. The simultaneous growth and assembly of crystallites are underpinned by the cavernous internal structure of the nanoassemblies evident from the SAXS study. This allows crystallites both at the surface and in bulk to consume monomers from the solution.

The concomitant growth and assembly of crystallites differentiate this pathway from a classical mechanism. In conclusion, only with the combination of modern X-ray spectroscopic and scattering methods, we can elucidate the emergence of nanoassemblies in solution both from a chemical and a morphological perspective. The resulting mechanistic insights with a high level of microscopic detail help to pave the way towards a generalised understanding of non-classical formation processes.

Author contact: Dorota Koziej, [dkoziej@physnet.uni-hamburg.de](mailto:dkoziej@physnet.uni-hamburg.de)  
Bert Nickel, [nickel@physik.uni-muenchen.de](mailto:nickel@physik.uni-muenchen.de)  
Lukas Grote, [lukgrote@physnet.uni-hamburg.de](mailto:lukgrote@physnet.uni-hamburg.de)

## References

1. M. Jehannin, A. Rao and H. Colfen, 'New horizons of nonclassical crystallization', *J. Am. Chem. Soc.* **141**, 10120–10136 (2019).
2. M. Niederberger, G. Garnweitner, J. Ba, J. Polleux and N. Pinna, 'Nonequilibrium synthesis, assembly and formation of metal nanocrystals', *Int. J. Nanotechnol.* **4**, 263–272 (2007).
3. M. Staniuk, O. Hirsch, N. Kränzlin, R. Böhlen, W. van Beek, P. M. Abdala and D. Koziej, 'Puzzling mechanism behind a simple synthesis of cobalt and cobalt oxide nanoparticles: *in situ* synchrotron X-ray absorption and diffraction studies', *Chem. Mater.* **26**, 2086–2094 (2014).

## Original publication

'X-ray studies bridge the molecular and macro length scales during the emergence of CoO assemblies', *Nature Communications* **12**, 4429 (2021). DOI: 10.1038/s41467-021-24557-z



Lukas Grote<sup>1,2</sup>, Cecilia A. Zito<sup>1,3</sup>, Kilian Frank<sup>4</sup>, Ann-Christin Dippel<sup>2</sup>, Patrick Reisbeck<sup>4</sup>, Krzysztof Pitala<sup>5,6</sup>, Kristina O. Kvashnina<sup>7,8</sup>, Stephen Bauters<sup>7,8</sup>, Blanka Detlefs<sup>9</sup>, Oleh Ivashko<sup>9</sup>, Pallavi Pandit<sup>2</sup>, Matthias Rebber<sup>1,10</sup>, Sani Y. Harouna-Mayer<sup>1,10</sup>, Bert Nickel<sup>4</sup> and Dorota Koziej<sup>1,10</sup>

1. Institute for Nanostructure and Solid-State Physics, Centre for Hybrid Nanostructures (CHyN), Universität Hamburg, Hamburg, Germany
2. Deutsches Elektronen-Synchrotron DESY, Hamburg, Germany
3. São Paulo State University UNESP, São José do Rio Preto, Brazil
4. Faculty of Physics and Center for NanoScience (CeNS), Ludwig-Maximilians-Universität München, Munich, Germany
5. Faculty of Physics and Applied Computer Science, AGH University of Science and Technology, Krakow, Poland
6. Academic Center for Materials and Nanotechnology, AGH University of Science and Technology, Krakow, Poland
7. The Rossendorf Beamline at the European Synchrotron Radiation Facility ESRF, Grenoble, France
8. Institute of Resource Ecology, Helmholtz-Zentrum Dresden-Rossendorf (HZDR), Dresden, Germany
9. European Synchrotron Radiation Facility ESRF, Grenoble, France
10. The Hamburg Centre for Ultrafast Imaging (CUI), Universität Hamburg, Hamburg, Germany

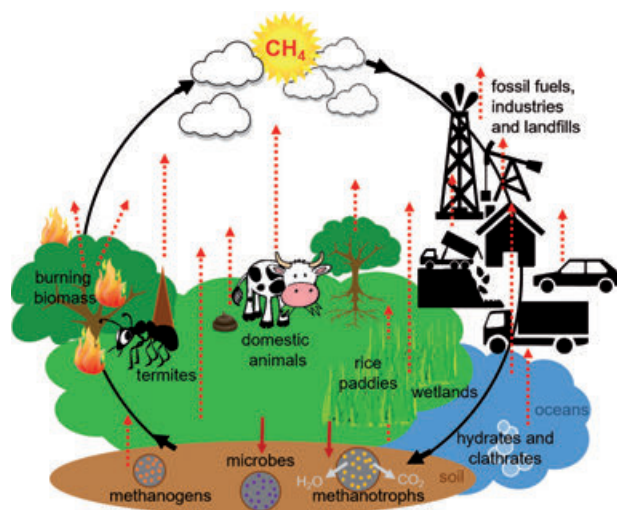
# Fighting a greenhouse gas

## Dinuclear copper complexes as models of methane oxidation

Methane monooxygenases (MMOs) mediate the first step of bacterial methane oxidation by converting methane to methanol. For the most abundant, copper-dependent form of MMO, the mechanism of this reaction is unknown. We have synthesised copper complexes that bind dioxygen and activate it for incorporation into aliphatic substrates such as methane. Using a combination of resonance-Raman (RR) and X-ray absorption spectroscopy (XAS) as well as mass spectrometry (MS), at beamlines P64 and P65, the electronic and geometric structures of the relevant intermediates were elucidated. A key step in the reactivity of the investigated systems is the cleavage of the O–O bond which leads to highly electrophilic mono- $\mu$ -oxo dicopper intermediates, which in turn mediate H-atom abstraction from hydrocarbons, coupled to an O-transfer.

After carbon dioxide, methane is the most dominant anthropogenic greenhouse gas. While its atmospheric concentration is much lower than that of CO<sub>2</sub>, methane is one to two orders of magnitude more effective in terms of its global warming potential (GWP). About 60% of the current methane flux from landmass to the atmosphere is the result of human activities, originating from fermentation processes associated with livestock, from cultivated rice paddy fields, fossil fuel use, biomass burning or landfills (Fig. 1). With the global methane pledge, the reduction of anthropogenic methane emissions has recently also been put on the political agenda. Natural sources of methane emission include wetlands, where methane is produced by microbes (methanogens), but also termites, oceans and other sources. On the other hand, soil methane is consumed by methanotrophs, microorganisms that feed on methane, constituting an important sink in the global methane cycle [1–3].

The first step of bacterial methane oxidation is mediated by MMO enzymes, which convert methane to methanol.



This reaction is highly challenging from a chemical point of view as methane is the most inert hydrocarbon and has the strongest C–H bond with a bond dissociation energy of 105 kcal/mol [3,4]. Moreover, the further oxidation of methanol to formaldehyde, formic acid and carbon oxides is difficult to avoid. Industrial processes circumvent the direct oxidation of methane to methanol by first converting methane to syngas (CO + H<sub>2</sub>), from which methanol is produced at high temperatures and pressures. The way in which biological systems mediate direct methane oxidation at room temperature and ambient pressure thus is of profound interest. For the iron-based, soluble form of MMO (sMMO), the corresponding mechanism has been elucidated whereas for the more common, copper-dependent form of this enzyme (particulate MMO, pMMO), details of this reaction are still unknown [3,4]. We have synthesised two catalytically active dinuclear copper complexes that bind oxygen and activate it for insertion into the C–H bonds of hydrocarbons. By using a combination of techniques (RR, XAS and MS), we were able to understand the fate of oxygen in our model systems, from its initial binding to the copper centres to its final incorporation into aliphatic substrates.

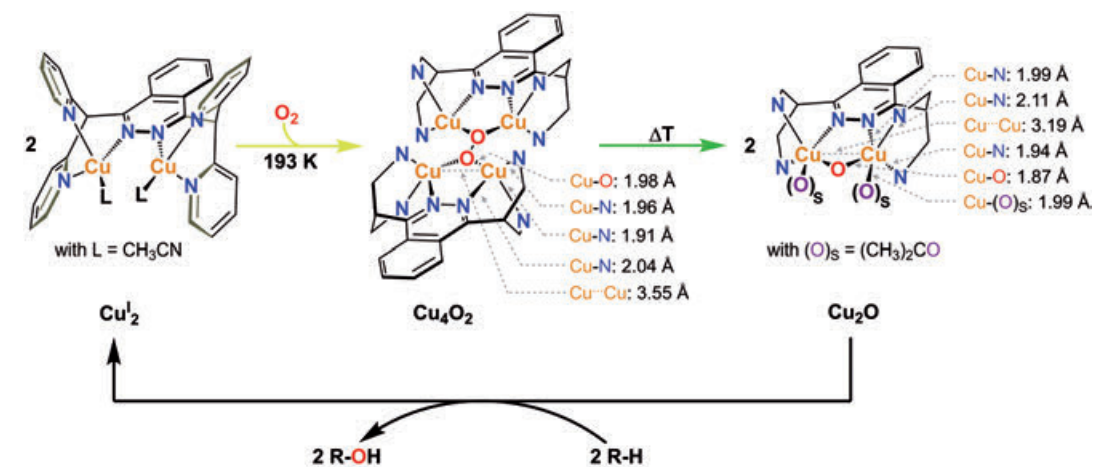
The structure of the complexes and the reactive cycle are shown in Fig. 2. When exposed to dioxygen, two of the dinuclear copper(I) precursors bind one molecule of O<sub>2</sub> as peroxide and form a tetranuclear cluster. This intermediate was trapped at 193 K and investigated with RR and XAS as well as cryogenic electrospray ionisation MS. Upon heating to 238 K, the O–O bond of the bridging peroxo unit is

Figure 1

The methane flux from the land to the atmosphere comprises natural and human sources. Methanotrophs convert methane to carbon dioxide and water, constituting an important sink in the global methane cycle [1–3].

Figure 2

The catalytic cycle starts with the bonding of O<sub>2</sub> to the dicopper(I) complex (Cu<sub>2</sub>, left), resulting in the formation of the tetranuclear copper cluster (Cu<sub>4</sub>O<sub>2</sub>, middle). Homolytic O–O-bond cleavage leads to the active Cu<sub>2</sub>O species (right) which catalytically oxygenates a variety of hydrocarbons. Key geometric parameters (selected bond lengths and Cu–Cu distances) of the oxygenated complexes (Cu<sub>4</sub>O<sub>2</sub> and Cu<sub>2</sub>O) based on EXAFS data are shown as well. In the Cu<sub>4</sub>O<sub>2</sub> and Cu<sub>2</sub>O complexes the pyridine rings of the ligand have been omitted for clarity and simplified by the N-donor atoms.



cleaved and two dicopper complexes with so-called mono- $\mu$ -oxo cores are formed in which one oxygen atom is bound between the two Cu(II) centres. Due to this special environment, the mono- $\mu$ -oxo species is highly electrophilic and can abstract a hydrogen atom from organic substrates (R–H). Thereby, an organic radical (R) is formed which in turn combines with the OH group formed at the dinuclear metal site, leading to an alcohol (R–OH). This reaction sequence is denoted as rebound mechanism and applies to many biological oxygenation reactions. However, these processes are usually mediated by high-valent metal-oxo intermediates (Fe(IV), Cu(III)), whereas our systems only require two Cu(II) centres to enable this pathway.

RR has provided valuable information about the structure of the tetranuclear (Cu<sub>4</sub>O<sub>2</sub>) intermediate and the splitting of the O–O bond, leading to the very reactive mono- $\mu$ -oxo dicopper (Cu<sub>2</sub>O) complexes. Moreover, detailed insights into the oxidation state and the nearest-neighbour environment of the copper centres in the Cu<sub>2</sub>O and Cu<sub>4</sub>O<sub>2</sub> complexes were obtained from X-ray absorption fine structure (EXAFS; Fig. 2) and X-ray absorption near-edge structure (XANES). Notably, the edge position in the Cu K-edge XANES spectra was found to shift to higher energy upon oxygenation of the Cu(I) precursor to the Cu<sub>4</sub>O<sub>2</sub> intermediate and further conversion to the Cu<sub>2</sub>O complex, reflecting a stepwise transition from Cu(I) to Cu(II). Furthermore, information regarding the structure of the Cu<sub>4</sub>O<sub>2</sub> and Cu<sub>2</sub>O species was obtained from EXAFS, which showed good agreement with the results of density functional theory calculations.

The results provide new insights into the biomimetic oxidation of methane to methanol, a reaction of significant environmental impact. Direct methane oxidation to methanol, occurring under ambient conditions, is of fundamental chemical interest and may also become important in the

context of moving toward a methanol economy or reducing methane levels in the atmosphere [1,2,4].

Author contact: Ramona Jurgeleit, [rjurgeleit@ac.uni-kiel.de](mailto:rjurgeleit@ac.uni-kiel.de)  
Benjamin Grimm-Lebsanft, [benjamin.lebsanft@physik.uni-hamburg.de](mailto:benjamin.lebsanft@physik.uni-hamburg.de)  
Michael Rübhausen, [mruebhau@physnet.uni-hamburg.de](mailto:mruebhau@physnet.uni-hamburg.de)  
Felix Tuczek, [ftuczek@ac.uni-kiel.de](mailto:ftuczek@ac.uni-kiel.de)

### References

1. H. Schaefer, 'On the causes and consequences of recent trends in atmospheric methane', *Curr. Clim. Chang. Rep.* 5, 259–274 (2019).
2. M. Saunio et al., 'The global methane budget 2000–2017', *Earth Syst. Sci. Data* 12, 1561–1623 (2020).
3. C. W. Koo and A. C. Rosenzweig, 'Biochemistry of aerobic biological methane oxidation', *Chem. Soc. Rev.* 50, 3424–3436 (2021).
4. R. B. Jackson, E. I. Solomon, J. G. Canadell, M. Cargnello and C. B. Field, 'Methane removal and atmospheric restoration', *Nat. Sustain.* 2, 436–438 (2019).

### Original publication

'Catalytic oxygenation of hydrocarbons by mono- $\mu$ -oxo dicopper(II) species resulting from O–O cleavage of tetranuclear CuI/CuII peroxo complexes', *Angewandte Chemie International Edition* 60, 14154–14162 (2021). DOI: 10.1002/anie.202101035



Ramona Jurgeleit<sup>1</sup>, Benjamin Grimm-Lebsanft<sup>2</sup>, Benedikt Maria Flöser<sup>1,3</sup>, Melissa Teubner<sup>2,4</sup>, Sören Buchenau<sup>2</sup>, Laura Senft<sup>5</sup>, Jonas Hoffmann<sup>6,7</sup>, Maria Naumova<sup>8</sup>, Christian Näther<sup>1</sup>, Ivana Ivanović-Burmazović<sup>5,9</sup>, Michael Rübhausen<sup>2</sup> and Felix Tuczek<sup>1</sup>

1. Institute of Inorganic Chemistry, Christian-Albrechts-University of Kiel, Kiel, Germany
2. Institut für Nanostruktur- und Festkörperphysik, Center for Free Electron Laser Science (CFEL), DESY, Hamburg, Germany
3. Max Planck Institute for Chemical Energy Conversion, Mülheim an der Ruhr, Germany
4. Department of Inorganic Chemistry, RWTH Aachen University, Aachen, Germany
5. Department of Chemistry and Pharmacy, Friedrich-Alexander-University of Erlangen-Nürnberg, Erlangen, Germany
6. Institute for Analytical and Organic Chemistry, University of Bremen, Bremen, Germany
7. MAPEX, Center for Materials and Processes, University of Bremen, Bremen, Germany
8. Deutsches Elektronen-Synchrotron DESY, Hamburg, Germany
9. Department Chemie, Ludwig-Maximilians-Universität München, München, Germany

# What determines the elastic properties of teeth?

XRD and pressurisation quantify tooth nanocrystal stiffness

**Dentine, the bone-like tissue that makes up the core of teeth, comprises a composite of carbonated hydroxyapatite nanocrystals (c-Ap) embedding a fibrillar collagen matrix. The elastic properties of the nanoparticles critically define the response of teeth to load but the nanometre dimensions render standard mechanical tests very challenging. X-ray diffraction on the PETRA III beamline P07, combined with *in situ* water pressurisation, allowed us to directly measure mineral strain and bulk modulus. Backed by electron and atom probe methods, our results improved the understanding of the elastic properties of the biogenic nanocomposite.**

Tooth dentine is a bony biocomposite material consisting of carbonated apatite nanocrystal mineral (c-Ap, 50 vol.%, [1]) and an organic component made of protein fibrils (collagen type I, ~30 vol.%) (Fig. 1). Together with water, these constituents form a stiff and tough material that elastically and reversibly survives many years of mechanical loading without failure. We have shown that the combined action of tensile and compressive stresses between the protein nanofibers and the c-Ap mineral crystals strongly contribute to the longevity of dentine [2]. Quantification of these stresses remains elusive, since it is not yet possible to directly measure the elastic properties of c-Ap nanoparticles due to their sub-micrometre dimensions.

We measured the deformation of c-Ap nanocrystals within pig dentine samples by X-ray diffraction using a hydrostatic

pressurisation chamber [3] mounted at the P07 High Energy Materials Science beamline (HEMS). Heat treatment was used to remove the collagen constituent (annealing, 250 °C) or removal of  $\text{CO}_3^{2-}$  (ashing, 550 °C) to separate the effects of protein-induced stresses from chemical strain in the crystals. This allowed us to study the effects of de-carbonation on the properties of the biogenic apatite crystals.

We observed picometre deformations in reversible linear decreases in both *a*- and *c*-lattice parameters of the crystals using X-ray diffraction. From these, we determined experimental values of both bulk moduli (*K*) and the ratios of *a*- over *c*-lattice deformation ( $\eta$ ) (Fig. 2) for which we observed that deformation along the *a*-axis is almost twice as high as along the *c*-axis for annealed c-Ap, whereas upon removal of  $\text{CO}_3^{2-}$ , deformations become more similar

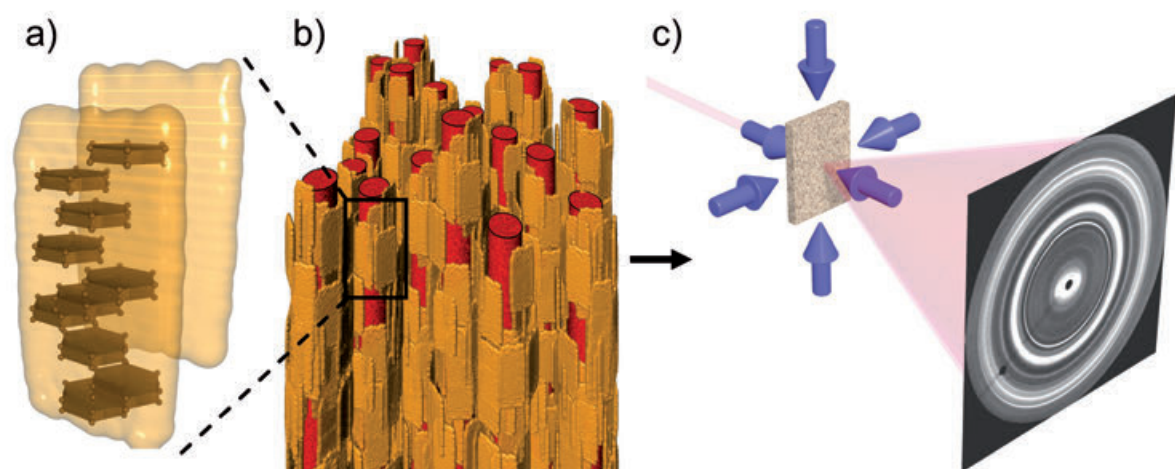


**Figure 1**  
Schematic illustration of mineralised collagen fibrils. a) Hexagonal unit cells of c-Ap crystals (illustrated in brown) bond to neighbouring crystals to create mineral clusters and thus, a polycrystalline structure. The c-Ap nanoparticles attach and partly wrap around collagen fibrils (marked red), forming b) bundles of mineralised fibrils creating a composite. Note that the schematic composition is not drawn to scale. c) Heat-treated samples were hydraulically compressed in water while measuring diffraction patterns before, during and after applying load. This provided diffraction patterns in which the deformation along the *a*- and *c*-lattice axes of the nanocrystals were determined.

along both axes. The larger standard deviations obtained with annealed dentine highlight the natural variation in carbonate content found in different teeth and different locations in teeth.

To better understand results from the experiments at PETRA III, transmission electron microscopy (TEM) and atom probe tomography (APT) were performed by our international team. These methods confirmed that no recrystallisation occurred upon our heat treatment and revealed a dense packing of elongated tablet-shaped nanocrystals, packed into high-density crystalline domains, surrounded by low-density carbon and nitrogen-rich clusters. These measurements further helped confirm that in dentine, carbon is present inside the apatite crystalline nanoparticle domains, likely in the form of carbonate.

Using the X-ray diffraction measurements, we were able to determine the elastic constants of biogenic apatite nanocrystals. In order to convert the deformation measurements into mechanical characteristics of the nanocrystals, it was necessary to match experimental compression measurements and synthetically derived elastic constants.

We achieved this by comparing each experimental result with all possible combinations of elastic constants ( $C_{11}$ ,  $C_{12}$ ,  $C_{13}$  and  $C_{33}$ ) of the c-Ap hexagonal crystal system, generated within a range of 0–200 GPa. More than 6 million combinations of these parameters yielded theoretical *K* and  $\eta$  values, which we matched with our diffraction-derived results, to create distributions in which we identified best matches. Only synthetically generated elastic constants that yielded bulk modulus and lattice strain ratios close to experimental values were considered. Histograms of the selected values allowed us to clearly quantify two of the elastic constants,  $C_{11}$  and  $C_{33}$ . These were matched with literature values obtained over the last five decades. Together with estimators of  $C_{11}$  and  $C_{12}$  we could finally determine possible bounds on Young's moduli  $E_{11}$  and  $E_{33}$  as well as the basal and prismatic Poisson's ratios, i.e. the Poisson's ratio along base and side faces of the hexagonal crystal structure of apatite (see grey faces in Fig. 3), of the apatite nanocrystals in the annealed and ashed states. All results demonstrate a marked increase in stiffness upon removal of the  $\text{CO}_3^{2-}$  from apatite in the biogenic apatite nanocrystals (Fig. 3).

The presented extensive characterisations of biological carbonate hydroxyapatite nanoparticles are extremely valuable to clarify the relationship between carbonate content and mechanical properties of bony tissues. The results of this study will support development of more accurate bone-like materials models.

**Author contact:** Jean-Baptiste Forien, [forien1@lnl.gov](mailto:forien1@lnl.gov)  
Paul Zaslansky, [paul.zaslansky@charite.de](mailto:paul.zaslansky@charite.de)

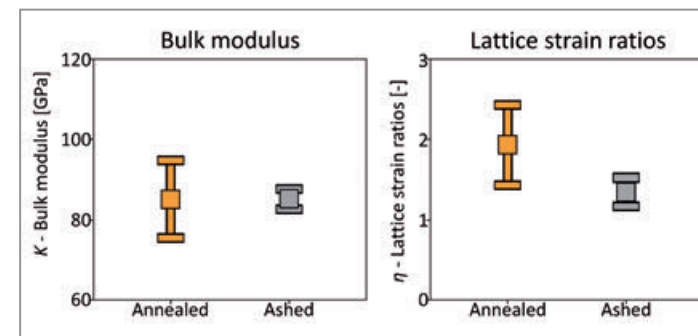


**Figure 2**  
Plots of the experimentally measured bulk moduli (*K*) and lattice strain ratios ( $\eta$ ) in annealed c-Ap and ashed nanocrystals of pig dentine. Means and standard deviations are presented in the plots and are larger (more variable) prior to carbonate removal by heating to 500 °C.

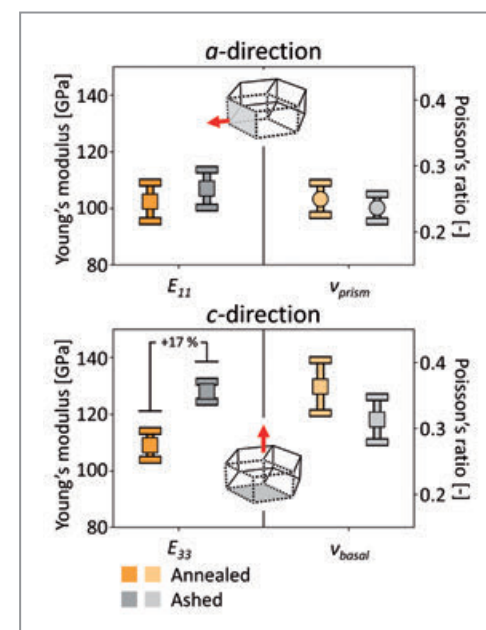


**Figure 3**  
Calculated Young's moduli and Poisson's ratios of annealed and de-carbonated crystals of apatite along the *a*- and *c*-lattice direction ( $E_{11}$  and  $E_{33}$ , respectively). Plots indicate means and standard deviations, calculated based on experimentally derived  $C_{33}$  and  $C_{13}$  and literature models for  $C_{11}$  and  $C_{12}$ .

## References

- R. Z. LeGeros, 'Apatites in biological systems', *Prog. Cryst. Growth Charact. Mater.* 4, 1–45 (1981).
- J.-B. Forien, I. Zizak, C. Fleck, A. Petersen, P. Fratzi, E. Zolotoyabko, P. Zaslansky, 'Water-mediated collagen and mineral nanoparticle interactions guide functional deformation of human tooth dentin', *Chem. Mater.* 28, 3416–3427 (2016).
- C. Krywka, C. Sternemann, M. Paulus, M. Tolan, C. Royer and R. Winter, 'Effect of osmolytes on pressure-induced unfolding of proteins: a high-pressure SAXS study', *ChemPhysChem.* 9, 2809–2815 (2008).

## Original publication

'X-ray diffraction and *in situ* pressurization of dentine apatite reveals nanocrystal modulus stiffening upon carbonate removal', *Acta Biomaterialia* 120, 91–103 (2021).  
DOI: 10.1016/j.actbio.2020.09.004



Jean-Baptiste Forien<sup>1</sup>, Jun Uzuhashi<sup>2</sup>, Tadakatsu Ohkubo<sup>3</sup>, Kazuhiro Hono<sup>2</sup>, Lucy Luo<sup>3</sup>, Henry P. Schwarcz<sup>3</sup>, Alix C. Deymier<sup>4</sup>, Christina Krywka<sup>5</sup>, Claudia Fleck<sup>6</sup> and Paul Zaslansky<sup>7</sup>

- Lawrence Livermore National Laboratory, Livermore, USA
- National Institute for Materials Science, Tsukuba, Japan
- McMaster University, School of Geography and Earth Sciences, Hamilton, Canada
- University of Connecticut Health Center, Farmington, USA
- Helmholtz-Zentrum Hereon, Geesthacht, Germany
- Technische Universität Berlin, Materials Science & Engineering, Berlin, Germany
- Charité – Universitätsmedizin Berlin, Restorative and Preventive Dentistry, Berlin, Germany

# Unexpected twist of catalytic nanoparticles

Precise orientation affects shape, size and behaviour

Nanoparticles that make up catalysts can arrange themselves in slightly different ways, and behave significantly differently as a result. This is revealed by an X-ray study of palladium nanoparticles carried out at the DESY NanoLab and PETRA III. The structure of the palladium nanoparticles in terms of its size and shape was monitored under varying oxidation and reduction conditions *in situ* using X-ray diffraction. The experiments provide systematic insights into the self-organisation of catalyst particles and how the catalytic behaviour is dependent on their orientation, size and shape.

Catalysts often consist of certain metals, such as platinum, rhodium or palladium, which promote the desired chemical reactions without being consumed themselves. The catalytic converters used in the exhaust system of cars, for instance, promote the oxidation of toxic carbon monoxide to carbon dioxide and the reduction of harmful nitrogen oxides. Metallic catalysts usually have the form of nano-

particles, because these have larger surface areas for a given amount of material.

More active centres of the catalyst nanoparticles are often located at corners and along edges. The shape and size of the particles can therefore have a substantial influence on their function and efficiency. The connection between the function of catalytic particles and its detailed structure is only just beginning to be understood [1]. With insights into the optimal size and shape of a nanoparticle, for example, catalysts could be made significantly better or cheaper. In particular, the role of the particles' precise orientation on the substrate has scarcely been explored. It is commonly assumed that around 90% of the metal used in present day catalysts contributes nothing to their functionality.

In this systematic study, palladium nanoparticles were grown on a magnesium oxide substrate. Both of these materials are typically found in a range of different catalysts, so the system studied serves as a model for numerous applications, including the catalytic converters installed in cars [2]. The nanoparticles were deposited on the substrate in a vacuum by means of molecular beam epitaxy at DESY NanoLab. The size and orientation of the resulting nanoparticles were analysed *in situ* using high-intensity X-rays at the PETRA III *in situ* X-ray Diffraction and Imaging beamline P23.

It clearly emerges that the nanoparticles have a preferred orientation upon deposition. The particles line up along the crystal lattice of the magnesium oxide substrate and almost all of them grow in a certain direction and to a certain size. But only almost all of them: about one in a

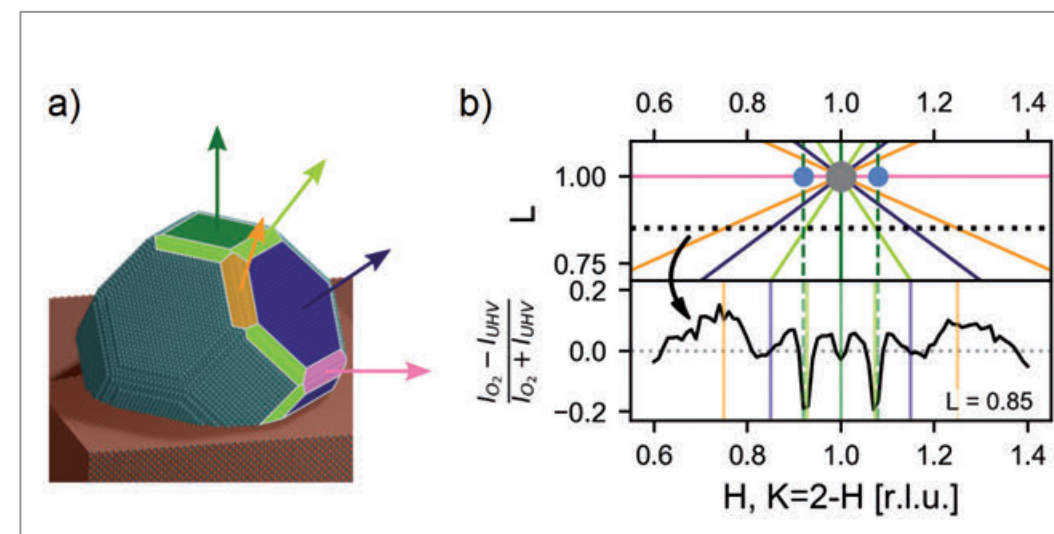


**Figure 2**  
(a) Illustration of the nanoparticles with different types of facets highlighted with colours corresponding to the lines in (b). (b) top, reciprocal space map of a plane around the Pd 111 reflex showing the location of the scattering from different facets. Bottom, a line scan along this plane showing the difference in the X-ray scattering signal in an oxidising environment compared to in vacuum conditions. (Reprinted with permission from ACS Nano 15 8, 13267–13278 (2021). Copyright 2021 American Chemical Society.)

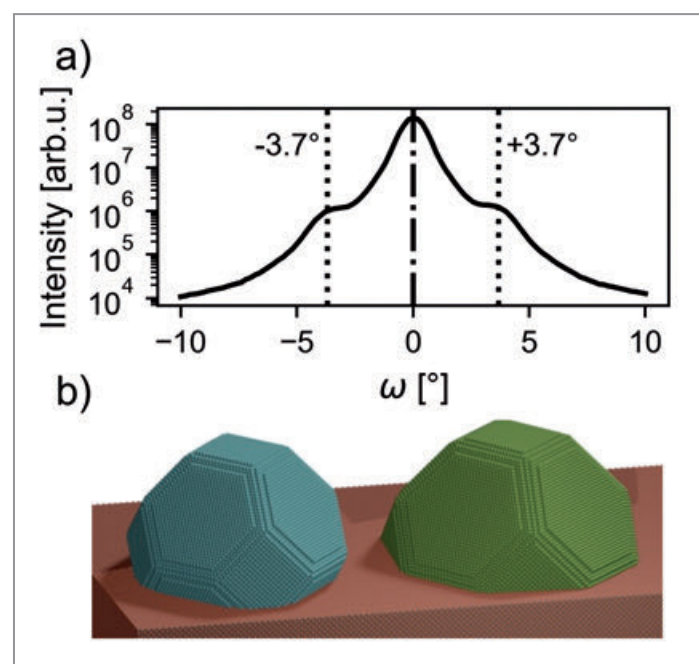


**Figure 1**  
a) Sample rotation,  $\omega$ , rocking scan around the Pd111 reflex, showing nanoparticle mosaicity. The two shoulders at  $\pm 3.7^\circ$  are indicative of particles which are rotated by a fixed amount in plane from the preferred [001] epitaxy on magnesium oxide. (b) Illustrations of the particle in preferred orientation (right) and the slightly rotated one (left) differ in shape and thus in function.

hundred nanoparticles aligns itself at a small angle,  $3.7^\circ$  to the right or left of the preferred direction (Fig. 1a). This 1% of the particles adopts a second alignment and their shape is also slightly different (Fig. 1b). As a result, the corners and edges with the active centres also differ in the two types of particles, and they behave differently as a catalyst in operation.

The operation of the nanoparticles under nearly real conditions was simulated by heating the sample to more than  $400^\circ\text{C}$  and their shape was investigated with *in situ* X-ray diffraction during oxidation and reduction reactions. During these reactions, the nanoparticles typically change their shape, which in turn means that the active sites shift.

The shape of the nanoparticles and its changes in different oxidising and reducing environments was elucidated by probing the scattering signal from the nanoparticle facets in reciprocal space. Figure 2a shows an illustration of such a particle in the preferred orientation with highlighted different facets. The coloured lines illustrated in the top panel of Fig. 2b shows where the corresponding crystal truncation rods arising from the nanoparticle facets are located in reciprocal space. X-ray diffraction data in specific along specific directions in reciprocal space covering different facets were acquired to deduce how the nanoparticle facets respond in different catalytic environments. The bottom panel of Fig. 2b shows the difference in X-ray diffraction signal along H, K=2-H direction at L = 0.85 in an oxidative compared to in vacuum. The changes in scattering signal in this region of reciprocal space provides information on how the different facets of the preferred [001] orientated and slightly rotated nanoparticles behave in oxidising and reducing environments.

The operational data for the two types of nanoparticles differ considerably, but in view of the complexity of their interaction it is not yet possible to give a simple answer as to which type of particle works better. The study provides insights to the positions of all the atoms and, in addition, how each individual atom contributes to the catalytic effect. These results may potentially lead to the ability to tailor the optimal catalyst for every application [3]. Studying the palladium nanoparticles is itself the first step along this path. On a qualitative level, our observations apply quite generally to catalytic nanoparticles on a substrate.

Author contact: Simon Chung, [simon.chung@desy.de](mailto:simon.chung@desy.de)

## References

1. B. Roldan Cuenya and F. Behafarid, 'Nanocatalysis: size- and shape-dependent chemisorption and catalytic reactivity', *Surf. Sci. Rep.* **70**, 135–187 (2015).
2. A. Stierle, J. Gustafson and E. Lundgren, 'Surface-sensitive X-ray diffraction across the pressure gap'. in: J. Frenken, I. Groot (eds), 'Operando research in heterogeneous catalysis', Springer Ser. Chem. Phys. **114**, 59–87 (2017).
3. M. Ahmadi, H. Mistry and B. Roldan Cuenya, 'Tailoring the catalytic properties of metal nanoparticles via support interactions', *J. Phys. Chem. Lett.* **7**, 3519–3533 (2016).

## Original publication

'Epitaxy and shape heterogeneity of a nanoparticle ensemble during redox cycles', *ACS Nano* **15**, 13267–13278 (2021). DOI: 10.1021/acsnano.1c03002



Simon Chung<sup>1</sup>, Jan-Christian Schöber<sup>1,3</sup>, Steffen Tober<sup>1,3</sup>, Daniel Schmidt<sup>3</sup>, Azat Khadiev<sup>2</sup>, Dmitri V. Novikov<sup>2</sup>, Vedran Vonk<sup>1</sup> and Andreas Stierle<sup>1,3</sup>

1. Centre of X-ray and Nano Science (CXNS) c/o DESY, Hamburg, Germany
2. Deutsches Elektronen-Synchrotron DESY, Hamburg, Germany
3. Fachbereich Physik, Universität Hamburg, Hamburg, Germany

# New pathway to harnessing the sun for a clean energy future

Ultrafast X-ray measurement provides important findings for the solar industry

Over the past 50 years, scientists have made great advances in photovoltaic technologies that convert sunlight into electricity and artificial photosynthesis devices that convert sunlight and water into carbon-free fuels. Crystalline silicon is by now the accepted standard for solar cells, but there are still opportunities to develop low-cost, flexible, readily processable (paintable) materials for photovoltaics based on organic materials. The charge generation processes in these materials are distinctly different from those in conventional semiconductors. Understanding ultrafast dynamics of photon-to-charge conversion is paramount for optimising such novel light-harvesting systems.

At the heart of many emerging sunlight-to-fuel and sunlight-to-electricity concepts are interfacial processes that require an optimised, concerted flow of charge and energy on the molecular level. Processes evolving on spatial and temporal scales spanning orders of magnitudes have to be connected in order to gain a comprehensive understanding of the fundamental dynamics and scaling laws that enable molecular, interfacial and macroscopic charge and energy transport. Soft X-ray spectroscopy techniques are particularly well-suited to monitor electronic and chemical states of matter with the elemental site specificity and chemical sensitivity that is required to test and improve our fundamental understanding of interfacial chemistry and photo-physics in complex systems.

Photoinduced charge generation plays a central role in a broad range of physical, chemical and biological processes that underlie natural and engineered photocatalytic and photovoltaic systems. Organic donor-acceptor systems are particularly intriguing candidates for light-harvesting applications as their properties can be readily modified using well-established chemical synthesis techniques. Improving the efficiency of the underlying light-harvesting and charge generation processes, however, requires detailed knowledge of all the steps from the initial light-induced excitation of the chromophore to the final state where charges are separated in the donor and acceptor phases. Monitoring the evolution of the interfacial electronic structure, as it proceeds in real-time and with the atomic-site specificity and chemical sensitivity of X-ray spectroscopy, holds great promise for improving our fundamental understanding of the reaction mechanisms that underlie the function of such devices.

By using femtosecond X-ray pulses from the free-electron laser FLASH at the plane-grating monochromator beamline PG2 in combination with the wide-angle electron spectrometer (WESPE) end station, we extended the experimental technique of time-resolved X-ray photoemission spectroscopy (trXPS) [1,2] into the femtosecond regime. This enabled us to monitor free charge carrier formation in a model donor-acceptor system — a heterojunction between a copper-phthalocyanine (CuPc) electron donor and a C<sub>60</sub> electron acceptor — on their natural timescale for the first time (Fig. 1). The basic principle of trXPS, as depicted in Fig. 1a, is the combination of two light pulses, whereas a 'pump' pulse initiates electronic dynamics inside the sample and their time evolution is monitored by a second, delayed X-ray 'probe' pulse [3,4]. Figure 2 illustrates the central results of the trXPS study. The binding energy of the C 1s core electrons of C<sub>60</sub> directly reflects the charge transfer

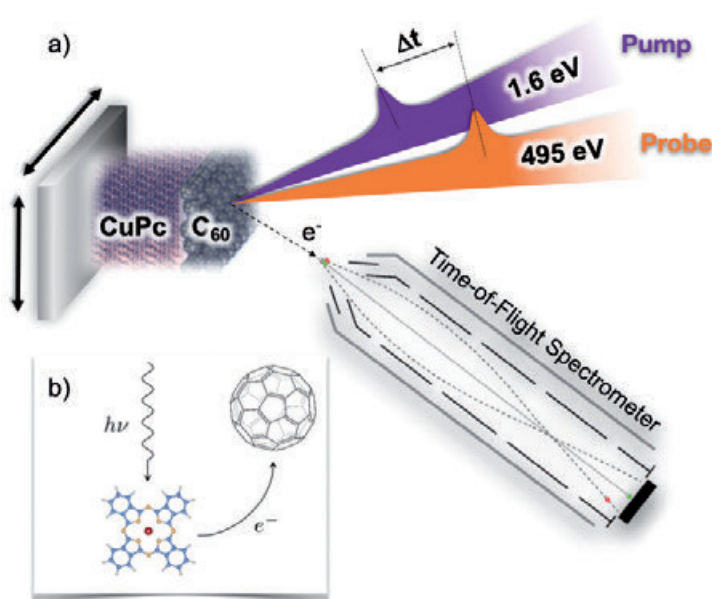


**Figure 1**  
a) Schematic of the performed trXPS experiment. b) Sketch of the photoinduced charge-transfer between the electron donor (CuPc) and the electron acceptor (C<sub>60</sub>).

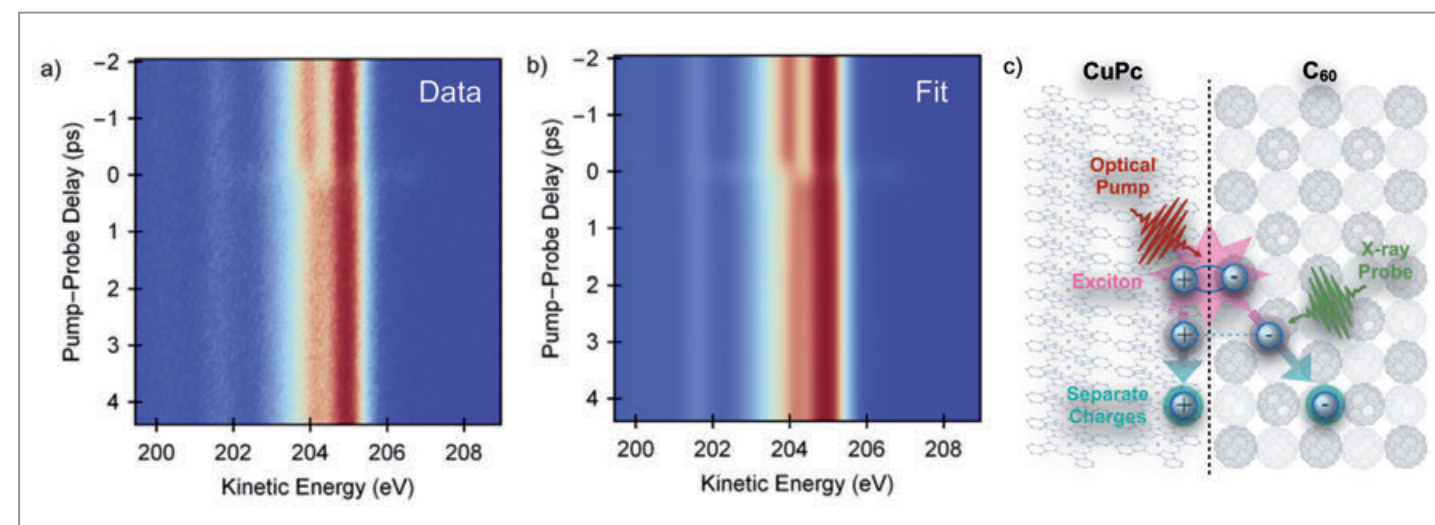


**Figure 2**  
a) Measured femtosecond time-resolved XPS C 1s spectra of the CuPc:C<sub>60</sub> heterojunction as a function of time-delay (vertical) and kinetic energy (horizontal).  
b) Result of a global fit procedure that decomposes the heterojunction spectra into contributions associated with the two separate components CuPc and C<sub>60</sub>.  
c) Schematic representation of the time-resolved XPS experiment and the observed kinetics.

on a local atomic scale. A shift of the C 1s line to higher kinetic energy, i. e. lower binding energy, indicates that an additional electronic charge is present near the carbon atom that is ionised. Accordingly, XPS enables direct, local and quantitative insight into the critically important step of the generation of separated charges.

The initial excitation results in a locally bound electron hole pair, a so-called exciton. Our studies unveiled a previously unobserved channel for exciton dissociation into mobile charge carriers providing the first direct, real-time characterisation of the timescales and efficiency of charge generation in an organic heterojunction. We demonstrate that the previously reported lifetime of interfacial charge-transfer (ICT) states of about 1 ps [5] results from the competition between two separate relaxation channels: interfacial electron-hole recombination and ICT dissociation into delocalised charges. Moreover, our data provide direct access to the efficiency for free charge carrier generation from ICT states at the CuPc:C<sub>60</sub> interface (Fig. 2c). Approximately 20% of photogenerated ICT states relax into delocalised charge carriers that can be extracted from the heterojunction while the remaining 80% recombine and relax within about 1 ps.

The reported findings give strong support to the emerging realisation that charge separation, even from energetically disfavoured excitonic states, is contributing significantly, indicating new options for light-harvesting in organic heterojunctions. The direct determination of energetics, temporal dynamics and relative channel efficiencies for an archetypical organic heterojunction hold great promise that other light-harvesting processes in complex multi-compound systems may be studied on their natural timescales and with the unprecedented site-specificity provided by ultrafast trXPS. This could pave a way towards a

better understanding of emerging photovoltaic and photocatalytic frameworks.

Author contact: Friedrich Roth,  
friedrich.roth@physik.tu-freiberg.de

## References

1. T. Arion et al., 'Site-specific probing of charge transfer dynamics in organic photovoltaics', *Appl. Phys. Lett.* **106**, 121602 (2015).
2. F. Roth et al., 'Efficient charge generation from triplet excitons in metal-organic heterojunctions', *Phys. Rev. B* **99**, 020303(R) (2019).
3. A. Shavorskiy et al., 'Sub-nanosecond time-resolved ambient-pressure X-ray photoelectron spectroscopy setup for pulsed and constant wave X-ray light sources', *Rev. Sci. Instrum.* **85**, 093102 (2014).
4. S. Neppi and O. Gessner, 'Time-resolved X-ray photoelectron spectroscopy techniques for the study of interfacial charge dynamics', *J. Electron Spectrosc. Relat. Phenomena* **200**, 64–77 (2015).
5. A. E. Jaiilaubekov et al., 'Hot charge-transfer excitons set the time limit for charge separation at donor/acceptor interfaces in organic photovoltaics', *Nat. Mater.* **12**, 66–73 (2013).

## Original publication

'Direct observation of charge separation in an organic light harvesting system by femtosecond time-resolved XPS', *Nature Communications* **12**, 1196 (2021).  
DOI: 10.1038/s41467-021-21454-3



Friedrich Roth<sup>1</sup>, Mario Borgward<sup>2</sup>, Lukas Wenthous<sup>3,4</sup>, Johannes Mahl<sup>2</sup>, Steffen Palutke<sup>4</sup>, Günter Brenner<sup>4</sup>, Giuseppe Mercurio<sup>5</sup>, Serguei Molodtsov<sup>1,5,6</sup>, Wilfried Wurth<sup>3,4,7</sup>, Oliver Gessner<sup>2</sup> and Wolfgang Eberhardt<sup>3</sup>

1. Institute of Experimental Physics, TU Bergakademie Freiberg, Freiberg, Germany
2. Chemical Sciences Division, Lawrence Berkeley National Laboratory, Berkeley, CA, USA
3. Center for Free-Electron Laser Science (CFEL), DESY, Hamburg, Germany
4. Deutsches Elektronen-Synchrotron DESY, Hamburg, Germany
5. European XFEL GmbH, Schenefeld, Germany
6. ITMO University, St. Petersburg, Russia
7. Universität Hamburg, Hamburg, Germany

# One zeptosecond for a quantum beat

Magnetisation dynamics controls nuclear states — precisely

Nuclei are small which makes them intrinsically quantum. At the same time nuclei are hard to control due to their large energy scales. While quantum systems are typically manipulated by lasers, regular lasers do not operate at X-ray energies. This is where X-ray quantum optics start. It aims to control photons, atoms and nuclei at X-ray energies via tailor-made quantum interactions. Demanding as the topic already is for static interactions, dynamic control of nuclei goes even one step further. And as shown in this work, transient quasiparticles of a solid are very useful in tuning quantum systems, not only at X-ray energies but also in general. In the experiment the phase of a nuclear quantum system is controlled by magnetisation dynamics with an extreme precision down to one zeptosecond and a stability of below 50 yoctoseconds.

Quantum systems will be crucial to future technologies. However, in order to use such systems in practice, it is necessary to control and manipulate them with great precision. Applications of precision control range from quantum computing over quantum communication to quantum metrology. In the X-ray regime, photon and atomic transition energies are on the order a few kiloelectronvolt. Accompanying the high transition energies are extremely short quantum state oscillation periods of sub-attoseconds. We are entering the realm of zeptoseconds ( $1 \text{ zs} = 10^{-21} \text{ s}$ ). Recent progress just hit the border between atto- and zeptoseconds, covering stability on zeptosecond time scales [1,2] or retrieving those time scales from path differences [3]. The way pursued in our work determines and controls phase changes in the nucleus corresponding to approximately 1 zs with a stability below 50 yoctoseconds ( $1 \text{ ys} = 10^{-24} \text{ s}$ ).

It is a big challenge to apply schemes known in quantum optics at X-ray energies. Although X-ray free-electron lasers like the European XFEL reach high X-ray energies,

they are far away from the tunability and flexibility of typical lasers available in the visible range. In order to control high-energy quantum systems, other schemes are called for. Numerous methods have been developed using X-ray cavities, piezo-controlled Doppler shifts or magnetisation switching [4]. A new approach is pursued in this work. In X-ray quantum optics experiments, the atoms are typically in a solid state. Solids host different types of quasiparticles, i. e. excitations of the vibrational, electronic or magnetic degrees of freedom. Here, the quasiparticles of the magnetisation, called magnons, are utilised. As shown in an earlier study, the quantum interactions of the solid structure with the nuclei can be tuned when magnons are excited [5]. These transient magnons are now specifically timed to tune the nuclear transitions with a hitherto unreachable precision.

The experiment has been carried out at beamline P01 at PETRA III. The iron isotope  $^{57}\text{Fe}$  is embedded in a 13 nm thin magnetic film and features a nuclear transition at 14.4 keV corresponding to an oscillation period of 287 zs. This transition is excited by a short synchrotron pulse (Fig. 1). The

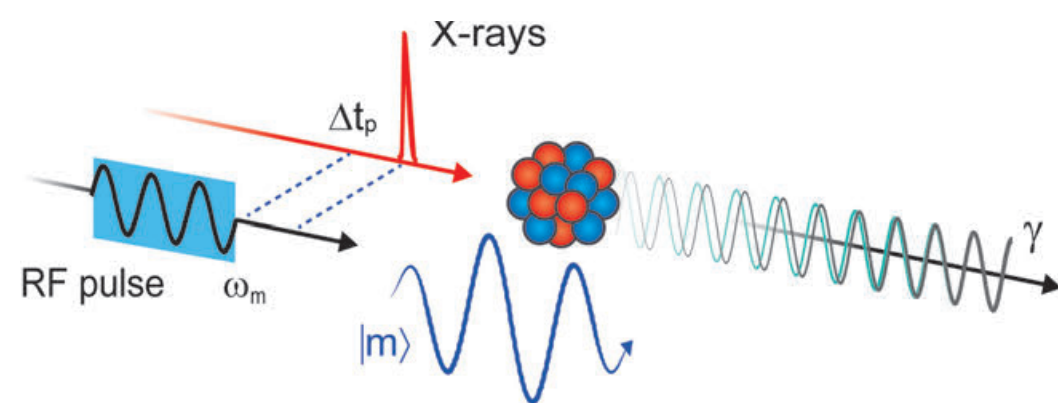


Figure 1

Scheme of the experiment: a nucleus is excited by a short X-ray pulse. It emits a gamma quantum in a superposition of two quantum states with slightly different frequency (grey and green) that will form an interference pattern — a quantum beat. The oscillation period of both transitions is about 287 zs. A timed radio-frequency burst excites magnons (blue) for a couple of nanoseconds in the solid hosting the nuclei. The magnon oscillation proceeds on the picosecond time scale.

magnetic interaction in the solid actually splits the transition, such that two transitions with different frequencies are excited and interfere (green and black oscillations in Fig. 1). From the superposition a quantum beat forms in the nuclear decay pattern as shown in Fig. 2a in black. The beat occurs on the nanosecond time scale. This is twelve orders of magnitude slower than the actual oscillation period of the transition dipole moments due to the very small difference of the two transition energies. The emitted photon intensity is detected by a fast photo diode and the nanosecond temporal decay is recorded.

When magnons are excited for a few nanoseconds during the lifetime of the nuclearexcited state, the nuclear transitions slightly change their energy. After the magnon excitation all energy levels fall back to their original energy while accumulating a temporal shift of their 287 zs oscillation. Thus, the dynamic phase of the system has changed. This is visible as a temporal shift of the quantum beat (red in Fig. 2a). Hence, zeptosecond shifts of the transition are transformed to nanoseconds in the quantum beat. The principle is the same as within an interferometer but is of quantum nature. Interestingly, knowledge of the overall phase change of the quantum beat is enough to determine the phases of the two transitions due to the known magnetic interactions in the sample. The smallest delay that we can control and detect, corresponds to 1.3 zs with a stability below 50 ys.

The magnon offers high flexibility to manipulate the quantum system. Parameters like the magnon's excitation power, frequency, duration or its time delay all determine how strongly the phase changes and when the change is applied to the quantum system. This is shown in Fig. 2b where the magnon's time delay is changed with respect to the nuclear excitation. The quantum beat starts to change as soon as the magnon is excited. After the magnon is damped out and given the same excitation duration, the accumulated phase shift is the same for all data shown (vertical lines).

The experiments demonstrate zeptosecond interferometry and the possibility to tune an embedded quantum system by exciting the surrounding solid. The method could be applied to quantum systems that are already considered for quantum computers, such as nitrogen vacancy centres in diamonds or ion-doped solids. Precise adjustments of this kind are important when building quantum sensors, for example to establish extremely precise time standards or to detect minute changes in general.

Author contact: Lars Bocklage, [lars.bocklage@desy.de](mailto:lars.bocklage@desy.de)

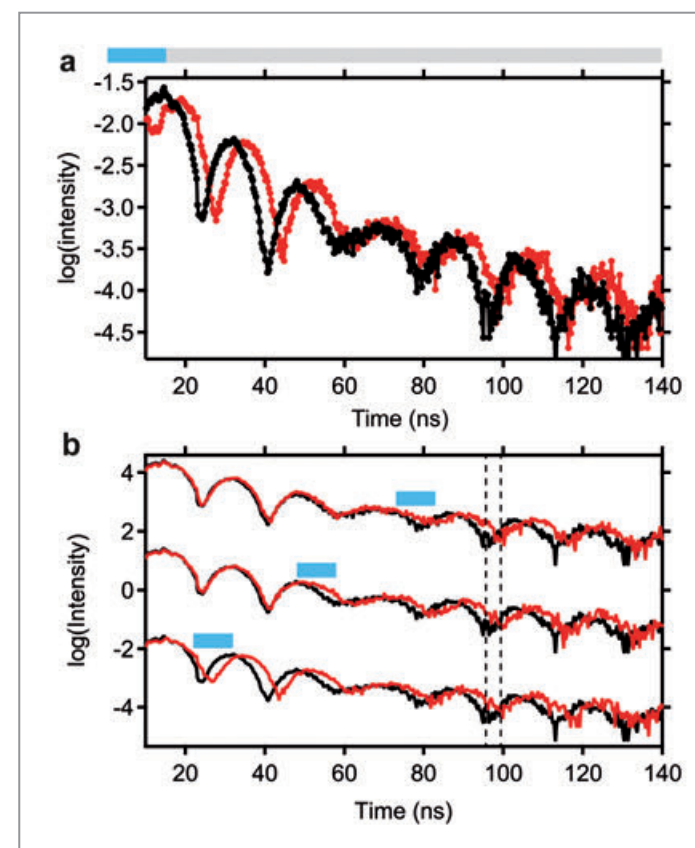


Figure 2

a) Measured quantum beats without (black) and with magnon excitation (red). The magnon is excited during the time indicated by the blue bar. Both quantum beats are the same but the one with magnon excitation is shifted in time. b) Magnon excitations can be applied at different times (blue bars). The detected time delay is the same as long as the magnon duration is not changed.

## References

1. M. Ossiander et al., 'Attosecond correlation dynamics', *Nat. Phys.* **13**, 280–285 (2017).
2. K. P. Heeg et al., 'Coherent X-ray-optical control of nuclear excitons', *Nature* **590**, 401–404 (2021).
3. S. Grundmann et al., 'Zeptosecond birth time delay in molecular photoionization', *Science* **370**, 339–341 (2020).
4. E. Kuznetsova and O. Kocharovskaya, 'Quantum optics with X-rays', *Nat. Photonics* **11**, 685–686 (2017).
5. L. Bocklage et al., 'Spin precession mapping at ferromagnetic resonance via nuclear resonant scattering of synchrotron radiation', *Phys. Rev. Lett.* **114**, 147601 (2015).

## Original publication

'Coherent control of collective nuclear quantum states via transient magnons', *Science Advances* **7**, eabc3991 (2021). DOI: 10.1126/sciadv.abc3991



Lars Bocklage<sup>1,2</sup>, Jakob Gollwitzer<sup>1</sup>, Cornelius Strohm<sup>1</sup>, Christian F. Adloff<sup>1,2</sup>, Kai Schlage<sup>1</sup>, Ilya Sergeev<sup>1</sup>, Olaf Leupold<sup>1</sup>, Hans-Christian Wille<sup>1</sup>, Guido Meier<sup>3,2</sup> and Ralf Röhlsberger<sup>1,2,4,5,6</sup>

1. Deutsches Elektronen-Synchrotron DESY, Hamburg, Germany
2. The Hamburg Centre for Ultrafast Imaging (CUI), Universität Hamburg, Hamburg, Germany
3. Max Planck Institute for the Structure and Dynamics of Matter, Hamburg, Germany
4. Friedrich-Schiller Universität Jena, Germany
5. Helmholtz-Institut Jena, Germany
6. GSI Helmholtzzentrum für Schwerionenforschung GmbH, Darmstadt, Germany

Required Credit:  
Reprinted with permission. Copyright 2020 American Chemical Society.

# Making monopoles visible

Soft X-ray angle-resolved photoelectron spectroscopy reveals magnetic monopoles in momentum space

An outstanding feature of condensed matter physics is that phenomena predicted in high-energy physics can be realised in the low-energy quasiparticle excitations in the electronic band structure of modern materials. In a new class of those quantum materials, the Weyl semimetals (WSM), the crossing points of the valence and conduction bands can be considered as momentum-space analogues of magnetic monopoles in real space. The monopole character is encoded in the momentum-dependence of the electronic wave functions, namely the topologically non-trivial winding of the so-called Berry curvature around the monopole. Soft X-ray angle-resolved photoelectron spectroscopy (ARPES) combined with circular dichroism (CD) and spin resolution provides momentum-resolved access to this characteristic monopole texture in momentum space.

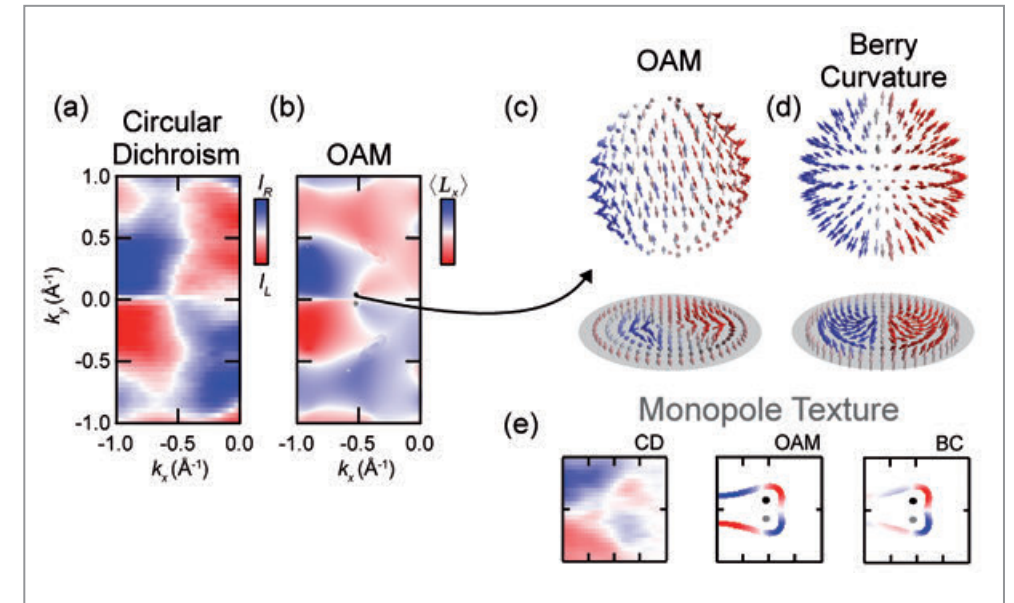
It is known that — on the basis of classical electromagnetism — magnetic monopoles, i.e. quantised magnetic charges, cannot exist. However, in the framework of topological quantum matter physics such objects can be realised in WSM, but instead of real space they are rather located in momentum space. More precisely, the valence and conduction bands in WSM cross each other in the three-dimensional bulk-band structure and the field configuration of the momentum-space magnetic field, the so-called Berry curvature, around these Weyl points forms a monopole or anti-monopole texture (Fig. 2d).

In the present work, the electronic structure of the paradigmatic WSM candidate TaAs is investigated by means of soft X-ray ARPES experiments performed at the ASPHERE III end station of the P04 beamline at Petra III. The beamline

provides variable circularly polarised light at bulk-sensitive soft X-ray photon energies that allow us to study the bulk-band structure of TaAs in great detail. Moreover, the experimental setup is equipped with a spin detector which gives additional access to the spin structure of the electronic states. The spin polarisation of the bulk bands in general is an important prerequisite of the WSM phase. In TaAs, it arises from the interplay of spin-orbit coupling and the broken inversion symmetry in the crystal structure. For the first time, we have succeeded in demonstrating the bulk-band spin polarisation of a WSM experimentally, as shown in Fig. 1b.

The breaking of inversion symmetry has another important effect on the electronic wave functions, namely the formation of a finite orbital angular momentum (OAM) (see Fig. 1a). The OAM can be considered as an orbital analogue of the

**Figure 2** Circular dichroism (CD), orbital angular momentum (OAM) and Berry curvature (BC) around the Weyl points. Momentum distribution of the measured CD (a) and the calculated OAM (b) integrated over an energy range from 0 eV to  $-1.2$  eV corresponding to the width of the highest valence band. (c,d) Calculated momentum space-field configuration on a small sphere around a Weyl point and corresponding azimuthal equidistant projections. (e) Constant energy cuts of CD, OAM and BC at  $-0.2$  eV below the Fermi level.



electron spin, and recently a connection between OAM and Berry curvature has been predicted [1,2]. Density functional theory band structure calculations directly demonstrate the existence of OAM in the wave functions in TaAs (Fig. 1a). Importantly, CD, i.e. the photoemission intensity difference between ARPES spectra taken with left and right circularly polarised light, accurately reflects the calculated OAM texture  $L_x$ . Several sign changes appearing in the calculations are reproduced in the experimental data (Fig. 1a and 2a,b), providing evidence for a strong OAM-sensitivity of our experiment.

The momentum distribution of the OAM  $L_x$  and the CD can be explored in more detail in Fig. 2a,b. It becomes directly evident that the OAM is strongly modulated around the WP pair marked in Fig. 2b, so that a characteristic checkerboard pattern appears. Indeed, it can be shown that the OAM texture around the WP is strongly related to the topological character: As can be seen in Fig. 2e, the Berry curvature of the Weyl fermion band qualitatively resembles the characteristics of the OAM and the measured CD. Although a detailed evaluation of the three-dimensional field configuration (Fig. 2c,d) shows that OAM and BC are not completely aligned, both share the same topologically non-trivial winding number. Thus, from a band topology perspective, BC and OAM are equivalent around the WP, and they both represent a monopole structure. The OAM, in turn, is accessible experimentally, and the measured CD pattern provides a direct momentum-resolved signature for the Berry curvature monopoles in TaAs.

Our approach goes beyond previous studies in which the mere band dispersion of WSM was investigated using ARPES. In this work, the wave function character of the

electronic bulk states carrying the topological information is directly unveiled. Our findings might therefore be applicable to a wide range of topological quantum materials.

Author contact: Maximilian Ünzelmann, [muenzelmann@physik.uni-wuerzburg.de](mailto:muenzelmann@physik.uni-wuerzburg.de)  
Hendrik Bentmann, [hendrik.bentmann@physik.uni-wuerzburg.de](mailto:hendrik.bentmann@physik.uni-wuerzburg.de)

## References

- M. Schüler, U. De Giovannini, H. Hübener, A. Rubio, M. A. Sentef and P. Werner, 'Local Berry curvature signatures in dichroic angle-resolved photoelectron spectroscopy from two-dimensional materials', *Sci. Adv.* 6, eaay2730 (2020).
- S. Cho, J.-H. Park, J. Hong, J. Jung, B. S. Kim, G. Han, W. Kyung, Y. Kim, S.-K. Mo, J. D. Denlinger, J. H. Shim, J. H. Han, C. Kim and S. R. Park, 'Experimental observation of hidden Berry curvature in inversion-symmetric bulk 2H-WSe<sub>2</sub>', *Phys. Rev. Lett.* 121, 186401 (2018).

## Original publication

'Momentum-space signatures of Berry flux monopoles in the Weyl semimetal TaAs', *Nature Communications* 12, 3650 (2021).  
DOI: 10.1038/s41467-021-23727-3



Maximilian Ünzelmann<sup>1</sup>, Hendrik Bentmann<sup>1</sup>, Tim Figgemeier<sup>1</sup>, Philipp Eck<sup>2</sup>, Jennifer N. Neu<sup>3,4</sup>, Begmuhammet Geldiyev<sup>1</sup>, Florian Diekmann<sup>5,6</sup>, Sebastian Rohlf<sup>5,6</sup>, Jens Buck<sup>5,6</sup>, Moritz Hoesch<sup>7</sup>, Matthias Kalläne<sup>5,6</sup>, Kai Rossnagel<sup>5,6,7</sup>, Ronny Thomale<sup>2</sup>, Theo Siegrist<sup>3,4</sup>, Giorgio Sangiovanni<sup>2</sup>, Domenico Di Sante<sup>2,8,9</sup> and Friedrich Reinert<sup>1</sup>

- Experimentelle Physik VII and Würzburg-Dresden Cluster of Excellence ct.qmat, Universität Würzburg, Würzburg, Germany
- Theoretische Physik I, Universität Würzburg, Würzburg, Germany
- Department of Chemical and Biomedical Engineering, FAMU-FSU College of Engineering, Tallahassee, USA
- National High Magnetic Field Laboratory, Tallahassee, USA
- Institut für Experimentelle und Angewandte Physik, Christian-Albrechts-Universität zu Kiel, Kiel, Germany
- Ruprecht Haensel Laboratory, Deutsches Elektronen-Synchrotron DESY, Hamburg, Germany
- Deutsches Elektronen-Synchrotron DESY, Hamburg, Germany
- Department of Physics and Astronomy, University of Bologna, Bologna, Italy
- Center for Computational Quantum Physics, Flatiron Institute, New York, USA

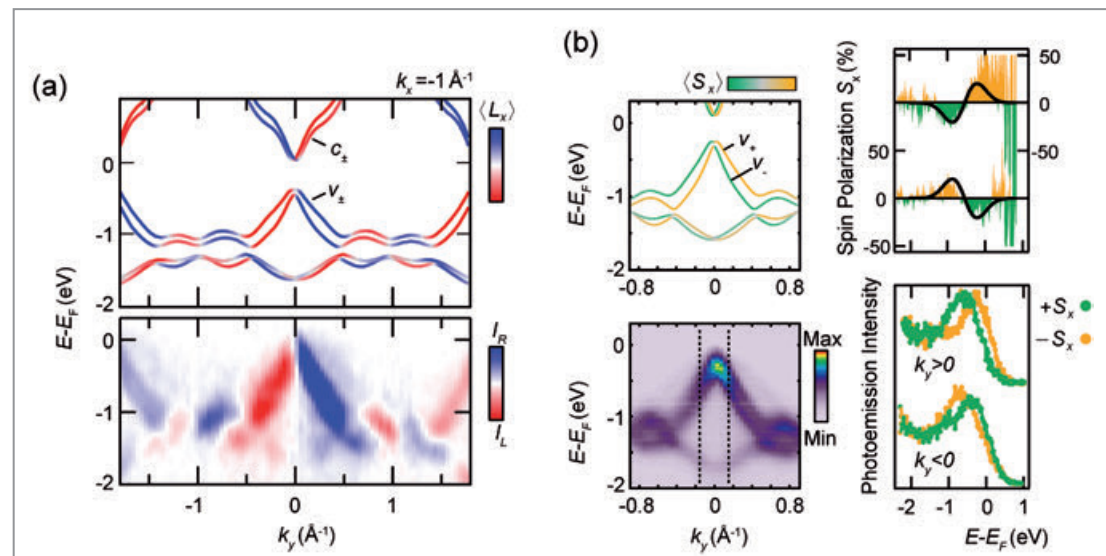


**Figure 1** Spin and orbital angular momentum (SAM and OAM) of the TaAs bulk bands. (a) Comparison between calculated OAM texture (upper panel) and measured circular dichroism (lower panel) in a band structure cut. (b) Spin polarisation of the bulk bands obtained from DFT (upper left panel) in comparison to the spin-resolved soft X-ray ARPES spectra (right panels) taken at  $k_y$ , as marked in the spin-integrated measurement in the lower left panel.

# Ultrafast THz Ohmmeter at extreme temperatures

Multi-cycle terahertz free-electron lasers reveal microscopic origins of electrical conductivity in super-heated solids

Electrical conductivity of matter is dictated by its electronic and structural properties. The conductivity is therefore an important measure of materials under high-energy density conditions that are relevant to planetary science and advanced material processing. These extreme conditions can be produced in laboratory by isochorically heating of solid density targets using high-intensity optical or free-electron lasers (FELs). Utilising synchronised terahertz (THz) and extreme ultraviolet (XUV) FEL pulses, both generated at FLASH, a time-resolved high-precision measurement of DC conductivity of intense XUV-FEL excited nanofoil samples has been achieved. The conductivity evolution during the solid to plasma transition is resolved with a time resolution better than 500 fs.

Electromagnetic waves at THz frequencies have been successfully implemented to measure the electrical conductivity of ultrafast laser-excited samples for decades [1]. It has unique advantages, such as sub-picosecond temporal resolution and contact-free measurements, allowing one to study the conductivity of high energy density matter in a laboratory. However, these novel studies also face several challenges, which includes high plasma density shielding, in case the solid density plasma frequency is  $>10^{15}$  Hz, leading to a reduced transmission of the THz radiation through the target. Furthermore, the irreversible solid-plasma phase transition forbids high-repetition rate measurements as applied in conventional solid-state studies.

To overcome these hurdles, we recently applied an FEL-pump-THz-probe experiment at the FLASH BL3 beamline in combination with high-sensitive single-shot electro-optical

sampling [2] of the THz-field to measure the conductivity of 30 nm thick gold foils strongly heated by the XUV-FEL pulses to electron temperatures up to 16000 K (experimental setup shown in Fig. 1). As the absorbed XUV energy transfers from the electrons to the ions, the sample transits from a cold to superheated solid and eventually melts into a warm dense liquid. We have determined the DC electrical conductivity over these material states by the measurements of transmitted THz electric field through the heated samples in a time-resolved manner. The multi-cycle THz pulses from FLASH provide continuous measurements with temporal resolutions better than 500 fs. An example of the experimental data is presented in Fig. 2.

These ultrafast time-resolved measurements offer unique insight into the electrical conductivity. The broadband electrical conductivity from our THz measurements and previ-

ous optical measurement (Fig. 3) allows us to differentiate between the individual contributions from electron-electron and electron-ion scattering that limit the conductivity at high temperatures. We found that the electron-electron scattering frequency increased drastically after ultrafast heating of the sample, following the so-called Fermi-Liquid theory that so far was only observed in cryogenic cooled samples in previous studies. The close relation between electron-ion scattering frequency and the structure of the ions based entirely on experimental data is also observed. The study has showcased a new experimental platform that fully utilise the unique capabilities of both the THz and

XUV pulses at FLASH. The high-quality data acquired from this experiment will help researchers to test and improve their models on strongly heated materials. In this regime, sophisticated theories, such as quantum molecular dynamics, are required to describe the phenomena.

Author contact: Zhijiang Chen, [zchen@slac.stanford.edu](mailto:zchen@slac.stanford.edu)  
Siegfried H. Glenzer, [glenzer@slac.stanford.edu](mailto:glenzer@slac.stanford.edu)

## References

1. R. Ulbricht, E. Hendry, J. Shan, T. F. Heinz and M. Bonn, 'Carrier dynamics in semiconductors studied with time-resolved terahertz spectroscopy', *Rev. Mod. Phys.* **83**, 543–586 (2011).
2. B. K. Ofori-Okai, A. Descamps, J. Lu, L. E. Seipp, A. Weinmann, S. H. Glenzer and Z. Chen, 'Toward quasi-DC conductivity of warm dense matter measured by single-shot terahertz spectroscopy', *Rev. Sci. Instrum.* **89**, 10D109 (2018).

## Original publication

'Ultrafast multi-cycle terahertz measurements of the electrical conductivity in strongly excited solids', *Nature Communications* **12**, 1638 (2021). DOI: 10.1038/s41467-021-21756-6



Zhijiang Chen<sup>1</sup>, Chandra B. Curry<sup>1,2</sup>, Ruoheng Zhang<sup>2</sup>, Franziska Treffert<sup>1,3</sup>, Nikola Stojanovic<sup>4,5</sup>, Sven Toleikis<sup>4</sup>, Rui Pan<sup>4</sup>, Maxence Gauthier<sup>1</sup>, Ekaterina Zapolnova<sup>4</sup>, Lars E. Seipp<sup>1,5</sup>, Anthea Weinmann<sup>1,6</sup>, Mianzhen Z. Mo<sup>1</sup>, Jongjin B. Kim<sup>1</sup>, Bastian B.L. Witte<sup>1,7</sup>, Saša Bajt<sup>4,8</sup>, Sergey Usenko<sup>4,9,10</sup>, Regina Soufli<sup>11</sup>, Tom Pardini<sup>11</sup>, Stefan Hau-Riege<sup>11</sup>, Catherine Burcklen<sup>11</sup>, Jochen Schein<sup>6</sup>, Ronald Redmer<sup>7</sup>, Ying Y. Tsui<sup>2</sup>, Benjamin K. Ofori-Okai<sup>1</sup> and Siegfried H. Glenzer<sup>1</sup>

1. SLAC National Accelerator Laboratory, Menlo Park, CA, USA
2. University of Alberta, Edmonton, Alberta, Canada
3. Technische Universität Darmstadt, Darmstadt, Germany
4. Deutsches Elektronen-Synchrotron DESY, Hamburg, Germany
5. DLR - Institute for Optical Sensor Systems, Berlin, Germany
6. Universität der Bundeswehr München, Neubiberg, Germany
7. Institut für Physik, Universität Rostock, Rostock, Germany
8. The Hamburg Centre for Ultrafast Imaging, Hamburg, Germany
9. Institut für Experimentalphysik, Universität Hamburg, Hamburg, Germany
10. European XFEL, Schenefeld, Germany
11. Lawrence Livermore National Laboratory, Livermore, CA, USA

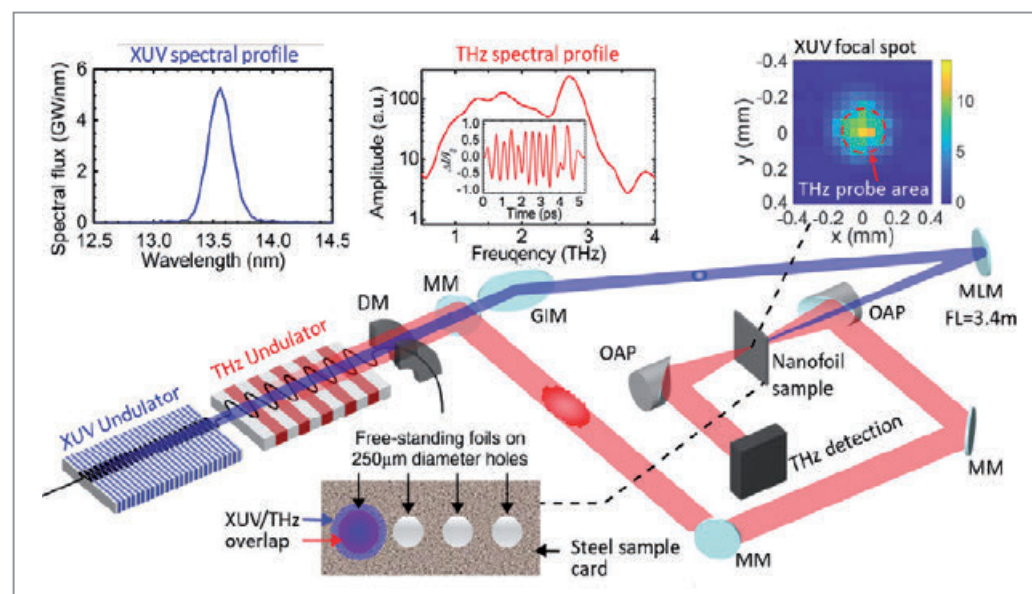


**Figure 1** Experimental setup at the BL3 beamline of FLASH. The XUV-pulses of 13.6 nm (spectral profile on top-left) are focused by a multilayer mirror (MLM) onto the nanofoil samples (focal spot profile on top right), heating its electrons to over 16000 K temperature. Multi-cycle THz pulses (spectral and temporal profile on top middle) are focused by an off-axis parabolic mirror (OAP) to probe the heated samples. The probe signal is detected by a single-shot electro-optical sampling method.

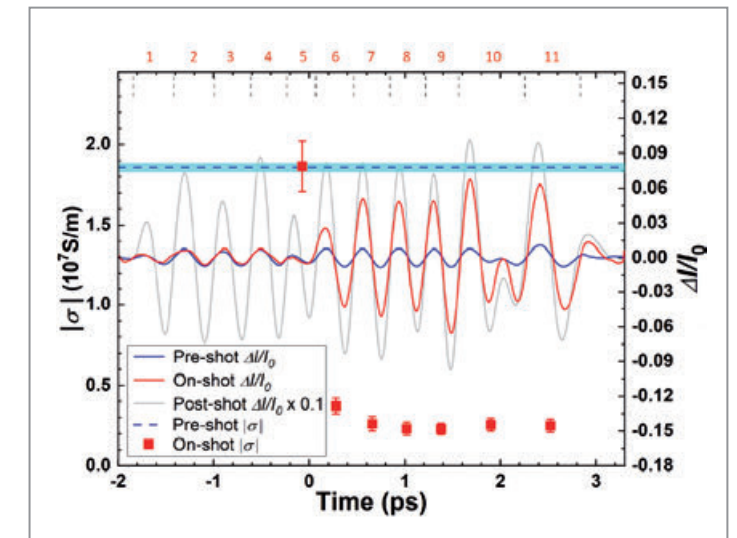


**Figure 2** Time-resolved electrical conductivity  $\sigma$  (left axis) of a XUV-FEL heated sample determined by the THz transmission measurements (right axis). 'Pre-shot' represents measurement on a cold gold sample, 'on-shot' is the measurement of XUV-FEL heated sample and 'post-shot' is the measurement when no sample is present, i.e. ablated by the XUV-FEL pulse.

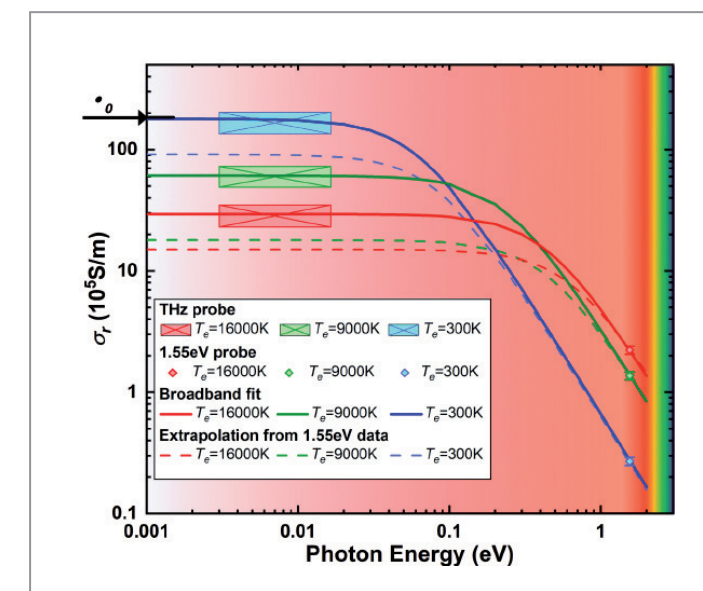


**Figure 3** Broadband electrical conductivity  $\sigma_r$  of gold with various electron temperatures  $T_e$ . The THz data are shown on the left (rectangular blocks) and the optical data are on the right. The frequency-dependent conductivity is fit to a Drude model that subsequently reveals electron carrier densities and electron scattering frequencies.

# Spin fluctuations unfreeze on cooling

Coherent X-rays reveal low-temperature decay of spin-density wave

In virtually all matter, lower temperatures mean less mobility of its microscopic components. The less heat energy is available, the less atoms vibrate, the less magnetic moments change their direction — they freeze. We have now observed the opposite behaviour: Spin-order fluctuations in a layered nickelate do not freeze on cooling, but actually speed up. When the material is cooled below a threshold temperature, the energy barriers for fluctuations start shrinking faster than the thermal energy. This low-temperature loss of energy barrier height shows an intriguing similarity to an observation in superconducting cuprates.

In high-temperature superconducting cuprates, spin and charge degrees of freedom form nanoscale order into density waves (DW) [1]. This kind of order seems to compete with superconductivity as DW order decays at low temperatures when superconductivity sets in. Remarkably, a similar decay of DW order has been observed in isostructural layered nickelates, which are not superconducting but otherwise share many properties with the cuprate superconductors. Similar to what is found in cuprates, DW order in nickelates develops on cooling and then starts to decay when cooled further. This decay, which sets in at about half of the onset temperature of the DW order, is not driven by competition with superconductivity. In turn, the mechanism responsible in nickelates may also occur in cuprates and contribute to the energy balance between DW order and superconductivity in these materials.

In a recent study, we investigated the low-temperature decay of nickelate DWs. We used resonant soft X-ray diffraction with the photon energy tuned to the Ni  $2p \rightarrow 3d$  electronic excitations, which provides a high sensitivity to spin and charge order [2]. The experiments were carried out at beamline P04 of PETRA III at DESY and at beamline 12.0.2.2 at the Advanced Light Source in Berkeley. We found the low-temperature DW decay to occur largely via a loss of spatial correlations. Either the ordered regions shrink or dislocations form in these regions. Soft X-rays with a high degree of coherence allowed us to track the evolution of disorder in the DW order in a soft X-ray photon correlation experiment (Fig. 1a) [3]. The spatial distribution of disorder in the sample leads to an interference pattern on the detector such that the diffraction signal breaks into a myriad of speckles (Fig. 1a). Any change of

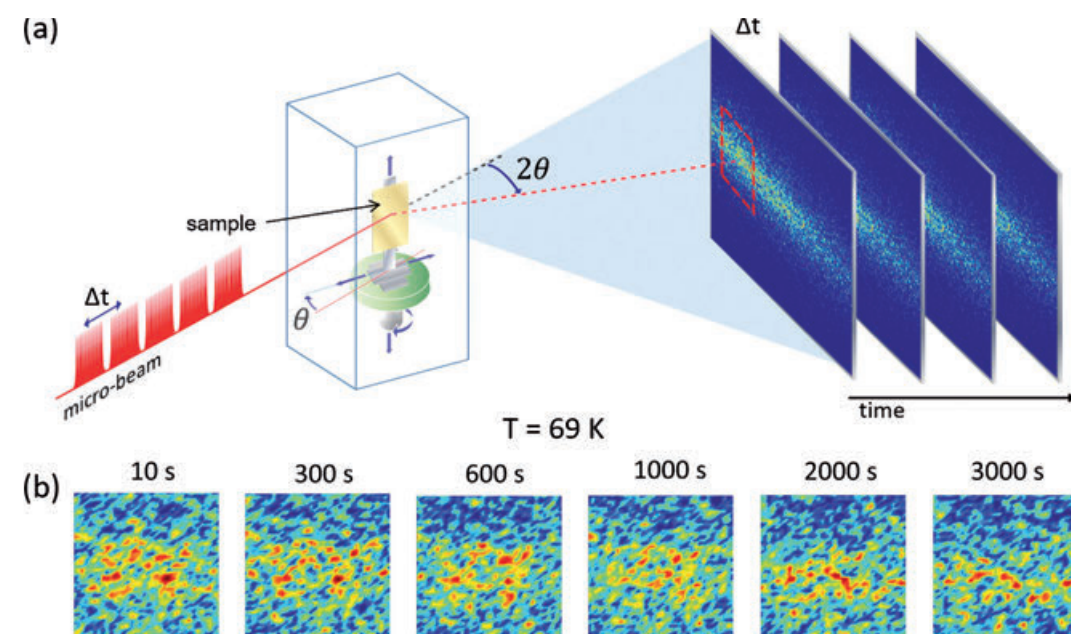
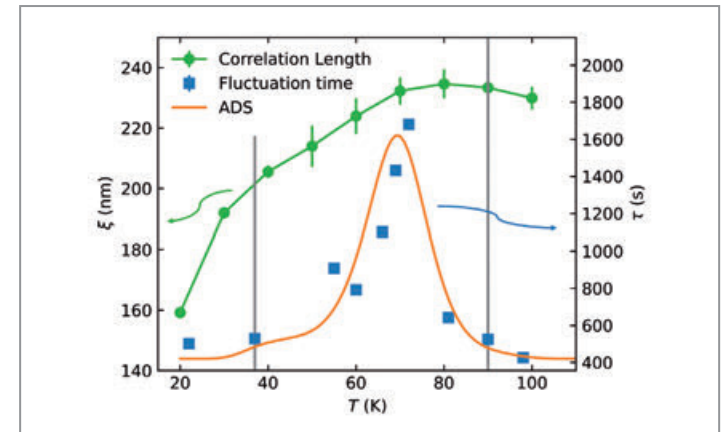


**Figure 1**  
a) Diffraction of coherent soft X-rays from a spin density wave cause a speckle pattern on the detector reflecting the spatial distribution of order in the sample. b) Fluctuations in this distribution affect the speckle pattern such that images become increasingly dissimilar when taken with larger time intervals.

**Figure 2**  
At low temperatures the correlation length of the DW order (green) decreases. The characteristic time for fluctuations (blue) has its maximum at a temperature close to where the correlation length is largest. Still the correlation length alone does not explain how fluctuation times evolve with temperature. A model of activated dynamic scaling (orange) describes the relation between fluctuations, correlation length and temperature.



disorder, i.e. the motion of a dislocation or the shift of a domain wall changes the speckle pattern, which allows us to track fluctuations of disorder in time. Figure 1b contains a typical series of speckle patterns. The closer in time the images were recorded the more they resemble each other; when the time separation is larger, images differ more and more. From a statistical analysis we obtain the time, on which all similarity gets lost. This fluctuation time describes the dynamics in our DW order pattern.

For our sample, we found fluctuation times of several tens of minutes with quite a drastic temperature dependence (blue squares in Fig. 2). Around 70 K, the order is most stable with a fluctuation time of about 30 minutes. At higher temperatures, fluctuations speed up, which is quite commonly observed when higher thermal energy makes fluctuations faster. Quite unexpectedly, though, also when cooled to below 70 K, the fluctuation times start decreasing again, i. e. the fluctuations speed up there too.

Around the temperature where fluctuations are slowest, the spatial correlations are largest (green symbols in Fig. 2). In fact, a monotonous relation between correlation length and fluctuations speed has been observed in several materials. For the present case, though, we find that the correlation length alone cannot describe the observed temperature dependence of the fluctuations: We find the same fluctuation times at pairs of high and low temperatures where correlation lengths clearly differ (see grey lines in Fig. 2). Hence, temperature must play a role as well.

A model describing describes a relationship between fluctuation times, correlation length and temperatures is that of activated dynamic scaling (ADS) [4]. In this model, the correlation length defines an effective energy barrier for thermally activated fluctuations. An extended ADS model describes our experimental findings well (Fig. 2) and explains the unusual behaviour: Below 70 K the loss of spatial correlations causes a reduction of energy barriers that proceeds faster on cooling than the loss of thermal energy. In consequence, the fluctuations do not freeze but rather unfreeze.

Given the striking similarity in the low-temperature decays in nickelates and cuprates one may wonder, to what extent our observation matters for the energy balance between DW order and superconductivity. While the low-temperature

fluctuations we observe are probably too slow to have a sizeable effect on material properties, we expect much faster fluctuations to be present as well and those may indeed play a relevant role. We had to concentrate on the most intense region of the DW Bragg peak related to fluctuations on long spatial length scales, while faster fluctuations on shorter length scales should be visible in the wings of the Bragg peak. Next-generation X-ray sources with higher coherent soft X-ray flux and faster detectors will allow us to study these fast fluctuations directly.

Author contact: Christian Schüßler-Langeheine, christian.schuessler@helmholtz-berlin.de

## References

1. A. Frano et al., 'Charge ordering in superconducting copper oxides', *J. Phys. Condens. Matter* **32**, 374005 (2020).
2. C. Schüßler-Langeheine et al., 'Spectroscopy of stripe order in  $\text{La}_{1-x}\text{Sr}_x\text{NiO}_3$  using resonant soft X-ray diffraction', *Phys. Rev. Lett.* **95**, 156402 (2005).
3. G. Grübel and F. Zontone, 'Correlation spectroscopy with coherent X-rays', *J. Alloys Compd.* **362**, 3–11 (2004).
4. D. S. Fisher, 'Activated dynamic scaling in disordered systems (invited)', *J. Appl. Phys.* **61**, 3672–3677 (1987).

## Original publication

'Measurement of spin dynamics in a layered nickelate using X-ray photon correlation spectroscopy: evidence for intrinsic destabilization of incommensurate stripes at low temperatures', *Physical Review Letters* **127**, 057001 (2021). DOI: 10.1103/PhysRevLett.127.057001



Alessandro Ricci<sup>1</sup>, Nicola Poccia<sup>2</sup>, Gaetano Campi<sup>3</sup>, Shrawan Mishra<sup>4,5</sup>, Leonard Müller<sup>1</sup>, Boby Joseph<sup>6</sup>, Bo Shi<sup>7</sup>, Alexey Zozulya<sup>1</sup>, Marcel Buchholz<sup>8</sup>, Christoph Trabant<sup>8,9</sup>, James C. T. Lee<sup>4,10,12</sup>, Jens Viehhaus<sup>1,9</sup>, Jeroen B. Goedkoop<sup>7</sup>, Agustinus Agung Nugroho<sup>11</sup>, Markus Braden<sup>8</sup>, Sujoy Roy<sup>4</sup>, Michael Sprung<sup>1</sup> and Christian Schüßler-Langeheine<sup>9</sup>

1. Deutsches Elektronen-Synchrotron DESY, Hamburg, Germany
2. Leibniz Institute for Solid State and Materials Research, IFW, Dresden, Germany
3. Institute of Crystallography, CNR, Roma, Italy
4. Advanced Light Source, Berkeley, USA
5. Indian Institute of Technology, Varanasi, India
6. Elettra Sincrotrone, Trieste, Italy
7. Van der Waals-Zeeman Institute, University of Amsterdam, Netherlands
8. II. Physikalisches Institut, Universität zu Köln, Germany
9. Helmholtz-Zentrum Berlin für Materialien und Energie, Berlin, Germany
10. Department of Physics and Astronomy, Sonoma State University, Rohnert Park, USA
11. Faculty of Mathematics and Natural Sciences, Institut Teknologi Bandung, Indonesia
12. Department of Physics, Concordia College, Moorhead, USA

# Imaging the electronic states of quantum materials

A new X-ray method creates images of the charge cloud of transition metal ions in the ground and excited states

To understand the spectacular properties of transition metal (TM) compounds, it is often necessary to determine the orbital degrees of freedom of the TM ions. One needs to know which orbitals are occupied in the ground state, which orbitals are available for excitations, and where they are in energy. Various spectroscopies are being used, but the necessary quantitative spectral analysis is far from straightforward due to strong correlations. Heavy approximations are required, producing results which are not free from ambiguities. Here, we present a new spectroscopic method capable of creating a visual image of the charge cloud of the ground and excited states, and thus provide clear insight into the electronic states of the material without the need for complex calculations.

It was recently shown that a new spectroscopic technique, so-called 'non-resonant inelastic X-ray scattering from an s-core hole' (*s*-NIXS), can make visual images of the spatial distribution of the TM *d* holes, thus producing a 'negative' of the ground-state electronic charge cloud around the TM ion [1]. In this *s*-NIXS process, an impinging X-ray photon is scattered from a TM ion, thereby making an electronic transition from an *s*-core into the valence *d*-shell. This is a rather special transition since it is dipole forbidden and becomes only allowed if the experiment is carried out in such a way that the momentum transfer  $\mathbf{q}$  is sufficiently large ( $|\mathbf{q}| \lesssim 1/R_{\text{core}}$ ,  $h\nu \lesssim 5$  keV). The beauty of using an *s*-core shell is that it is spherical. The angular dependence of the integrated intensity of the *s* → *d* transition then only depends on the density of the *d* holes in the direction of  $\mathbf{q}$ . In other words, by rotating a single crystal over multiple angles, (see Fig. 1a) and recording the corresponding *s*-NIXS intensities, one can obtain a 'negative' of the *d* elec-

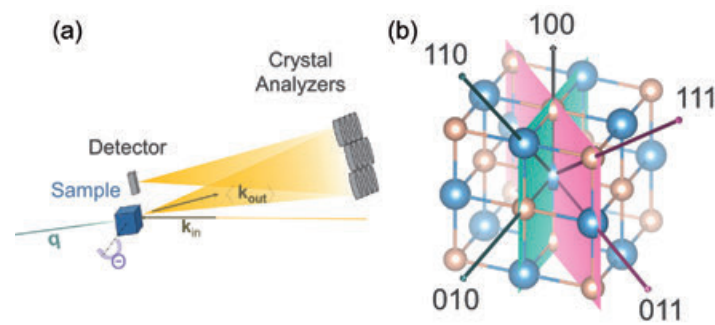


**Figure 1**  
1 a) Schematic representation of the NIXS spectrometer of P01 (DESY). During an *s*-NIXS experiment, the sample angle  $\theta$  is varied to collect spectra with  $\mathbf{q}$  parallel to several directions within the same crystal plane.  
b) Crystal structure of  $\alpha$ -MnS. The two planes explored in the experiment are indicated in dark cyan and magenta.

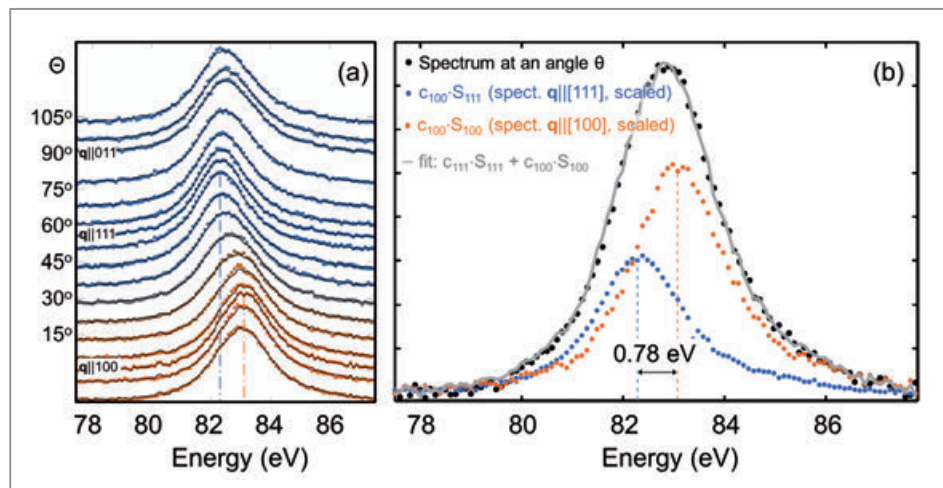
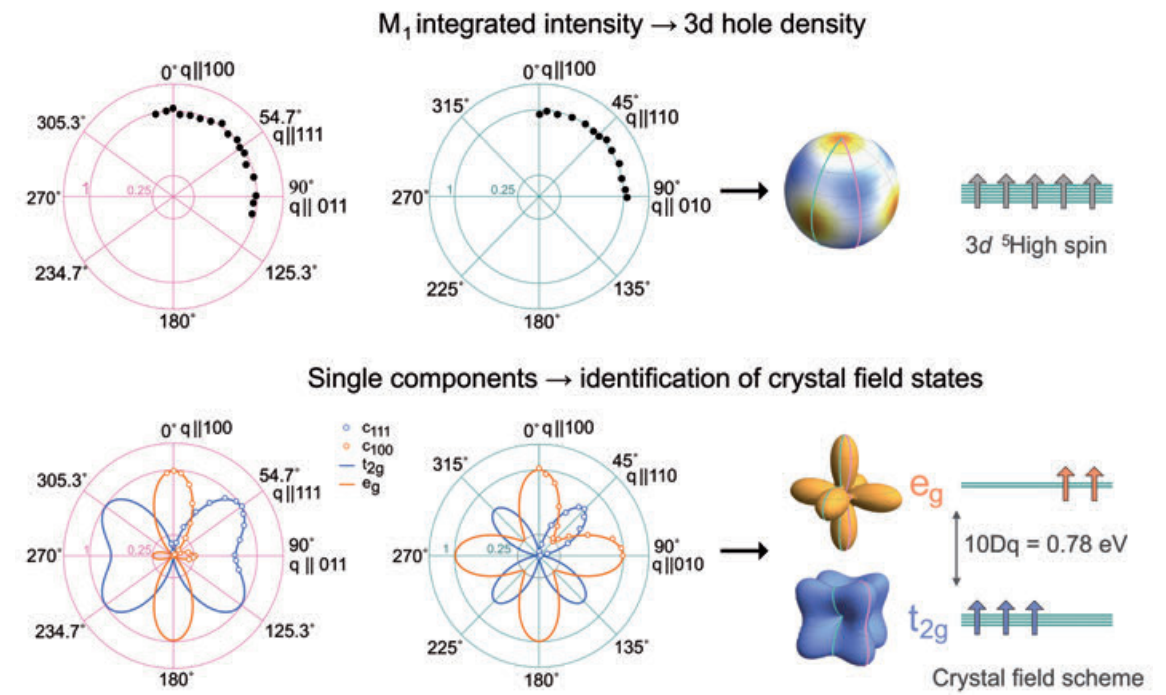


**Figure 2**

a) Stack of Mn  $M_1$  NIXS spectra acquired for several sample orientations relative to  $\mathbf{q}$ . Note that the centre of the spectra shifts in energy, with extremes for  $\mathbf{q} \parallel [111]$  (82.37 eV) and  $\mathbf{q} \parallel [100]$  (83.15 eV). The black lines are the result of fitting. b) Fitting procedure: The experimental spectrum for each angle  $\theta$  (black dots) is decomposed using the weighted sum of the two extreme spectra for  $\mathbf{q} \parallel [111]$  (blue dots) and  $\mathbf{q} \parallel [100]$  (orange dots) which provides the best fit (gray line).

**Figure 3**  
Top: Polar plot of the integrated intensity of the Mn  $M_1$  edge in the  $[100] \rightarrow [111] \rightarrow [011]$  plane (magenta) and in the  $[100] \rightarrow [110] \rightarrow [010]$  plane (dark cyan). Their circular shape indicates a spherical three-dimensional hole density of the Mn high-spin  $3d^5$  configuration.  
Bottom: The intensity of the  $\mathbf{q} \parallel [100]$  (orange) and  $\mathbf{q} \parallel [111]$  (blue) components follow the angular dependence of the  $e_g$  (orange) and  $t_{2g}$  (blue) orbitals, respectively. The  $e_g/t_{2g}$  crystal field splitting  $10Dq$  is 0.78 eV as read from the  $\mathbf{q} \parallel [111]$  and  $\mathbf{q} \parallel [100]$  peak separation in Fig. 2b.



tron density of the TM ions in that crystal. This *imaging* ability has recently been used to determine the ground-state orbital character of several TM compounds including those with complex crystal structures [2].

In the present work, we went one step further. Here we investigate the excited states and identify their orbital character via *imaging*. To demonstrate its feasibility, we performed *s*-NIXS experiments on  $\alpha$ -MnS (cubic rocksalt structure), see Fig. 1b, at the dedicated NIXS end station of the P01 beamline at PETRA III. Figure 2a shows a selection of the  $M_1$  edge ( $3s \rightarrow 3d$ ) spectra collected for several sample orientations. First, we plot the integrated intensity of each spectrum against the angle, see Fig. 3, top. The plot shows no orientational dependence, indicating a spherical ground-state charge density which is in fact fully consistent with the  $3d^5$  ( ${}^6A_1 - e_g^3 t_{2g}^2$ ) high-spin ground-state configuration of the  $\text{Mn}^{2+}$  ions in  $\alpha$ -MnS. Next, we take a closer look at the set of spectra in Fig. 2a. They are not the same: their centre moves on the energy axis and their widths vary. This is due to the presence of two peaks, i.e. two possible transitions, whose relative intensity is a function of the angle. The two narrowest spectra are those for  $\mathbf{q} \parallel [111]$  and  $\mathbf{q} \parallel [100]$ , and they are the two farthest apart in energy. Taking these as references, it is possible to fit the other spectra using their linear combination, see Fig. 2b. The corresponding weights ( $c_{111}$  and  $c_{100}$ ) can now be drawn on a polar plot, and they follow the known shapes of the  $t_{2g}$  and  $e_g$  orbitals, respectively, see Fig. 3, bottom. The final states are of the  $3s^1 3d^{5+1}$  type, and as far as the  $3d$  part is concerned, we thus can identify them as the  ${}^5T_2 - t_{2g}^3 e_g^2$  and  ${}^5E - t_{2g}^3 e_g^2$  states, respectively. Their energy separation is the cubic crystal-field splitting  $10Dq$ , and we can read directly from Fig. 2b that it is 0.78 eV.

In summary, with the imaging capability of the new *s*-NIXS technique, it is now possible to directly determine not only the  $3d$  charge distribution in the ground state but also the orbital character of the excited states. This gives us additional access to energy parameters that are relevant for the properties of the material. There is no need to rely on spectral analysis using complex calculations.

Author contact: Andrea Amorese, amorese@cpfs.mpg.de  
Liu Hao Tjeng, hao.tjeng@cpfs.mpg.de

## References

1. H. Yavaş, M. Sundermann, K. Chen, A. Amorese, A. Severing, H. Gretarsson, M. W. Haverkort and L. H. Tjeng, 'Direct imaging of orbitals in quantum materials', *Nat. Phys.* **15**, 559–562 (2019).
2. B. Leedahl, M. Sundermann, A. Amorese, A. Severing, H. Gretarsson, L. Zhang, A. C. Komarek, A. Maignan, M. W. Haverkort and L. H. Tjeng, 'Origin of Ising Magnetism in  $\text{Ca}_3\text{Co}_2\text{O}_8$ , unveiled by orbital imaging', *Nat. Commun.* **10**, 5447 (2019).
3. S. Sugano, Y. Tanabe and H. Kamimura, 'Multiplets of transition-metal ions in crystals' Academic Press, New York (1970).

## Original publication

'Selective orbital imaging of excited states with X-ray spectroscopy: the example of  $\alpha$ -MnS', *Physical Review X* **11**, 011002 (2021). DOI: 10.1103/PhysRevX.11.011002



Andrea Amorese<sup>1,2</sup>, Brett Leedahl<sup>1</sup>, Martin Sundermann<sup>1,2</sup>, Hlynur Gretarsson<sup>1,3</sup>, Zhiwei Hu<sup>4</sup>, Hong-Jin Lin<sup>4</sup>, Chien-Te Chen<sup>4</sup>, Marcus Schmidt<sup>1</sup>, Horst Borrmann<sup>1</sup>, Juri Grin<sup>1</sup>, Andrea Severing<sup>1,2</sup>, Maurits W. Haverkort<sup>5</sup> and Liu Hao Tjeng<sup>1</sup>

1. Max Planck Institute for Chemical Physics of Solids, Dresden, Germany
2. Institute of Physics II, University of Cologne, Cologne, Germany
3. Deutsches Elektronen-Synchrotron DESY, Hamburg, Germany
4. National Synchrotron Radiation Research Center, Hsinchu, Taiwan
5. Institute for Theoretical Physics, Heidelberg University, Heidelberg, Germany

# Twisting magnetisation with light

Laser pulses enable faster creation of skyrmions in ferromagnets

**Smaller, faster, more energy-efficient:** The requirements to computing and data storage become increasingly demanding and alternative concepts are continuously explored. Small magnetic textures, so-called skyrmions, are proposed as an ingredient in novel memory and logic devices. However, technological application requires fast and energy-efficient control of these nanometre-sized skyrmions. In our study, we demonstrate that skyrmions can be created and annihilated with single pulses of an ultrashort laser. Combining high-resolution X-ray imaging and time-resolved scattering, we reveal the fundamental mechanism leading to the creation of skyrmions on a time scale of only 300 ps. Based on our findings, we make first proposals for applying the concept in devices.

Skyrmions in thin magnetic films are localised, chiral magnetisation textures where the magnetisation continuously reverses from the outside to the inside (see inset in Fig. 1a). In particular, they are distinguished from other textures by their spherical topology. As a result, the creation or annihilation of a skyrmion involves a transition of the magnetic system's topology which is considered to cause a certain topological protection against this transition. This topological stability of skyrmions makes them attractive for data storage and data-processing technologies but also renders their fast creation very difficult.

Here, we investigate laser-mediated skyrmion creation in thin-film magnetic multilayer materials with perpendicular magnetic anisotropy. In these materials, a skyrmion phase is stabilised by competing local and non-local interactions, most notably interface-induced antisymmetric exchange and long-range stray-field interaction. We find that this skyrmion phase can be created by a single femtosecond infrared laser pulse of sufficient intensity. As shown in Fig. 1a, the laser pulse transforms a previously homogeneously magnetised film into a dense pattern of nanometre-scale skyrmions which appear as black circular domains in our images. The images were recorded at beamline P04 of PETRA III, using holography-based X-ray microscopy. The mobile holography end station operated by the Max Born

Institute is equipped with a fibre laser system for *in situ* excitation of the magnetic film. We used this unique instrumental combination to systematically map out the properties of laser-based skyrmion creation.

First, we discovered that the density of the skyrmion phase depends linearly on the magnetic field applied in the film's out-of-plane direction (Fig. 2a). The applied field, therefore, provides an easy and direct handle to control the number of skyrmions generated in a certain area. At high fields, the created number of skyrmions reduces to a single skyrmion in our microscopic field of view (Fig. 1b). After increasing the field strengths but preserving the skyrmion, it is possible to even annihilate the skyrmion by another laser pulse. A laser can, therefore, be used to write and erase information encoded by skyrmions.

As our second main finding, we observed an extremely sharp threshold for the laser fluence required to create skyrmions in a single pulse (Fig. 2b). Below the threshold, skyrmions only form after irradiation with thousands or millions of laser pulses. Above the threshold, the skyrmion density created is almost constant. Such a sharp threshold cannot be explained with a creation mechanism via thermal activation but is indicative of a phase transition taking place to form the topological skyrmion phase. In addition,

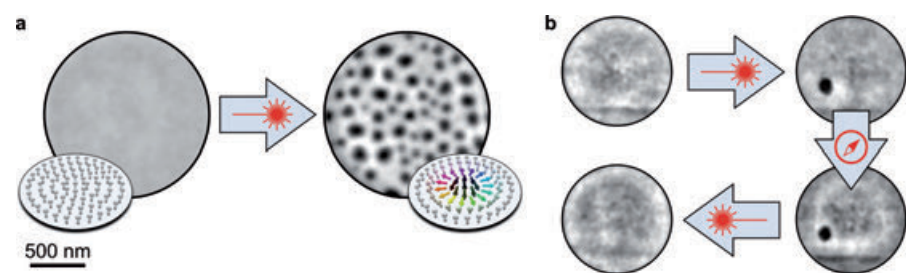
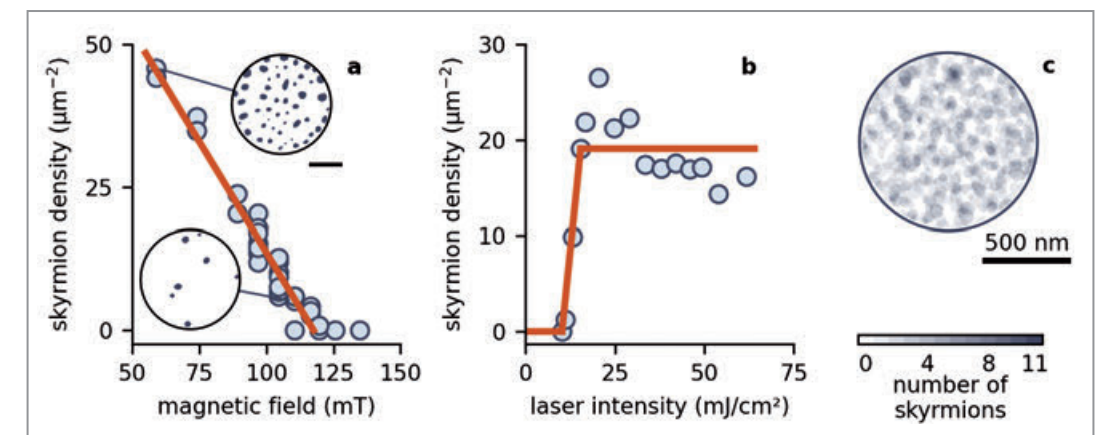


**Figure 1** Laser-induced ultrafast creation of magnetic skyrmions imaged with holography-based X-ray microscopy. a) A uniformly magnetised layer is transformed to a skyrmion phase after irradiation with a single laser pulse. Insets show the spin texture of the initial state and a single skyrmion. b) Skyrmion creation and annihilation cycle: first, laser-induced skyrmion creation, then slight increase of applied field, at last, laser-induced annihilation of the same skyrmion.

**Figure 2** Properties of laser-induced skyrmion creation. a) Linear dependence of the skyrmion density on the applied field. Insets show examples of the skyrmion phase. b) Sharp laser intensity threshold for skyrmion creation. c) Completely random and uniform spatial creation probability. The map was compiled as the sum of 20 skyrmion patterns independently created by single laser pulses in the same field of view.



the skyrmion creation probability is spatially surprisingly homogenous and skyrmions appear randomly distributed in the film (Fig. 2c). This finding is in contrast to skyrmion creation by spin-orbit torques where skyrmions preferentially form at natural or artificial pinning sites [1]. Therefore, we can rule out creation mechanisms based on optically generated spin torques.

To investigate the mechanism and speed of the topological transition, we performed complementary time-resolved X-ray scattering experiments at the SCS beamline at European XFEL. In these experiments, the small-angle scattering from the transient magnetic structures is detected during skyrmion formation after laser excitation. Surprisingly, we found that the transition to the skyrmion phase proceeds on a time scale of only 300 ps which is significantly faster than any magnetic switching process in a ferromagnet observed so far [2]. In concert with atomistic spin simulations, the scattering experiments reveal that the laser promotes the magnetic system into a high-temperature state of strongly fluctuating spins. In this — so far undisclosed — fluctuation phase the barrier for topological switching is reduced and skyrmions can appear in large numbers as short-range ordered nuclei. Subsequently, the nuclei coarsen to their equilibrium skyrmion size and density.

Given that skyrmions can have a size in the range of ten nanometres [3] and yet be stable at room temperature, our findings may have interesting implications for future computing concepts based on skyrmions as logic entities. Here, we bring forward the idea of an ultrafast 'skyrmion reshuffler'. Such a device is used to randomise bit streams for probabilistic computing. In this computing scheme, numbers are represented as strings of random bits of '0' and '1', with the probability to encounter '1' encoding the number value. Computations can then be carried out via logic operations between individual bits of different input numbers. While this scheme is inherently very error tolerant, it requires decorrelated inputs of the gates. A laser could generate such random skyrmion strings in a device where their density, i.e. the probability computing value, is controlled by the applied field. With our work we demonstrate

that 'reshuffling' of skyrmions can be performed optically on a timescale of picoseconds, compatible with state-of-the-art computer clock speed and much faster than in previous concepts based on thermal diffusion [4] operating on the timescale of seconds.

Author contact: Bastian Pfau, [bastian.pfau@mbi-berlin.de](mailto:bastian.pfau@mbi-berlin.de)  
Felix Büttner, [felix.buettner@helmholtz-berlin.de](mailto:felix.buettner@helmholtz-berlin.de)

## References

1. F. Büttner et al., 'Field-free deterministic ultrafast creation of magnetic skyrmions by spin-orbit torques', *Nat. Nanotechnol.* **12**, 1040–1044 (2017).
2. N. Berger et al., 'Irreversible transformation of ferromagnetic ordered stripe domains in single-shot infrared-pump/resonant-X-ray-scattering-probe experiments', *Phys. Rev. B* **91**, 054416 (2015).
3. L. Caretta et al., 'Fast current-driven domain walls and small skyrmions in a compensated ferrimagnet', *Nat. Nanotechnol.* **13**, 1154–1160 (2018).
4. J. Závorka et al., 'Thermal skyrmion diffusion used in a reshuffler device', *Nat. Nanotechnol.* **14**, 658–661 (2019).

## Original publications

'Observation of fluctuation-mediated picosecond nucleation of a topological phase', *Nature Materials* **20**, 30–37 (2021).  
DOI: 10.1038/s41563-020-00807-1



Felix Büttner, Bastian Pfau, Marie Böttcher, Michael Schneider, Giuseppe Mercurio, Christian M. Günther, Piet Hessing, Christopher Klose, Angela Wittmann, Kathinka Gerlinger, Lisa-Marie Kern, Christian Strüber, Clemens von Korff Schmising, Josefín Fuchs, Dieter Engel, Alexandra Churikova, Siying Huang, Daniel Suzuki, Ivan Lemesh, Mantao Huang, Lucas Caretta, David Weder, John H. Gaida, Marcel Möller, Tyler R. Harvey, Sergey Zayko, Kai Bagschik, Robert Carley, Laurent Mercadier, Justine Schlappa, Alexander Yaroslavtsev, Loïc Le Guyader, Natalia Gerasimova, Andreas Scherz, Carsten Deiter, Rafael Gort, David Hickin, Jun Zhu, Monica Turcato, David Lomidze, Florian Erdinger, Andrea Castoldi, Stefano Maffessanti, Matteo Porro, Andrey Samartsev, Jairo Sinova, Claus Ropers, Johan H. Mentink, Bertrand Dupé, Geoffrey S. D. Beach and Stefan Eisebitt

'Application concepts for ultrafast laser-induced skyrmion creation and annihilation', *Applied Physics Letters* **118**, 192403 (2021).  
DOI: 10.1063/5.0046033



Kathinka Gerlinger, Bastian Pfau, Felix Büttner, Michael Schneider, Lisa-Marie Kern, Josefín Fuchs, Dieter Engel, Christian M. Günther, Mantao Huang, Ivan Lemesh, Lucas Caretta, Alexandra Churikova, Piet Hessing, Christopher Klose, Christian Strüber, Clemens von Korff Schmising, Siying Huang, Angela Wittmann, Kai Litzius, Daniel Metternich, Riccardo Battistelli, Kai Bagschik, Alexandr Sadovnikov, Geoffrey S. D. Beach and Stefan Eisebitt

For affiliation details refer to original publications.

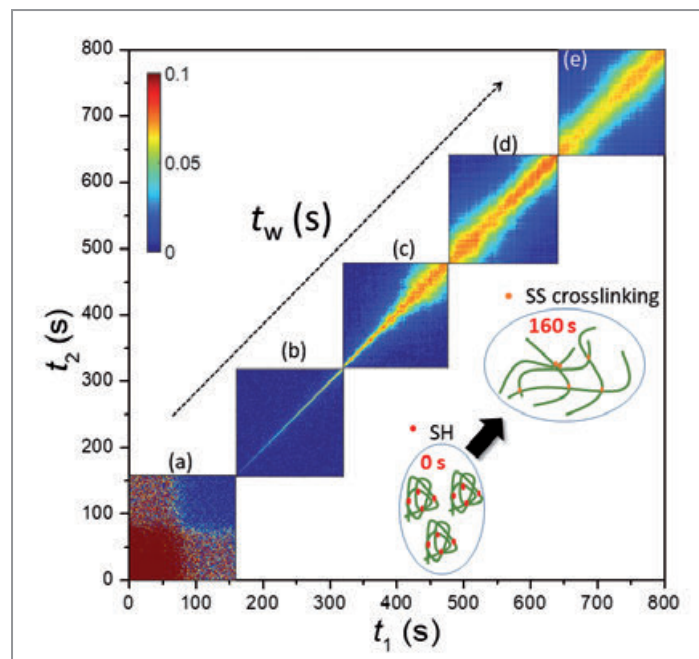
# Dynamical heterogeneity in a cooked egg

Microscopic dynamics of a heat-induced protein gel revealed using coherent X-ray scattering

Protein gelation is a fundamental topic in food chemistry as well as in condensed-matter physics. Gelation, as a result of heat-induced denaturation, leads to a three-dimensional network structure through the formation of disulfide cross-links and hydrogen bonds [1]. The properties of such gels, which form through a non-equilibrium process, are closely related to the microscopic dynamics of the network. Thus, understanding the microscopic dynamics of a gel at the lengthscales of the network structures is of interest in the fields concerning gelation of colloids, polymers and proteins.

Reorganisation of the microscopic structures which are under stress in a protein gel network can lead to heterogeneity in its relaxation dynamics. Understanding such reorganisation requires the understanding of the structure and dynamics of protein gels on a broad range of lengthscales and timescales, ranging from single proteins (nanometres) up to the network mesh size (micrometres), and milliseconds up to hundreds of seconds. However, the studies on the dynamic properties of thermal gels of proteins, so far, have only focused on the understanding of internal or short-time processes [2,3].

We have demonstrated the applicability of the sophisticated state-of-the-art technique low-dose X-ray photon correlation spectroscopy (XPCS) in ultra-small-angle X-ray



scattering (USAXS) geometry on a real protein gel [4,5]. In this experiment, a series of time-resolved scattering patterns is recorded using an area detector. Each of these scattering patterns is divided into different wavevector modulus ( $q$ ) regions and the intensity autocorrelation functions from each region are calculated using

$$g_2(q, t) = \frac{\langle I(t_1)I(t+t_1) \rangle}{\langle I(t_1) \rangle^2},$$

where  $I(t_1)$  is the scattered intensity at a measurement time  $t_1$  and  $\langle \dots \rangle$  indicates the average over the measurement time  $t_1$  and the pixels within the wavevector modulus range  $q \pm \delta q$ . This intensity autocorrelation function can be described by the Kohlrausch-Williams-Watts (KWW) function [4,5]

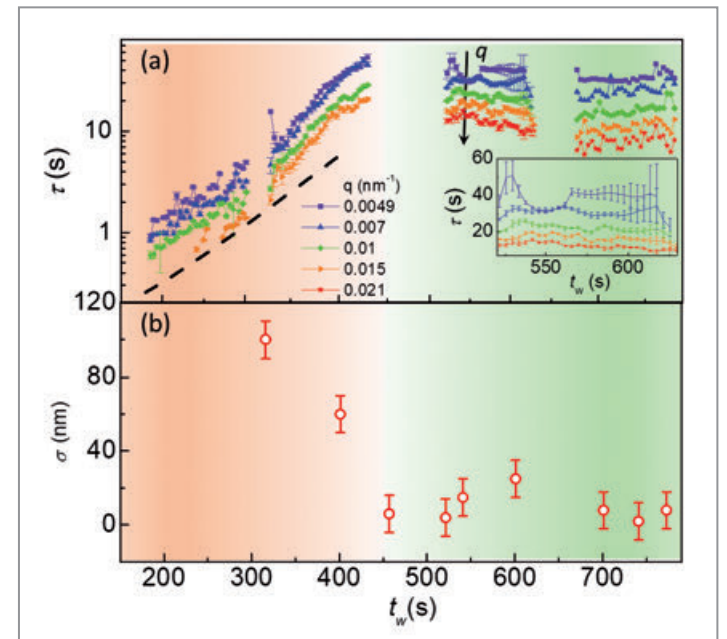
$$g_2(q, t) = 1 + \beta \exp\left[-2\left(\frac{t}{\tau}\right)^\gamma\right],$$

where  $\tau$  is the characteristic relaxation time of the system and  $\gamma$  is the stretching exponent, reflecting the deviations from the exponential behaviour. In the case of a non-equilibrium system, it is common to calculate the two-time correlation function given by

$$C_l(q, t_1, t_2) = \frac{\langle I_p(q, t_1)I_p(q, t_2) \rangle_{\text{pixels}}}{\langle I_p(q, t_1) \rangle_{\text{pixels}} \langle I_p(q, t_2) \rangle_{\text{pixels}}},$$

**Figure 1** Two-time correlation functions collected at 80 °C (at  $q=0.01 \text{ nm}^{-1}$ ) in five time intervals after reaching the temperature: a) 0–160 s, b) 160–320 s, c) 320–480 s, d) 480–640 s, e) 640–800 s. Temporal fluctuations can be observed in Fig. d–e. Inset schematic shows the native state of the proteins before denaturation (0 s after heating at 80 °C) and after unfolding due to heat denaturation (160 s after heating at 80 °C).

**Figure 2** a) Evolution of the relaxation time  $\tau$  as a function of  $t_w$  at 80 °C at different  $q$  as indicated in the legend. The inset shows the data within the time window  $t_w \approx 480\text{--}640 \text{ s}$  on a linear scale to visualise the temporal fluctuations. The dashed black line represents an exponential growth function. b)  $\sigma$  as a function of  $t_w$  showing a reduction with waiting time.



where  $I_p$  is the intensity at the pixel  $p$  and  $\langle \dots \rangle_{\text{pixels}}$  indicates an average over the pixels within the wavevector modulus range  $q \pm \delta q$ . The lines perpendicular to the diagonal of all the two-time correlation plots can be extracted to obtain the intensity correlation functions,  $g_2(q, t)$ .

Using this technique, we followed the simultaneous evolution of the microscopic dynamics on lengthscales of the network mesh size and the structural evolution corresponding to the gelation kinetics of a hen egg white. XPCS experiments were performed at the beamline P10 of PETRA III, using an X-ray wavelength of 1.54 Å. During the gelation, we performed five consecutive XPCS runs, each run corresponding to 160 s, at different fresh sample spots. The corresponding two-time correlation functions are depicted in Figs. 1a–e, and allow us to follow the evolution throughout the entire measurement time. The corresponding growth kinetics of the network structure show that, under the chosen conditions, the network structure evolution is remarkably well separated from the dynamics, i.e. the dynamics are observable only after 160 s (the bottom left corner of Fig. 1b) when the major part of the structural evolution is complete. The microscopic dynamics are observed to be hyper-diffusive and a pronounced slowing-down with time  $t_w$  is observed in Fig. 1. The stress-activated dynamics exhibit an exponential rise of the relaxation time (ageing) and a subsequent steady-state ballistic motion displaying significant temporal heterogeneity (Fig. 2a). The lengthscale (inversely proportional to the wavevector modulus  $q$ ) dependence of the dynamics is used to calculate the spatial extension  $\sigma$  of the decorrelation events using the method described in [6]. Figure 2b depicts that  $\sigma$  decreases from 100 nm to a few nanometres upon ageing, accompanied by a lowering of the degree of dynamical heterogeneity as a result of the discrete rearrangement events in the gel. These dynamical events are such that they do not change the structure of the gel.

Our investigation paves the way for future studies of dynamics following protein gelation, aggregation, liquid–liquid phase separation, as well as other phase transitions on lengthscales from nanometres to microns. Thus, the estab-

lished framework in this research has profound implications both for the food industry and the fundamental study of phase transitions of various soft-matter systems.

**Author contact:**  
Nafisa Begam, [nafisa.begam@ifap.uni-tuebingen.de](mailto:nafisa.begam@ifap.uni-tuebingen.de)

**References**

- Y. Mine, T. Noutomi and N. Haga, 'Thermally induces changes in egg white proteins', *J. Agric. Food Chem.* **38**, 2122–2125 (1990).
- M. Grimaldo, F. Roosen-Runge, F. Zhang and F. Schreiber, T. Seydel, 'Dynamics of proteins in solution', *Q. Rev. Biophys.* **52**, E7 (2019).
- M. Hennig, F. Roosen-Runge, F. Zhang, S. Zorn, M. W. A. Skoda, R. M. J. Jacobs, T. Seydel and F. Schreiber, 'Dynamics of highly concentrated protein solutions around the denaturing transition', *Soft Matter* **8**, 1628–1633 (2012).
- A. Girelli, H. Rahmann, N. Begam, A. Ragulskaya, M. Reiser, S. Chandran, F. Westermeier, M. Sprung, F. Zhang, C. Gutt and F. Schreiber, 'Microscopic dynamics of liquid-liquid phase separation and domain coarsening in a protein solution revealed by X-ray photon correlation spectroscopy', *Phys. Rev. Lett.* **126**, 138004, (2021).
- A. Ragulskaya, N. Begam, A. Girelli, H. Rahmann, M. Reiser, F. Westermeier, M. Sprung, F. Zhang, C. Gutt and F. Schreiber, 'Interplay between kinetics and dynamics of liquid-liquid phase separation in a protein solution revealed by coherent X-ray spectroscopy', *J. Phys. Chem. Lett.* **12**, 7085–7090 (2021).
- A. Duri and L. Cipelletti, 'Length scale dependence of dynamical heterogeneity in a colloidal fractal gel', *Europhys. Lett.* **76**, 972–978 (2006).

**Original publication**  
'Kinetics of network formation and heterogeneous dynamics of an egg white gel revealed by coherent X-ray scattering', *Physical Review Letters* **126**, 098001 (2021). DOI: 10.1103/PhysRevLett.126.098001

Nafisa Begam<sup>1</sup>, Anastasia Ragulskaya<sup>1</sup>, Anita Girelli<sup>2</sup>, Hendrik Rahmann<sup>3</sup>, Sivasurender Chandran<sup>3</sup>, Fabian Westermeier<sup>4</sup>, Mario Reiser<sup>2,5</sup>, Michael Sprung<sup>4</sup>, Fajun Zhang<sup>1</sup>, Christian Gutt<sup>2</sup> and Frank Schreiber<sup>1</sup>

- Institut für Angewandte Physik, Universität Tübingen, Germany
- Department Physik, Universität Siegen, Germany
- Department of Physics, Indian Institute of Technology Kanpur, India
- Deutsches Elektronen-Synchrotron DESY, Hamburg, Germany
- European XFEL, Schenefeld, Germany

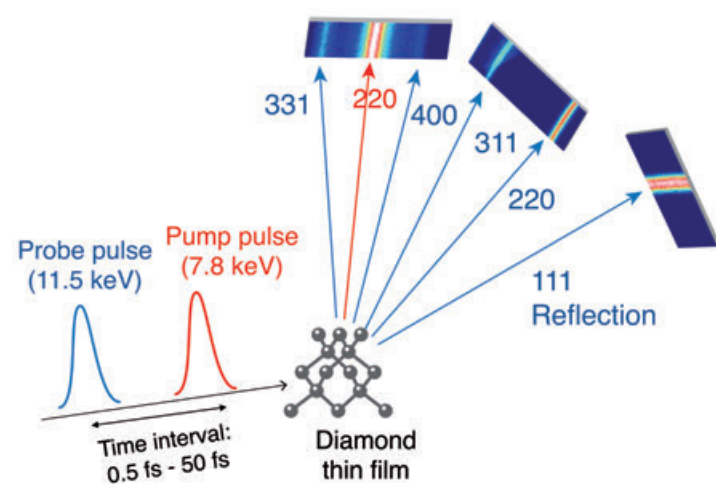
# Unusual melting in diamond

Atomic-scale time-resolved visualisation of ultrafast bond breaking by X-ray laser

In a conventional melting process, the application of heat or pressure causes large thermal vibrations of atoms at first and their bonds break apart later. When matter interacts with ultraintense X-ray pulses melting occurs in a different way. We have found evidence of an unconventional melting process in diamond induced by an X-ray laser beam. Using an X-ray pump-X-ray probe technique, we have demonstrated that covalent bonds in diamond break apart straight away, and only afterwards the atoms start moving underway to the melting.

Since their discovery in 1895, X-rays have become established as an invaluable probe for gaining an atomic insight into the structure of matter through various kinds of X-ray-matter interaction processes, such as scattering, absorption, emission of photoelectrons and fluorescence. These interactions were usually weak with the previous generation X-ray sources, and therefore it was assumed that X-ray irradiation did not modify matter. This situation has been totally changed by the recent advent of X-ray free-electron lasers (XFELs) which can generate high-brilliance X-ray pulses with femtosecond durations.

When an XFEL pulse irradiates matter, photoionisation and emission of Auger electrons occur almost simultaneously during or shortly after the irradiation with the pulse. The photoelectrons and Auger electrons collide with bound electrons in the surrounding atoms and strip outer shell electrons, triggering a cascade of collisional ionisations [1].

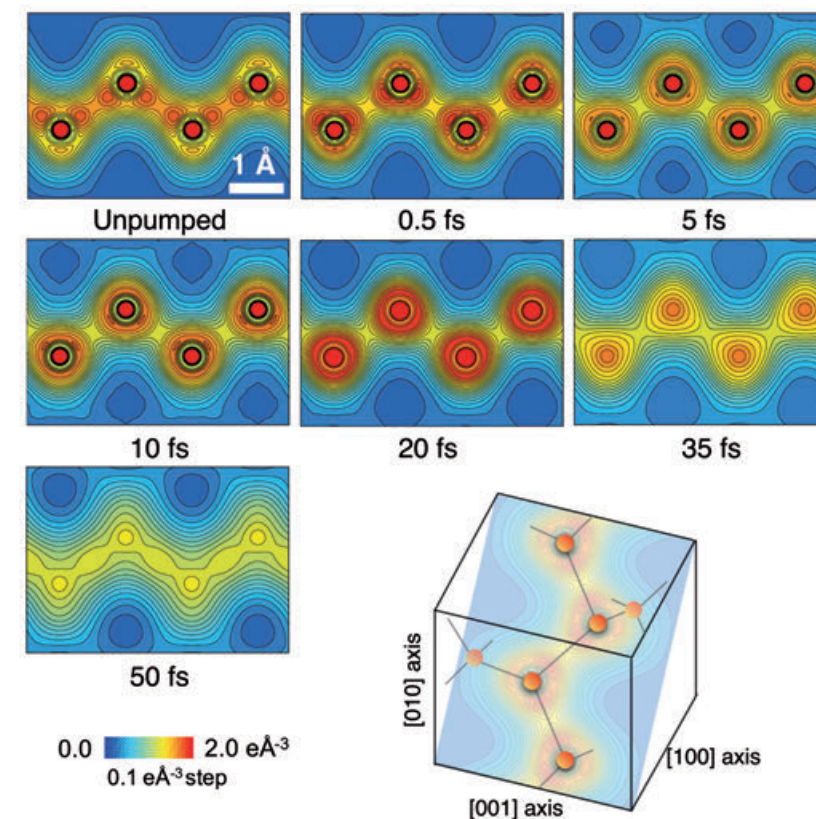


Thereby, a massive number of electrons are excited almost at once. A numerical simulation [2] predicts that a nanometre-focused XFEL beam with intensity of about  $10^{19}$  W/cm<sup>2</sup> [3] may excite approximately 30% of valence electrons to the conduction band of diamond. Such an enormously high electron excitation makes interaction of X-rays with matter irreversible, resulting in atomic disordering of matter. Deep understanding of such transient XFEL interaction with matter is essential not only because of fundamental interest but also for all potential XFEL applications.

In the reported experiment, an atomic-scale time-resolved visualisation of XFEL-matter interaction using diamond as a benchmark sample was performed. By employing the unique capability of the SPring-8 Angstrom Compact free-electron Laser (SACLA) [4], multiple diffraction peaks of diamond were measured in the X-ray pump-X-ray probe experiment (Fig. 1). For explanation, the first pulse (pump pulse) excited the diamond and the second pulse (probe pulse), with a controlled delay time, was used to investigate the changing structure of the sample with Bragg diffraction technique. By carefully analysing the diffraction intensity of the probe pulse, we determined the electron density maps in diamond after excitation with the pump pulse, as depicted in Fig. 2.

**Figure 1**  
Schematic illustration of the experiment. The focused double XFEL pulse irradiated a diamond film. The shot-by-shot diffraction images were measured using three two-dimensional detectors.

**Figure 2**  
Temporal changes of valence electron-density distribution and atomic displacement in diamond after irradiation with the pump pulse. The plots show valence charge-density distribution for the (110) plane at different delay times. The undamaged case (unpumped) is also shown for reference. The contour lines are drawn from 0.1 to 2.0 eÅ<sup>-3</sup> with 0.1 eÅ<sup>-3</sup> step width (e is the electron charge).



The measurement revealed that the covalent bonds between the carbon atoms of the diamond were broken and the electron distribution around each atom became almost isotropic within about 5 fs after the pump pulse, followed by the onset of the atomic movement underway to the melting. The temporal order of the bond breaking and the atomic disordering was opposite to the conventional melting process, where the application of heat or pressure causes large thermal vibrations of atoms at first and later the bond breaking.

The measured results were interpreted on the basis of dedicated theoretical simulations with the code XTANT [2]. These simulations showed that the observed displacement of carbon atoms was due to an ultrafast transition of the diamond's crystal structure caused just by the presence of many electrons excited by the intense XFEL pulse. The structural 'non-thermal' transformation forced atoms to quickly relocate their positions. It was called 'non-thermal' [5,6] as it was not triggered by 'thermal' heating of atoms in the crystal lattice, which takes longer time. The simulations allowed to unambiguously identify the mechanism and the stages of the observed transition which ended in rapid diamond melting.

The X-ray-induced non-thermal melting should be ubiquitous for many experiments with high intensity XFELs, such as single-particle imaging, protein nanocrystallography and generation of warm dense matter and plasma in high-energy-density regime. Particularly, the finding of this study should contribute to developing methodologies for structure determination with intense XFEL pulses, as the X-ray-induced damage, first electronic and later structural, occurring in this regime during the irradiation, should be carefully treated.

Author contact: Beata Ziaja, [ziaja@mail.desy.de](mailto:ziaja@mail.desy.de)  
Ichiro Inoue, [inoue@spring8.or.jp](mailto:inoue@spring8.or.jp)  
Eiji Nishibori, [nishibori.eiji.ga@u.tsukuba.ac.jp](mailto:nishibori.eiji.ga@u.tsukuba.ac.jp)

## References

1. B. Ziaja, R. A. London and J. Hajdu, 'Unified model of secondary electron cascades in diamond', *J. Appl. Phys.* **97**, 064905 (2005).
2. N. Medvedev and B. Ziaja, 'Multistep transition of diamond to warm dense matter state revealed by femtosecond X-ray diffraction', *Sci. Rep.* **8**, 5284 (2018).
3. H. Mimura et al., 'Generation of  $10^{20}$  W cm<sup>-2</sup> hard X-ray laser pulses with two-stage reflective focusing system', *Nat. Commun.* **5**, 3539 (2014).
4. T. Ishikawa et al., 'A compact X-ray free-electron laser emitting in the sub-ångström region', *Nat. Photon.* **6**, 540-544 (2012).
5. C. W. Siders et al., 'Detection of nonthermal melting by ultrafast X-ray diffraction', *Science* **286**, 1340-1342 (1999).
6. S. K. Sundaram and E. Mazur, 'Inducing and probing non-thermal transitions in semiconductors using femtosecond laser pulses', *Nat. Mater.* **1**, 217-224 (2002).

## Original publication

'Atomic-scale visualization of ultrafast bond breaking in X-ray-excited diamond', *Physical Review Letters* **126**, 117403 (2021).  
DOI: 10.1103/PhysRevLett.126.117403



Ichiro Inoue<sup>1</sup>, Yuka Deguchi<sup>2</sup>, Beata Ziaja<sup>3,4</sup>, Taito Osaka<sup>1</sup>, Malik M. Abdullah<sup>5</sup>, Zoltan Jurek<sup>6</sup>, Nikita Medvedev<sup>5,6</sup>, Victor Tkachenko<sup>4,7,8</sup>, Yuichi Inubushi<sup>8,1</sup>, Hidetaka Kasai<sup>2,9</sup>, Kenji Tamasaku<sup>1</sup>, Toru Hara<sup>1</sup>, Eiji Nishibori<sup>2,9</sup> and Makina Yabashi<sup>1,8</sup>

1. RIKEN SPring-8 Center, Sayo, Japan
2. Graduate School of Pure and Applied Sciences, University of Tsukuba, Tsukuba, Japan
3. Center for Free-Electron Laser Science (CFEL), DESY, Hamburg, Germany
4. Institute of Nuclear Physics, Polish Academy of Sciences, Krakow, Poland
5. Institute of Physics, Czech Academy of Sciences, Prague, Czech Republic
6. Institute of Plasma Physics, Czech Academy of Sciences, Prague, Czech Republic
7. European XFEL, Schenefeld, Germany
8. Japan Synchrotron Radiation Research Institute, Sayo, Japan
9. Faculty of Pure and Applied Sciences and Tsukuba Research Center for Energy Materials Science, University of Tsukuba, Tsukuba, Japan

# Structural dynamics of laser-induced shock waves

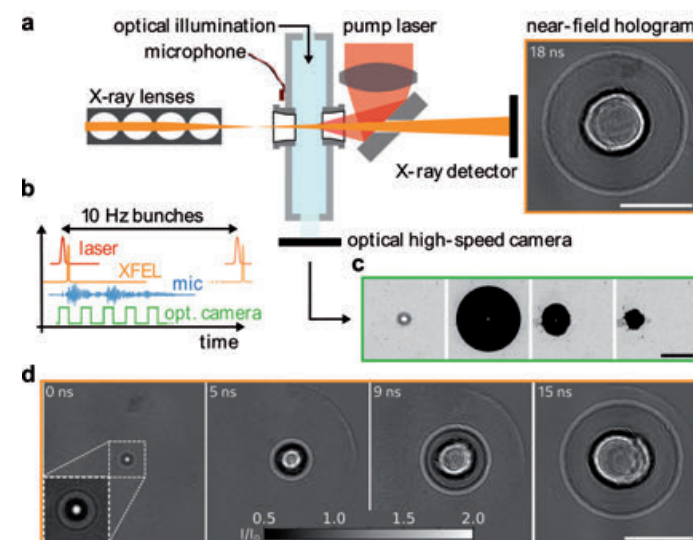
Pump-probe X-ray holographic imaging of laser-induced cavitation bubbles with femtosecond FEL pulses

Gas bubbles in a liquid are a frequent phenomenon in our daily environment, from a glass of sparkling water to the surf of the sea. They also occur in extreme non-equilibrium states of cavitation bubbles, involving fast dynamics and highest states of density, temperature and pressure. Apart from fundamental questions, cavitation bubbles are also relevant for a range of important applications, from laser surgery to material processing. Here, we generate cavitation bubbles by focusing a nanosecond infrared (IR) laser pulse into water. Following dielectric breakdown and a rapid plasma expansion, a shock wave is emitted and a cavitation bubble is formed. We investigated the early structural dynamics of this process by holographic flash imaging with X-ray free-electron laser (XFEL) pulses.

In this experiment we have studied laser-induced cavitation in water, i.e. the process of generating vapour-gas bubbles following optical breakdown and plasma formation. The initial supersonic regime of bubble expansion leads to the emission of a shock wave. The cavitation bubble grows up to a point of maximum radius and subsequently collapses which may again result in the emission of a shock wave. Over the last decades, several applications of laser-induced

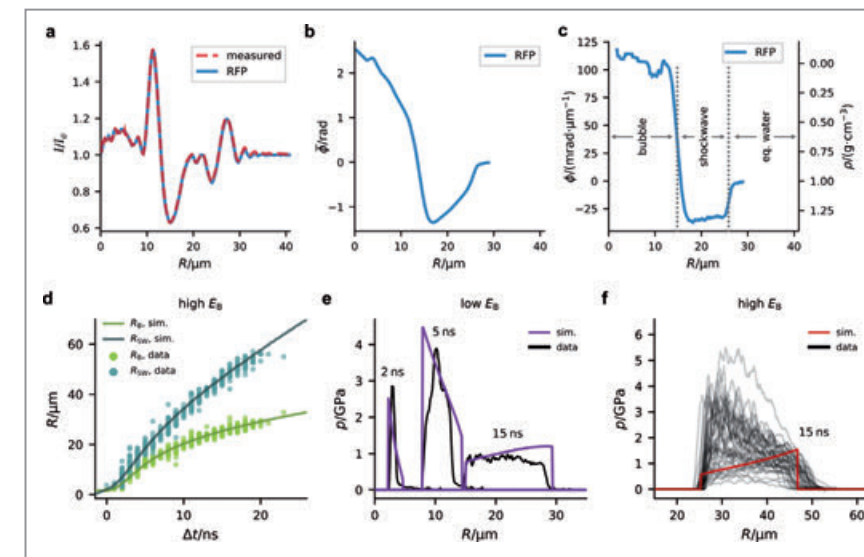
cavitation have evolved, ranging from material and surface processing, sonochemistry to medical laser surgery. Formation mechanisms and dynamics of laser-induced cavitation have been studied intensively by optical and acoustical methods [1,2]. The observation of cavitation dynamics requires imaging techniques with high spatial and temporal resolution. Near-field X-ray holography with ultrashort XFEL pulses fulfils these requirements, as it is a single-shot wide field technique with spatial resolution up to 20 nm [3].

Figure 1 shows a schematic of the experiment at the MID instrument at EuXFEL. 14 keV XFEL pulses are focused by nano-compound refractive lenses (CRL) to a spot size of about 100 nm. Cavitation bubbles are seeded by an IR pump laser with a pulse duration of 6 ns, which is aligned coaxially with the X-ray beam and is focused into a water cuvette, placed at a distance of 140 mm behind the X-ray focus. The XFEL pulse probes the cavitation bubble with a time delay  $\Delta t$  after seeding. The single-pulse holograms are recorded at a distance of 9 m behind the CRL focus. The process is repeated with 10 Hz and  $\Delta t$  is varied to acquire a time series of cavitation dynamics (Fig. 1d) [4]. The X-ray holograms contain quantitative information on the projected phase shift which is directly related to the density distribution  $\rho$  of the cavitation bubble. In order to extract this information, modulations by the empty-beam need to be separated from the object contribution, and in a second step, the phase has to be recovered by phase retrieval algorithms. The empty-beam correction of holographic recordings with FEL pulses is considerably more challenging than for synchrotron experiments since the self-amplified spontaneous emission process results in strong pulse-to-pulse variations of the X-ray beam. For this reason, we use an approach based on a principal component analysis to decompose the empty-beam in its main eigenmodes, as previously shown for synchrotron radiation in [5,6].



**Figure 1**  
(a) Experimental setup. A water cuvette is placed behind the focus of an XFEL pulse. An IR laser is focused into the cuvette to seed a cavitation bubble inside the water. The X-ray pulse probes the bubble with a time delay  $\Delta t$  after the laser pulse. The X-ray hologram is detected by a scintillation-based CMOS detector. (b) Timing scheme of the experiment. The laser pulse excites a cavitation bubble prior to the X-ray pulse to obtain the maximum expansion radius and collapse time of the cavitation bubble. An optical high-speed camera observes the cavitation process and a microphone detects the pressure waves. (c) Image sequence of the optical high-speed camera. (d) Empty-beam corrected holograms of cavitation bubbles for different  $\Delta t$ . Scale bars: (a,d) 50  $\mu\text{m}$ , (c) 500  $\mu\text{m}$ .

**Figure 2**  
RFP reconstruction steps and results obtained from the X-ray holograms. (a) Radial intensity profile of a single recorded hologram together with the optimised phase profile propagated to the detector plane. (b) Projected radially fitted phase in the sample plane. (c) 3D radial phase profile (left ordinate) and density profile (right ordinate). (d) Radial dynamics of the bubble boundary and shock wave front for a selected set of events with high  $E_B$ . The solid line represents simulations with parameters optimised to fit the data. (e) Exemplary radial shockwave pressure profiles for selected time delays and low  $E_B$ . (f) Set of shockwave profiles at  $\Delta t = 15$  ns and high  $E_B$ . We observe pronounced discrepancies between experimental data and the simulated curve.



We used two different phase retrieval approaches — an iterative scheme based on alternating projections [7] and an algorithm working on the radial intensity distribution for radially symmetric objects. The latter approach, which we denote radially fitted phase (RFP), uses an optimiser to find the projected radial phase distribution. Such an optimiser minimises the mismatch between the measured radial intensity profile and the profile obtained by numerical propagating of the modelled phase profile to the detector (Fig. 2a). Exploiting spherical or elliptical symmetry, the 3D radial phase (Fig. 2c) is obtained from the projected phase (Fig. 2b) and by proportionality also the radial density distribution  $\rho(R)$ . Combined with a modified Tait equation of state (EOS) for water, this yields the pressure profile  $\rho(R)$  of the shock wave which is in the gigapascal range.

This analysis is applied to over 5000 individual cavitation events which are categorised in terms of delay  $\Delta t$  and deposited bubble energy  $E_B$ . Figure 2d depicts the radial dynamics of the shock front and the bubble boundary for a range of high  $E_B$ , obtained from the X-ray holograms together with simulations based on the Gilmore model for cavitation dynamics and the Kirkwood-Bethe hypothesis for shock wave propagation. Figure 2e shows selected shock wave profiles at low  $E_B$ . While our simulations describe the experimental data for low  $E_B$  quite well, we observe pronounced discrepancies between simulations and the shock wave structure for higher  $E_B$  (see Fig. 2f). Standard models for cavitation dynamics and the Tait EOS at high pressures do not accurately describe the observations.

In summary, the quantitative analysis of near-field diffraction patterns in the holographic regime gives access to physical conditions of cavitation, including transition from plasma to a cavitation bubble, density waves and compression at different  $\Delta t$ . The structural dynamics, in particular the measured density in the shock wave, provides an important constraint and pushes the limits of standard EOS and numerical simulations. In a follow-up beamtime we will extend the work to study the bubble collapse. Today, the

shape in the final stages of collapse associated with strongest compression and sonoluminescence phenomena are still unknown.

Author contact: Malte Vassholz, [mvassho@gwdg.de](mailto:mvassho@gwdg.de)  
Tim Salditt, [tsaldit@gwdg.de](mailto:tsaldit@gwdg.de)

## References

1. A. Vogel, S. Busch and U. Parlitz, 'Shock wave emission and cavitation bubble generation by picosecond and nanosecond optical breakdown in water', *J. Acoust. Soc. Am.* **100**, 148–165 (1996).
2. W. Lauterborn and T. Kurz, 'Physics of bubble oscillations', *Rep. Prog. Phys.* **73**, 106501 (2010).
3. M. Bartels, M. Krenkel, J. Haber, R. N. Wilke and T. Salditt, 'X-ray holographic imaging of hydrated biological cells in solution', *Phys. Rev. Lett.* **114**, 048103 (2015).
4. M. Osterhoff, M. Vassholz, H. P. Hoeppe, J. M. Rosselló, R. Mettin, J. Hagemann, J. Möller, J. Hallmann, M. Scholz, R. Schaffer, U. Boesenberg, C. Kim, A. Zozulya, W. Lu, R. Shayduk, A. Madsen and T. Salditt, 'Nanosecond timing and synchronization scheme for holographic pump-probe studies at the MID instrument at European XFEL', *J. Synchrotron Radiat.* **28**, 987–994 (2021).
5. V. Van Nieuwenhove, J. De Beenhouwer, F. De Carlo, L. Mancini, F. Marone and J. Sijbers, 'Dynamic intensity normalization using eigen flat fields in X-ray imaging', *Opt. Express* **23**, 27975–27989 (2015).
6. J. Hagemann, M. Vassholz, H. P. Hoeppe, M. Osterhoff, J. M. Rosselló, R. Mettin, F. Seiboth, A. Schropp, J. Möller, J. Hallmann, C. Kim, M. Scholz, U. Boesenberg, R. Schaffer, A. Zozulya, W. Lu, R. Shayduk, A. Madsen, C. G. Schroer and T. Salditt, 'Single-pulse phase-contrast imaging at free-electron lasers in the hard X-ray regime', *J. Synchrotron Radiat.* **28**, 52–63 (2021).
7. J. Hagemann, M. Töpperwien and T. Salditt, 'Phase retrieval for near-field X-ray imaging beyond linearisation or compact support', *Appl. Phys. Lett.* **113**, 041109 (2018).

## Original publication

'Pump-probe X-ray holographic imaging of laser-induced cavitation bubbles with femtosecond FEL pulses', *Nature Communications* **12**, 3468 (2021). DOI: 10.1038/s41467-021-23664-1



Malte Vassholz<sup>1</sup>, Hannes P. Hoeppe<sup>1</sup>, Johannes Hagemann<sup>2</sup>, Juan M. Rosselló<sup>3</sup>, Markus Osterhoff<sup>4</sup>, Robert Mettin<sup>5</sup>, Thomas Kurz<sup>2</sup>, Andreas Schropp<sup>2</sup>, Frank Seiboth<sup>2</sup>, Christian G. Schroer<sup>2,4</sup>, Markus Scholz<sup>5</sup>, Johannes Möller<sup>5</sup>, Jörg Hallmann<sup>5</sup>, Ulrike Boesenberg<sup>5</sup>, Chan Kim<sup>5</sup>, Alexey Zozulya<sup>5</sup>, Wie Lu<sup>5</sup>, Roman Shayduk<sup>5</sup>, Robert Schaffer<sup>5</sup>, Anders Madsen<sup>5</sup> and Tim Salditt<sup>1</sup>

1. Institut für Röntgenphysik, Georg-August-Universität Göttingen, Göttingen, Germany
2. Deutsches Elektronen-Synchrotron DESY, Hamburg, Germany
3. Drittes Physikalisches Institut, Georg-August-Universität Göttingen, Göttingen, Germany
4. Fachbereich Physik, Universität Hamburg, Hamburg, Germany
5. European XFEL, Schenefeld, Germany

# Probing the interior of water-rich planets

The deep water layer of low-density planets would be 'fuzzy' with dissolved magnesium from the rocky core

Water-rich planets such as Uranus and Neptune in our Solar system could be the most common type in our galaxy. Direct exploration for such planets is difficult, if not impossible, due to the distance from the Earth, resulting in limitations of geophysical data to infer the planet's internal structures and compositions. Conventional models have assumed separate layers of water and rock based on their chemical behaviours at low pressures. However, recent models have suggested a compositional gradient in the interior in order to explain the low surface temperature of the planet. Our research provides experimental evidence of atomic-scale mixing between water and rock which can support the thermal boundary layer model.

Astrophysical surveys so far have suggested that water-rich planets, like Uranus and Neptune, could be prevalent in our galaxy [1]. However, their internal structures and geochemical cycles are not well understood. According to the conventional models, the water-rich planets have been assumed to have distinct layers of atmosphere, an icy (mostly H<sub>2</sub>O) mantle and a rocky (and/or metallic) core, positioning the layer interface between H<sub>2</sub>O and rocky layers in a range of high-pressure and high-temperature conditions [2,3]. However, recent internal models seeking to explain the low luminosity of Uranus invoked a compositional gradient model associated with a thermal barrier [4].

To understand the interior of water-rich planets by experiments, typical mantle-rock-forming minerals, olivine [(Mg,Fe)<sub>2</sub>SiO<sub>4</sub>] and ferroperricite [(Mg,Fe)O], were immersed in water and compressed between two gem-quality diamond culets in a diamond-anvil cell (DAC) and heated by an infrared laser to set the sample conditions in the pressure range of 15–80 GPa and the temperature range of 1000–4000 K. Under such simultaneous high-pressure and temperature conditions, we monitored the chemical reactions between the minerals and water using bright synchrotron X-rays provided by the P02.2 extreme conditions beamline (ECB) at PETRA III and the beamline 13-IDD at APS. Our data showed that (liquid) water could leach Mg from

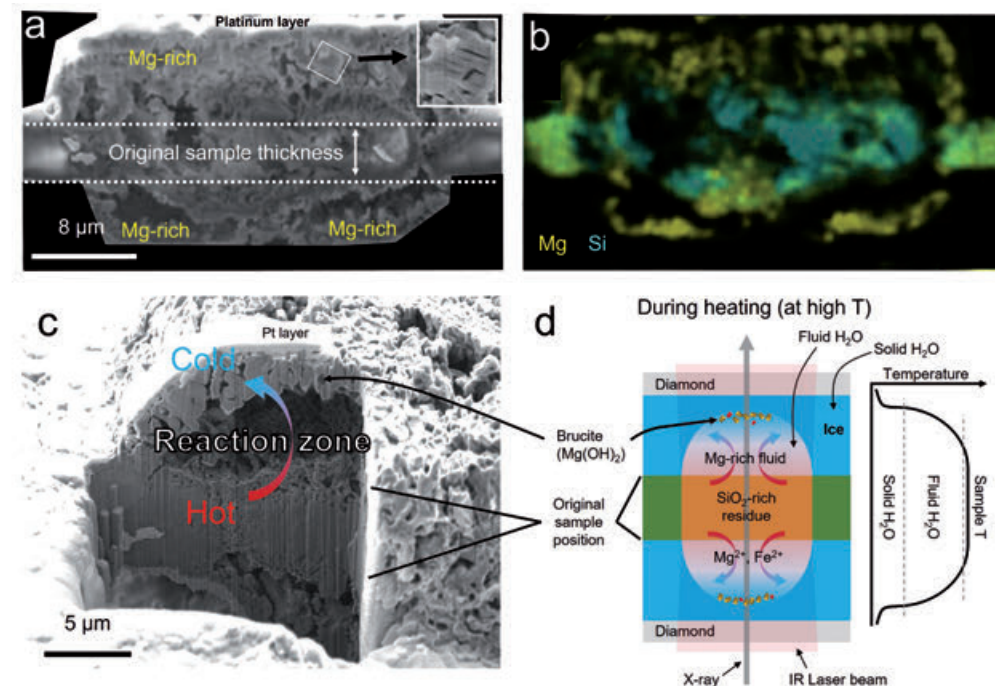
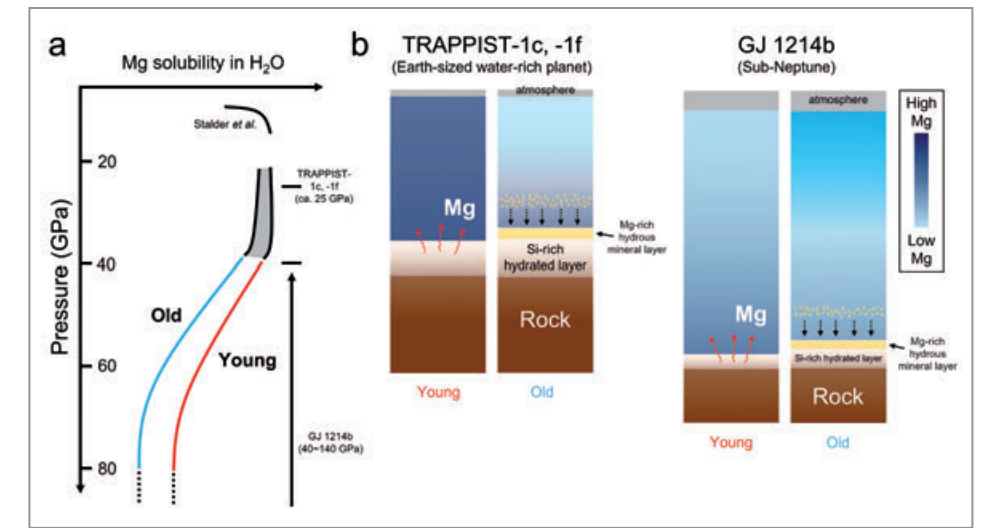
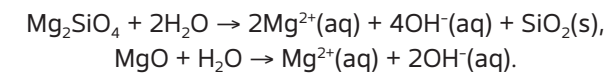


**Figure 1** SEM analysis of the recovered sample from laser heating of the olivine starting material in H<sub>2</sub>O medium. a) A cross-sectional view of the olivine heated to 1770 K at 33 GPa. b) Elemental distribution for Mg (yellow) and Si (cyan) throughout the cross section in (a). c) Another cross-sectional view of the olivine heated to 1330 K at 30 GPa. The pore would have been filled with Mg-rich fluid at high temperature and high pressure. d) A schematic diagram to illustrate the formation of the dome-like structure in (a) and (c) upon laser heating.

**Figure 2** Preliminary models of water-rich planetary interiors. a) Schematic diagram of pressure-dependent Mg solubility in H<sub>2</sub>O. b) Models for internal layering of four different types of water-rich planets by mass and thermal gradient. The red wavy arrows indicate leaching out of Mg from the rocky layer. The black dashed arrows indicate precipitation of Mg-rich hydrous minerals (yellow dots) due to the reduction in Mg solubility upon cooling.



the mineral phases at the high-pressure and temperature conditions relevant for the interior of water-rich planets:



A sudden decrease of X-ray diffraction intensity from the starting minerals was observed, concomitant to the appearance of new diffraction peaks from brucite [Mg(OH)<sub>2</sub>]. This demonstrates that the Mg component is dissolved in water from both olivine and ferroperricite, and precipitates as Mg(OH)<sub>2</sub> in a low-temperature region due to the decrease in solubility.

Details of the reaction processes were confirmed by scanning electron microscopy (SEM) and energy-dispersive X-ray spectroscopy of the recovered samples (Fig. 1). We found a dome-like structure (Fig. 1a,c) as a result of the dissolution and precipitation of the Mg component, together with a porous silica-rich layer left in the original sample position (Fig. 1b). We interpret this as selective dissolution, transportation and precipitation of Mg by water/ice under the thermal gradient within the sample chamber (Fig. 1d).

Mg dissolution is strongest in the pressure range of 20–40 GPa above 1500 K (Fig. 2a). Such conditions are close to the pressure-temperature conditions expected for the boundary between water and rocky layers of Earth-sized water-rich exoplanets, such as TRAPPIST-1f [5] (Fig. 2b). In the case of large water-rich planets such as GJ1214b [6], water-rock interactions would still occur, albeit in a reduced degree which will limit the range of chemical gradients at the boundary (Fig. 2b). Alternatively, water-rock reactions can occur during the hot and early stages of planetary accretion for yet larger planets, such as Uranus, which would remain as a thermal boundary layer in the top portion of the mantle [7], explaining its unusually low surface luminosity.

We plan to extend our investigations for the interior of water-rich planets to chemical mixing between other icy materials, such as CO<sub>2</sub>, NH<sub>3</sub> and lithophile (rock-loving)

elements. When the pressure range is extended, possible changes in the properties of H<sub>2</sub>O are expected as well, for example, into the superionic state. Future studies on volatiles-rock reactions will thus provide important thermodynamic data for advancing our knowledge on water-rich planets which could be common in our galaxy.

Our study was performed as a part of the Early Science Program of the Centre for Molecular Water Science (CMWS) that is currently being set up at DESY.

Author contact: Taehyun Kim, [ppower306@yonsei.ac.kr](mailto:ppower306@yonsei.ac.kr)  
Yongjae Lee, [yongjaelee@yonsei.ac.kr](mailto:yongjaelee@yonsei.ac.kr)  
Sang-Heon Dan Shim, [shdshim@asu.edu](mailto:shdshim@asu.edu)

## References

1. N. M. Batalha, 'Exploring exoplanet populations with NASA's Kepler Mission', *Proc. Natl. Acad. Sci. U.S.A.* **111**, 12647–12654 (2014).
2. A. Léger et al., 'A new family of planets? "Ocean-Planets"', *Icarus* **169**, 499–504 (2004).
3. T. Guillot, 'The interiors of giant planets: models and outstanding questions', *Annu. Rev. Earth Planet. Sci.* **33**, 493–530 (2005).
4. A. Vazan and R. Helled, 'Explaining the low luminosity of Uranus: a self-consistent thermal and structural evolution', *Astron. Astrophys.* **633**, A50 (2020).
5. C. T. Unterborn, S. J. Desch, N. R. Hinkel and A. Lorenzo, 'Inward migration of the TRAPPIST-1 planets as inferred from their water-rich compositions', *Nat. Astron.* **2**, 297–302 (2018).
6. D. Charbonneau et al., 'A super-Earth transiting a nearby low-mass star', *Nature* **462**, 891–894 (2009).
7. A. Vazan, R. Sari and R. Kessel, 'A new perspective on interiors of ice-rich planets: ice-rock mixture rather than a layered structure', preprint at <https://arxiv.org/abs/2011.00602> (2020).

## Original publication

'Atomic-scale mixing between MgO and H<sub>2</sub>O in the deep interiors of water-rich planets', *Nature Astronomy* **5**, 815–821 (2021).  
DOI: 10.1038/s41550-021-01368-2



Taehyun Kim<sup>1</sup>, Stella Chariton<sup>2</sup>, Vitali Prakapenka<sup>3</sup>, Anna Pakhomova<sup>3</sup>, Hanns-Peter Liermann<sup>3</sup>, Zhenxian Liu<sup>4</sup>, Sergio Speziale<sup>5</sup>, Sang-Heon Shim<sup>6</sup> and Yongjae Lee<sup>1</sup>

1. Yonsei University, Seoul, South Korea
2. The University of Chicago, Argonne, USA
3. Deutsches Elektronen-Synchrotron DESY, Hamburg, Germany
4. University of Illinois at Chicago, Chicago, USA
5. GFZ German Research Centre for Geosciences, Potsdam, Germany
6. Arizona State University, Tempe, USA

# Zeptoseconds across the molecule

Molecular double-slit experiment uncovers the travel time of light from one end to the other

Two stones dropped simultaneously into water create a double-slit-like interference pattern on the surface which is symmetric around the centre of the two drop points. A skipping flat pebble, which jumps off the water surface once before it sinks at a position further away, results in an asymmetric interference pattern that is shifted towards the position where the stone sunk. The reason for the asymmetry is the time delay between the births of the two waves on the water's surface. The electron angular distribution from photoionisation of the hydrogen molecule also shows a double-slit-like interference pattern, and we investigated its asymmetry to measure the travel time of light across the molecule.

Photoelectron emission from the hydrogen molecule ( $H_2$ ) mimics the double-slit experiment. The two centres of the diatomic molecule behave like independent photon absorbers and as indistinguishable sources of coherent photoelectron waves [1]. Subsequently, their interference fringes become observable in the angular emission pattern of the outgoing electron in the molecular frame of reference. In the past, this molecular double-slit experiment has provided insight into some of the most fundamental concepts of quantum mechanics like wave-particle duality of the electron, decoherence of a quantum system or entanglement among quantum particles [2,3]. In this work, we showed that the double-slit behaviour of  $H_2$  photoionisation unveils yet another fundamental concept of nature: the finite speed of light.

During the process of photoionisation, a wavefront of constant phase, i.e. a photon, sweeps from one end of the molecule to the other. The finite speed of light should affect the photoionisation of  $H_2$  because the photoelectron wave cannot be launched at the same time from the two atomic centres while the photon arrives at different times. Accordingly, the contributions from the two centres to the total photoelectron wave are subject to 'birth time delay' and we expected the corresponding interference pattern to be asymmetric. From a simple model perspective, this birth time delay should correspond to the travel time of the photon across the molecule which is 247 zeptoseconds ( $1 \text{ zs} = 10^{-21} \text{ s}$ ) for the average bond length of molecular hydrogen ( $R = 1.4 \text{ au}$  [atomic units]).

In the present work, we searched for the birth time delay of electron emissions in one-photon double ionisation of  $H_2$  at a photon energy of 800 eV. Our experiment employed a cold target recoil ion momentum spectroscopy (COLTRIMS) reaction microscope and it was performed at the PIPE end station of beamline P04 at PETRA III using circularly polarised light. For each detected photoionisation event, the experiment produced the three-dimensional momentum vectors of all four reaction fragments (two electrons and two protons). The two proton momentum vectors are antiparallel and point in the direction of the molecular axis. We used this information during the data analysis to transform the electron momentum vectors into the molecular frame of reference and to identify the orientation of the molecule with respect to the light propagation direction.

**Figure 1** Emission angle  $\alpha$  of fast electrons in the molecular frame of reference as a function of the kinetic energy release (KER) and the molecular bond length. The fringes underline the double-slit nature of fast electron emission in one-photon double ionisation of  $H_2$  at a photon energy of 800 eV.

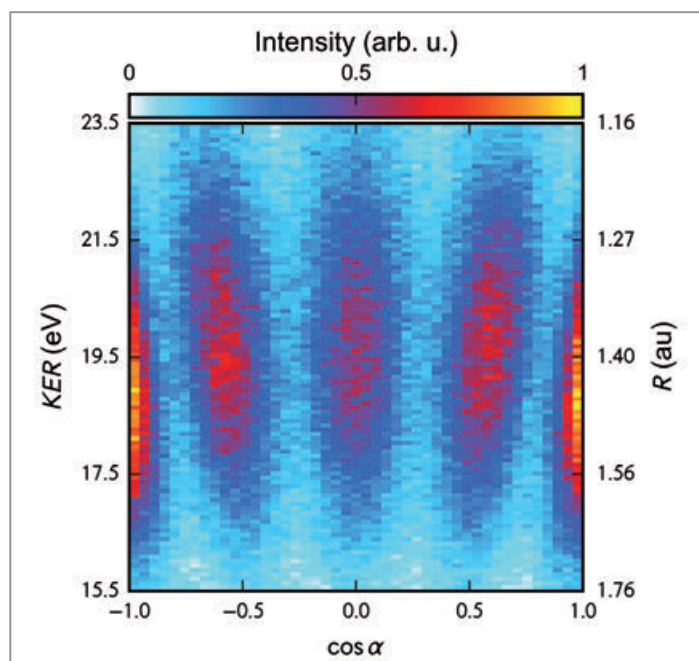
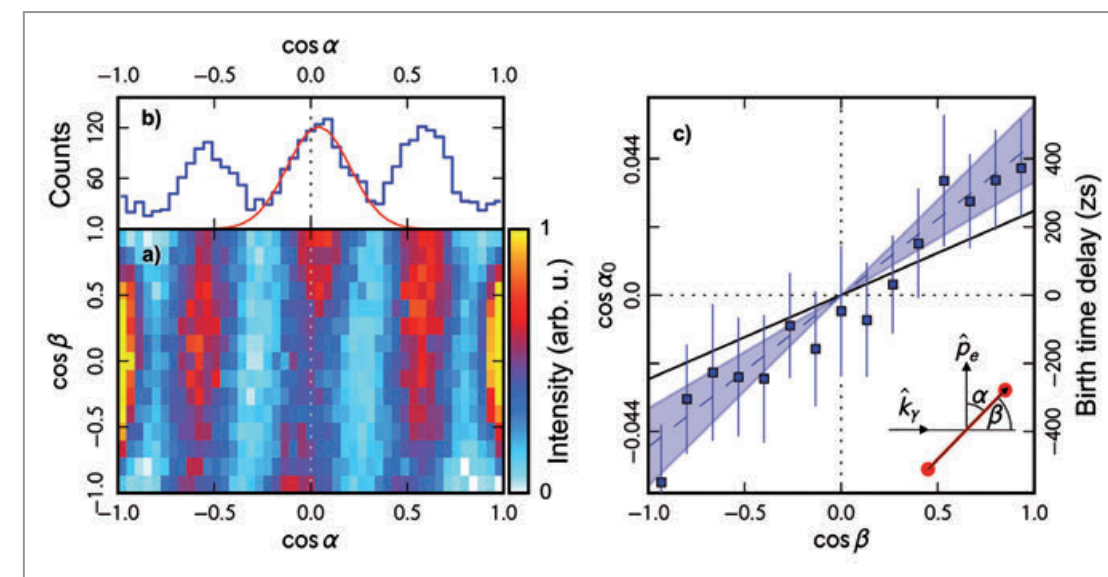


**Figure 2** Birth-time-delay measurement for fast electrons and an average molecular bond length. a) Electron angular distribution as a function of  $\beta$ . b) Electron angular distribution for parallel alignment of light and molecule ( $\cos \beta = 1$ ; blue). Gaussian fit to identify the position of the zeroth-order interference maximum  $\alpha_0$  (red). c) Birth time delay (calculated from  $\alpha_0$ ) as a function of  $\beta$  (blue) and the simple model prediction for comparison (black). The blue-shaded region indicates the systematic error range.



In double ionisation of  $H_2$ , the excess energy is shared between the two electrons and for highly asymmetric energy sharing the fast electron practically behaves like a photoelectron in single ionisation. Hence, we had to restrict our investigation to fast electrons that carried more than 96% of the excess energy. Figure 1 shows the electron angular distribution of those fast electrons as a function of the kinetic energy release that equals the sum of the kinetic energies of the protons which is inversely proportional to the molecular bond length  $R$  at the moment of ionisation. As one would expect from the behaviour of the interference pattern of a classical double-slit experiment, where the number of interference fringes increases as the slit distance increases, the angular separation of the maxima becomes smaller with growing  $R$ . Here, we averaged over all molecular orientations in the laboratory frame of reference.

Subsequently, we investigated the interference pattern as a function of the angle  $\beta$  between the molecular axis and the light propagation direction for the subset data,  $R = 1.40 \pm 0.04 \text{ au}$ , from Fig. 1. The interference fringes in Fig. 2a are tilted because of the asymmetry expected from birth time delay. For the quantitative analysis, we determined the angular positions of the zeroth-order interference maxima for each  $\beta$  through Gaussian fits as indicated in Fig. 2b. The angular position of the zeroth-order interference maximum  $\alpha_0$  and the birth time delay  $\tau$  are related through  $\tau = \cos \alpha_0 (R/v_{ph})$  where  $v_{ph}$  is the phase speed of the electron wave. The resulting calculated birth time delay as a function of  $\beta$  is shown in Fig. 2c and compared to the simple model case of  $\tau = \cos \beta (R/c)$  where the time delay is simply given by the projection of the molecular bond length onto the light propagation axis divided by the speed of light  $c$ .

Interestingly, the measured birth time delay overestimates the values expected from the simple model calculation.

Following up on our initial experimental work, this deviation has fuelled interest to investigate the birth time delay from a theoretical perspective. While the issue is not yet entirely resolved, we strongly suspect that the discrepancy originates from the two-electron nature of the investigated process [4].

**Author contact:**  
Sven Grundmann, grundmann@atom.uni-frankfurt.de  
Till Jahnke, jahnke@atom.uni-frankfurt.de  
Florian Trinter, florian.trinter@desy.de  
Reinhard Dörner, doerner@atom.uni-frankfurt.de

## References

- H. D. Cohen and U. Fano, 'Interference in the photo-ionization of molecules', *Phys. Rev.* **150**, 30–33 (1966).
- D. Akoury et al., 'The simplest double slit: interference and entanglement in double photoionization of  $H_2$ ', *Science* **318**, 949–952 (2009).
- M. Waitz et al., 'Two-particle interference of electron pairs on a molecular level', *Phys. Rev. Lett.* **117**, 083002 (2016).
- H. Liang et al., 'Nondipole effects in interference patterns of a two-electron wave', *Phys. Rev. A* **104**, L021101 (2021).

## Original publication

'Zeptosecond birth time delay in molecular photoionization', *Science* **370**, 339–341 (2020). DOI: 10.1126/science.abb9318



Sven Grundmann<sup>1</sup>, Daniel Trabert<sup>1</sup>, Kilian Fehre<sup>1</sup>, Nico Strenger<sup>1</sup>, Andreas Pier<sup>1</sup>, Leon Kaiser<sup>1</sup>, Max Kircher<sup>1</sup>, Miriam Weller<sup>1</sup>, Sebastian Eckart<sup>1</sup>, Lothar Ph. H. Schmidt<sup>1,2,3</sup>, Florian Trinter<sup>1,2,3</sup>, Till Jahnke<sup>1</sup>, Markus S. Schöffler<sup>1</sup> and Reinhard Dörner<sup>1</sup>

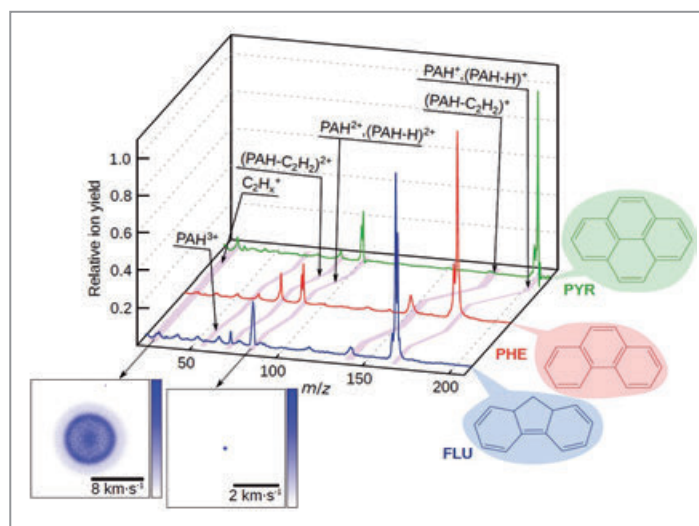
- Goethe-Universität, Institut für Kernphysik, Frankfurt am Main, Germany
- Deutsches Elektronen-Synchrotron DESY, Hamburg, Germany
- Fritz-Haber-Institut, Molecular Physics, Berlin, Germany

# Exploring astrochemistry with ultrafast XUV pulses at FLASH

A time-resolved study of polycyclic aromatic hydrocarbons

Satellite infrared measurements show signatures of aromatic vibrations in practically every corner of the universe, attributed to polycyclic aromatic hydrocarbons in the interstellar medium. These molecules account for up to 20% of carbon in space. Utilising ultrafast XUV pulses of the free-electron laser FLASH replicates some of the harsh radiation of the interstellar medium and allows a detailed insight into the various molecular processes occurring after the initial photoionisation.

Aromatic infrared vibrational signatures show that polycyclic aromatic hydrocarbons (PAHs) exist virtually everywhere in space. These molecules play an important role in interstellar chemistry, including providing reaction surfaces, aggregating into larger species such as fullerenes, fragmenting to provide building blocks for other molecules and absorbing high energy photons (UV and above) and emitting IR photons. Given their prevalence and quantity in the interstellar medium (ISM), PAHs and their derivatives are often cited as candidates contributing to the unidentified infrared emission bands and the diffuse interstellar bands and as such have been the subject of laboratory experiments for many decades. Astrochemical molecules are typically identified by their unique microwave rotational spectrum, but the low dipole moment in most PAHs has made this challenging. Substituted PAHs may have a sufficient dipole moment to record a rotational spectrum to match with astronomical spectra, as shown in 2021 when two isomers of cyanonaphthalene were finally identified as the first PAH derivatives in the ISM [1].

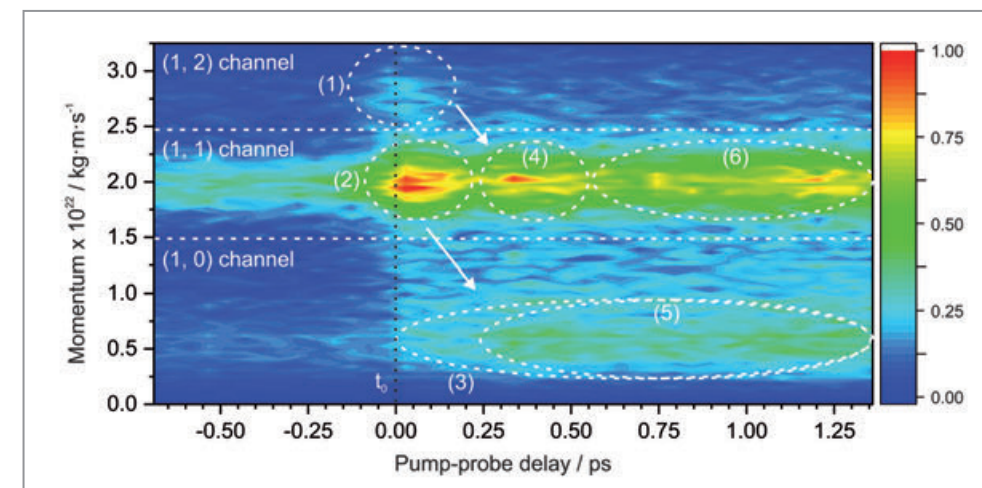


Our experiment aims at understanding the reaction dynamics of PAH molecules following interaction with ionising radiation prevalent in the interstellar medium. Photons in the XUV range can lead to multiple ionisation and trigger complex relaxation processes. Previous studies have shown that larger PAH molecules have efficient relaxation pathways, which transforms the energy of excited electronic states into vibrational excitation. Our work investigates the reaction dynamics of three small PAH molecules, fluorene, phenanthrene and pyrene (Fig. 1), following the initial ionisation in a pump-probe experiment. Using the CAMP end station at BL1 at FLASH, the time-dependent electron images, ion time-of-flight spectra and ion images were simultaneously acquired [2,3].

Having these multiple observables in our experiment allowed a detailed view into the absorption of an XUV photon by a PAH molecule. An example of our data is shown in Fig. 2, tracking the momentum of the  $C_3H_x^+$  ion as a function of XUV-IR pump-probe delay. Several time-dependent signatures can be seen in the data, such as feature (1) in the (1, 2) channel. The (X, Y) channel refers to the charges in the fragments, with the (1, 2) channel referring to the monocation  $C_3H_x^+$  being formed with a dication fragmentation partner. In the (1, 2) channel, the Coulombic interaction between the ions leads to an increase in the observed momentum of the  $C_3H_x^+$  ion. A peak in the (1, 2) channel, labelled as feature (1), occurs around  $t_0$  when the XUV pulse and IR probe overlap in time. This is attributed to highly-excited fluorene dications being formed by the XUV photon; before the dications are able to internally relax, the IR

**Figure 1** The PAH molecules studied in this experiment, fluorene (FLU), phenanthrene (PHE) and pyrene (PYR), with their XUV-induced mass spectra in blue, red and green, respectively. The ion images of the  $C_3H_x^+$  and  $PAH^{2+}$  ions from FLU are shown as insets. This figure is licensed under CC BY 4.0.

**Figure 2** The momentum profile of the  $C_3H_x^+$  ion formed through fragmentation of fluorene as a function of XUV-IR laser pulse delay. Positive pump-probe delay times correspond to XUV pulse first, IR pulse second, and  $t_0$ , where the pulses are simultaneous, is denoted by the vertical black dotted line. The (1, 2), (1, 1) and (1, 0) channels refer to the  $C_3H_x^+$  ion being formed with a dication, monocation and neutral fragmentation partner, respectively. Some highlighted features are described in the main text. This figure is licensed under CC BY 4.0.



pulse induces dissociative ionisation and fragmentation of the trication, thus leading to signal in the (1, 2) channel. If the IR pulse is delayed relative to the XUV pulse, rapid internal relaxation of the dication takes place and the IR pulse instead induces direct dissociation without further ionisation. The resulting peak in the (1, 1) channel, delayed from  $t_0$ , is highlighted as feature (4) where the  $C_3H_x^+$  ion is formed with a monocation partner fragment. Fitting the time-dependence of feature (1), backed up with theoretical studies, allows the femtosecond electronic relaxation rate of the fluorene dication to be determined.

Similar features are seen in other channels, for example, feature (2) in the (1, 1) channel. Feature (2) is attributed to the formation of highly excited fluorene monocations by the XUV pulse; close to  $t_0$ , the IR pulse induces dissociative ionisation, forming the dication and fragmenting it. Again, if a delay is introduced before the IR pulse, the monocation can internally decay, and the IR pulse dissociates the monocation, leading to an increase in signal in the (1, 0) channel, labelled as feature (5).

Through combining the ion images, the electron images and the ion TOF data, ultrafast relaxation of the PAHs in the neutral, monocation and dication states has been measured for the first time. These results suggest that ultrafast relaxation may be ubiquitous amongst PAHs, likely due to these molecules possessing a complex potential energy landscape with numerous conical intersections to mediate the relaxation. Yielding results by performing such a complex experiment and data analysis is a testament to the multiple expertise and collaborative efforts that accompany beamtimes at FLASH. Building on our experience of obtaining rich datasets on PAHs at FLASH, we recently completed another beamtime (August 2021) exploring how different levels of binding between aromatic rings affects

**Author contact:** Jason Lee, [jason.lee@desy.de](mailto:jason.lee@desy.de)  
Denis Tikhonov, [denis.tikhonov@desy.de](mailto:denis.tikhonov@desy.de)  
Bastian Manschwetus, [bastian.manschwetus@desy.de](mailto:bastian.manschwetus@desy.de)  
Melanie Schnell, [melanie.schnell@desy.de](mailto:melanie.schnell@desy.de)

the electronic relaxation and fragmentation patterns and we look forward to presenting these results to the community.

## References

1. A. B. McGuire et al., 'Detection of two interstellar polycyclic aromatic hydrocarbons via spectral matched filtering', *Science* **371**, 1265–1269 (2021).
2. B. Erk et al., 'CAMP@FLASH: an end-station for imaging, electron- and ion-spectroscopy, and pump-probe experiments at the FLASH free-electron laser', *J. Synchrotron Radiat.* **25**, 1529–1540 (2018).
3. A. T. Clark et al., 'Multimass velocity-map imaging with the pixel imaging mass spectrometry (PIMMS) sensor: an ultra-fast event-triggered camera for particle imaging', *J. Phys. Chem. A* **116**, 10897–10903 (2012).

## Original publication

'Time-resolved relaxation and fragmentation of polycyclic aromatic hydrocarbons investigated in the ultrafast XUV-IR regime', *Nature Communications* **12**, 6107 (2021).  
DOI: 10.1038/s41467-021-26193-z



Jason W. L. Lee<sup>1,2</sup>, Denis S. Tikhonov<sup>1,3</sup>, Pragya Chopra<sup>1,3</sup>, Sylvain Maclot<sup>4,5</sup>, Amanda L. Steber<sup>1,3,6</sup>, Sébastien Gruet<sup>1</sup>, Felix Allum<sup>2</sup>, Rebecca Boll<sup>7</sup>, Xuemei Cheng<sup>1</sup>, Stefan Düsterer<sup>1</sup>, Benjamin Erk<sup>1</sup>, Diksha Garg<sup>1,8</sup>, Lanhai He<sup>9</sup>, David Heathcote<sup>2</sup>, Melby Johnny<sup>9</sup>, Mehdi M. Kazemi<sup>1</sup>, Hansjochen Köckert<sup>2</sup>, Jan Lahl<sup>4</sup>, Alexander K. Lemmens<sup>10,11</sup>, Donatella Loru<sup>1,3</sup>, Robbie Mason<sup>2</sup>, Erland Müller<sup>1</sup>, Terence Mullins<sup>9</sup>, Pavel Olshin<sup>12</sup>, Christopher Passow<sup>1</sup>, Jasper Peschel<sup>4</sup>, Daniel Ramm<sup>1</sup>, Dimitrios Rompotis<sup>1,7</sup>, Nora Schirmel<sup>1</sup>, Sebastian Trippel<sup>1,9</sup>, Joss Wiese<sup>9,13</sup>, Farzaneh Ziaee<sup>14</sup>, Sadia Bari<sup>1</sup>, Michael Burt<sup>2</sup>, Jochen Küpper<sup>6,8,9,13</sup>, Anouk M. Rijs<sup>10,15</sup>, Daniel Rolles<sup>14</sup>, Simone Techert<sup>1,16</sup>, Per Eng-Johnsson<sup>1,4</sup>, Mark Brouard<sup>2</sup>, Claire Vallance<sup>2</sup>, Bastian Manschwetus<sup>1</sup> and Melanie Schnell<sup>1,3</sup>

1. Deutsches Elektronen-Synchrotron DESY, Hamburg, Germany
2. The Chemistry Research Laboratory, University of Oxford, Oxford, United Kingdom
3. Institute of Physical Chemistry, Christian-Albrechts-Universität zu Kiel, Kiel, Germany
4. Department of Physics, Lund University, Lund, Sweden
5. Physics Department, University of Gothenburg, Gothenburg, Sweden
6. The Hamburg Centre for Ultrafast Imaging (CUI), Universität Hamburg, Hamburg, Germany
7. European XFEL, Schenefeld, Germany
8. Department of Physics, Universität Hamburg, Hamburg, Germany
9. Center for Free-Electron Laser Science (CFEL) DESY, Hamburg, Germany
10. Radboud University, FELIX Laboratory, Nijmegen, The Netherlands
11. Van't Hoff Institute for Molecular Sciences, University of Amsterdam, Amsterdam, The Netherlands
12. Saint Petersburg State University, Saint Petersburg, Russia
13. Department of Chemistry, Universität Hamburg, Hamburg, Germany
14. J.R. Macdonald Laboratory, Department of Physics, Kansas State University, Manhattan, KS, USA
15. Division of BioAnalytical Chemistry, Vrije Universiteit Amsterdam, Amsterdam, The Netherlands
16. Institute for X-Ray Physics, Georg-August-Universität, Göttingen, Germany

# An ultrafast photoprotection mechanism against radiation damage

Real-time tracking of electron dynamics — using attosecond technology — allows preventing dissociation of a DNA building block

Ionising radiation causes damage to DNA when bonds are broken, and a better understanding of the ionisation and dissociation of its subunits would have implications beyond the scope of physical chemistry. We tracked, in real time, the photofragmentation of the DNA subunit adenine ionised by an extreme ultraviolet (XUV) attosecond pulse. We found that ultrafast electronic rearrangement before the atoms start to move opens up an efficient stabilisation pathway, in which a second ionisation step by a shortly delayed laser pulse leads to the production of structurally intact and stable doubly charged adenine.

The interaction of ionising radiation with large biomolecules such as DNA is complex, involving the subunits and the environment. In a bottom-up approach, the study of photoionisation in isolated nucleic-acid bases allows the primary relaxation mechanisms to be identified in the absence of environmental effects. In particular, removal of a core or inner-valence electron leads to an internal electronic rearrangement, often governed by correlated processes such as charge migration, shake-up, Auger-Meitner decay or interatomic Coulombic decay (ICD). These processes may initiate a chain of events leading to fragmentation, i.e. damage, and they occur on an extremely

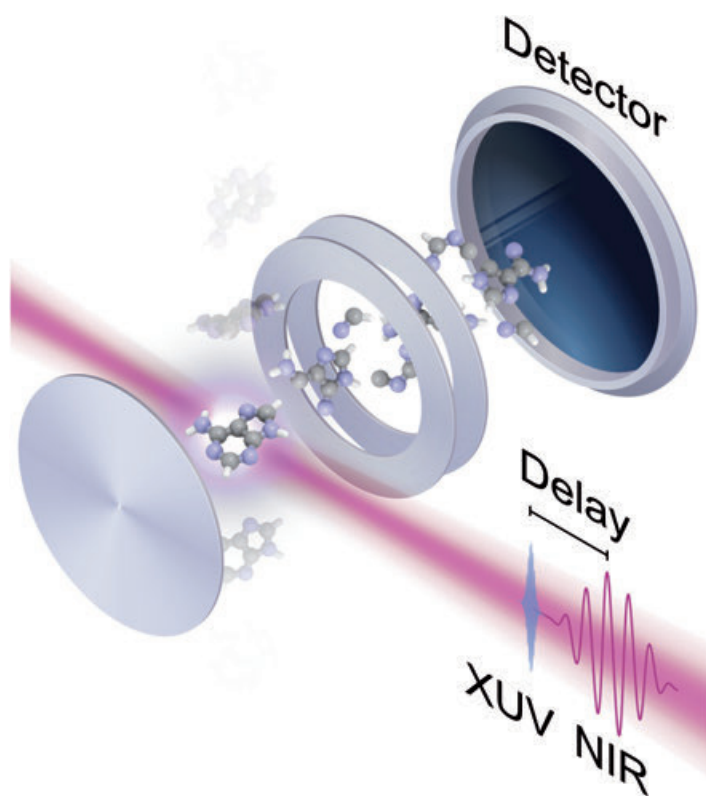
fast time scale now accessible by attosecond laser technology [1]. We report the first few-femtosecond time-resolved study of the dissociative dynamics of the nucleic-acid base adenine, with the motivation to track many-body effects *before* non-adiabatic effects take place, and potentially take advantage of them to control the molecular dissociation.

In our experiment (Fig. 1), adenine is ionised by an isolated sub-300-as pulse containing XUV photon energies from 15 to 35 eV, very similar to the kinetic energy range where DNA damage by secondary electrons is most likely to occur [2]. A waveform-controlled 4 fs near-infrared (NIR) probe pulse is combined with the XUV pump pulse using an interferometric approach. Adenine is sublimated and carried to the laser interaction region where the mass spectrum of the resulting ions is recorded as function of the pump-probe delay. Upon XUV ionisation, adenine shows a relatively low photostability with more than 80% of the ion mass spectrum consisting of fragments. Further deposition of energy by the NIR pulse leads to an overall increase of fragmentation. In particular, the yield of small fragment ions is enhanced at the expense of large fragments, indicating that the combination of XUV and NIR pulses leads to further excitation and therefore more efficient bond breaking. One could thus assume that the only effect of using a control NIR laser pulse would be to decrease the photostability of the XUV-ionised molecule.

However, an intriguing observation in the delay-dependent mass spectrum is the appearance of the adenine dication,

Figure 1

Adenine is exposed to an XUV attosecond pulse and an NIR pulse at an adjustable delay. A mass spectrometer detects the resulting ions. This figure is licensed under CC BY 4.0.



i.e. the doubly charged intact adenine molecule, at small positive delays as reported in Fig. 2. Although the XUV spectrum extends well above the dication's 23.5 eV appearance energy, we hardly observe it with the XUV pulse alone. In the process responsible for producing the dication, the added NIR pulse must somehow not facilitate dissociation but surprisingly stabilise the molecule through ionisation.

Thanks to the extremely high temporal resolution of our experimental apparatus, it is clear that to accurately fit the time-dependent yield of the adenine dication we need to include a short non-zero rise-time parameter ( $\tau_1$ ) of around 2.3 fs, unlike for the other ions where the step can be approximated as instantaneous. On the one hand, such a very short rise time suggests that an electronic rearrangement is involved in the formation of the adenine dication, on the other hand, it is puzzling for several reasons. First, inner-valence electronic relaxations are often assumed to be completed within a femtosecond. Second, nuclear motion would not be expected to make much of a difference so quickly. In order to disclose the origin of our experimental observation, an advanced theoretical model using the non-equilibrium Green's function method was employed. With the capability of capturing, with unique accuracy, the role of electron correlations, the time-dependent simulation led to the following explanation: The dication is efficiently produced only after an electronic rearrangement (shake-up) has put an electron in a specific high-lying unoccupied state which turns out to take a few femtoseconds. Once this state is populated, there is a higher probability for the NIR pulse to remove a second electron and to promote the molecule in a stable state of the dication. Without this last and crucial ionisation step, the molecule relaxes via various fragmentation pathways.

In conclusion, a multi-electron process was tracked in real-time in ionised adenine which has not been done experimentally for any polyatomic molecule before. That we achieve a degree of control over the molecular dissociation by taking advantage of the electronic dynamics and acting with extreme time resolution before notable nuclear motion begins, is promising for the outlook of chemistry at the natural time scale of electronic dynamics [3,4].

Author contact: [Francesca Calegari, francesca.calegari@desy.de](mailto:francesca.calegari@desy.de)

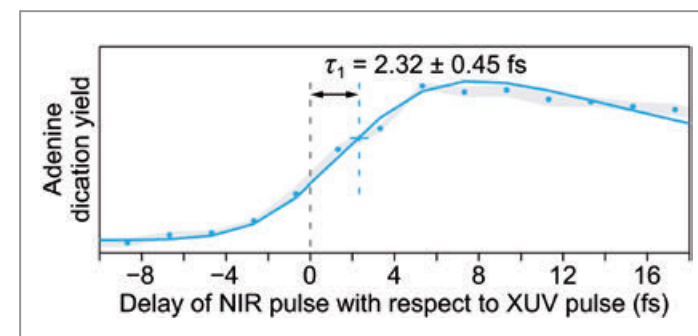


Figure 2

Adenine dication signal as function of pump-probe delay.

## References

1. M. Nisoli, P. Decleva, F. Calegari, A. Palacios and F. Martín, 'Attosecond electron dynamics in molecules', *Chem. Rev.* **117**, 10760–10825 (2017).
2. M. A. Huels, B. Boudaïffa, P. Cloutier, D. Hunting and L. Sanche, 'Single, double, and multiple double strand breaks induced in DNA by 3–100 eV electrons', *J. Am. Chem. Soc.* **125**, 4467–4477 (2003).
3. F. Lépine, M. Y. Ivanov and M. J. J. Vrakking, 'Attosecond molecular dynamics: fact or fiction?', *Nat. Photonics* **8**, 195–204 (2014).
4. A. Palacios and F. Martín, 'The quantum chemistry of attosecond molecular science', *Wiley Interdiscip. Rev. Comput. Mol. Sci.* **10**, e1430 (2019).

## Original publication

'Real-time observation of a correlation-driven sub 3 fs charge migration in ionised adenine', *Communications Chemistry* **4**, 73 (2021). DOI: 10.1038/s42004-021-00510-5



Erik P. Månsson<sup>1,2</sup>, Simone Latini<sup>3</sup>, Fabio Covito<sup>3</sup>, Vincent Wanie<sup>1,2,4</sup>, Mara Galli<sup>1,5</sup>, Enrico Peretto<sup>6,7</sup>, Gianluca Stefanucci<sup>7,8</sup>, Hannes Hübener<sup>3</sup>, Umberto De Giovanni<sup>3,9</sup>, Matteo C. Castrovilli<sup>10</sup>, Andrea Trabattoni<sup>1</sup>, Fabio Frassetto<sup>11</sup>, Luca Poletto<sup>11</sup>, Jason B. Greenwood<sup>12</sup>, François Légaré<sup>4</sup>, Mauro Nisoli<sup>2,5</sup>, Angel Rubio<sup>3,13</sup> and Francesca Calegari<sup>1,2,14</sup>

1. Center for Free-Electron Laser Science (CFEL), DESY, Hamburg, Germany
2. Inst. for Photonics and Nanotechnologies CNR-IFN, Milano, Italy
3. Max Planck Institute for the Structure and Dynamics of Matter and Center for Free-Electron Laser Science, Hamburg, Germany
4. INRS-EMT, Varennes, Canada
5. Department of Physics, Politecnico di Milano, Milano, Italy
6. CNR-ISM, Division of Ultrafast Processes in Materials (FLASHit), Monterotondo Scalo, Italy
7. Dipartimento di Fisica, Università di Roma Tor Vergata, Roma, Italy
8. INFN, Sezione di Roma Tor Vergata, Roma, Italy
9. Dipartimento di Fisica e Chimica, Università degli Studi di Palermo, Palermo, Italy
10. Inst. for the Structure of Matter CNR-ISM, Monterotondo Scalo, Italy
11. Inst. for Photonics and Nanotechnologies CNR-IFN, Padova, Italy
12. Centre for Plasma Physics, School of Maths and Physics, Queen's University Belfast, Belfast, UK
13. Center for Computational Quantum Physics (CCQ), The Flatiron Institute, New York, USA
14. Institut für Experimentalphysik, Universität Hamburg, Hamburg, Germany

# Attoseconds on a chip

Integrated electronic platform measures optical waveforms in the time-domain

At the core of photon science is the study of how matter interacts with light. Common techniques rely on the measurement of the frequency content of light, while losing critical information on the phase of the wave. It is highly desirable to measure the full waveform in time to gain the complete set of amplitude and phase information. Time-domain measurement techniques are well established in the microwave to THz frequency range and have been fundamental in understanding the full response of matter to electromagnetic radiation. Bringing such tools to higher frequencies, up to the PHz regime, can potentially enable exciting new insights into the generation of high harmonics in solids or other highly non-linear phenomena.

Time-domain techniques require sub-cycle time resolution to fully resolve a waveform. One way is to use a sufficiently short electrical or optical gate to measure the instantaneous electric field of the wave without smearing out the individual oscillations. A standard technique to tackle this problem is to use electro-optical sampling to measure low frequency GHz and THz up to mid-infrared waves. Recently it was demonstrated that temporal electric field echoes in the mid-infrared of excited biological molecules can be efficiently captured. These field echoes provide superior molecular sensitivity compared to conventional spectroscopic techniques [1]. However, electro-optical sampling has not been demonstrated to measure waveforms shorter in wavelength than the near-infrared. To further push the envelope in bandwidth, techniques like attosecond streaking have been developed which use attosecond-short XUV pulses to record waveforms up to the PHz bandwidth [2]. While attosecond streaking presents a powerful technique, it is lacking in sensitivity to weak electric fields. Most light-matter interactions result in very weak signatures in the

electric field and therefore cannot be detected with attosecond streaking methods.

Recently it has been demonstrated that attosecond electron pulses can be generated by field emission from plasmonic nanoantennas [3,4]. In our work, we demonstrate that attosecond electron bursts from such a nanoantenna can sample near-infrared electric fields, with sub-cycle precision in the time domain corresponding to a maximum frequency of  $\sim 0.35$  PHz. The total energy of the electric field can be just 5 fJ. This technique is less complex in its experimental requirements, capable of operating in ambient conditions using only pico-Joule optical sources. Moreover, these plasmonic nanoantennas can be fully integrated into electronic circuits without need for sophisticated detectors.

To accomplish this scheme, we generated a sub-cycle electronic gate using a 2.5-cycle near-infrared pulse at a wavelength of 1.2  $\mu\text{m}$  with 50 pJ pulse energy to collectively excite a network of plasmonic nanoantennas (Fig. 1a). The sharp

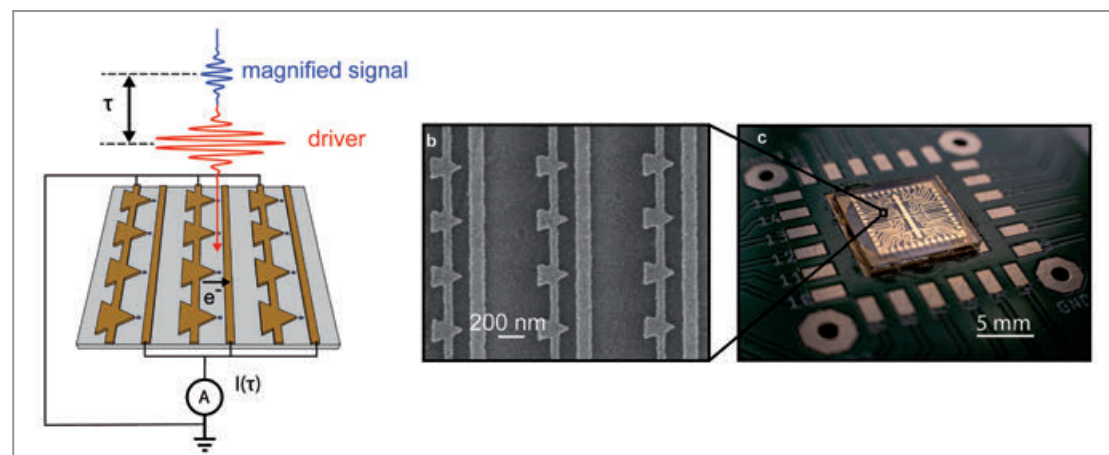


**Figure 1**  
Overview of the integrated detector. a) (left) Concept of the arrayed detector, showing the charge generation in the device by the driver pulse and the magnified signal wave. b) Scanning electron micrograph of the device. c) Photograph of the detector integrated to a printed circuit board.

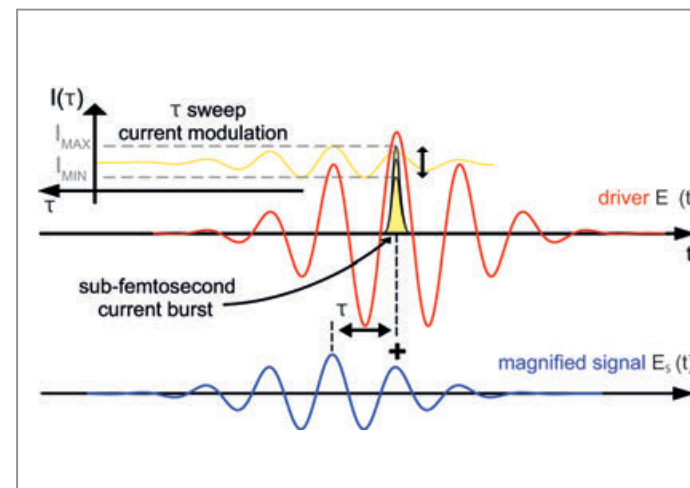


**Figure 2**  
Sketch of the optical field sampling process. The driver pulse generates an attosecond electron burst, that is modulated in its amplitude by the weak signal waveform. The current is generated as a function of delay between signal and driver and is proportional to the signal itself. Here, the signal is magnified for better visibility; the actual ratio is  $\sim 100:1$  (driver to signal).

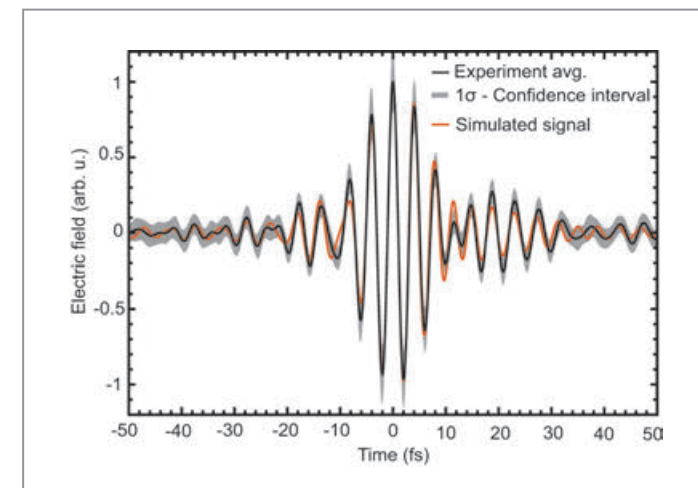


**Figure 3**  
Averaged electrical field and its standard deviation compared to the expected simulated signal.

tips of the nanoantennas locally enhance the incident electric field by a factor of around 20 to provide enough field strength for field emission of electrons from the antennas' surface. Due to its high non-linearity, the field emission generates an electron pulse with a duration of around 600 as. This electron pulse is much shorter than a half-cycle of the exciting wave ( $\sim 2$  fs) and is collected by an anode wire separated by 50 nm from the antenna tip (Fig. 1b). The attosecond generation process of the electron pulse creates the necessary resolution to sample a second electromagnetic waveform. When a sufficiently weak second field is present during the short generation time, it linearly perturbs the number of generated electrons. By simply measuring the generated current as a function of delay between the electron gate pulse and the second waveform (Fig. 2), the second waveform is recorded.

The results of our measurement are shown in Fig. 3 and demonstrate the detection of the normalised local electric field at the antenna tip. The measured current is proportional to the measured signal's electric field and is estimated to be at its peak around 5 MV/m with an estimated noise floor of around 500 kV/m. When comparing the recorded waveform to the expected waveform, it shows that our method clearly retrieves the local field of the nanoantenna. With *a priori* knowledge of the incident laser field, our technique can even measure the characteristic properties of the nanoantenna itself. These results suggest that by using the 600 as electron generation process, measuring frequencies of even higher bandwidth of up to 1 PHz are feasible.

The extreme bandwidth of our measurement technique combined with a high sensitivity down to only femtojoules will allow direct time-domain studies of highly non-linear phenomena such as high-harmonic generation in solids.

Experiments driving solids with strong THz fields exhibit highly non-linear responses, which can be captured over many octaves with a single measurement setup. Another avenue for exploration will be the fingerprinting of biological molecules in the notoriously hard to detect mid-infrared spectral region, enabling efficient detection of many species of molecules.

Overall, our results enable exciting possibilities for future experiments of sampling electric waveforms in the time-domain over broad frequency ranges with only a single on-chip detector.

Author contact: Felix Ritzkowsky, [felix.ritzkowsky@desy.de](mailto:felix.ritzkowsky@desy.de)

## References

1. I. Pupeza et al., 'Field-resolved infrared spectroscopy of biological systems', *Nature* 577, 52–59 (2020).
2. G. M. Rossi et al., 'Sub-cycle millijoule-level parametric waveform synthesizer for attosecond science', *Nat. Photonics* 14, 629–635 (2020).
3. M. Ludwig et al., 'Sub-femtosecond electron transport in a nanoscale gap', *Nat. Phys.* 16, 341–345 (2020).
4. P. D. Keathley, W. P. Putnam, P. Vasireddy, R. G. Hobbs, Y. Yang, K. K. Berggren and F. X. Kärtner, 'Vanishing carrier-envelope-phase-sensitive response in optical-field photoemission from plasmonic nanoantennas', *Nat. Phys.* 15, 1128–1133 (2019).

## Original publication

'On-chip sampling of optical fields with attosecond resolution', *Nature Photonics* 15, 456–460 (2021).  
DOI: 10.1038/s41566-021-00792-0



Mina R. Bionta<sup>1,2</sup>, Felix Ritzkowsky<sup>1,2</sup>, Marco Turchetti<sup>1</sup>, Yujia Yang<sup>1</sup>, Dario Cattozzo Mor<sup>1</sup>, William P. Putnam<sup>3</sup>, Franz X. Kärtner<sup>2</sup>, Karl K. Berggren<sup>1</sup> and Phillip D. Keathley<sup>1</sup>

1. Massachusetts Institute of Technology, Cambridge, USA
2. Deutsches Elektronen-Synchrotron DESY, Hamburg, Germany
3. University of California at Davis, Davis, USA

# Chirping FEL pulses

## Spectro-temporal measurements in transient absorption spectroscopy

Time-resolved ultrafast spectroscopy with atomic site specificity is one of the key applications of free-electron lasers (FELs). Hereby transient absorption spectroscopy, an all-optical technique which is well-established in the infrared and visible regime, creates a promising new direction for FELs. In a nutshell, one measures the absorption spectrum of an FEL pulse after transmission through a target (gas, liquid, plasma or even solid) by dispersing the pulses with a grating-based spectrometer. Probing with a second FEL pulse at various time delays, one can thus time-resolve the initiated electronic dynamics. Independently tuning the photon energies of the pump and probe pulses increases the possibilities of the technique further.

One particular benefit of transient absorption spectroscopy is its combined high spectral and temporal resolution which is not limited by the Fourier time-bandwidth relationship. An absorption measurement of a sample is hereby recorded through the detection of the attenuated light in forward direction with a grating-based photon spectrometer. Individual spectral lines can be covered and resolved within the spectral bandwidth of the probing FEL pulses. While it is this latter bandwidth, which sets the ultimate limit on the time resolution of the experiment, the spectroscopic resolution is only determined by the resolving power of the grating spectrometer. For a controlled experiment, it is crucial to measure the arrival

times of the different spectral components of the FEL pulses *in situ*.

Here, we utilise an ultrafast atomic plasma switch which allows us to measure the spectro-temporal distribution of FEL pulses during a transient absorption experiment in neon. The experiment has been carried out at the open-port beamline BL2 at FLASH. It is equipped with a split-and-delay unit [1], which cuts the FEL beam profile in two halves, spatially separate. Subsequently, two identical copies ('pump' and 'probe') of the FEL pulses with a variable temporal delay are focused into a moderately dense neon gas target. After the interaction the probe pulse is

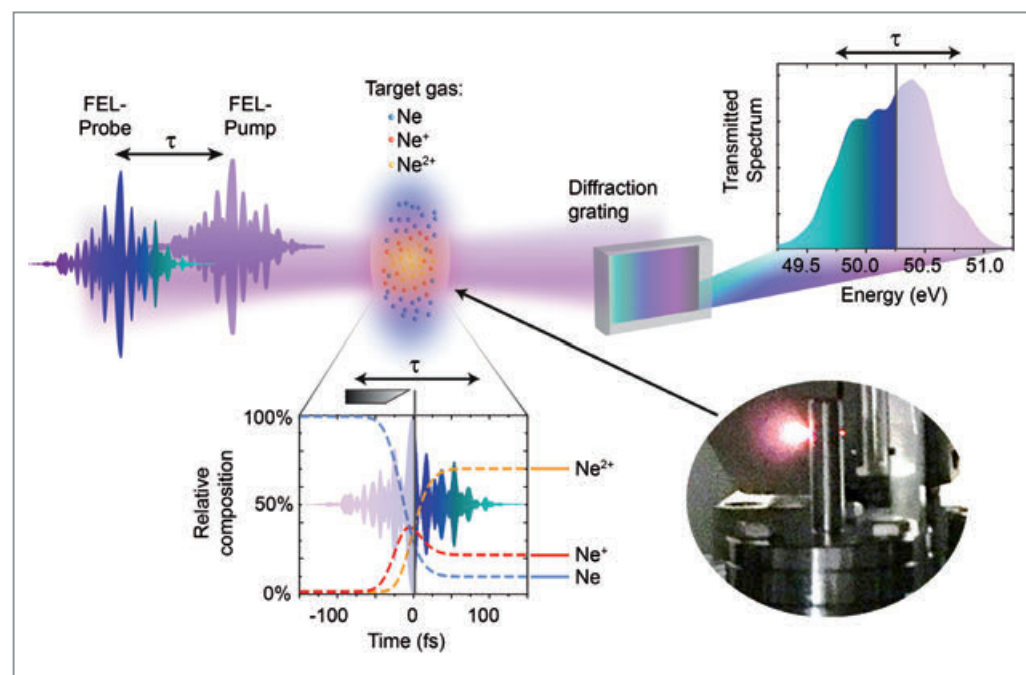
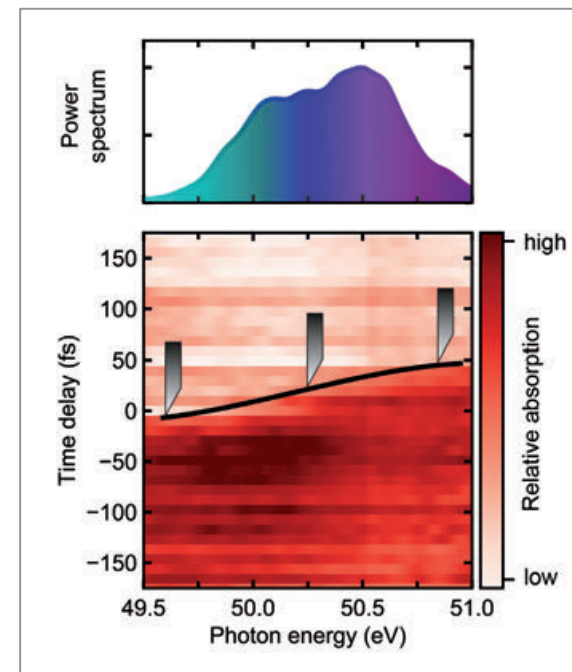


Figure 1

Schematic setup of the pump-probe experiment for characterising the chirp of FEL pulses in transient absorption spectroscopy. Two copies of the same FEL pulse are focused into a moderately dense neon target (see also photographic image, with visible radiation due to plasma recombination) where the pump pulse rapidly ionises the target up to  $\text{Ne}^{2+}$ . The time-delayed probe pulse, after transmission through the target, is spectrally dispersed with a grating spectrometer, detecting a change in attenuation of the target for different spectral components at different delays. The calculated abundancies of the different ionic species and the temporal knife-edge action of this plasma switch due to the pump pulse, which is centred at time zero, is depicted in the lower inset.

Figure 2  
Absorption of the probe pulse as a function of the photon energy and the time delay relative to the pump pulse. The pump-induced increase in transmission (from high to low absorption) through the neon target shows a characteristic spectro-temporal trend which is indicated by the solid black line, where the temporal plasma switch transmits different spectral components of the probe pulse at different delays as indicated by the knife pictograms.



again spatially separable by means of mechanical slits and is detected with an XUV grating spectrometer.

The measurement technique and experimental setup is described in more detail in Ref. [2] and is illustrated in Fig. 1. The first pump pulse efficiently ionises the target, such that, up to 70% doubly charged  $\text{Ne}^{2+}$  ions are rapidly produced. These are nearly transparent to XUV radiation while neutral and singly charged neon still absorb quite strongly. The plasma target thus acts like an ultrafast switch for the transmission of the probe pulse where the neon atoms respond quasi instantaneously to the pump pulse following the well-understood effect of atomic photoionisation of valence electrons. Depending on the time delay between pump and probe pulses, only those parts of the FEL probe pulse are then efficiently transmitted that see the ionised transparent medium. Due to the action of this ultrafast atomic plasma switch, which acts like a temporal knife edge, the arrival times of the FEL pulse's different spectral components are directly encoded in the probe-pulse's transmission spectra.

Figure 2 shows the experimental result for the relative absorption as a function of the photon energy and the time delay of pump and probe FEL pulses. The frequency power spectrum of the relatively broadband pulses is depicted in the upper region of the figure. In the case shown here, the higher photon energies of the probe pulse arrive ahead in time and are therefore only transmitted at a greater positive delay (the pump pulse arrives first) than the lower-frequency components that follow later. This is indicated in the figure by the knife symbols. The temporal absorption edge is therefore tilted and slightly curved. From this behaviour, the temporal frequency evolution in the pulses, i.e. their chirp, can be directly determined. This is also in good agreement with simulations.

This new method allows direct access to the temporal and spectral signature of the FEL pulses within a transient absorption spectroscopy experiment. Knowing the arrival times of the different frequency components not only improves the temporal resolution of an experiment when probing different electronic transitions, but also the spectro-temporal waveform of the FEL pulses can be further optimised for more efficient pumping, e. g. for triggering a chemical reaction in a molecule from a specific atomic site. The realisation in the short-wavelength XUV to

X-ray range allows for a much more precise control of individually selectable atoms in larger molecules. It is also a key-building block for non-linear multidimensional spectroscopy in the X-ray range with ultrashort broadband attosecond (X)FEL pulses.

Author contact: Christian Ott, christian.ott@mpi-hd.mpg.de  
Thomas Ding, thomas.ding@mpi-hd.mpg.de  
Thomas Pfeifer, thomas.pfeifer@mpi-hd.mpg.de

## References

1. M. Wöstmann, R. Mitzner, T. Noll, S. Roling, S. Siemer, F. Siewert, S. Eppenhoff, F. Wahler and H. Zacharias, 'The XUV split-and-delay unit at beamline BL2 at FLASH', *J. Phys. B: At. Mol. Opt. Phys.* **46**, 164005 (2013).
2. T. Ding, M. Rebholz, L. Aufleger, M. Hartmann, V. Stooß, A. Magunia, P. Birk, G. D. Borisova, C. da Costa Castanheira, P. Rupprecht, Y. Mi, T. Gaumnitz, Z.-H. Loh, S. Roling, M. Butz, H. Zacharias, S. Düsterer, R. Treusch, C. Ott and T. Pfeifer, 'XUV pump-XUV probe transient absorption spectroscopy at FELs', *Faraday Discuss.* **228**, 519–536 (2021).

## Original publication

'Measuring the frequency chirp of extreme-ultraviolet free-electron laser pulses by transient absorption spectroscopy', *Nature Communications* **12**, 643 (2021). DOI: 10.1038/s41467-020-20846-1



Thomas Ding<sup>1</sup>, Marc Rebholz<sup>1</sup>, Lennart Aufleg<sup>2</sup>, Maximilian Hartmann<sup>1</sup>, Veit Stooß<sup>1</sup>, Alexander Magunia<sup>1</sup>, Paul Birk<sup>1</sup>, Gergana Dimitrova Borisova<sup>1</sup>, David Wachs<sup>1</sup>, Carina da Costa Castanheira<sup>1</sup>, Patrick Rupprecht<sup>1</sup>, Yonghao Mi<sup>1</sup>, Andrew R. Attar<sup>2</sup>, Thomas Gaumnitz<sup>2</sup>, Zhi-Heng Loh<sup>4</sup>, Sebastian Roling<sup>5</sup>, Marco Butz<sup>5</sup>, Helmut Zacharias<sup>5</sup>, Stefan Düsterer<sup>6</sup>, Rolf Treusch<sup>6</sup>, Arvid Eislage<sup>6</sup>, Stefano M. Cavalletto<sup>1</sup>, Christian Ott<sup>1</sup> and Thomas Pfeifer<sup>1</sup>

1. Max-Planck-Institut für Kernphysik, Heidelberg, Germany
2. Department of Chemistry, University of California, Berkeley, USA
3. Laboratorium für Physikalische Chemie, ETH Zürich, Switzerland
4. Division of Chemistry and Biological Chemistry, and Division of Physics and Applied Physics, School of Physical and Mathematical Sciences, Nanyang Technological University, Singapore
5. Physikalisches Institut, Westfälische Wilhelms-Universität Münster, Germany
6. Deutsches Elektronen-Synchrotron DESY, Hamburg, Germany

# Towards ultimate time resolution in speckle correlation dynamics

Recording nanosecond dynamics with pulsed synchrotron light

Recording speckle movies via X-ray photon correlation spectroscopy (XPCS) enables the study of slow dynamics in complex systems at synchrotron sources on time scales from milliseconds to hours. The time resolution of XPCS is defined by the detector frame rate and the X-ray pulse repetition rate. Recent progress in ultrafast detector development brought a very promising prospect into perspective for utilising the MHz pulsed nature of storage rings to extend the time resolution down to nanoseconds. By resolving single X-ray pulses of PETRA III with the AGIPD detector we measured nanosecond equilibrium dynamics in a colloidal liquid, marking the first demonstration of pulse-resolved XPCS at a storage ring. Successful demonstration of this technique paves the way to study dynamics of very relevant soft matter biological systems at future diffraction-limited storage rings such as PETRA IV.

Recording X-ray speckle correlations via XPCS is a powerful tool to study slow dynamics in various complex and disordered systems in condensed matter including colloids, polymers, capillary fluctuations, metallic glasses and water [1]. Nowadays, the accessible timescales in XPCS measurements are set by X-ray area-detector technology, the limited coherent flux and the X-ray pulse repetition frequency. At up-to-date 3rd generation storage rings, typically, time scales from hours down to milliseconds can be accessed. Although, 3rd generation synchrotron sources offer MHz pulse repetition rates, commercially available 2D X-ray detector systems provide frame rates only up to few kilo-

hertz. Advanced techniques have been developed and demonstrated at X-ray free-electron lasers (FELs) to access femto- to nanosecond dynamics independent of the detector frame rate via split-pulse XPCS [2] or X-ray speckle visibility spectroscopy (XSVS) [3]. However, split-pulse XPCS requires special X-ray optics while XSVS requires very precise control of the X-ray pulse duration. Recent significant improvements in X-ray detector readout time and detection efficiency allowed to employ the intrinsic time structure of the storage ring to XPCS. In particular, the AGIPD detector has been developed for resolving MHz pulsed X-ray beams.

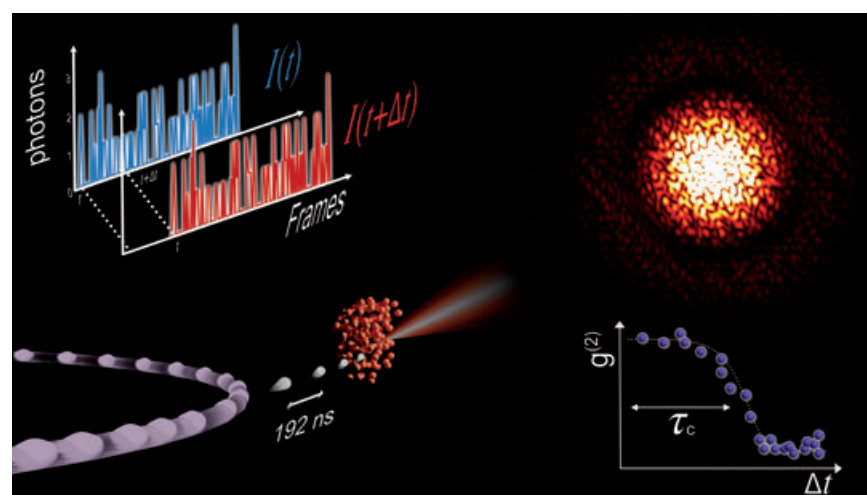


**Figure 1** Sketch of the XPCS experiment at the coherence beamline P10 of PETRA III. X-ray pulses are delivered to the sample position with 192 ns time separation. Speckle patterns are recorded in a small-angle X-ray scattering geometry with the AGIPD. Sample dynamics are acquired from intensity auto-correlation function (upper-left). The intensity auto-correlation function  $g^{(2)}$  provides access to the characteristic time  $\tau_c$  of the investigated system (bottom-right).

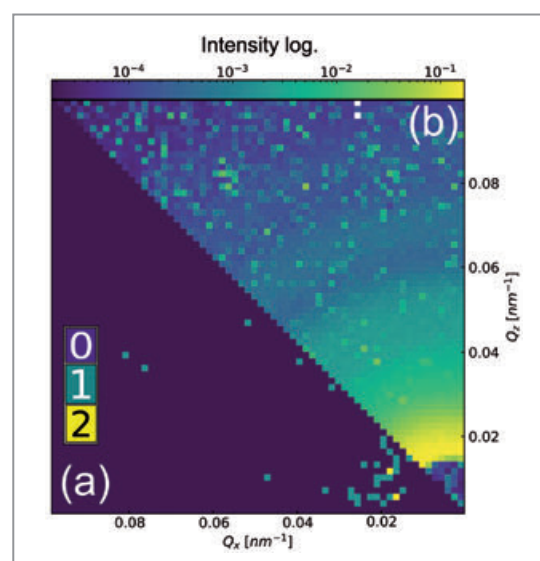
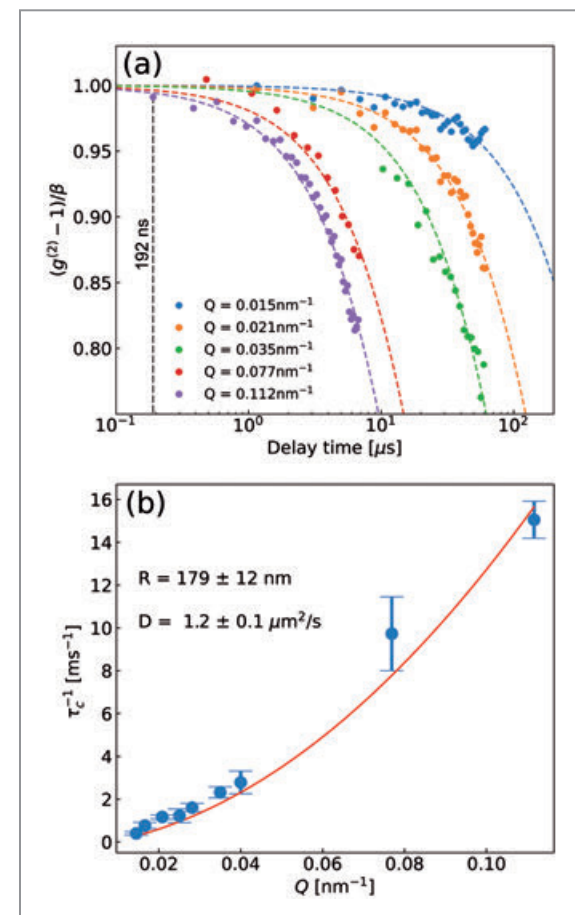


**Figure 2** a) Single-pulse speckle pattern showing single and two-photon scattering events. b) Sum of one million single-pulse speckle patterns.

**Figure 3** a) Normalised intensity auto-correlation functions measured with 192 ns time resolution. The first correlation point is denoted by the vertical dashed line. Fits of the corresponding  $g^{(2)}$  functions are given by dashed lines. b) The solid line shows a fit to  $\tau_c^{-1} = D_0 Q^2$ , the particle radius  $R$  is obtained from the Stokes-Einstein relation.



Low coherent flux of synchrotron sources presents a challenge in acquiring sufficient photon statistics on pulse to pulse basis. Up to now only FEL studies have proven that it is possible to obtain meaningful speckle patterns from low intensity scattering patterns ( $< 0.005$  photons/pixel). Here, we demonstrate the feasibility of using single pulses of PETRA III together with the AGIPD to study nanosecond dynamics in a system of colloidal particles via XPCS.

We have carried out conventional XPCS with 8 keV photons at the coherence beamline P10 of PETRA III. The experimental scheme is shown in Fig. 1. The 40-bunch filling pattern of the storage ring delivered X-ray pulses, each separated by 192 ns. Colloidal silica nanoparticles with a radius of 180 nm dispersed in water were filled into a 700  $\mu\text{m}$  thick glass capillary. The challenge of the experiment was to extract temporal speckle correlations from extremely weak scattering patterns originating from individual X-ray pulses. The collected scattered intensity was analysed by taking into account the analog-to-digital conversion and gain values of the AGIPD to resolve single and two-photon events from individual speckle patterns (Fig. 1, bottom-right).

In XPCS, each speckle pattern collected in the far field detection plane corresponds to the spatial arrangement of the colloidal particles. Upon motion of the particles, the corresponding speckle pattern changes accordingly. Hence, the dynamics of the investigated sample is traced by measuring temporal speckle correlations of intensity fluctuations and calculating an auto-correlation function  $g^{(2)}$ . The value of the  $g^{(2)}$  function at time zero corresponds to the speckle contrast and is related to the coherence properties of the X-ray source. In our colloidal liquid,  $g^{(2)}$  follows a single exponential decay function with a characteristic time  $\tau_c$  of the system. For  $\tau \gg \tau_c$ , the lack of correlation between the speckle patterns results in  $g^{(2)}$  converging to unity. Figure 3a shows the normalised auto-correlation functions as a function of delay time with 192 ns resolution for varying wave-vector transfer  $Q$ . For Brownian diffusion,  $\tau_c$  is related to the free particle diffusion coefficient via  $D_0 = (\tau_c Q^2)^{-1}$ . Figure 3b shows the corresponding fit of the model to the data providing  $\tau_c$ , which is very good agreement with the expected diffusion coefficient.

In conclusion, the advent of future diffraction-limited storage rings and the technological development of ultrafast

detectors pave the way for XPCS studies down to nanosecond timescales. The study is also very timely in the context of the ongoing PETRA IV project, i.e. the upgrade of PETRA III to a diffraction-limited storage ring with expected 400 times higher coherent photon flux.

Author contact: Wonhyuk Jo, [wonhyuk.jo@desy.de](mailto:wonhyuk.jo@desy.de)  
Wojciech Roseker, [wojciech.roseker@desy.de](mailto:wojciech.roseker@desy.de)

## References

1. F. Lehmkuhler, W. Roseker and G. Grubel, 'From femtoseconds to hours—measuring dynamics over 18 orders of magnitude with coherent X-rays', *Appl. Sci.* **11**, 6179 (2021).
2. W. Roseker et al., 'Towards ultrafast dynamics with split-pulse X-ray photon correlation spectroscopy at free electron laser sources', *Nat. Commun.* **9**, 1704 (2018).
3. F. Perakis et al., 'Coherent X-ray reveal the influence of cage effect on ultrafast water dynamics', *Nat. Commun.* **9**, 1917 (2018).

## Original publication

"Nanosecond X-ray photon correlation spectroscopy using pulse time structure of a storage-ring source", *International Union of Crystallography Journal* **8**, 124–130 (2021). DOI: 10.1107/S2052252520015778

Wonhyuk Jo<sup>1</sup>, Fabian Westermeier<sup>1</sup>, Rustam Rysov<sup>1</sup>, Olaf Leupold<sup>1</sup>, Florian Schulz<sup>2,3</sup>, Steffen Tober<sup>2</sup>, Verena Markmann<sup>1</sup>, Michael Sprung<sup>1</sup>, Allesandro Ricci<sup>1</sup>, Torsten Laurus<sup>1</sup>, Allahgholi Aschkan<sup>1</sup>, Alexander Klyuev<sup>1</sup>, Ulrich Trunk<sup>1</sup>, Heinz Graafsma<sup>1</sup>, Gerhard Grubel<sup>1,3</sup> and Wojciech Roseker<sup>1</sup>

1. Deutsches Elektronen-Synchrotron DESY, Hamburg, Germany
2. Institute of Physical Chemistry, Universität Hamburg, Hamburg, Germany
3. The Hamburg Centre for Ultrafast Imaging (CUI), Universität Hamburg, Hamburg, Germany



# New XFEL techniques to understand rapid synthesis at high pressures and dynamics of planetary interiors

Pulsed heating with the European XFEL opens a new pathway to high-pressure synthesis

Scientists using static high-pressure experiments have dreamed of performing time resolved X-ray diffraction experiments with a MHz probe rate during laser heating or dynamic compression within a Diamond Anvil Cell (DAC). By doing so, contamination of the samples through e.g. the diffusion of carbon from the anvil or other elements enclosing the sample can be avoided, which becomes an increasing challenge at higher pressures and temperatures. Such experiments are now possible at the High-Energy-Density (HED) instrument of the European XFEL by exposing samples in a DAC to 20 fs long X-ray pulses at 18 keV and MHz repetition rates. Furthermore, the highly intense X-ray pulses can be used to heat a sample mixture and synthesise compounds such as  $\epsilon$ -iron nitride very rapidly. This new setup is enabling unprecedented time resolved X-ray diffraction and imaging experiments, opening new avenues to explore the dynamics of planetary interiors or new synthesis pathways to yet unknown materials.

Nitrides consisting of nitrogen (N) and transition metal elements like iron (Fe) make up an important class of industrially relevant materials that exhibit outstanding magnetic, electrical and mechanical properties. In particular  $\epsilon$ -iron nitride ( $\epsilon$ -Fe<sub>3</sub>N<sub>1+x</sub>) has been studied extensively because of its usage in high-density magnetic recording media, as catalyst and high wear- or corrosion-resistant materials [1].

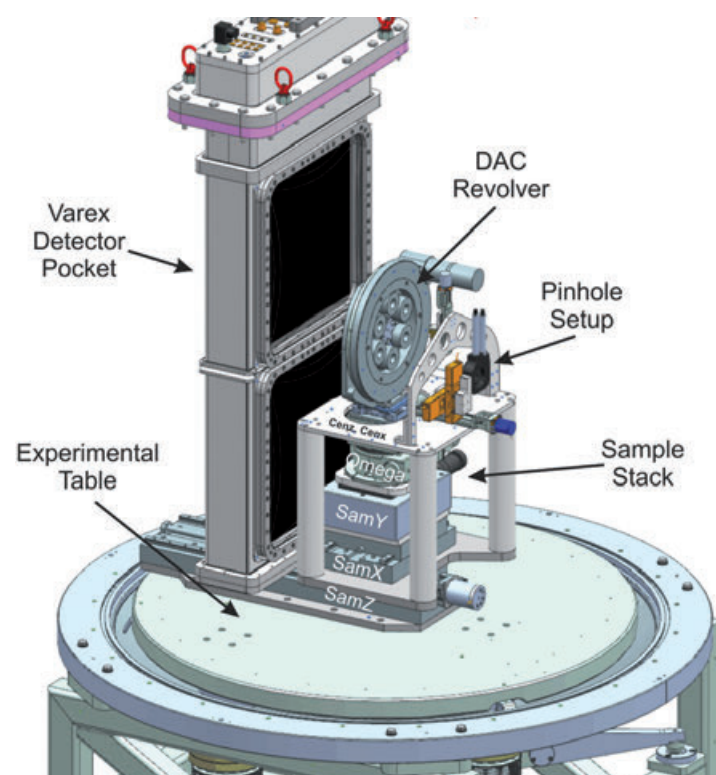


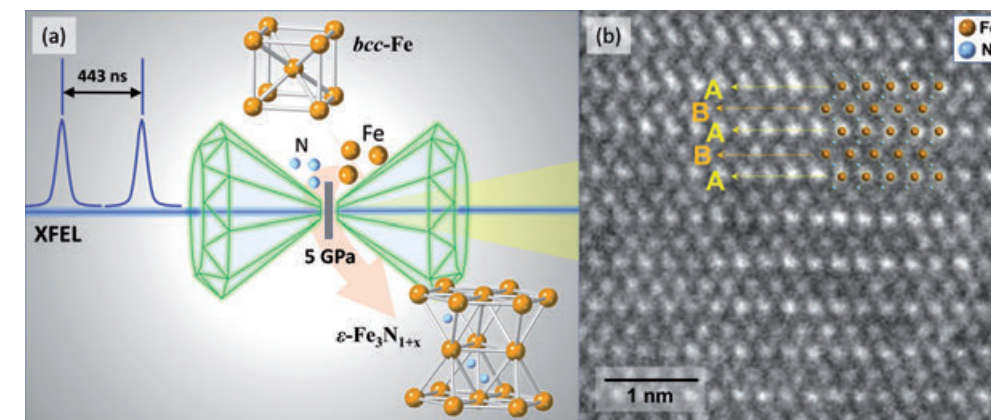
Figure 1  
CAD drawing of the sample stack and area detector.

However, the synthesis of a stoichiometrically pure and homogeneous form of  $\epsilon$ -iron nitride is rather challenging because of the inability to control the reaction rate of nitrogen and iron in a conventional high-pressure and -temperature setup. Using the new static DAC setup at the HED instrument (Fig. 1) it was possible to rapidly synthesise non-stoichiometric but homogenous  $\epsilon$ -Fe<sub>3</sub>N<sub>1+x</sub> with  $x = 0.33$  using 20 fs pulses from the European XFEL arriving at a repetition rate of 2.25 MHz (Fig. 2a). 4  $\mu$ m-thin iron foil was pre-compressed in nitrogen gas to 5 GPa. When the sample was irradiated by pulses from the European XFEL repeating at every 443 ns, sample temperatures in excess of 1400 K were detected through the transformation of  $\alpha$ - to  $\gamma$ -iron and subsequently, the uniform reaction of Fe and N<sub>2</sub> along the beam path to form Fe<sub>3</sub>N<sub>1.33</sub>. This demonstrated that the activation energy provided by intense X-ray exposures with an XFEL can be coupled with the source time structure to examine the time dependence of synthesis reactions under high-pressure conditions.

The synthesis of Fe<sub>3</sub>N<sub>1.33</sub> was not only demonstrated in the 20 fs X-ray diffraction images collected at the HED instrument but was also subsequently confirmed by X-ray diffraction mapping of the irradiated area in the DAC at the beamline P02.2 at PETRA III. Further analysis of the recovered samples using the FIB and STEM, including chemical analysis, confirmed the homogeneity of the Fe<sub>3</sub>N<sub>1.33</sub> in the irradiated sample area (Fig. 2b).

Coupling intense X-ray laser pulses with sufficiently high energy to initiate distinctive chemical reactions emerges as new research field in static high-pressure science with the

Figure 2  
a) Cartoon demonstrating the synthesis of  $\epsilon$ -Fe<sub>3</sub>N<sub>1+x</sub> in the DAC using 25 fs long X-ray pulses. b) STEM image of the iron foil area irradiated by the EuXFEL X-ray beam indicating that  $\epsilon$ -iron nitride with a composition of Fe<sub>3</sub>N<sub>1.33</sub> was formed.



potential to study reaction pathways at high pressure. This is particularly true since recently the Adaptive Gain Integrating Pixel Detector (AGIPD) has become operational to collect femtosecond short diffraction images after each pump pulse providing a nanosecond movie with femtosecond snapshots into the synthesis pathway. Systematic exploration of chemical reactivity across different reactants at extreme pressures and temperatures could lead to the discovery of hitherto unknown compounds and pathways not only of industrial relevance but also for a better understanding of the chemistry of astrophysical processes.

Besides the use of the X-ray beam for the exploration and search for new fast synthesis pathways, yet other types of DAC setups at HED are planned to be used for fast compression experiments using a dynamic Diamond Anvil Cell (dDAC) [2] and a pulsed laser heating technique [3]. The latter could heat a sample such as iron with an infrared laser at very high pressures to simulate and study the core of planetary bodies such as the Earth and super earths. The methodology of pulsed laser heating and dDAC experiments have been discussed in detail by Liermann et al. 2021 (see original publication), indicating that contaminations of the sample can be avoided by rapidly exposing the sample to the short X-ray pulses of the European XFEL. In this work it was shown how a set of 25 X-ray pulses can be laid over the infrared laser heating pulse of 23  $\mu$ s duration with a 6  $\mu$ s material response [3].

In addition, fast dDAC experiments make use of the maximum pulse train length of the European XFEL of 200 (600)  $\mu$ s to collect up to 325 images on the AGIPD detector to cover a fast compression path. This may be used to explore the compression and strain dependence of phase transitions in low- and high-z materials and even the formation of amorphous ice as described recently [4] as a function of the compression rate.

Author contact:

Hanns-Peter Liermann, [hanns-peter.liermann@desy.de](mailto:hanns-peter.liermann@desy.de)  
Yongjae Lee, [yongjaelee@yonsei.ac.kr](mailto:yongjaelee@yonsei.ac.kr)  
Cornelius Strohm, [cornelius.strohm@desy.de](mailto:cornelius.strohm@desy.de)  
Stewart McWilliams, [rs.mcwilliams@ed.ac.uk](mailto:rs.mcwilliams@ed.ac.uk)

## References

1. S. Bhattacharyya, 'Iron nitride family at reduced dimensions: a review of their synthesis protocols and structural and magnetic properties', *J. Phys. Chem. C* **119**, 1601–1622 (2015).
2. Z. Jenei, H. P. Liermann, R. Husband, A. S. J. Méndez, D. Pennicard, H. Marquardt, E. F. O'Bannon, A. Pakhomova, Z. Konopkova, K. Glazyrin, M. Wendt, S. Wenz, E. E. McBride, W. Morgenroth, B. Winkler, A. Rothkirch, M. Hanfland and W. J. Evans, 'New dynamic diamond anvil cells for tera-pascal per second fast compression X-ray diffraction experiments', *Rev. Sci. Instrum.* **90**, 065114 (2019).
3. V. Cerantola, A. D. Rosa, Z. Konopkova, R. Torchio, E. Brambrink, A. Rack, U. Zastrau and S. Pascarelli, 'New frontiers in extreme conditions science at synchrotrons and free electron lasers', *J. Phys. Cond. Matt.* **33**, 274003 (2021).
4. C. Lin and J. S. Tse, 'High-pressure nonequilibrium dynamics on second-to-microsecond time scales: application of time-resolved X-ray diffraction and dynamic compression in ice', *J. Phys. Chem. Lett.* **12**, 8024–8038 (2021).

## Original publication

'Novel experimental setup for megahertz X-ray diffraction in a diamond anvil cell at the High Energy Density (HED) instrument of the European X-ray Free-Electron Laser (EuXFEL)', *Journal of Synchrotron Radiation* **28**, 688–706 (2021). DOI: 10.1107/S1600577521002551



Hanns-Peter Liermann, Zuzana Konópková, Karen Appel, Clemens Prescher, Andreas Schropp, Valerio Cerantola, Rachel J. Husband, James D. McHardy, Malcolm I. McMahon, R. Stewart McWilliams, Charles. M. Pépin, Jona Mainberger, Michael Roeper, Andreas Berghäuser, Horst Damker, Peter Talkovski, Manon Foese, Naresh Kujala, Oriana B. Ball, Marzena A. Baron, Richard Briggs, Maxim Bykov, Elena Bykova, Julien Chantel, Amy L. Coleman, Hyunchoe Cynn, Dana Dattelbaum, Leora E. Dresselhaus-Marais, Jon H. Eggert, Lars Ehm, William J. Evans, Guillaume Fiquet, Mungo Frost, Konstantin Glazyrin, Alexander F. Goncharov, Huijeong Hwang, Zsolt Jenei, Jaeyong Kim, Falko Langenhorst, Yongjae Lee, Mikako Makita, Hauke Marquardt, Emma E. McBride, Sébastien Merkel, Guillaume Morard, Earl F. O'Bannon III, Christoph Otzen, Edward J. Pace, Alexander Pelka, Jeffrey S. Pigott, Vitali B. Prakapenka, Ronald Redmer, Carmen Sanchez-Valle, Markus Schoelmerich, Sergio Speziale, Georg Spiekermann, Blake T. Sturtevant, Sven Toleikis, Nenad Velisavljevic, Max Wilke, Choong-Shik Yoo, Carsten Baehtz, Ulf Zastrau and Cornelius Strohm

'X-ray free electron laser-induced synthesis of  $\epsilon$ -iron nitride at high pressures', *Journal of Physical Chemistry Letters* **12**, 3246–3252 (2021). DOI: 10.1021/acs.jpcllett.1c00150



Huijeong Hwang, Taehyun Kim, Hyunchoe Cynn, Thomas Vogt, Rachel J. Husband, Karen Appel, Carsten Baehtz, Oriana B. Ball, Marzena A. Baron, Richard Briggs, Maxim Bykov, Elena Bykova, Valerio Cerantola, Julien Chantel, Amy L. Coleman, Dana Dattelbaum, Leora E. Dresselhaus-Marais, Jon H. Eggert, Lars Ehm, William J. Evans, Guillaume Fiquet, Mungo Frost, Konstantin Glazyrin, Alexander F. Goncharov, Zsolt Jenei, Jaeyong Kim, Zuzana Konópková, Jona Mainberger, Mikako Makita, Hauke Marquardt, Emma E. McBride, James D. McHardy, Sébastien Merkel, Guillaume Morard, Earl F. O'Bannon III, Christoph Otzen, Edward J. Pace, Alexander Pelka, Charles M. Pépin, Jeffrey S. Pigott, Vitali B. Prakapenka, Clemens Prescher, Ronald Redmer, Sergio Speziale, Georg Spiekermann, Cornelius Strohm, Blake T. Sturtevant, Nenad Velisavljevic, Max Wilke, Choong-Shik Yoo, Ulf Zastrau, Hanns-Peter Liermann, Malcolm I. McMahon, R. Stewart McWilliams and Yongjae Lee

For affiliation details refer to original publications.

# Automatic differentiation is capturing X-ray images

Realising soft X-ray ptychography at FLASH

**Differentiable programming (also known as automatic differentiation) is a broadly used tool in optimisation and large-scale artificial intelligence data handling. The gradient values crucial for numerical optimisation in X-ray ptychography imaging are computed with automatic differentiation.**

Hard X-ray imaging enables quantifying heavy elemental compositions, crystal lattice structures and strain fields in crystalline materials. On the other hand, imaging of complex chemistry with light elements possessing low X-ray scattering cross-sections becomes feasible with soft X-rays (below 1 keV photon energy) [1]. Due to the limitations of optics at soft X-ray wavelengths, imaging at short wavelengths is challenging. Lensless imaging methods are a powerful alternative seeking to measure diffraction patterns of a sample and to algorithmically convert them into a high-resolution image — a well-known technique that is broadly called phasing. Coherent diffraction imaging (CDI) became an important scientific field with the emergence of highly intense synchrotron and FEL sources combined with the advancement of X-ray detectors. Advanced computation enables the phasing of diffraction patterns; a revolutionary step towards discovering the nanoworld. Nevertheless, the CDI phasing techniques have a limited ability to

retrieve images for extended samples or complex-valued samples from single measurements [2].

Ptychography was introduced as a scanning diffraction imaging technique. A series of diffraction patterns is recorded by scanning a finite X-ray probe over an extended sample with an overlap between the adjacent scan positions (Fig. 1) [3]. Afterwards, the stack of diffraction patterns is numerically converted to retrieve an image of the sample and, at the same time, the illuminating pulse. The redundancy in measurements removes the ambiguities commonly linked to single-shot CDI of extended samples [4]. Thus, X-ray ptychography gained significant momentum to study large samples, especially at synchrotron sources in the hard X-ray regime.

A high degree of spatial coherence and exceptional photon flux, together with ultrashort pulses, make free-electron lasers ideal facilities for ptychography imaging [5]. However, standard ptychography algorithms require a light pulse that is stable from shot to shot. Thus, the fluctuations of the FEL pulses, which are typical for the self-amplified spontaneous emission (SASE) process, complicate the implementation of this technique and the data analysis at X-ray sources like FLASH.

X-ray ptychography can be recognised as an optimisation problem. The sample can be recovered by optimising an error metric that quantifies the difference between measured and synthetic diffraction patterns. Most of the optimisation approaches used for ptychography rely on an analytical calculation of the error metric's derivatives. Any change in the optimisable parameters potentially requires massive, time-consuming and complicated recalculation. An elegant way to solve this problem is to use various numerical methods that allow automatic differentiation (AD) of the error metric with respect to optimisable parameters. AD is a family of computational techniques that automatically calculate derivatives for numerical functions [6].

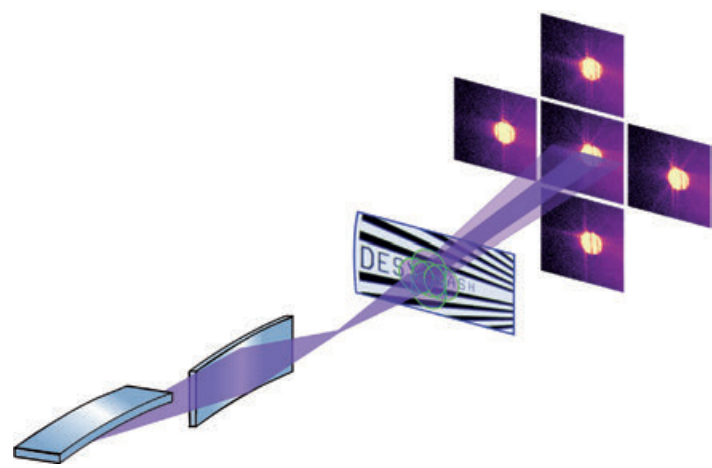
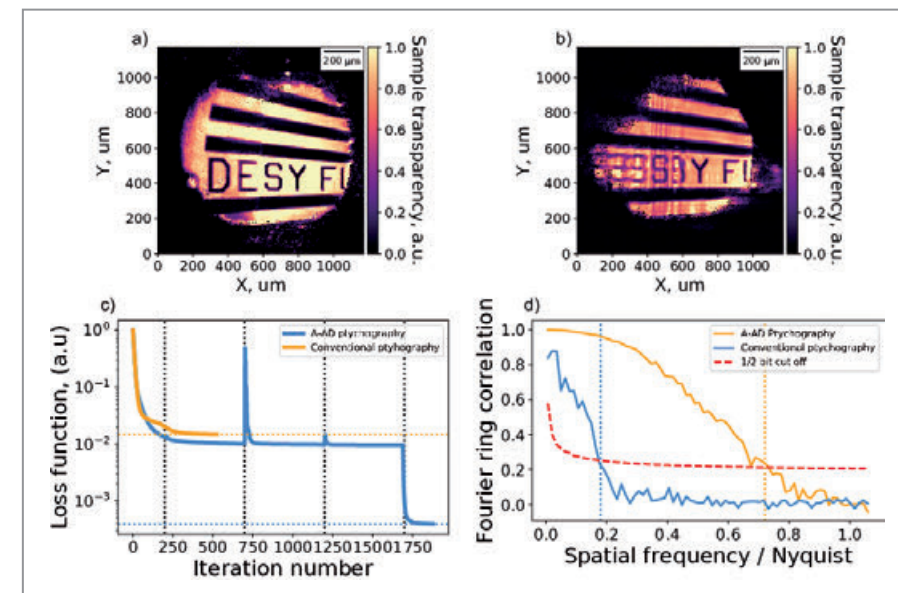


**Figure 1**  
Schematic layout of the ptychography experiment at FLASH2 beamline FL24. The sample is scanned with overlapping FEL pulses to obtain a series of diffraction patterns. An iterative conversion of diffraction patterns retrieves an image of the sample and the modal composition of the FEL pulses.

**Figure 2**  
Sample reconstructions using a) A-AD ptychography versus b) conventional ptychography, which does not consider fluctuating FEL parameters as optimisable. c) Optimisation with A-AD starts with a conventional ptychography algorithm, which is followed by a differentiable scan position refinement and expresses the FEL illumination as its coherent modes. d) Resolution estimated by applying a half-bit threshold to the Fourier ring correlation shows a three-times improved resolution obtained by using A-AD ptychography compared to conventional ptychography.



Also, AD has been widely used in deep learning to automate optimisation tasks.

We have successfully established a prototype-adaptive automatic differentiation (A-AD) routine for streamlining ptychography at FELs. Fluctuations of pulses, partial spatial coherence (typical for FLASH) and scanning imprecisions can be numerically integrated into the model. The entire routine uses a forward model. This model guesses measured diffraction patterns. Then, the routine optimises the error metric with different optimisation methods to obtain a global minimum. The forward model, the type of error metric and the optimisation approach can be changed independently without the need for any analytical re-derivation. The computational power of the A-AD routine to analyse the measured data provides very high flexibility for performing ptychography experiments.

For the first time, ptychography was performed at the FLASH2 beamline FL24 which is equipped with KB micro-focusing optics employing bendable mirrors [7]. By using the A-AD model for reconstruction, a resolution below 3  $\mu\text{m}$  was achieved at 13.5 nm wavelength for an intermediate-field geometry (Fig. 2). This geometry was chosen to realise a non-destructive setup for ptychography at FELs where the sample is placed a few centimetres downstream of the focus. Without integrating fluctuating FEL parameters, such as beam position instabilities and partial coherence, into the ptychography routine, the reconstructions permanently fail to converge. During the ptychography experiment at FLASH, near- and intermediate-field diffraction patterns of a test sample were measured with the same setup, and collected datasets were retrieved successfully. Additionally, the A-AD ptychography routine yielded insight into the mode structure of every FEL pulse and captured them shot-by-shot. Single-shot characterisation of FEL pulses is of vital importance to precisely monitor the experiment parameters and perform successful imaging experiments.

Applications of our A-AD routine can be extended to the recently growing field of electron ptychography, as well as 3D ptycho-tomography at FELs and synchrotrons. A-AD ptychography paves the way to non-destructive and high-resolution imaging at FEL facilities. Soft X-rays down to 1.5 nm, coupled to high-dynamic-range soft X-ray detectors (such as PERCIVAL developed at DESY) and combined with high-performance computing algorithms, open new avenues to study complex engineered materials at FLASH.

Author contact: Masoud Mehrjoo, [masoud.mehrjoo@desy.de](mailto:masoud.mehrjoo@desy.de)  
Elke Ploenjes, [elke.ploenjes@desy.de](mailto:elke.ploenjes@desy.de)

## References

1. M. R. Howell, T. Beetz, H. N. Chapman, C. Cui, J. M. Holton, C. J. Jacobsen, J. Kirz, E. Lima, S. Marchesini, H. Miao, D. Sayre, D. A. Shapiro, J. C. H. Spence and D. Starodub, 'An assessment of the resolution limitation due to radiation-damage in X-ray diffraction microscopy', *J. Electron Spectrosc. Relat. Phenom.* **170**, 4–12 (2009).
2. A. Barty, J. Kopper and H. N. Chapman, 'Molecular imaging using X-ray free-electron lasers', *Annu. Rev. Phys. Chem.* **64**, 415–435 (2013).
3. F. Pfeiffer, 'X-ray ptychography', *Nat. Photonics* **12**, 9–17 (2018).
4. P. Thibault and A. Menzel, 'Reconstructing state mixtures from diffraction measurements', *Nature* **494**, 68–71 (2013).
5. A. He, L. Yang and L. Yu, 'High-gain free-electron laser theory, introduction', in 'Synchrotron light sources and free-electron lasers: accelerator physics, instrumentation and science applications', 149–190, Springer (2020).
6. T. J. Barth, D. E. Keyes and D. Roose, 'Automatic differentiation: applications, theory, and implementations, engineering', Vol. 50, of 'Lecture notes in computational science and engineering', Springer (2006).
7. E. Plönjes, B. Faatz, M. Kuhlmann and R. Treusch, 'FLASH2: operation, beamlines, and photon diagnostics', *AIP Conf. Proc.* **1741**, 020008 (2016).

## Original publication

'Flexible ptychography platform to expand the potential of imaging at free-electron lasers', *Optics Express* **22345–22365** (2021). DOI: 10.1364/OE.426931



Konstantin Kharitonov<sup>1</sup>, Masoud Mehrjoo<sup>1</sup>, Mabel Ruiz-Lopez<sup>2</sup>, Barbara Keitel<sup>1</sup>, Svea Kreis<sup>1</sup>, Martin Seyrich, Mihai Pop<sup>2</sup> and Elke Plönjes<sup>1</sup>

1. Deutsches Elektronen-Synchrotron DESY, Hamburg, Germany
2. Lund University, Lund, Sweden

# A microscope with soft X-ray spectroscopy eyes

Soft X-ray imaging spectroscopy with micrometre resolution to analyse domains in quantum materials

Functionality of quantum materials appears through the correlated interaction of microscopic degrees of freedom like spin, charge, orbital and lattice [1]. Their intricate energy balance enables the material to display hugely different properties as a result of small perturbations, while often spatially inhomogeneous textures lead to separate electronic properties in domains which extend from the nano- to the micrometre scale [2]. An understanding requires electronic structure studies to be combined with high-resolution imaging. Here, we present a setup with a resolution of better than 2  $\mu\text{m}$  in soft X-ray resonant inelastic and elastic scattering as well as absorption spectroscopy. With such a setup, percolation networks and spatial details of phase transition behaviour can be studied directly in the electronic structure.

A few examples, which highlight the importance of phase coexistence and inhomogeneity in solids, include the high- $T_c$  superconductor  $\text{HgBa}_2\text{CuO}_{4+y}$  [3], or vanadium dioxide with its insulator-metal transition close to room temperature [4].

Soft X-ray spectroscopies, like X-ray absorption spectroscopy (XAS) and resonant inelastic X-ray scattering (RIXS), are well-established techniques for the study of the electronic structure of quantum materials. By resonantly addressing core transitions in solids, selected elements are probed with sensitivity for charge, spin and orbit. However, the detected signal is usually averaged across the entire illuminated area on the sample, which typically extends tens of micrometres in each dimension, thus averaging over multiple domains of potentially different character.

Our RIXS imaging setup (Fig. 1a) successfully demonstrates XAS and RIXS in combination with imaging having a spatial resolution better than 2  $\mu\text{m}$ . The measurements were carried out at the PETRA III beamline P04. There is an off-axis Fresnel analyser zone plate (AZP) at the heart of the setup which images the sample in one direction and disperses scattered X-rays in the orthogonal dimension [5]. Using a 2D charge-coupled device (CCD) detector yields the combined imaging and spectroscopic information on the two dimensions of a single exposure.

With the beamline exit slit opened as far as possible, the highest possible X-ray flux is transmitted onto the sample. A linear zone plate focuses the resulting X-ray 'rainbow' in the horizontal to a width below 1  $\mu\text{m}$  (Fig. 1a). In the verti-

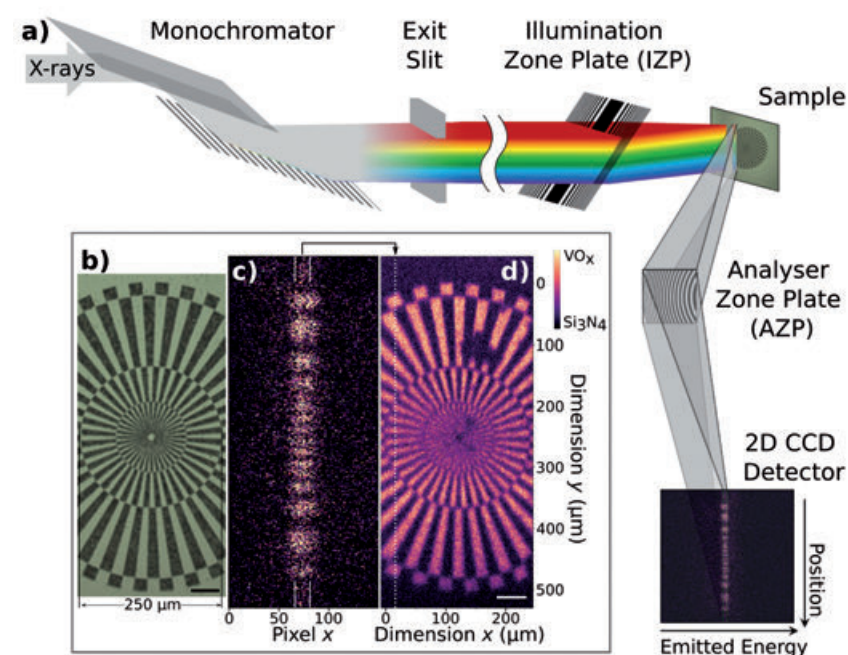
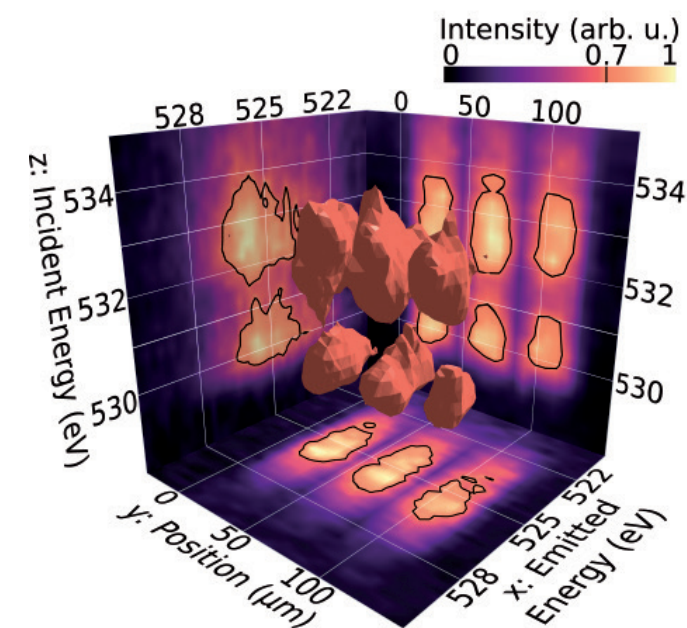


**Figure 1**  
a) Experimental setup: The monochromator exit slit is fully opened. A linear zone plate focuses transmitted energies to a vertical line of sub-micrometre width at the position of the sample. An analyser zone plate combines imaging and spectroscopy: Along the vertical, the sample is imaged, while X-ray emission is dispersed in the horizontal. b) Test structure for measurement of spatial resolution (dark: vanadium oxide; bright: silicon nitride). c) Single-exposure detector image of the test structure. The signal is averaged between the white lines along the horizontal and comprises the highlighted slice of the reconstruction shown in d). This procedure is repeated while scanning the sample along the horizontal in steps of 250 nm. Scale bars are 50  $\mu\text{m}$ .

**Figure 2**  
An energy scan on  $\text{VO}_2$  squares of size 30  $\mu\text{m} \times 30 \mu\text{m}$  yields a 3D dataset. Each detector exposure is a 2D image of position vs. emitted energy (bottom projection). Scanning the incident photon energy additionally yields a RIXS map (left plane) and spatially resolved partial fluorescence yield absorption data (right plane). As an example, the 3D iso-surface in the centre visualises relative intensities of 70%.



cal, this line focus measures approximately 1 mm and contains spatially separated photon energies from 528.2 eV to 531.8 eV when the central photon energy is set to 530 eV (oxygen K-edge). The energy resolution in the measured data is preserved despite this broad-incident photon energy bandwidth, since the AZP disperses the emission from every illuminated point separately in this imaging setup. In summary, a single 2D detector exposure contains both spatial information and incident energy on the vertical axis, as well as emitted energy on the horizontal axis.

The spatial resolution was determined via a Siemens star test structure (Fig. 1b) with a diameter of 500  $\mu\text{m}$ . Bright and dark structures consist of vanadium oxide and silicon nitride, respectively. Fluorescence contrast is created by exciting oxygen fluorescence only in the vanadium oxide parts. With the focus line extending across the test structure, a detector image as shown in Fig. 1c is obtained. Scanning in horizontal direction and averaging the detector image between the white lines as indicated in Fig. 1c allow reconstructing the test structure as shown in Fig. 1d. Using a Fourier ring correlation algorithm, the spatial resolution was determined to be 1.8  $\mu\text{m}$ .

The flexibility of this RIXS imaging setup to record versatile information becomes apparent through the opportunity of different acquisition modes:

- 1) For homogeneous samples, a so-called RIXS map (inelastic scattering spectra for a range of excitation energies) can be obtained in a single detector exposure.
- 2) For heterogeneous samples with a rather featureless excitation spectrum, e.g. fluorescence, the line focus in combination with a scan in the orthogonal direction can be used to map the sample (this was used for determination of spatial resolution on the Siemens star test structure, see above). Also, unidimensional spectro-imaging can be used to measure XAS and RIXS in dependence of one spatial dimension by scanning only the incident photon energy (see Fig. 2).
- 3) For heterogeneous samples with a complex excitation spectrum, a combined scan of focus line position and incident photon energy can be used to obtain a high-dimensional information matrix of the sample.

In summary, the RIXS imaging setup offers flexibility which can be adjusted to individual experimental needs. While

making use of the entire bandwidth transmitted through the beamline monochromator, different schemes are proposed of how electronic structure analysis can be combined with micrometre resolution for the domain-resolved study of novel quantum materials.

Author contact: Jan O. Schunck, [jan.schunck@desy.de](mailto:jan.schunck@desy.de)  
Martin Beye, [martin.beye@desy.de](mailto:martin.beye@desy.de)

## References

1. Y. Tokura, M. Kawasaki and N. Nagaosa, 'Emergent functions of quantum materials', *Nat. Phys.* **13**, 1056–1068 (2017).
2. E. Dagotto, 'Complexity in strongly correlated electronic systems', *Science* **309**, 257–262 (2005).
3. G. Campi, A. Bianconi, N. Poccia, G. Bianconi, L. Barba, G. Arrighetti, D. Innocenti, J. Karpinski, N. D. Zhigadlo, S. M. Kazakov, M. Burghammer, M. v. Zimmermann, M. Sprung and A. Ricci, 'Inhomogeneity of charge-density-wave order and quenched disorder in a high- $T_c$  superconductor', *Nature* **525**, 359–362 (2015).
4. H. S. Choi, J. S. Ahn, J. H. Jung, T. W. Noh and D. H. Kim, 'Mid-infrared properties of a  $\text{VO}_2$  film near the metal-insulator transition', *Phys. Rev. B* **54**, 4621–4628 (1996).
5. F. Marschall, Z. Yin, J. Rehanek, M. Beye, F. Döring, K. Kubiček, D. Raiser, S. T. Veedu, J. Buck, A. Rothkirch, B. Rösner, V. A. Guzenko, J. Viehhaus, C. David and S. Teichert, 'Transmission zone plates as analyzers for efficient parallel 2D RIXS-mapping', *Sci. Rep.* **7**, 8849 (2017).

## Original publication

'Soft X-ray imaging spectroscopy with micrometer resolution', *Optica* **8**, 156–160 (2021). DOI: 10.1364/OPTICA.405977



Jan O. Schunck<sup>1,2</sup>, Florian Döring<sup>3</sup>, Benedikt Rosner<sup>3</sup>, Jens Buck<sup>4,5</sup>, Robin Y. Engel<sup>1,2</sup>, Piter S. Miedema<sup>1</sup>, Sanjoy K. Mahatha<sup>1</sup>, Moritz Hoesch<sup>1</sup>, Adrian Petraru<sup>6</sup>, Hermann Kohlstedt<sup>4</sup>, Christian Schüssler-Langeheine<sup>7</sup>, Kai Rossnagel<sup>1,4,5</sup>, Christian David<sup>3</sup> and Martin Beye<sup>1,2</sup>

1. Deutsches Elektronen-Synchrotron DESY, Hamburg, Germany
2. Universität Hamburg, Hamburg, Germany
3. Paul Scherrer Institut (PSI), Villigen, Switzerland
4. Institut für Experimentelle und Angewandte Physik, Christian-Albrechts-Universität zu Kiel, Kiel, Germany
5. Ruprecht-Haensel-Labor, Christian-Albrechts-Universität zu Kiel, Kiel, Germany
6. Nanoelektronik, Technische Fakultät, Christian-Albrechts-Universität zu Kiel, Kiel, Germany
7. Helmholtz-Zentrum Berlin für Materialien und Energie, Berlin, Germany

# First determination of the bulk spin polarisation of magnetite

Imaging spin-filtering meets time-of-flight energy recording

Magnetite — probably the oldest magnetic material known to mankind — is considered a promising material for spin electrodes in spintronics applications. Photoelectron spectroscopy with high-energy synchrotron radiation is an extremely powerful tool for studying the bulk electronic structure of complex oxide materials such as magnetite. The combination of this well-established technique with an imaging spin-filter and time-of-flight energy recording enables the spin-polarised investigation of the electronic structure. For this purpose, a novel momentum microscope has been developed and set up at the hard X-ray beamline P22.

Magnetite ( $\text{Fe}_3\text{O}_4$ ) has attracted humans for ages because of its magic magnetic properties which helped first pioneers navigate through deserts and sailors across the oceans. Wegener's theories on continental drifts were confirmed by changes of the earth magnetic field imprinted in magnetite. For a long time, theorists have predicted a hidden electronic property of magnetite: half-metallicity which leads to electrical transport by electrons with only one spin orientation. This rare property is ideal for spintronics, where the spin of the electron is used for the encoding of information. However, direct experimental access to the spin polarisation of the conduction electrons in bulk magnetite has been impeded by the pronounced surface sensitivity of conventional electron spectroscopies. For these reasons, half-metallic ferromagnetism in magnetite has remained elusive up to now.

Here, we have developed a new experimental approach to directly study the intrinsic spin polarisation in magnetite

using bulk-sensitive hard X-ray photoelectron spectroscopy (HAXPES). This non-destructive technique utilises the photoelectric effect to determine the electronic structure in a solid. Due to the high photon energy of several keV, the emitted photoelectrons propagate at high kinetic energies, thereby significantly enhancing the information depth to 10–20 nm and overcoming the atomic surface sensitivity of photoemission in the VUV or soft X-ray regime. However, this comes at a price, as high photon energies also lead to a sharp reduction of the photoionisation cross sections and hence signal strength. The signal strength is further reduced (by up to a factor of 100) when filtering the photoelectrons by their spin orientation, making spin-resolved HAXPES valence band spectroscopy a major challenge. In our new concept, these limitations are overcome by a dramatically improved detection efficiency. This is achieved by using a momentum microscope specifically developed for HAXPES operation, built and commissioned

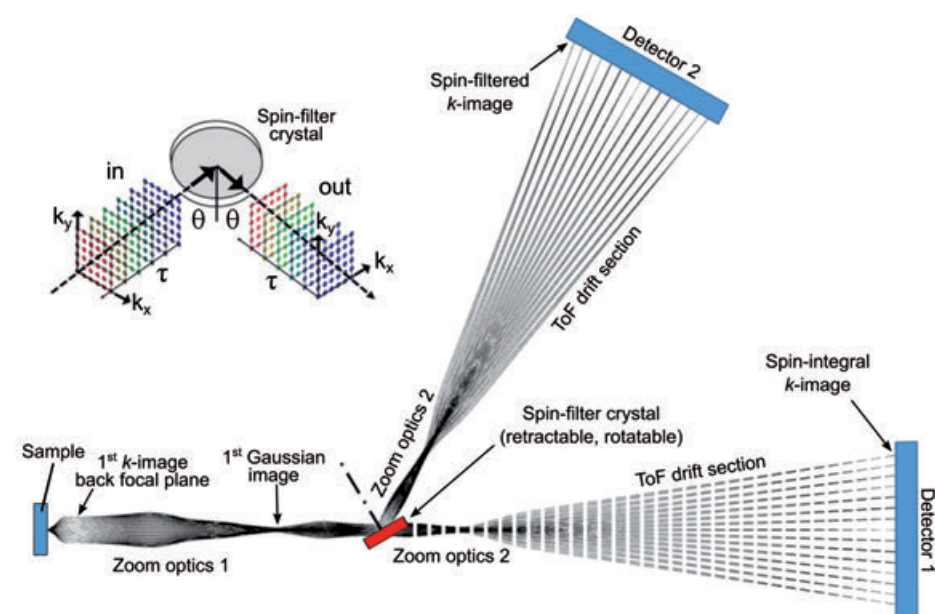


**Figure 1** Photoelectron trajectories (side view) and principal operation of the newly set up momentum microscope at beamline P22. Notice that the spin-filter also preserves the energy information encoded in the time-of-flight signal (see inset), resulting in a 3D ( $k_x, k_y, E_{kin}$ ) recording scheme.

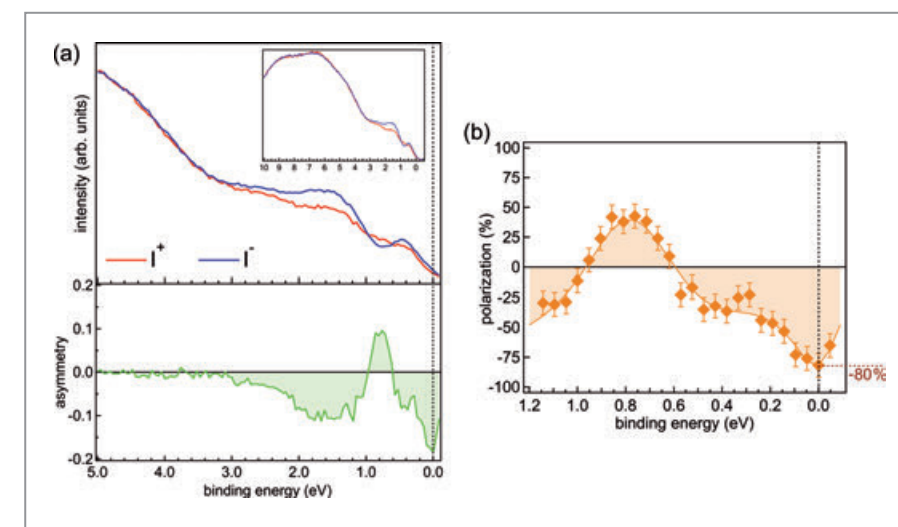


**Figure 2** a) Valence-band spectra measured with an excitation energy of  $h\nu = 5.0$  keV for two opposite in-plane magnetisations denoted by  $I^+$  and  $I^-$  together with the calculated energy-dependent asymmetry  $A$ . b) Spin polarisation of the magnetite film (the line serves as a guide to the eye). It is negative at  $E_F = 0$  eV with a value of  $-80\%$ . Between 0.60 and 0.95 eV, there is a sign change of the polarisation. The error bars denote the statistical error.

in close collaboration with DESY at beamline P22. It uses a special entrance lens that simultaneously accepts all photoelectrons emitted by the sample and employs a time-of-flight detection scheme for spectroscopy, using the 40-bunch mode of PETRA III as pulsed photon source. The microscope's electron optics converts the momentum distribution of the photoelectrons into a 2D spatial map. Spin-filtering is achieved by reflecting the photoelectrons off an  $\text{Ir}(1\ 1\ 1)$  crystal surface before detecting them, taking advantage of the reflection asymmetry between spin up and down electrons due to spin-orbit interaction. This setup enables full-field momentum imaging [1]. A schematic view of the microscope is shown in Fig. 1.

The power of this new instrumental milestone and its unprecedented efficiency is demonstrated by its application to the case of magnetite. The predicted half-metallicity of the ferrimagnet  $\text{Fe}_3\text{O}_4$  is attributed to its inverse-spinel structure with itinerant, uncompensated minority electrons on the octahedral iron sublattice, giving rise to a spin polarisation at the Fermi level ( $E_F$ ) of  $\sim 100\%$ . Although the spin polarisation of magnetite has been studied for almost 40 years, many contradicting results have been published so far. This is attributed to the surface sensitivity of the applied methods. The polarity of the surface of magnetite renders them inherently unstable, leading to a high sensitivity of experimental results on the specific surface state and treatment. Thus, bulk-sensitive and spin-resolved HAXPES is required to settle the question of magnetite's half-metallicity.

In our study we used an MBE-grown  $\text{Fe}_3\text{O}_4(1\ 1\ 1)/\text{ZnO}(0\ 0\ 0\ 1)$  film, cooled down to 30 K and magnetised parallel ( $I^+$ ) or antiparallel ( $I^-$ ) to the quantisation axis of the spin-filter. HAXPES performed with 5 keV photons was employed to measure the valence band for opposite magnetisation directions using the time-of-flight momentum microscope equipped with the spin-filter crystal. Figure 2a shows both photoelectron spectra along with the resulting spin asymmetry  $A = (I^+ - I^-)/(I^+ + I^-)$ . Calibrating the data with the known spin sensitivity  $S(E)$  of the spin-filter crystal yields the spin polarisation  $P = A/S$  as shown in Fig. 2b.

Taking statistical errors into account, as well as the fact that the magnetite film was measured in remanence (and therefore not fully magnetised at 30 K), yields an experimental estimate of the intrinsic, i.e. bulk-representative, Fermi-level spin polarisation of  $P(E_F) = -80^{+10}_{-20}\%$ .

This value indeed strongly points to a complete minority spin polarisation for charge carriers in agreement with theoretical predictions from density-functional theory [2]. This establishes magnetite as a potential key material for novel spin-based information technology. Having fostered interest on magnetism for centuries, magnetite might again attract scientists in a hot research field.

Author contact: Matthias Schmitt, [matthias.schmitt@physik.uni-wuerzburg.de](mailto:matthias.schmitt@physik.uni-wuerzburg.de)  
Michael Sing, [sing@physik.uni-wuerzburg.de](mailto:sing@physik.uni-wuerzburg.de)

## References

1. K. Medjanik, S. V. Babenkov, S. Chernov, D. Vasilyev, B. Schönhense, C. Schlueter, A. Gloskovskii, Y. Matveyev, W. Drube, H.-J. Elmers and G. Schönhense, 'Progress in HAXPES performance combining full-field k-imaging with time-of-flight recording', *J. Synchrotron Radiat.* 26, 1996-2012 (2019).
2. P. Piekarz, K. Parlinski and A. M. Oles, 'Origin of the Verwey transition in magnetite: group theory, electronic structure, and lattice dynamics study', *Phys. Rev. B* 76, 165124 (2007).

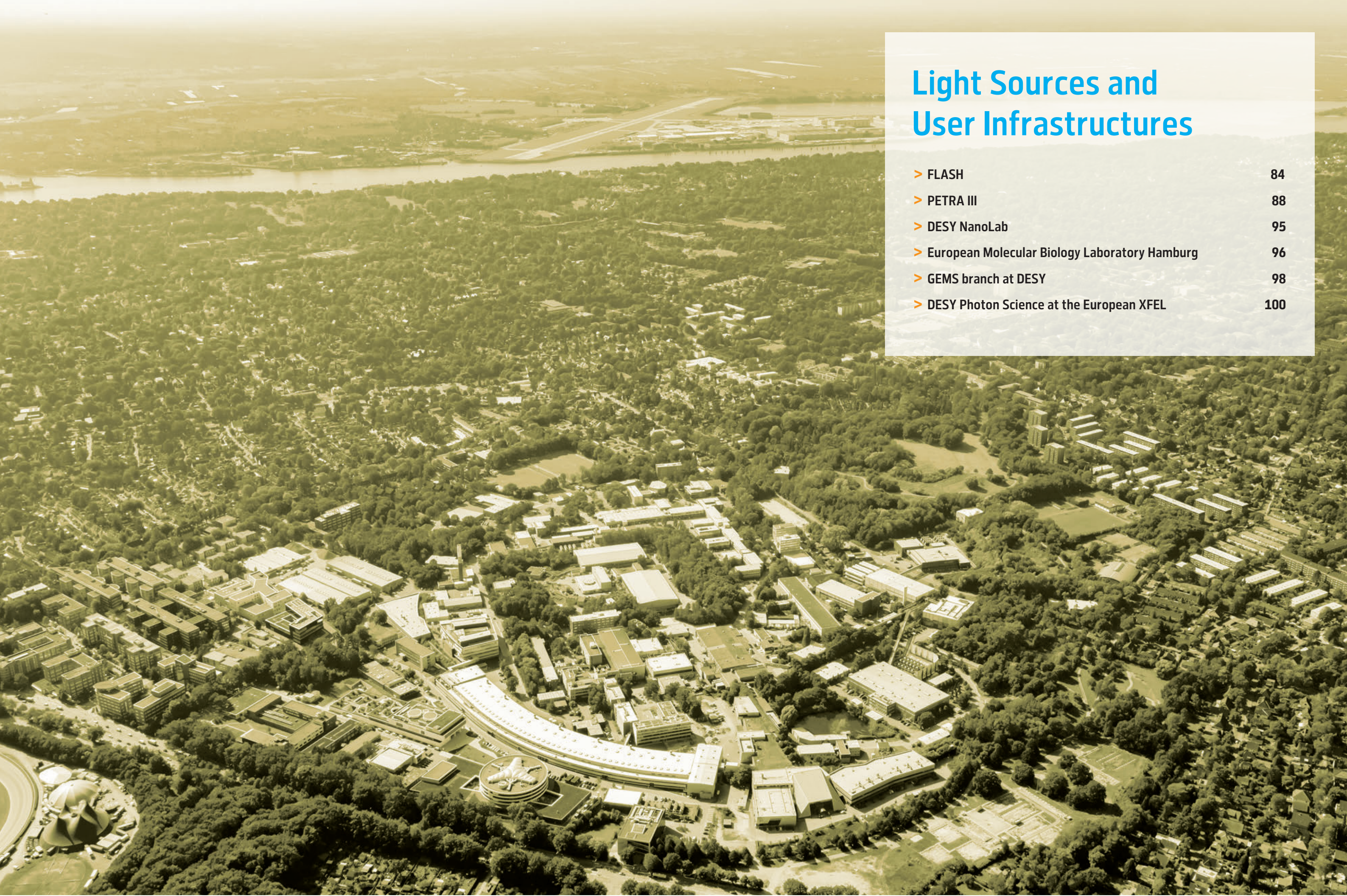
## Original publication

'Bulk spin polarization of magnetite from spin-resolved hard X-ray photoelectron spectroscopy', *Physical Review B* 104, 045129 (2021). DOI: 10.1103/PhysRevB.104.045129



Matthias Schmitt<sup>1</sup>, Ozan Kirilmaz<sup>2</sup>, Sergii Chernov<sup>2</sup>, Sergey Babenkov<sup>2</sup>, Dmitry Vasilyev<sup>2</sup>, Olena Fedchenko<sup>2</sup>, Katerina Medjanik<sup>2</sup>, Yuri Matveyev<sup>3</sup>, Andrei Gloskovskii<sup>3</sup>, Christoph Schlueter<sup>3</sup>, Aimo Winkelmann<sup>4</sup>, Lenart Dudy<sup>5</sup>, Hans-Joachim Elmers<sup>2</sup>, Gerd Schönhense<sup>2</sup>, Michael Sing<sup>1</sup> and Ralph Claessen<sup>1</sup>

1. Physikalisches Institut und Würzburg-Dresden Cluster of Excellence ct.qmat, Julius-Maximilians-Universität, Würzburg, Germany
2. Institut für Physik, Johannes Gutenberg-Universität, Mainz, Germany
3. Deutsches Elektronen-Synchrotron DESY, Hamburg, Germany
4. Academic Centre for Materials and Nanotechnology (ACMIN), AGH University of Science and Technology, Kraków, Poland
5. SOLEIL Synchrotron, Saint-Aubin, France



# Light Sources and User Infrastructures

> FLASH	84
> PETRA III	88
> DESY NanoLab	95
> European Molecular Biology Laboratory Hamburg	96
> GEMS branch at DESY	98
> DESY Photon Science at the European XFEL	100

### Covid-19 pandemic: stress-test for user operation

In 2021, the pandemic situation has still substantially hampered the scientific user operation at FLASH. Nevertheless, 23 out of 31 initially planned user experiments could still be performed successfully. However, eight beamtimes had to be cancelled in the first half of 2021, most of them due to the extended lockdown in Germany as well as travel and quarantine restrictions for users from abroad. Out of the 23 experiments, 19 (83%) were conducted at local experimental end stations operated by FLASH personnel who put in extensive efforts to substitute manpower for the user groups in addition to their other duties. Due to the pandemic situation, fewer users were allowed on site but all made best use of video conferences and remote access to the data. The local teams were thus often complemented by colleagues abroad who contributed quite efficiently by taking care of near real-time data analysis and who provided input and feedback for necessary adaptations of the experimental plan.

Unfortunately, the decreased number of operable experiments also led to less parallel operation of FLASH1 and FLASH2. Thus, in only about 20% of the cases, experiments matched for parallel operation in both experimental halls. Under normal conditions, the degree of parallel user operation would be 30–40%, hence yielding substantially more beamtime for users.

### Setup of 'time-delay compensating monochromator' beamline FL23 started

The new time-delay compensating monochromator (TDCM) beamline, previously presented in the DESY Photon Science Annual Report 2019 [1,2], is currently set up in the FLASH2 experimental hall 'Kai Siegbahn' (Fig. 1).

The double grating monochromator design of beamline FL23 will provide a narrow spectral bandwidth of the FLASH2 photon pulses while preserving the ultrashort free-electron laser (FEL) pulse duration of less than 50 fs. A Kirkpatrick-Baez (KB) mirror system employing bendable mirrors focuses the monochromatised radiation down to about  $5 \times 5 \mu\text{m}^2$  beam size at the target, independent of the monochromator slit width (Tab. 1). Due to a movable exit arm, the monochromator can be used in double- or single-grating configuration. The latter allows higher throughput and is particularly interesting when using harmonics at short wavelengths. FL23 will offer an open port for user or FLASH provided mobile end stations.

Table 1: Key parameters of the time-delay compensating monochromator beamline FL23

Wavelength	(nm)	1.2–20.0 (including harmonics)
Pulse length	(fs)	< 50
Resolution	( $\lambda/\Delta\lambda$ )	$\geq 2000$
Flux at beamline end	(photons/pulse)	$10^{10}$

Meanwhile, most of the beamline components have been built and delivered, and the installation of the individual components has started in October 2021. Figure 2 shows the assembly of the interior monochromator mechanics ongoing in November 2021.

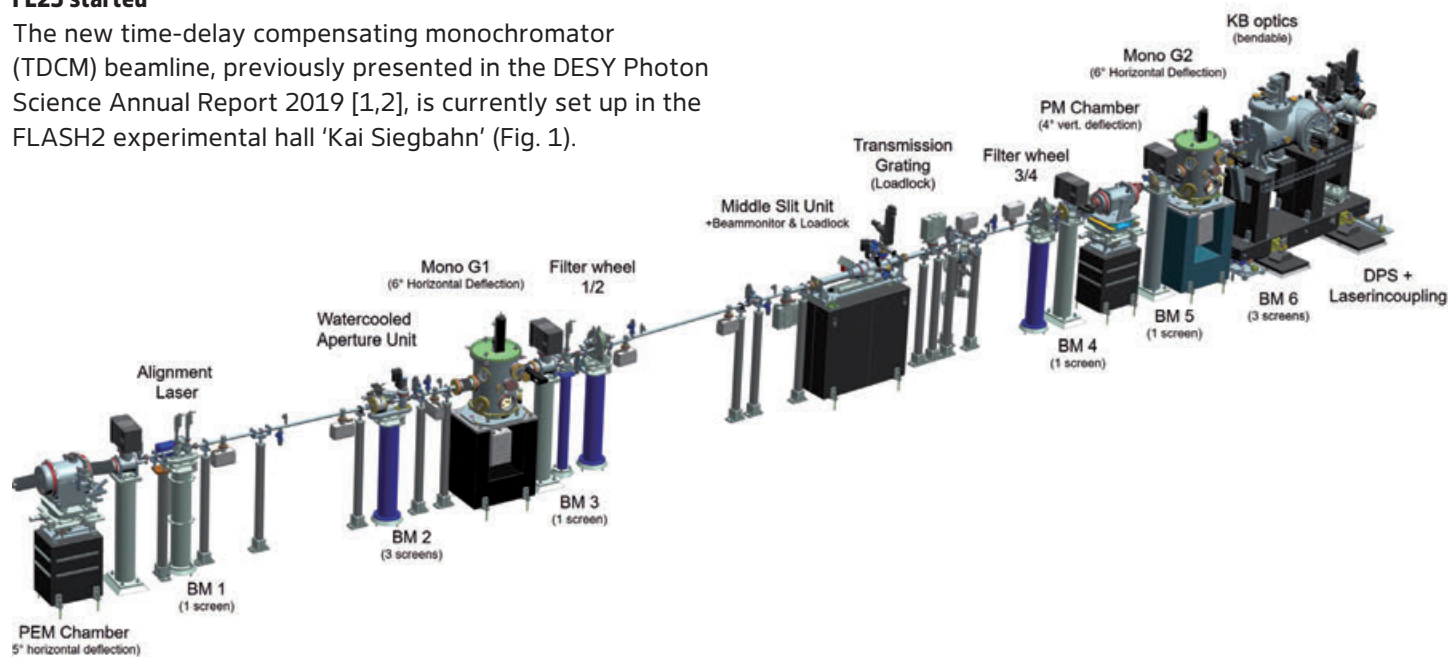


Figure 1  
3D construction drawing of the time-delay compensating monochromator (TDCM) beamline FL23 at FLASH (PEM = plane elliptical mirror, BM = beam monitor, G1/2 = gratings, PM = plane mirror, DPS = differential pumping stage).



Figure 2  
Assembly of the mechanics for the FL23 monochromator gratings in the cleanroom.

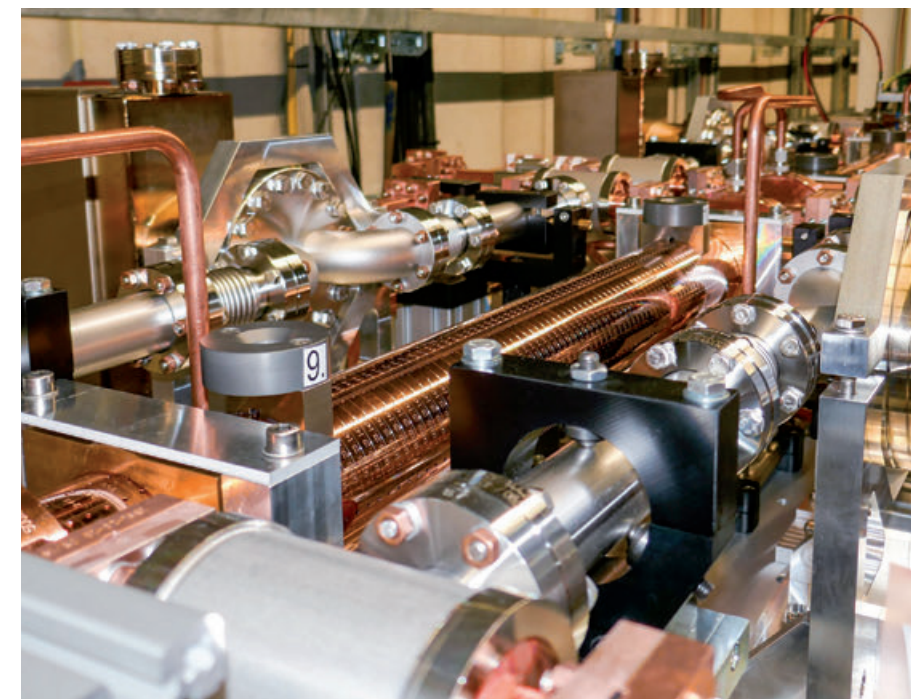


Figure 3  
The new PolariX cavities at FLASH2 are two copper structures, one of them is visible here in the centre. The electron beam propagates from lower left to upper right.

Assuming no further delays (in particular, pandemic-related), we expect to be ready for commissioning of beamline FL23 with beam towards the end of 2022 and will accept experiments with 'friendly' users in 2023.

### Making space for the next generation of pump-probe lasers

In the FLASH1 experimental hall 'Albert Einstein', the 45 m<sup>2</sup> pump-probe laser hut was cleared out during the last months in order to provide space for a new, modern laser system. In autumn 2020, a new pulse train laser had already been set up in a laser tent close to the PG2 beamline end. Since then, it has replaced the old pulse train laser that was operated in the laser hut for over fifteen years and has been fully decommissioned by now. Once the interior of the pump-probe laser hut has been completely refurbished, the air-conditioning system on its roof will be upgraded as well to meet the new, enhanced requirements for temperature stability and humidity control. Afterwards, in autumn 2022, an established 10 Hz, millijoule laser system will be re-installed for the transition period of about one and a half years between the two FLASH2020+ upgrade shutdowns. This system will provide intense laser pulses for atomic and molecular physics as well as warm dense matter experiments at the beamlines BL1 and BL3, whereas the PG beamlines will be served by the aforementioned pulse train laser system.

After the planned second shutdown in 2024, the new pulse train laser system will provide shorter and more intense pulses to all beamlines in the FLASH1 hall. It is presently under development and will be installed in the refurbished, slightly enlarged laser hut.

### PolariX — measuring the FEL pulse length by 'streaking' the electron bunches

During the shutdown in winter 2020/2021, a new accelerator structure named PolariX [3] was installed in the FLASH2 accelerator tunnel just behind the SASE undulators (Fig. 3). Developed in a collaboration of DESY, PSI and CERN, PolariX is a transverse deflecting structure (TDS) similar to a streak camera. It kicks the accelerated electron bunches to the side with a time-dependent strength of this kick. This way, the longitudinal position along the electron bunch is mapped onto a horizontal coordinate on an imaging screen, or in other words, the arrival time of the individual electrons is mapped to a spatial coordinate. In the longitudinal phase space of the electrons, it allows to measure both, the energy profile as well as the charge distribution along the electron bunch. The longitudinal charge distribution can also be used to deduce the FEL pulse length with femtosecond time resolution. Since the electrons lose part of their energy during FEL emission, their energy profile behind the undulators can also be used to measure the FEL photon pulse length in a complementary way.

### Unique combination yielding new scientific opportunities at beamline FL26

In October 2021, the first FEL-pump-HHG-probe experiment was successfully conducted at the 'Reaction Microscope' (REMI) end station at FLASH2 beamline FL26. This was a collaborative effort of a large team from the Max Planck Institute for Nuclear Physics (MPIK) in Heidelberg led by Christian Ott and Thomas Pfeifer together with colleagues from the Leibniz University Hannover and many colleagues from different groups at DESY. The broadband

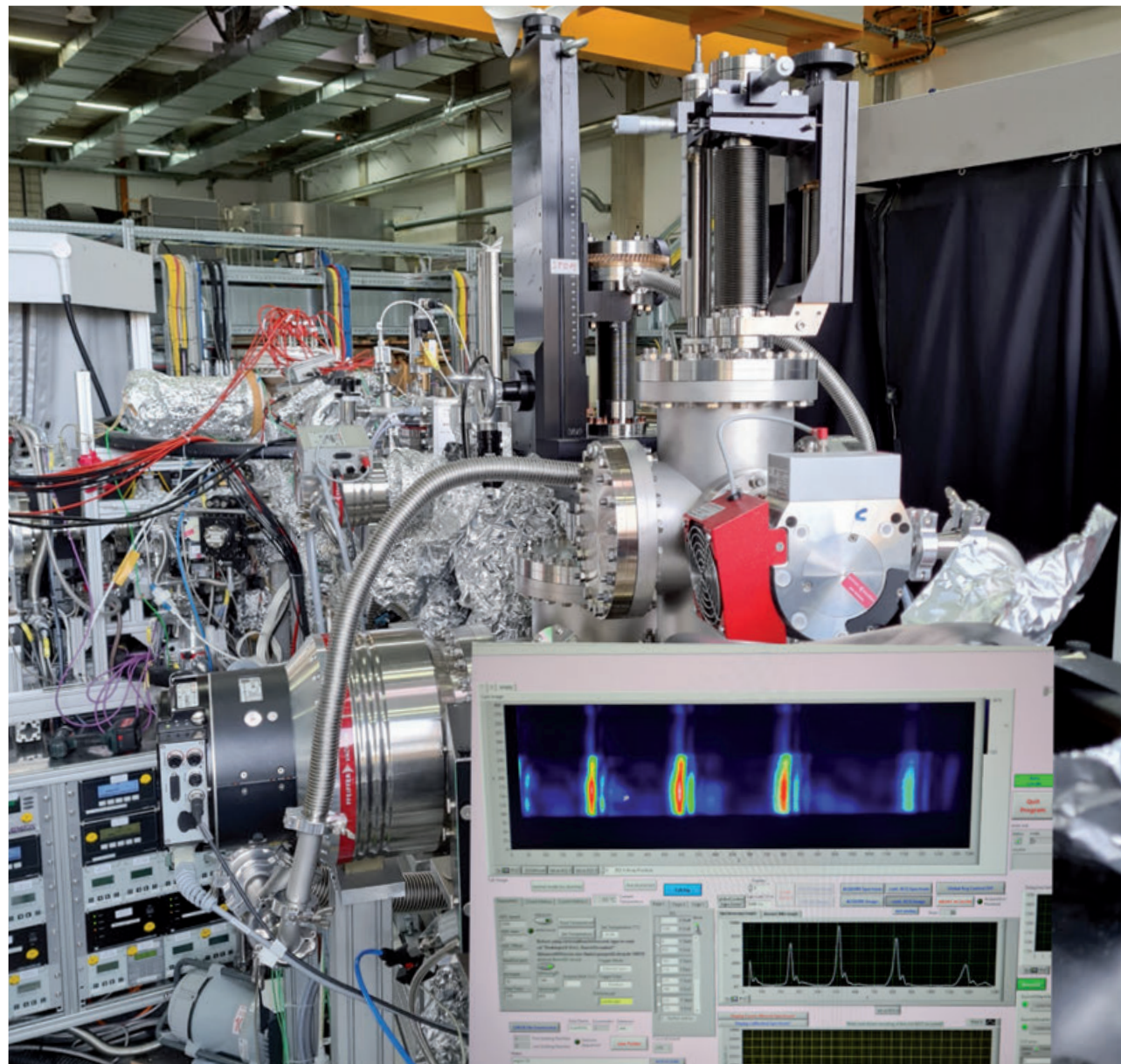


**Figure 4**  
New experimental apparatus for XUV transient absorption spectroscopy behind REMI at FLASH2 beamline FL26 together with recorded HHG spectra resolving individual harmonics (lower right corner).

high-harmonic generation (HHG) spectrum was utilised in femtosecond XUV transient absorption spectroscopy for tracking the dissociation of molecules and identifying the electronic states of the atomic fragments. This effect is highly relevant for understanding the interaction of extreme ultraviolet radiation (XUV) with atmospherically relevant molecules. The transient absorption was measured over the full harmonic spectrum of the HHG source. For that purpose, the colleagues from Heidelberg had installed a refocusing mirror behind REMI, focusing into their own interaction chamber, installed just after REMI. This experimental chamber was complemented by a grating spectrometer with an in-vacuum CCD behind it (Fig. 4). Since FLASH2 and the HHG source [4,5] were running again very reliably, dissociation dynamics of oxygen molecules could be characterised over a large parameter range. This included many different FEL photon energies,

profiting from the tunability of the variable gap undulators at FLASH2. A detailed data analysis is underway and the whole team is looking forward to many exciting insights achieved by ultrafast time-resolved spectroscopy at FL26.

**Contact (FLASH and FLASH2020+):**  
Rolf Treusch, [rolf.treusch@desy.de](mailto:rolf.treusch@desy.de)  
Martin Beye, [martin.beye@desy.de](mailto:martin.beye@desy.de)

#### References

1. L. Poletto et al., *J. Synchrotron Radiat.* **25**, 131–137 (2018).
2. M. Ruiz Lopez et al., *J. Synchrotron Radiat.* **26**, 899–905 (2019).
3. B. Marchetti et al., *Scientific Reports* **11**, 3560 (2021).
4. E. Appi et al., *Sci. Rep.* **10**, 6867 (2020).
5. E. Appi et al., *Rev. Sci. Instrum.* **92**, 123004 (2021).

# FLASH2020+ — first upgrade started

## Energy boost on the horizon

FLASH2020+ aims at providing greatly improved experimental capabilities for all users. Therefore, it encompasses major changes and upgrades to almost all sections of the accelerator, new undulators, as well as a new photon beamline and diagnostics in the FLASH1 tunnel. Furthermore, substantial improvements and new capabilities will be realised in the experimental halls.

The upgrade project involves all scientific and infrastructure groups responsible for FLASH at DESY. Enrico Allaria took over the project lead in 2020 and brought it into full swing. As the new project leader, Lucas Schaper is now in charge of further advancing the project and coordinating the upcoming construction phases (Fig. 1) of FLASH2020+.

**Phase 0** (shutdown November 2021 – August 2022): The exchange of two linear accelerator modules will boost the maximum achievable electron energy. A new injector laser system and an afterburner undulator at FLASH2 will be installed.

**Phase 1** (shutdown planned for 2024): Major upgrades of FLASH1: new undulator chain with variable gap and polarisation, seeding at full repetition rate, new photon beamline and diagnostics in the FLASH1 tunnel for FEL operation and for users; complemented by an upgrade of the THz–XUV pump–probe end station (as used throughout) as well as more flexible pump–probe lasers in both experimental halls.

**Phase 2** (shutdown anticipated for 2026): Upgrade of FLASH2: New configuration of magnet structures for novel lasing concepts towards multi-colour operation and shorter pulses.

The FLASH accelerator team, together with many groups specialised on technical subsystems and infrastructure, as well as the FLASH Photon Science groups are now working full steam to successfully realise major refurbishments and upgrades. The goal is to finish ‘Phase 0’ of the project in the first major shutdown of FLASH before the accelerator commissioning starts again.



**Figure 1**  
Timeline of the FLASH2020+ project construction phases.

Users will benefit most from an increased electron beam energy of the accelerator. It will allow FLASH to lase at about 20% shorter wavelengths than before. This will shift the wavelength limit to about 3.4 nm (365 eV) and thus enable measurements ‘deeper’ in the water window. In addition, FLASH2 will be equipped with a variable polarisation third-harmonic afterburner undulator (Fig. 2). Optimised to provide photon energies around the L-edges of iron, chromium and nickel, the new undulator will allow, for example, for dichroism studies in the field of ultrafast magnetisation dynamics.

After cooling down the superconducting accelerator again in August 2022, the new installations will be commissioned. It is planned to restart operation for users in November 2022, allocating experiments from the last proposal round; the deadline was on 1 October 2021.

The next call for proposals will be issued in spring 2022 for beamtimes in the second half of 2023 before FLASH goes into the next shutdown — planned for the full year 2024 to realise Phase 1.

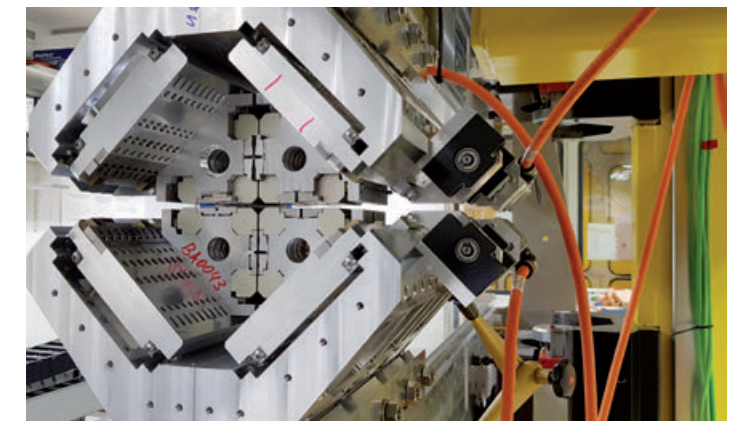


**Figure 2**  
Photograph of the prototype for the afterburner undulator for FLASH2. The pictured design will also serve as a testbed for the new undulators for FLASH1.



**Figure 3**  
New FLASH accelerator module during tests in the Accelerator Module Test Facility (AMTF) hall at DESY. The installation will be done during the first shutdown in 2022.



**Figure 1**  
View into the PETRA III experimental hall 'Max von Laue' during beamtime of users at the beamline P04 with the apparatus 'EASI' (Electronic structure from Aqueous Solution and Interfaces) of the Fritz Haber Institute Berlin (mounted diagonally on the right).

During the year 2021 the operation of PETRA III for users and the construction of beamlines were still affected by the worldwide pandemic. However, due to the experience gained in 2020 how to operate this facility under difficult pandemic conditions, an access mode of PETRA III could be realised which enables national and international users almost normal access to the beamlines and laboratories. In addition, most of the planned beamtimes, which have been postponed from 2020 to the future, could be carried out until August 2021. In the early months of 2021, conducting experiments was still strongly influenced by national and international pandemic regulations and travel restrictions which made it difficult to prepare samples in the users' home institutions or to travel to DESY. Later in the year, almost regular operation for users was possible (Fig. 1). More than 2800 individual users, including mail-in and remote access, performed experiments at PETRA III beamlines which almost corresponds to the number achieved before the pandemic. As usual, the operation time of PETRA III was split into two run periods: one from beginning of March until beginning of July and a second from beginning of August until end of December 2021. During the first run the number of users performing

experiments on-site at DESY was restricted to three person per experiment with exceptions with exceptions for complex and challenging experiments. During the second run, six persons per experiment were permitted.

In total, 4639 hours of beamtime were provided at PETRA III. During the first runs until beginning of July, 1975 hours were available at 23 beamlines: P01-P14 in the PETRA III experimental hall 'Max von Laue', P21.1-P24 in the hall 'Ada Yonath' and P61-P65 in the hall 'Paul Peter Ewald'. In the second half of the year, 2664 hours were available for now 25 beamlines, as beamlines P62 for small-angle scattering and P66 for luminescent spectroscopy have started user operation mode in fall 2021.

### PETRA III — machine operation

In 2021 the availability of the PETRA III storage ring was 97.3% with a mean time between failures of 53 hours (as of 14 December 2021). The PETRA III machine was performing relatively well under the unusual circumstances, although slightly better results have been achieved in recent years. Roughly a quarter of the down

time was caused by external power glitches from the Hamburg power net. A dedicated working group will discuss which measures can be taken to make the PETRA storage ring less sensitive to these glitches. As in previous years, two different electron bunch filling modes were offered for the PETRA III storage ring: a 'timing mode' with 40 bunches for time-resolved measurements and a 'multi bunch' mode with 480 bunches, both with approximately the same share. This bunch-mode distribution has proven to be an optimal scenario to provide a maximum number of 'timing mode' shifts while minimising the radioactive activation of ring components as well as radiation damage of undulators.

The shutdown period in January and February 2021 was used to install the front end for the PETRA III beamline P66 at a bending magnet (Fig. 2). For this, a modified quadrupole was inserted, as well as a synchrotron light extraction chamber and a vacuum flight tube running up to the P66 experimental hutch. Subsequently, the mirror chamber was installed in the summer shutdown 2021, reflecting the VUV beam originating from the bending magnet to the experiment.

With the finalisation of P62 and P66 in 2021, the only open beamline slots at PETRA III are P25 and P63. These beamlines are in the planning phase and will become operational in the next two to three years. The vacuum chambers for the undulators and the front-end hardware for P25 and P63 are already installed. Therefore, the PETRA III storage ring is now in its final configuration for operation with all possible PETRA III beamlines. A change of one cavity is foreseen for summer of 2022 but no further extensive work on the accelerator in the beamline sections is planned. In 2023 an upgrade of PIA, a part of the pre-accelerator installations of PETRA, is planned to ensure reliable operation of PETRA III for the coming years and to enable PETRA IV operations in the long term.

### PETRA III — new beamlines in user operation

In 2021 two more beamlines became operational for regular users: beamline P62 'Small-Angle X-ray Scattering beamline for MATerials research' (SAXSMAT) in the PETRA III experimental hall 'Paul Peter Ewald' and beamline P66 for 'time-resolved luminescence spectroscopy' (Superlumi) in a separate hutch in building 47K. Thus, the 'PETRA III Extension Project (PEX)' has been successfully completed. The PEX project was initiated in 2012 to relocate the most relevant X-ray techniques of the DORIS III light source after its shutdown to PETRA III.

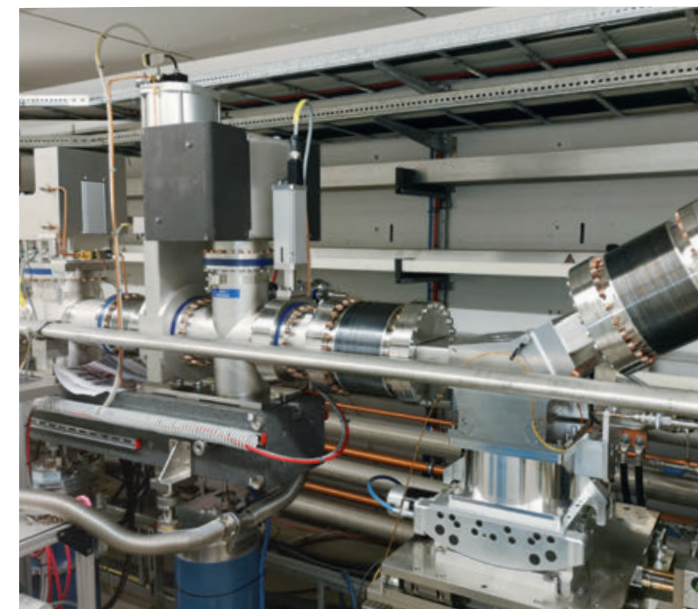


**Figure 2**  
Front end girder and mirror chamber for reflection of the VUV beam up to the experimental hutch of the PETRA III beamline P66.

The mission of the new beamline P62 (Fig. 3) is to serve the community of both hard and soft condensed matter and health research. It enables *in situ* investigation of bio-based hierarchical materials such as bones and health-related samples like cancer tissue. Beamline P62 is also well-suited to investigate the synthesis of nanoparticles and for *operando* studies of catalysts. Other topics of interest are energy storage and conversion materials as well as nano-confinement of materials.

Beamline P62 offers an X-ray small- and wide-angle scattering (SAXS/WAXS) setup, also in combination with computed tensor tomography. This setup is capable of *in situ* and *operando* SAXS/WAXS as well as high-throughput applications. The X-ray source is a 2 m undulator. X-ray beams are available in a photon energy range between 3.5 keV and 35.0 keV with a flux of  $10^{13}$  photons/sec. The focal size can be as low as a few micrometres. The SAXS detector is an in-vacuum Eiger2X 9M, whereas the WAXS detector is an Eiger2X 4M. Both detectors can be operated simultaneously and allow for > 200 Hz frame rate for *in situ* applications at full resolution. For contrast enhancement, the photon energy can be tuned to the relevant absorption edges of materials, thus offering anomalous SAXS.

The mission of beamline P66 is to investigate radiative decays which are created by electronic excitations. At



**Figure 3**  
View into the experimental hutch of the PETRA III beamline P62 with the wide SAXS flight tube extending to the back (left). First data obtained at P62 of 10 nm gold nanoparticles (right).

P66 (Fig. 4) the luminescence of previously excited samples can be measured, e. g. of future scintillator materials. For the time-resolved analysis of the luminescence decay the timing mode is inevitable. Here, PETRA III is of advantage for the beamline with 90 ps pulse width and 192 ns separation of the light pulses.

The photon energies of the beamline range from 3.7 eV (UV) to 40 eV (VUV) which corresponds to a wavelength range of 31 nm to 335 nm. The resolving power of the primary monochromator lies between  $6 \times 10^{-4}$  and  $9 \times 10^{-4}$ , depending on the photon energy. The experimental hutch is located between the PETRA hall 'Max von Laue' and the FLASH2 hall 'Kai Siegbahn' on top of the PETRA III wall.

At the experimental station, a helium flow cryostat is available to reach sample temperatures between 10 K and 380 K in a high-vacuum sample chamber.

#### PETRA III - design and construction of remaining beamlines

In 2021 two last remaining open beamlines are in the design phase and one end station is in the construction phase: the undulator beamline P25 and the undulator beamline P63, a cooperation project with Max Planck institutions as well as the end station HIKA at beamline P23, a cooperative activity with the Karlsruhe Institute of Technology (KIT). These beamlines are not part of the above mentioned PEX-project.

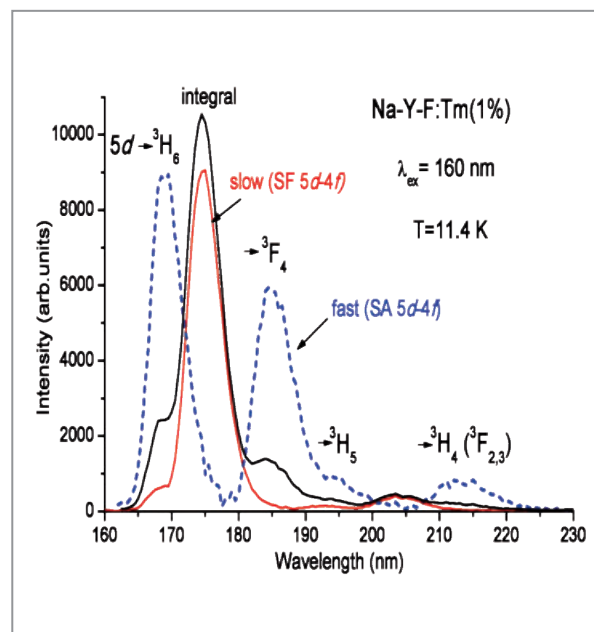
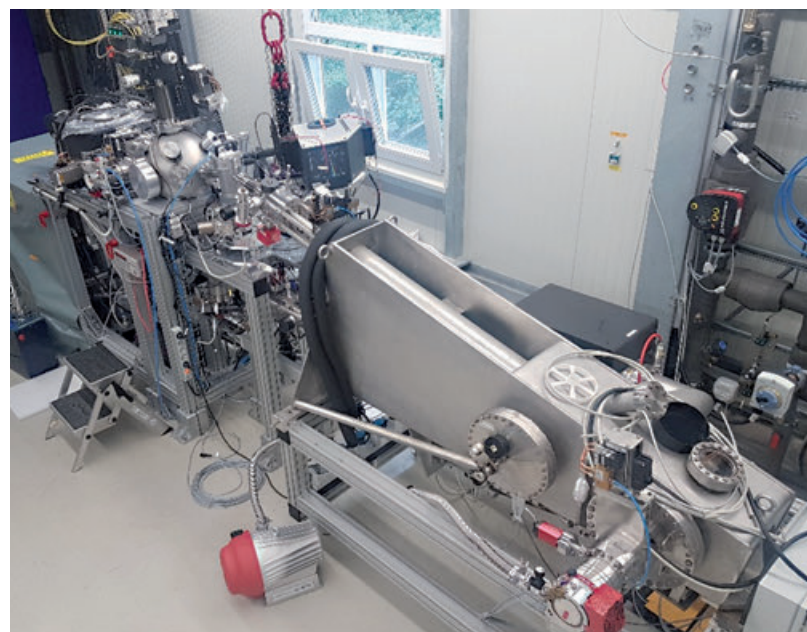


**Figure 4**  
(left) View of the experimental setup at the PETRA III beamline P66 with the sample chamber in the back and primary monochromator in the front. (right) The graph on the right shows a first energy-resolved luminescence spectrum of Na-Y-F:Tm for fast (20 ns) and slow (140 ns) response.



**Figure 5**  
Experimental hutch for the HIKA experiment at the PETRA III beamline P23 (left). Lifting the HIKA imager into the PETRA III hall 'Ada Yonath' through the opened hall roof (right).



In the PETRA III experimental hall 'Ada Yonath', the biggest activity is the upgrade of the *in situ* diffraction beamline P23 with an end station for hierarchical imaging (HIKA). This joint project of KIT and DESY is funded by the Helmholtz Association of German Research Centres (HGF). This upgrade complements the existing imaging techniques available at PETRA III by hierarchical imaging methods for materials research in life sciences and semiconductor research. The project is advancing rapidly. In 2021, the new experimental hutch was erected and the HIKA instruments delivered to DESY (Fig. 5). Due to the enormous weight and dimensions of HIKA, parts of the roof of

the PETRA hall 'Ada Yonath' were temporarily removed to enable the delivery and installation. Three staff members of KIT are on-site at PETRA III to realise the project in cooperation with DESY. In 2022, the installations will be completed and both the preparation and the control hutches will be built. The first beam in the hutch is expected end of 2022 or beginning of 2023.

Beamline P25 is part of a joint project of the PETRA III and the DESY group of PETRA III and the DESY group for innovation technology transfer (ITT). It will be serving customers from industry and academia who need imaging or

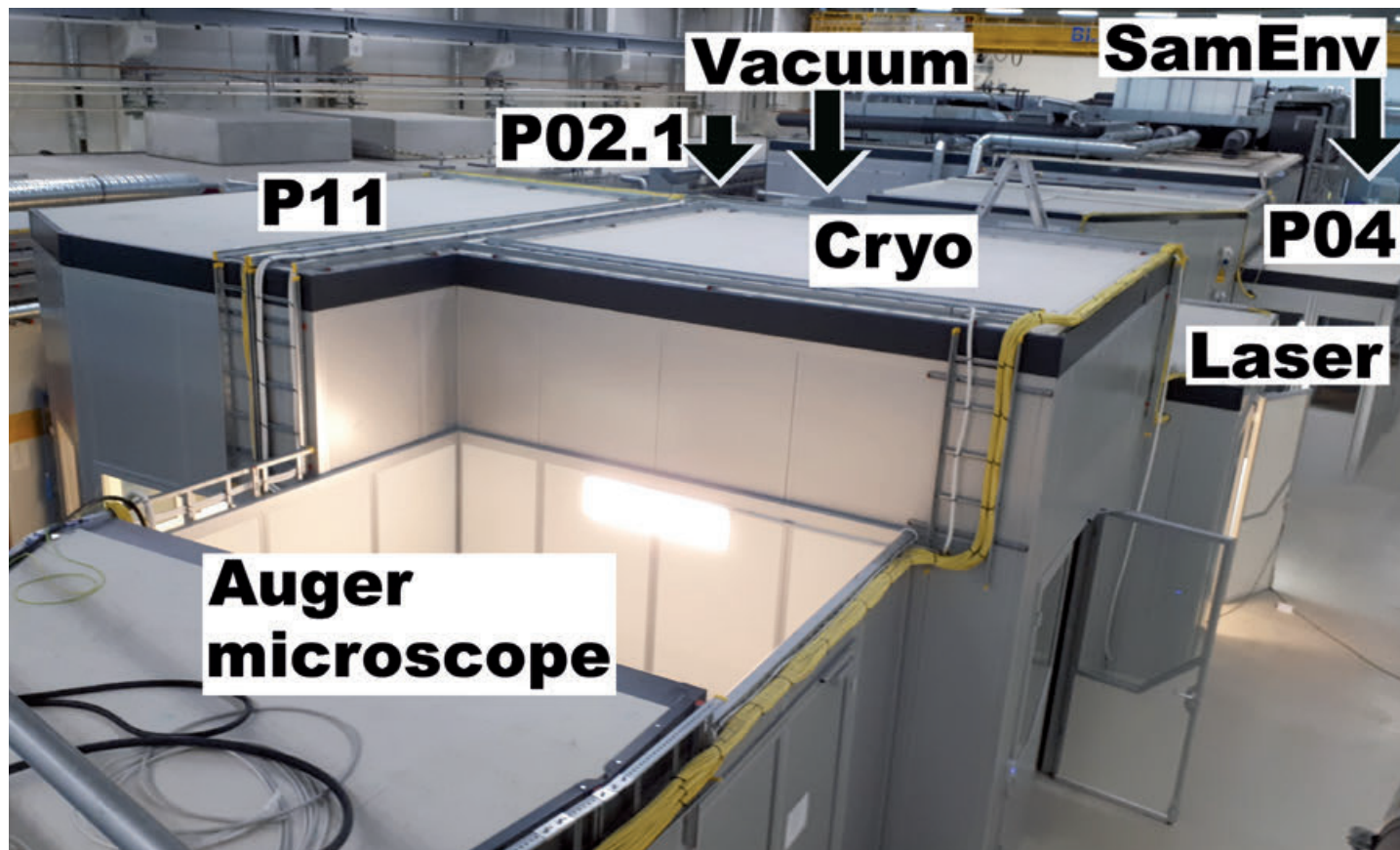


**Figure 5**  
New laboratories for beamlines, sample environment and technical support: The infrastructure is located in the PETRA III hall 'Max von Laue'. 'SamEnv' is a laboratory for the sample environment team of PETRA III.

powder diffraction applications for investigating their samples. Located in a hutch for monochromatic X-ray beams, both end stations will be designed for fully automated operation. In addition, an end station for white and pink beam applications will be constructed in a separate hutch. This hutch will also be used for testing and commissioning components needed for the PETRA IV project. It is planned to complete the design in early 2022 and start with the construction phase soon afterwards.

P63 is the last open beamline at PETRA III. In 2021 it was decided to start planning this beamline and to bring it into operation well in advance of the shutdown for the PETRA IV upgrade. Beamline P63 will be planned in very close cooperation with the Fritz Haber Institute in Berlin and the Max Planck Institute for Chemical Energy Conversion in Mülheim an der Ruhr. It will be dedicated to combined XAS/XRF/SAXS/powder diffraction studies and will partially add to already existing XAS capabilities at beamlines P64 and P65 which are heavily overbooked. It is planned to start the detailed technical design next year; the first beam shall be available in 2024.

#### **PETRA III — upgrade of laboratories and general services**

In 2021 the new PETRA III laboratory infrastructure is close to being finalised (Fig. 6). In total, eight specialised laboratories have been erected in sector 0 in the PETRA III

hall 'Max von Laue'. Four laboratories add to the capabilities of existing PETRA III infrastructure: a dedicated lab for preparation and maintenance of PETRA III sample environment, a laboratory for the soft X-ray beamline P04, one for the powder diffraction beamline P02.1 and one for the macromolecular diffraction beamline P11. Another four specialised laboratories offer new general services at PETRA III. These services will comprise a laboratory for construction, maintenance and preparation of cryogenic sample environments, a lab for vacuum applications, a laser lab for off-line laser experiments and preparation and a lab for Auger-microscopy which is operated by the DESY NanoLab group.

Particularly, the aforementioned new labs will be of high importance for the future support of users and services to the beamlines, especially for PETRA IV. These new infrastructures will be operated by additional technical personnel. It is planned to start the operation of the laboratories in summer 2022.

*Contact (PETRA III): Oliver Seeck, [oliver.seeck@desy.de](mailto:oliver.seeck@desy.de)  
Hans-Christian Wille, [hans.christian.wille@desy.de](mailto:hans.christian.wille@desy.de)  
Contact (PETRA IV): Kai Bagschik, [kai.bagschik@desy.de](mailto:kai.bagschik@desy.de)  
Stephan Klumpp, [stephan.klumpp@desy.de](mailto:stephan.klumpp@desy.de)*

# PETRA IV — The ultimate 3D X-ray microscope

Revised storage-ring lattice with improved performance and an updated beamline portfolio

Within the PETRA IV project, PETRA III is to be upgraded to a synchrotron radiation source with ultra-low emittance. This will turn PETRA IV into a giant 3D X-ray microscope for biological, chemical and physical processes. It covers all relevant length scales and will be able to uncover the structure and dynamics of complex matter in all fields of science. The technical design phase of the PETRA IV project reached the end of its second year in 2021. Three major tasks for the upgrade of PETRA III have been pursued: The detailed design of the new storage ring lattice, the definition and refinement of the future beamline portfolio and the planning of additional infrastructure for PETRA IV.

In early 2021, a new transformative storage-ring concept was developed and further refined over the year. It is based on a 'hybrid 6-bend achromat' (H6BA) lattice with damping undulators. It outperforms the previous designs, as described in the PETRA IV conceptual design report (CDR) published in 2019 and the combi-lattice proposed in 2020, in terms of electron-beam stability and lifetime and makes a more reliable and sustainable top-up injection possible. In addition, the new lattice enables improved operation modes for timing experiments.

The new lattice also allows us to preserve the sector layout in the existing experimental halls. This will guarantee a sustainable re-use of existing infrastructure and simplify the start of operation for users. Overall, this leads to a slight reduction of the brightness of each beamline com-

pared to the previous design, while it preserves the current sector layout and creates space for three additional beamline sectors. Figure 2 shows the brightness of undulators in normal (4.5 m) and long straight sections (10 m) in comparison to the current brightness at PETRA III. The brightness will be improved by two to three orders of magnitude at all PETRA IV beamlines and will enable an outstanding suite of experiments, many of which are not feasible at present. However, the lattice design change will require further detailed studies that will be incorporated into the PETRA IV technical design report (TDR) now planned for mid 2023. According to the new PETRA IV project plan, the shutdown of PETRA III is planned for the end of 2025, followed by a two year construction phase, leading to a start of operation in January 2028. Based on the science case of PETRA IV and its outstanding



**Figure 1**  
Artist's view of the DESY campus with the PETRA IV storage ring (dashed line) and the planned experimental hall West (left). (Copyright: Science Communication Lab and DESY)



# The European Molecular Biology Laboratory Hamburg

Facilities for integrated structural biology at PETRA III

The Hamburg site of the European Molecular Biology Laboratory (EMBL) connects research and services to generate scientific excellence. We offer access to our integrated structural biology facility which includes, among others, preparation, crystallisation, biophysical and structural characterisation of biological samples and data analysis. We work together with other EMBL sites to provide support and increase automation throughout the experiment: from sample preparations to data deposition. Due to the Covid-19 pandemic, most EMBL services have been provided by remote operation (user-driven experiment control from a remote location) or mail-in services (experiment performed by on-site staff). In addition, intensive efforts have aimed at shaping up a future research infrastructure portfolio for PETRA IV. This year's research highlights at EMBL Hamburg included work on the structure mycobacterial ESX-5 complex and analysis of pH-responsiveness inside lipid nanoparticles (see the highlight section of this report).

## EMBL Hamburg offers access to its integrated facility within Instruct-ERIC

The European Research Infrastructure Consortium (ERIC) Instruct makes high-end research infrastructures, technologies and methods in structural biology available to external researchers. Since 2019, EMBL has been an Instruct-ERIC member and in addition, the Instruct Centre EMBL was launched in 2021, providing services in integrated structural biology from its sites in Heidelberg, Grenoble and Hamburg.

## Benefits of AlphaFold at EMBL Hamburg

AlphaFold2 is an artificial intelligence-based program that predicts protein structures with unprecedented accuracy. AlphaFold2 and the AlphaFold Protein Structure Database, released by DeepMind and EMBL, respectively, are a breakthrough for structural biology and will benefit research and services at EMBL Hamburg. AlphaFold2 supports macromolecular crystallography as it helps solve challenging structures, provide initial models for molecular replacement, interpret electron densities and design optimal constructs for purification and crystallography. Advanced applications, such as time-resolved X-ray crystallography and SAXS, will complement AlphaFold2 by providing information about structural dynamics.

## Sample Preparation and Characterisation (SPC) Facility

The SPC Facility offers a pipeline from the lab bench to the

EMBL beamlines, helping optimise and prepare samples for structural studies. The facility has become a member of the Molecular-Scale Biophysics Research Infrastructure (MOSBRI) consortium which allows supported access to molecular biophysics services across Europe.

The SPC team released eSPC, a freely available online platform (Fig. 1) which enables users to analyse molecular biophysics data from a range of experimental techniques without the need to travel to the lab where the data have been generated [1].

## Beamline P12 for biological small-angle X-ray scattering (SAXS)

P12 is an undulator beamline optimised for low background data collection from macromolecular solutions and kinetic experiments with high temporal resolution. P12 provides fully automated and remote data acquisition and processing which has allowed to continue the provision of services in 2021.

Anomalous SAXS (ASAXS) provides element-specific information. ASAXS measurements of proteins are now possible at the beamline P12 thanks to new developments including the beamline control, data acquisition and reduction pipeline and new modelling tools [2,3].

In the frame of EMBL's Environmental Research Initiative, the Svergun Group is using P12 to study dispersion of plastics in the environment ending up as micro and nano-sized debris. SAXS is employed to study the structure of

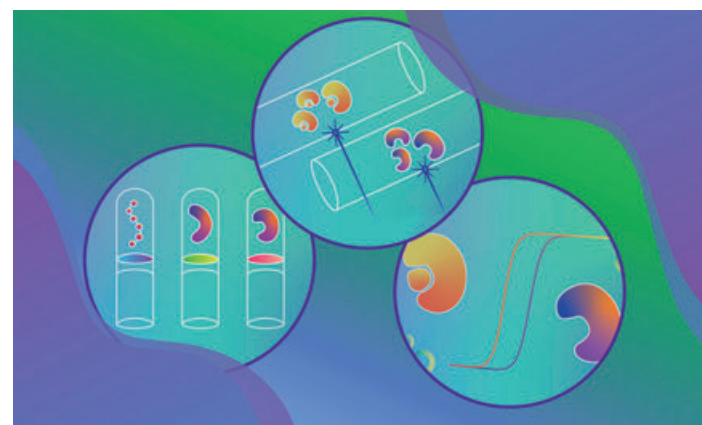


Figure 1

eSPC is a freely available online platform for analysis of molecular biophysics data (Credit: Silvia Burastero and Creative Team/EMBL).

nanoplastic particles in water to provide data in order to help remediation/elimination of nanoplastic pollution.

Scientists from several Hamburg research institutes led by the Svergun group collected the first SAXS curve of a protein using an X-ray free-electron laser (Fig. 2). The experiment, conducted at the European XFEL, used samples containing SARS-CoV-2 spike proteins complexed to specific antibodies. The results could improve understanding of the immune response in Covid-19.

The Small Angle Scattering Biological Data Bank (SASBDB), a searchable curated repository of SAXS experimental data run at EMBL, reached 2000 entries in spring.

## Beamlines P13 and P14 for macromolecular crystallography

The second P14 end station for time-resolved X-ray crystallography (T-REXX) is dedicated to serial synchrotron crystallography. The beamline graphical user interface MXCuBE and the automatic data processing and storage in our laboratory information management system ISPyB (recently renamed to EXI) were improved. The auto-processing results are now displayed as overview tables with downloadable diagrams and processed files. The resulting electron density is automatically available for inspection in a web browser minutes after data collection (Fig. 3). This fast feedback after a current measurement enables the adjustment of the subsequent data collection and allows remote users to follow the ongoing experiment almost in real time.

The Dectris CdTe 16M Eiger2 detector was installed at P14. Thanks to optimised beamline optics, an advanced Global Phasing Ltd's data-collection workflow [4] and CdTe-based high-resolution Eiger2 detector, users can now collect precise and accurate data on large unit-cell systems at high energies [5]. The setup can support the most demanding applications of X-ray crystallography to structural biology and enzyme-mechanistic studies.

## New team leader will establish biological X-ray imaging

EMBL Hamburg welcomes Liz Duke, a new team leader, who will establish biological X-ray imaging at P14. Hard X-ray biological imaging is an emerging technique that uses high energy X-rays to image tissues or even entire organisms. The technique will play a big role in EMBL Hamburg's future portfolio, enabling scientists to study life on multiple scales.

## Events and PETRA IV

EMBL Hamburg's events took place virtually this year. These included the workshop 'Strategy for future EMBL research infrastructures in the Life Sciences in Hamburg' which aimed to receive feedback from the international community on EMBL's plans for PETRA IV. EMBL forged closer ties with DESY by jointly organising a workshop on promoting industrial use of structural biology beamlines at PETRA III and PETRA IV as well as facilitating innovation. EMBL also presented its plans for future beamlines at the PETRA IV Beamline Portfolio Users' Workshop.

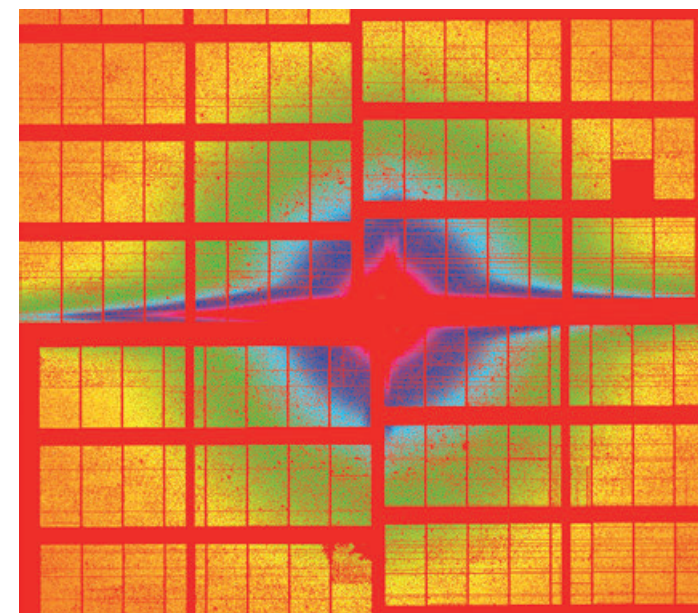


Figure 2

Scattering pattern of bovine serum albumin during the SAXS experiment at the European XFEL. The pattern was formed by X-ray pulses (from the European XFEL) which scattered when they hit the sample. They were captured by a AGIPD 1Mpx detector consisting of multiple panels, visible as rectangular tiles in the image. The colours indicate the scattered intensity. Image based on data generated by research groups at European XFEL, EMBL Hamburg and others (Credit: Andrey Gruzinov/EMBL).

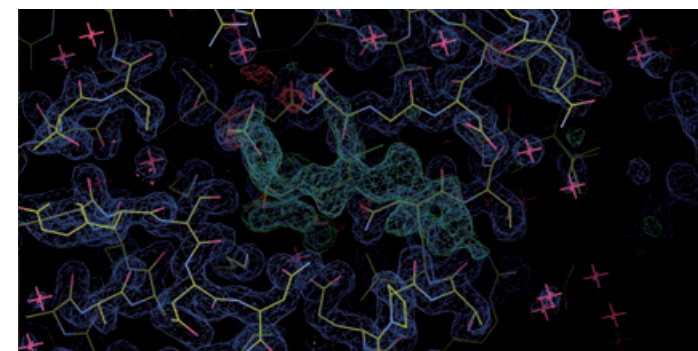


Figure 3

The information management system automatically provides the electron density of the collected dataset within a few minutes after data collection on T-REXX - the second end station at P14. (Credit: David von Stetten/EMBL).

To continue training and enable scientific exchange, EMBL has organised a SAXS course, a virtual P12 user meeting and the EMBO workshop 'Recent Advances in Structural Biology of Membrane Proteins'.

Contact: Dorota Badowska,  
dorota.badowska@embl-hamburg.de

## References

1. O. Burastero et al., *Acta Crystallogr. D* 77, 1241–1250 (2021).
2. A. Y. Gruzinov et al., *J. Synchrotron Radiat.* 28, 812–823 (2021).
3. D. C. F. Wieland et al., *J. Appl. Crystallogr.* 54, 830–838 (2021).
4. M. Oscarsson et al., *J. Synchrotron Radiat.* 26, 393–405 (2019).
5. S. L. S. Storm et al., *IUCr* 8, 896–904 (2021).

# The GEMS branch at DESY

Diffraction and imaging techniques optimised for the needs of materials research

Helmholtz-Zentrum Hereon operates the German Engineering Materials Science Centre (GEMS). The experimental stations of GEMS at PETRA III are continuously being developed and upgraded for (engineering) materials science users from institutions in Germany and all over Europe. The number of publications remains on a high level and a selection is presented below. Within the PETRA IV Beamline Portfolio process, GEMS has suggested plans for new beamlines to continue the successful work and to exploit the new possibilities at PETRA IV. A special issue of *Advanced Engineering Materials* published in 2021 gives an extensive overview of the experiments at the Hereon beamlines at PETRA III.

## Diffraction

The engineering materials station (Fig. 1) of the new white-beam beamline P61 at PETRA III started user operation in spring 2021 and is in high user demand. Many experiments focused on residual stress analysis in engineering materials and components. The white beam from the damping wiggler delivers excellent flux up to 200 keV, enabling diffraction experiments with several centimetre-thick steel samples. Experiments were also conducted to explore the microbeam radiotherapy technique. In summer, a heavy-load diffractometer was installed for the use with heavy samples or sample environments. A high-speed radiography station is currently developed within the framework of the Röntgen-Ångström Cluster project 'Track-AM'.

At the High Energy Materials Science Beamline P07, a series of experiments with the *in situ* selective laser melting (SLM) chamber was carried out. Two groups from TU Berlin studied the SLM process and the solidification of intermetallic TiAl alloys (Fig. 2). With the current setup, the rapid solidification and the corresponding phase transfor-

mations in a Ti-48Al-2Nb-2Cr alloy (in at. %) could be observed using high-energy X-ray diffraction with a time resolution of 20 ms [1]. Another experiment taking place was the *in situ* observation of precipitation kinetics in the Ni-based superalloy CMSX-4 using high-energy small- and wide-angle scattering (SAXS/WAXS) [2]. The high heating and cooling rates connected with the laser process lead to phase transformations far off from equilibrium, making model predictions more difficult, requiring experimental data for evaluation. Moreover, a hall-of-fame article was published in *Advanced Engineering Materials* that reviewed the impact of synchrotron X-ray techniques on the development of intermetallic TiAl alloys for high-temperature applications like, e. g. turbine blades in aircraft engines [3].

## Imaging

Materials research often requires the ability to use specifically designed *in situ* sample environments such as ovens, stress rigs, corrosion cells or nanoindenters which all are regularly used at our imaging instruments. Recently, a new nanoindenter was installed at the nanotomography end station of P05, enabling the collection of tomographic data during *in situ* nanoindentation [4]. The availability of a nanoindenter for full-field imaging complements the nanoindenter at the scanning nanodiffraction station of P03 Nanofocus End station. This has been available for many years and was recently used to study novel crosslinked super-crystalline nanocomposites materials made of organic functionalised nanoparticles [5]. The widely used stress rig at the P05 microtomography end station was improved and applied to the analysis of ten-

Figure 1

Experimental setup for measuring small samples with an energy-dispersive detector at P61A.



Figure 2  
Sketch of the experimental setup of the *in situ* SLM experiment at P07 (top) and diffraction patterns from the melt ( $t = 0.08$  s) and 20 ms after the laser beam crossed the gauge volume ( $t = 0.10$  s; bottom) [1].

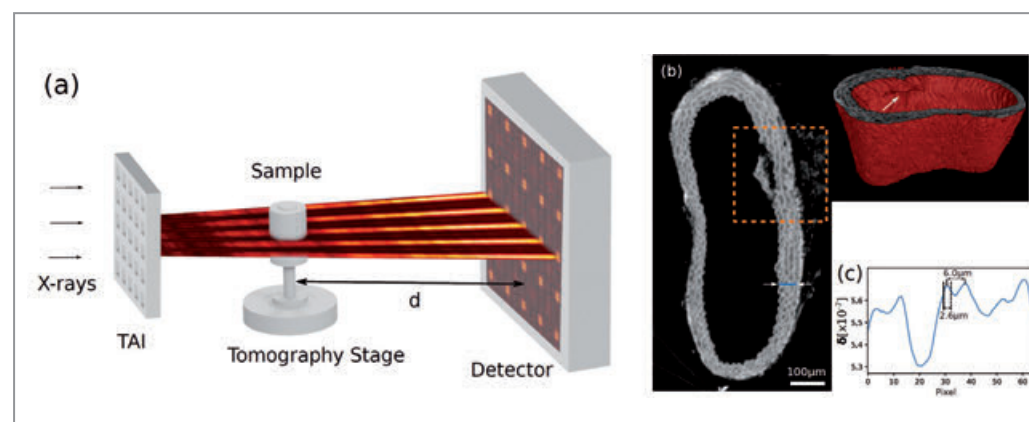
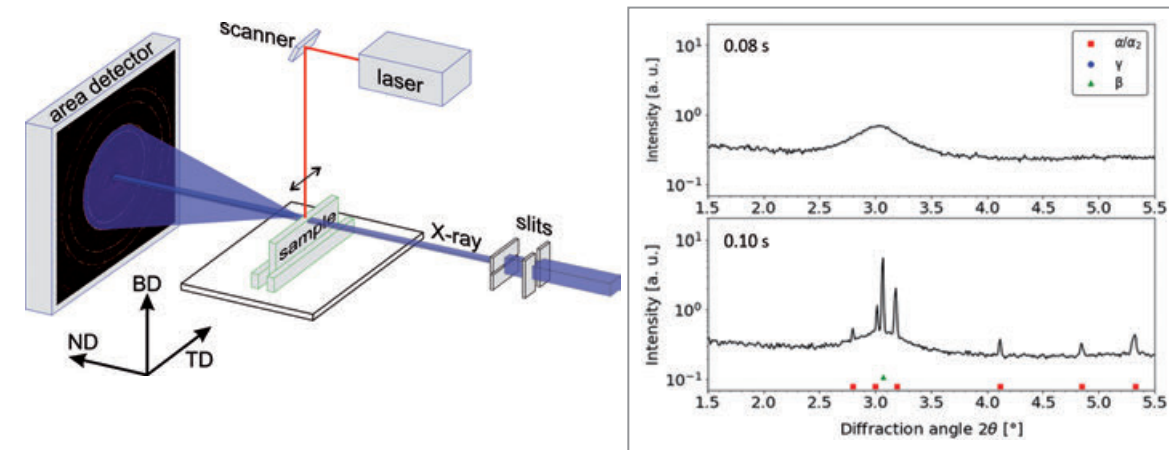


Figure 3

a) Phase-contrast imaging setup using Talbot array illuminators illustrating the formation of the intensity modulation. (b) Rendering of a mouse aorta phase-contrast scan depicting a fissure in the vascular wall (white arrow) and a respective slice showing its lamellar structure. (c) Line plot of blue line in (b) showing that two lamellae distanced  $6 \mu\text{m}$  apart can be well resolved [8].

sion wood [6], primate teeth, rubber or rodent tendons under mechanical load. The temporal resolution for *in situ* experiments was considerably improved.

The advancement of phase-contrast techniques was a key development at our full-field instruments. At the P05 nanotomography end station (spatial resolution below 40 nm), the world's first hard X-ray holo-tomography setup using Fresnel zone plates has been installed [7]. It allows to adjust the spatial resolution and the field-of-view by changing the focus-to-sample distance. Owing to the very good contrast in the well-established transmission X-ray microscopy mode (TXM) using Zernike phase contrast, the orientation of collagen fibres in human cortical bones was analysed and a relationship was found between the dark and bright osteons and the mechanical properties of bone(s) [4]. At tomographic scan times below three minutes the signal-to-noise ratio decreases significantly and classical image-filtering techniques reach their limitations. A machine-learning denoising algorithm was used to eliminate the noise in standard TXM scans enabling faster segmentation, e. g. *in situ* mechanical testing of biodegradable implants at the micro-tomography station. To make this approach available to all our users, an interactive framework is currently being developed within the HAICU (Helmholtz Artificial Intelligence Cooperation Unit) project Universal Segmentation Framework (UniSeF). Quantitative phase contrast, a technique which delivers tomography data normalised to effective atomic numbers, has been successfully implemented at the P05 and P07 micro-

tomography end stations using 2D Talbot array illuminators (Fig. 3). This approach also closes the gap in spatial resolution and allows to visualise soft tissues in the presence of highly attenuating materials, facilitating the use of contrast enhancing stains.

Two sets of molybdenum-silicon multilayer Laue lenses (MLL), developed by AXO (Dresden), have been implemented at the P03 Nanofocus end station within a long-term proposal from the Montanuniversität Leoben (Austria). Focal spots of 100 nm and 25 nm at working distances of 15 mm and 3 mm, respectively, are now available in addition to the 250 nm focus generated by Kirkpatrick-Baez mirrors at a focal distance of 100 mm. The MLL optics have already been successfully used for the characterisation of micrometre-sized layers for hard coating applications.

Author contact: Christina Krywka, christina.krywka@hereon.de  
Peter Staron, peter.staron@hereon.de  
Martin Müller, martin.mueller@hereon.de

## References

1. G. Graf et al., *Adv. Eng. Mater.* 2100557 (2021).
2. B. Wahlmann et al., *Adv. Eng. Mater.* 2100112 (2021).
3. P. Erdely et al., *Adv. Eng. Mater.* 2000947 (2020).
4. K. E. Stockhausen et al., *ACS Nano* 15, 455–467 (2021).
5. D. Guintini et al., *Nanoletters* 21, 2891–2897 (2021).
6. S. Schmelzle et al., *Adv. Eng. Mater.* 2100235 (2021).
7. S. Flenner et al., *Opt. Express* 28, 37514–37525, (2020).
8. A. Gustschin et al., *Optica* 8, 1588–1595 (2021).

# DESY Photon Science at the European XFEL

User consortia of the Helmholtz International Beamline (HIB)

Besides being responsible for the construction and the operation of the European XFEL linear accelerator, DESY plays an important role as user of the European XFEL. DESY is partner in several user consortia. The three largest of these are the Serial Femtosecond Crystallography (SFX) user consortium, the Helmholtz International Beamline for Extreme Fields (HIBEF) and the Heisenberg Resonant Inelastic X-ray Scattering (hRIXS) user consortium. Moreover, DESY scientists are developing lasers and detectors for usage at the European XFEL.

## SFX

The international SFX consortium provides methodologies and instrumentation for serial femtosecond crystallography experiments at the 'Single Particles, Clusters and Biomolecules and Serial Femtosecond Crystallography' (SPB/SFX) instrument of the European XFEL. It is now well recognised in the structural biology community that intense femtosecond-duration pulses overcome prior limitations in structure determination due to radiation damage and offer a unique capability of imaging macromolecules at ambient pressures and temperatures, all possible with ultrafast time resolution. With this in mind, the European XFEL issued a call for rapid-access experiments relevant to Covid-19-related research. Members of the SFX user consortium nucleated two collaborative proposals that were each awarded beamtime in early 2021 to examine the dynamic behaviour of the SARS-Cov-2 proteases. One group, led by T. J. Lane of DESY, is shown below (Fig. 1).



Both were successful experiments, collecting about 2 petabytes of data in total with the analysis ongoing at the time of writing.

The SFX user consortium has also contributed critically to the ongoing success of the SPB/SFX instrument through both funding and expert collaboration. As of September 2021, the SPB/SFX instrument has produced about 20 peer-reviewed publications using EuXFEL beam, many in high-impact journals. Much of the instrumentation used routinely at SPB/SFX was contributed by the SFX user consortium. For example, in 2021 the downstream station of the instrument enabled several experiments using an in-air extrusion jet of lipidic cubic phase in order to study the structure and dynamics of particular membrane proteins.

## HIBEF

The HIBEF user consortium is led by the Helmholtz-Zentrum Dresden-Rossendorf (HZDR) in collaboration with DESY and the Central Laser Facility (CLF) from Rutherford Appleton Laboratory (UK) as the major consortium partners. HIBEF contributes personnel and scientific input for experiments at the High Energy Density (HED) instrument of European XFEL.

After a successful community commissioning experiment in 2019 the high-pressure setup using diamond anvil cells (DAC) provided by DESY is an established experimental

Figure 1

T. J. Lane (left) coordinated a large collaboration for the rapid-access experiment 'New structures to fight Covid-19 solved by liquid jet SFX at the European XFEL'. Over 50 collaborators from more than 15 institutions took part. Many of the SPB/SFX beamline staff (shown here) ran the experiment, while others provided samples or ran remote analysis (Credit: European XFEL).

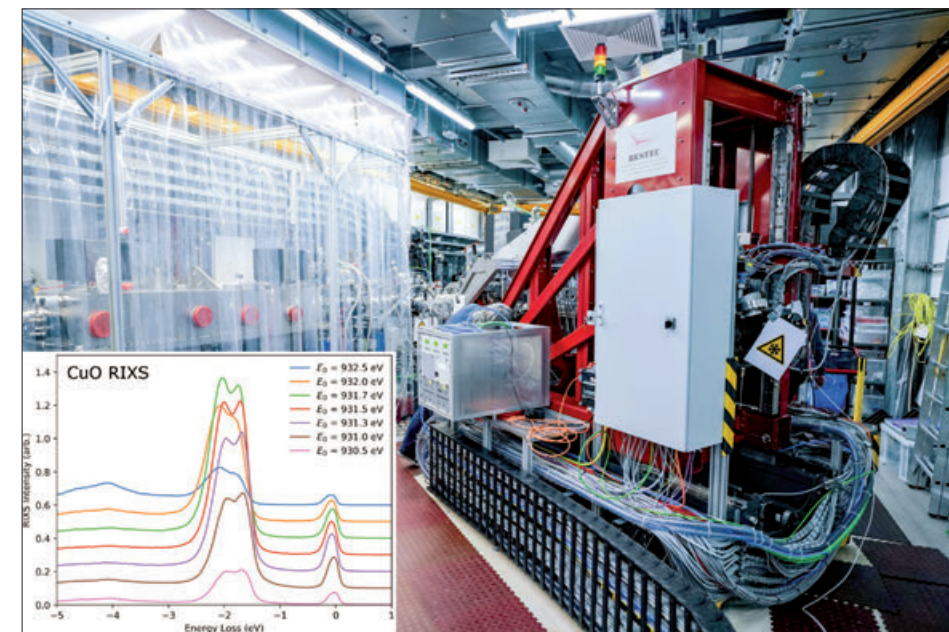


Figure 2

The Heisenberg RIXS spectrometer has undergone XFEL commissioning in 2021. Within minutes high-resolution RIXS spectra can be recorded. Now the next steps are on their way to get the temporal and energy resolution to the transform limit for chemical dynamics and changes in functional materials. hRIXS is looking forward to science-driven full user operation in 2022 (Credit: European XFEL).

setup, see also the highlight section of this report. In 2021 measuring campaigns with megahertz-time resolution in different fields of high pressure science were conducted. The high brilliance and the unique bunch train structure of the European XFEL were exploited for X-ray heating of low-Z materials using couplers, single shot pulsed laser heating and dynamic compression experiments utilising piezo-driven diamond anvil cells.

After successfully completing the internal commissioning of the Relativistic Laser at EuXFEL (ReLaX) [1], an international community performed a first user experiment combining the ReLaX high-intensity laser provided by HIBEF with the X-ray beam at HED. The goal was to have various physical settings and demonstrate in each the technical feasibility of several X-ray diagnostics, such as SAXS using an analysing highly annealed pyrolytic graphite (HAPG) crystal, phase-contrast imaging (PCI) and X-ray spectroscopy within the harsh radiation background generated by the laser-plasma interaction. The successful completion of this experiment paves the way for multiple novel science cases at HED.

The high-energy laser DiPOLE 100-X is on the track of recommissioning. Beam transport, velocity interferometer system for any reflector (VISAR) system and frequency doubling unit are installed or respectively in production. A community-commissioning proposal was submitted and accepted by the peer review panel and beamtime is foreseen in 2022. Sample preparation of shock compression targets has already started. Main parts of the high magnetic fields-setup provided by HZDR, like the heavy load goniometer and the capacitor bench with its dedicated room, will be built up in the first half of 2022. The coil design has been improved in order to reach higher fields than 45 T and will be tested.

## hRIXS

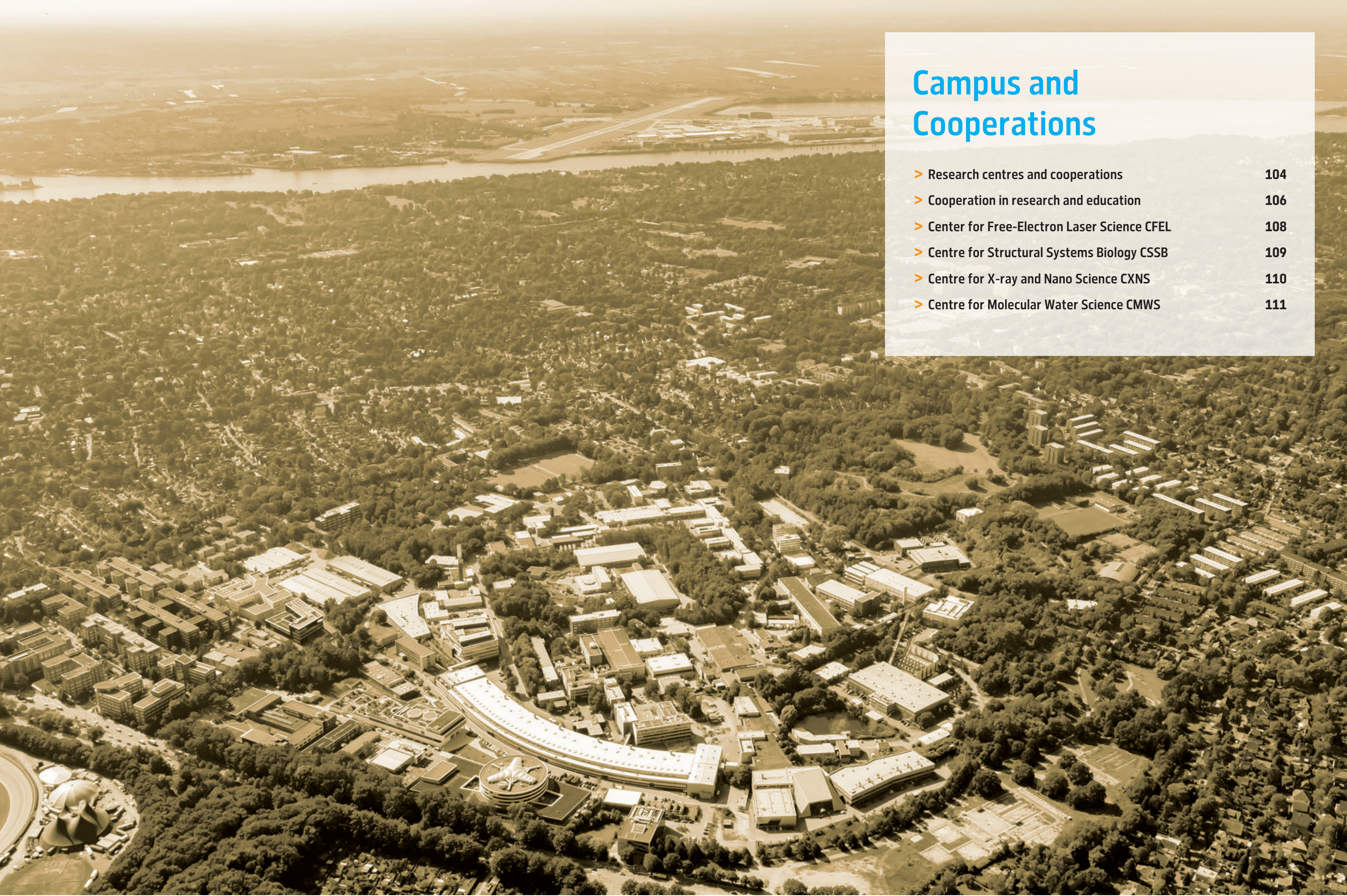
The Heisenberg RIXS consortium (hRIXS) has received the spectrometer (Fig. 2) and the 'Chem'-chamber from Bestec GmbH (design hRIXS consortium). Together with European XFEL's dedicated chamber for solids, this instrumentation is ready for studies of chemical dynamics and functional materials on the experimental floor of European XFEL. Commissioning shows exceedingly swift high-quality data acquisition. Here, joining the expertise of the hRIXS international consortium members with XFEL staff, was crucial. hRIXS with its high transmission and high resolution gratings (400–1600 eV energy range) brings new impetus to determine governing principles, trace dynamic pathways and non-equilibrium properties for chemical and physical science, materials, energy conversion and even bio-relevant systems. In 2022 full science-driven user operation will start. Funding for hRIXS is provided by the Helmholtz Association via strategic investment in the HIB and other national funds (Italy, Germany). The project is partially supported by the ERC Advanced Grant 'EDAX' at Potsdam University. A high-end detector is funded by Finnish partners through a FIRI grant. hRIXS includes partners from Germany, Switzerland, Finland, France, Sweden, Italy and the UK. The project is coordinated by Potsdam University in close collaboration with DESY and European XFEL.

## Contact:

SFX: Henry Chapman, CFEL/DESY and Universität Hamburg, henry.chapman@desy.de  
HIBEF: Thomas Cowan, HZDR, t.cowan@hzdr.de  
hRIXS: Alexander Föhlisch, Potsdam University and HZB, alexander.foehlich@helmholtz-berlin.de

## References

1. A. Laso Garcia et al., High Power Laser Sci. Eng. 9, E59 (2021).



# Campus and Cooperations

> Research centres and cooperations	104
> Cooperation in research and education	106
> Center for Free-Electron Laser Science CFEL	108
> Centre for Structural Systems Biology CSSB	109
> Centre for X-ray and Nano Science CXNS	110
> Centre for Molecular Water Science CMWS	111

# Research centres and cooperations

## Campus overview

DESY Photon Science is part of a worldwide scientific network. The cooperation landscape at DESY Photon Science is diversified and involves local as well as national and international partners.

Cooperation creates new scientific and technological opportunities at DESY's facilities, increases the pool of talents and is also indispensable for further coordination of research roadmaps and agendas. The image below highlights key points of cooperation

within the Science City Hamburg Bahrenfeld to which DESY Photon Science is connected. Some strategic highlights of the cooperation activities with universities, in networks and the interdisciplinary research platforms on campus are reported on within this chapter. German universities are also closely involved at PETRA III and FLASH, for example, via BMBF-funded collaborative research. Developments in connection to PETRA III, FLASH and European XFEL are described in the chapter 'Light Sources and User Infrastructures'.

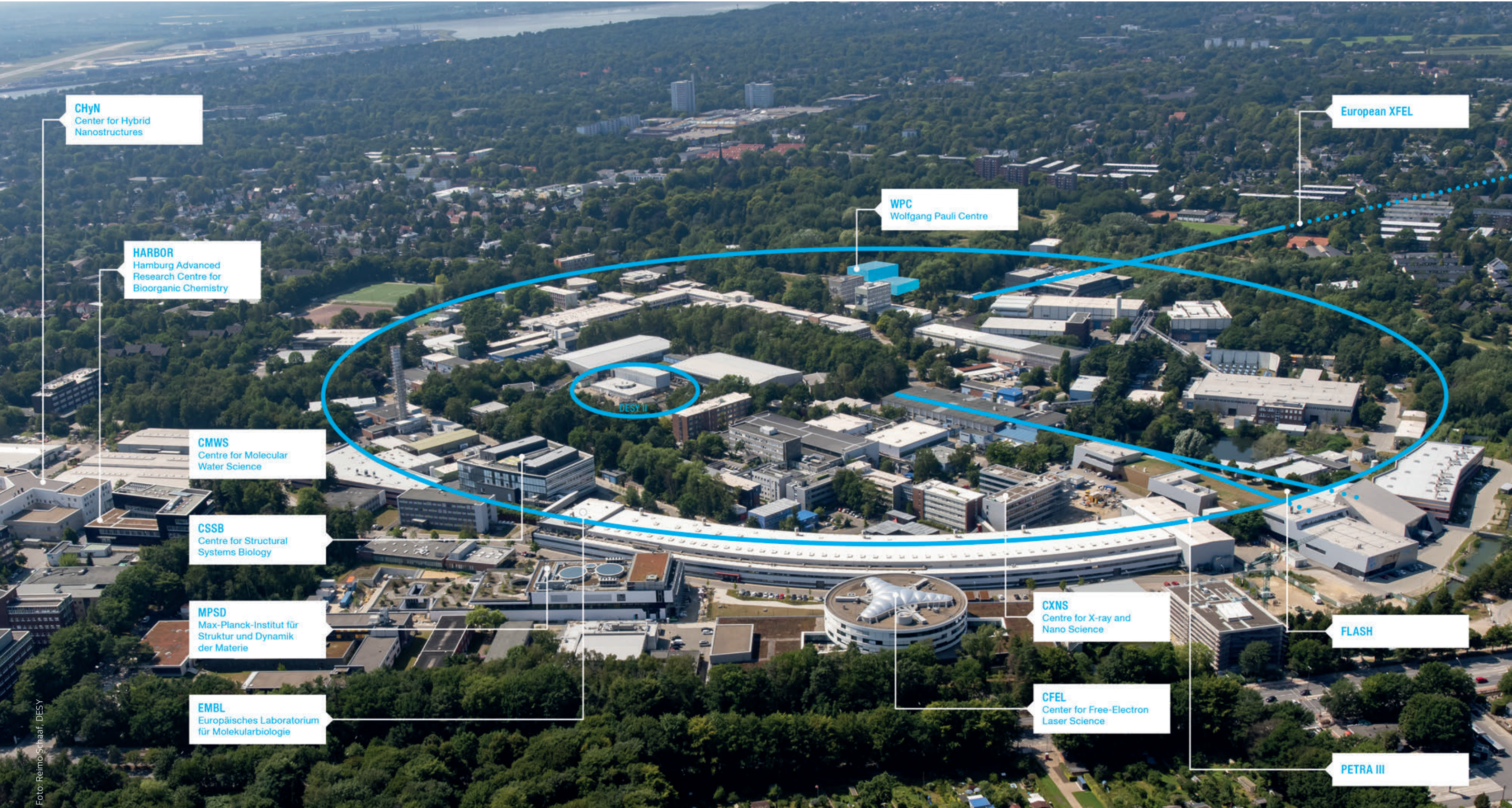


Foto: Reimo Schaaf, DESY

# Cooperation in research and education

## Universities and networks overview



Joint / cooperative appointments

Collaborative research structures

International and national cooperation

Graduate schools

### PHGS

Doctoral candidates at the PIER Helmholtz Graduate School (PHGS) benefit from outstanding research in particle and astroparticle physics, nano science, photon science, infection and structural biology, accelerators and theoretical physics. The PHGS is a graduate education programme at DESY in cooperation with Universität Hamburg (UHH).

### HELIOS

HELIOS (Helmholtz-Lund International Graduate School) includes particle physics, molecular physics, nano(bio) science and ultrafast photon science. The involved partners are UHH, Lund University, City of Hamburg and DESY.

### DASHH

DASHH (Data Science in Hamburg — Helmholtz Graduate School for the Structure of Matter) has the aim to harness data, computer and applied mathematical science to advance the understanding of nature. The involved partners are DESY, UHH, Technische Universität Hamburg (TUHH), Helmut-Schmidt-Universität, Hereon, Helmholtz-Zentrum für Infektionsforschung, Max Planck Institute for the Structure and Dynamics of Matter, European XFEL and Hochschule für Angewandte Wissenschaften Hamburg

### Strategic networks

- LEAPS — the League of European Accelerator-based Photon Sources — is a strategic consortium initiated by the directors of the synchrotron radiation and free-electron laser user facilities in Europe.
- PIER is the strategic partnership between DESY and Universität Hamburg ('Partnership for Innovation, Education and Research').

### Joint laboratories and institutes

- In the Helmholtz International Laboratory on Reliability, Repetition, Results at the most advanced X-ray Sources (HIR<sup>2</sup>X), DESY and the US National Accelerator Laboratory SLAC in California have joined forces to develop techniques and procedures that enable the reliable application of X-ray lasers.
- DESY is partner of the Helmholtz Institute Jena which is an outstation of the GSI Helmholtz Center for Heavy Ion Research on the campus of the Friedrich Schiller University of Jena. The institute is mainly focused on applied and fundamental research at the borderline of high-power lasers and particle accelerator facilities

### Excellence strategy

DESY Photon Science contributes to two clusters at the Universität Hamburg:

- 'CUI: Advanced Imaging of Matter'
- 'Understanding Written Artefacts'.

### Collaborative research with universities

Collaborative research centers with universities, involving DESY Photon Science, include:

- Tracking the active site in heterogeneous catalysis for emission control (SFB 1441), coordinated by Karlsruhe Institute of Technology (KIT);
- Tailor-made multi-scale materials systems (SFB 986), coordinated by TUHH;
- Extreme light for sensing and driving molecular chirality (SFB 1319), coordinated by University of Kassel;
- Atomic scale control of energy conversion (SFB 1073), coordinated by Georg-August-Universität Göttingen (GAU);
- Quantum cooperativity of light and matter (SFB 306), coordinated by Friedrich-Alexander-Universität Erlangen-Nürnberg (FAU);
- Centre for Integrated Multiscale Materials Systems (CIMMS), coordinated by TUHH;
- Centre for Data and Computing in Natural Science (CDCS), coordinated by UHH.

## Joint appointments

Andrea Trabattoni has been jointly appointed junior professor with Universität Hannover. For his activity in time-resolved angle-resolved photon electron spectroscopy, he has successfully acquired funding from the Helmholtz Young Investigator programme. Tobias Herr, who also acquired funding within the Helmholtz young investigator programme working on ultrafast non-linear microphotonics, was jointly appointed to a W2 professor position at UHH. Sadia Bari has been appointed associate professor equivalent to German 'W2' level at the University of Groningen to work in the field of soft X-ray research on the dynamic structure of isolated and solvated single biomolecules. This joint professorship with DESY is financed by Helmholtz funding for first-time professorial appointments. Patrick Huber — an expert on hierarchical material systems — has been jointly appointed to a W3 professorship with the TUHH.

## Graduate Schools

In January 2021 the Helmholtz Lund International Graduate School HELIOS was officially launched and the first HELIOS students started their projects throughout the year.

## Collaborative research structures

In 2021 several collaborative research centres (SFBs), to which DESY Photon Science researchers are contributing, started into a new term: SFB 986 'Tailor-made multi-scale material systems' (TUHH), SFB 1073 'Atomic scale control of energy conversion' (GAU), SFB 1441 'Tracking the active site in heterogeneous catalysis for emission control' (KIT) and the newly funded SFB 306 'Quantum cooperativity of light and matter' (FAU).

The UHH's excellence cluster CUI: Advanced Imaging of Matter organised a hybrid annual meeting during which the cluster's Mildred Dresselhaus Prizes were awarded. In 2021 the senior award went to Jie Shan, professor of applied and engineering physics and physics at Cornell University (USA), for her outstanding achievements in the field of experimental condensed matter physics. Prineha Narang, assistant professor of computational materials science at Harvard University (USA), was awarded the junior prize for her outstanding contributions to quantum science. The research building 'Hamburg Advanced Research Centre for Bioorganic Chemistry (HARBOR)' was opened in 2021 on the Bahrenfeld campus. CUI and various UHH groups are involved in HARBOR. HARBOR strengthens the links of the UHH and DESY in the context of time-resolved imaging for research on biomolecular physics. To promote science communication even during the Corona pandemic, UHH and DESY organised a digital version of 'Science on Tap' in 2021.

In 2021 the newly funded and user-driven consortium DAPHNE4NFDI started its work. It is coordinated by DESY and brings together several universities, including CAU and GAU, as well as research institutions to advance the state of data management in the photon and neutron science communities.

Update

# Center for Free-Electron Laser Science CFEL

Three institutions working successfully together

A new analytical technique is able to provide hitherto unattainable insights into the extremely rapid dynamics of biomolecules [1]. The team of developers from DESY and the University of Wisconsin presented a clever combination of quantum physics and molecular biology. They used the technique to track the way in which the photoactive yellow protein (PYP) undergoes changes in its structure in less than a picosecond after being excited by light. The detailed calculation shows how a conical intersection forms in four-dimensional space and how the PYP drops through it back to its initial state after being excited by light (Fig. 1). Now the scientists can describe this process in steps of a few tens of femtoseconds and thus advance the understanding of photoactive processes.

The LUX team at CFEL celebrated two milestones in the development of innovative plasma accelerators [2,3]. The scientists from the University of Hamburg and DESY used their accelerator to test a technique that allows the energy distribution of the electron beams produced to be kept particularly narrow. They also used artificial intelligence to allow the accelerator to optimise its own operation.

Plasma acceleration is an innovative technology that gives rise to a new generation of particle accelerators which are not only remarkably compact but also extremely versatile. This compactness is both a curse and a blessing: Since the acceleration process is concentrated in a tiny space that

is up to 1000 times smaller than conventional large-scale machines, the acceleration takes place under truly extreme conditions. Therefore, a number of challenges still have to be overcome before the new technology is ready to go into series production.

An international team of researchers from MPSD, the University of Toronto, the Diamond Light Source in Oxford and the EMBL Hamburg has found that two of the world's brightest light sources offer more common research possibilities than originally anticipated. Although they operate on very different timescales, synchrotrons and XFELs can produce data of equivalent quality as long as serial data collection is used in the imaging process. These findings open up a new avenue for collaborative applications [4].

Contact: Ralf Köhn, [ralf.koehn@cfel.de](mailto:ralf.koehn@cfel.de)

## References

1. A. Hosseinizadeh et al., *Nature* 599, 697–701 (2021).
2. S. Jalaš et al., *Phys. Rev. Lett.* 126, 104801 (2021).
3. M. Kirchen et al., *Phys. Rev. Lett.* 126, 174801 (2021).
4. P. Mehrabi, *Sci. Adv.* 7, eabf1380 (2021).

## CFEL Partner Institutions

- Deutsches Elektronen-Synchrotron DESY
  - Max Planck Institute for the Structure and Dynamics of Matter (MPSD)
  - Universität Hamburg (UHH)
- [www.cfel.de](http://www.cfel.de)

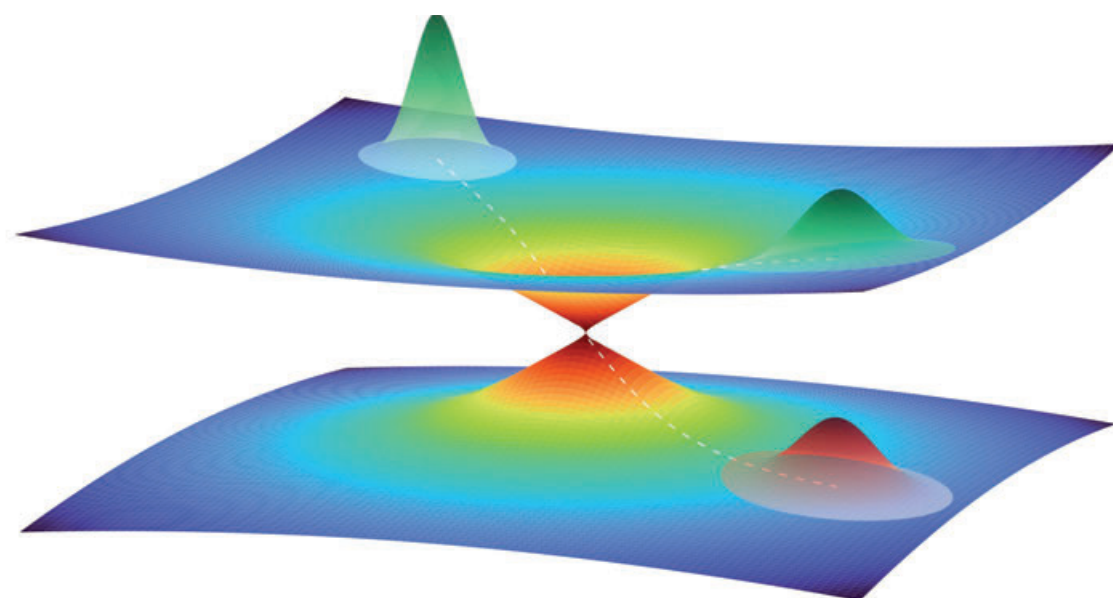


Figure 1

Illustration of a quantum wave packet in close vicinity of a conical intersection between two potential energy surfaces. The wave packet represents the collective motion of multiple atoms in the PYP. A part of the wave packet moves through the intersection from one potential energy surface to the other, while another part remains on the top surface, leading to a superposition of quantum states (Credit: CFEL, Niels Breckwoldt).

# Centre for Structural Systems Biology CSSB

Together against infectious diseases



Figure 1

Thomas Dobner (HPI), Helmut Dosch (DESY), Ulrich Schaible (FZB) and Chris Meier (CSSB) sign the cooperation agreement. (Photo: Kerstin Pukall)

## Research highlights

The coronavirus pandemic has demonstrated the importance of conducting fundamental research in order to investigate the mechanisms of disease-causing pathogens. In 2021, CSSB scientists have discovered a promising new antimalarial compound [1], revealed new insights into bacterial dinucleotidases [2], identified promising targets for the treatment of the human adenovirus [3] and unveiled the structure of the type VII secretion system from *Mycobacterium tuberculosis* [4,5]. Our scientists are also involved in the development of new tools and methods such as DNA origami signposts to pinpoint individual protein structures in electron cryotomography [6], the Protein Interface-score to assess protein-protein interfaces [7] and an online platform for analysing molecular biophysics data at our high-throughput crystallisation (HTX) and protein characterisation (PC) facilities [8].

## New partner

After five years of successful cooperation as associated partner, the Research Center Borstel, Leibniz Lung Center (FZB) became a full member of CSSB on 1 July 2021. The contract for this future cooperation was signed at a ceremony attended by CSSB and FZB scientists as well as representatives of CSSB funding bodies (Fig. 1). The FZB group will investigate the interaction of bacteria with surface structures of the lung in chronic lung diseases. For the establishment of this research group, a tenure track W2 professorship will be established at UHH and a new atomic force microscope will be installed at CSSB.

## New group leader

In October 2021, Charlotte Uetrecht began working at CSSB. Uetrecht has a joint appointment from the University of Siegen, where she is a W2 professor of Biochemistry, and from the Leibniz Institute for Experimental Virology (HPI). Uetrecht's group is affiliated with the European XFEL and DESY. She leads a team that will investigate the structural dynamics of viral protein complexes.

## Two collaborative projects funded

CSSB Director's funds were awarded to an ambitious flagship project called 'PLASMOFRACTION' which will use a bottom-up structural-systems biology approach to investigate membrane protein complexes in the transmissible gametocyte stages of the malaria parasite *Plasmodium falciparum*. While gametocytes are of high medical relevance, little is known about their molecular structure and function. PLASMOFRACTION will investigate *P. falciparum* gametocyte biology from a fresh angle with innovative shotgun structural-biology approaches that use cryo-EM to identify and determine structures of protein complexes directly from the parasite's cellular membranes.

CSSB's collaborative project 'Multiscale analysis of pathogen invasion strategies into clinically-relevant host cells' has been awarded funding from Hamburg's state research funding Hamburg-X supported project 'Infection Research'. This ambitious project, involving eight CSSB groups and three facilities, aims not only to investigate pathogen invasion strategies but also to increase synergies at CSSB and to lay the groundwork for future cooperative initiatives.

Contact: Chris Meier, [chris.meier@cssb-hamburg.de](mailto:chris.meier@cssb-hamburg.de)

## References

1. A. Alder et al., *Cell Chem. Biol.* 2451–9456 (2021).
2. J. D. Lormand et al., *eLife* 10, e70146 (2021).
3. J. M. Jung et al., *Sci. Immunol.* 6, eabe2942 (2021).
4. K. S. H. Beckham et al., *Sci. Adv.* 7, eabg9923 (2021).
5. C. M. Bunduc et al., *Nature* 593, 445–448 (2021).
6. E. Silvester et al., *Cell* 184, 1110–1121 (2021).
7. S. Malhotra et al., *Nat. Commun.* 12, 3399 (2021).
8. O. Burastero et al., *Acta Crystallogr. D* 77, 1241–1250 (2021).

## CSSB Partner Institutions

- Bernhard Nocht Institute for Tropical Medicine (BNITM)
- Deutsches Elektronen-Synchrotron DESY
- European Molecular Biology Laboratory (EMBL)
- Forschungszentrum Jülich (FZJ)
- Hannover Medical School (MHH)
- Leibniz Institute for Experimental Virology (HPI)
- Helmholtz Centre for Infection Research (HZI)
- Research Center Borstel (FZB)
- Universität Hamburg (UHH)
- University Medical Center Hamburg-Eppendorf (UKE)

## CSSB Investors

- Federal Republic of Germany
- Free and Hanseatic City of Hamburg
- Federal State of Lower Saxony
- Federal State of Schleswig-Holstein

[www.cssb-hamburg.de](http://www.cssb-hamburg.de)

# Centre for X-ray and Nano Science CXNS

Getting off the ground and taking shape — CXNS building starts operation

In August and September 2021 all staff working at the Centre for X-ray and Nano Science was able to move to the new building on campus close to the PETRA III experimental hall 'Max von Laue' (Fig. 1). The offices were occupied quickly while lab moves have required more time. Nevertheless, almost all labs are either in working condition or close to it by the end of 2021.

The spacious laboratories on the ground floor are divided up between Hereon's German Engineering Materials Science Centre (GEMS) and DESY Photon Science teams including the DESY NanoLab. The DESY NanoLab's X-ray and electrochemistry laboratories are situated in buildings in close proximity to the CXNS. A laser lab is planned in a joint cooperation between the Leibniz-Institut für Kristallzüchtung (IKZ) and the DESY NanoLab on the CXNS ground floor as well. CXNS will host offices for research groups of Christian-Albrechts-Universität zu Kiel (CAU) in the frame of the cooperative Ruprecht-Haensel Laboratory. Furthermore, a joint research group of DESY and the Technische Universität Hamburg (TUHH) within the Center for Integrated Multiscale Material Systems (CIMMS), has joined the CXNS.

These five strong research partners will be working together at the CXNS and will be using its excellent facilities either at the CXNS or in close vicinity at DESY's large-scale X-ray facilities PETRA III and FLASH. In addition, the CXNS is hosting the DESY Photon Science User Office.

The official opening ceremony for the CXNS is scheduled for spring 2022. It is planned to establish a regular interdisciplinary exchange of all CXNS scientific partners and also create a symposium in the field of X-ray and nanoscience.

Contact: *Andreas Stierle, andreas.stierle@desy.de*

## CXNS Partner Institutions

- Helmholtz-Zentrum Hereon, German Engineering Materials Science Centre (GEMS)
  - Christian-Albrechts-Universität zu Kiel (CAU), Ruprecht-Haensel-Labor
  - Technical University Hamburg (TUHH), Center for Integrated Multiscale Material Systems (CIMMS)
  - Leibniz-Institut für Kristallzüchtung (IKZ Berlin)
- [photon-science.desy.de/research/centres\\_for\\_research/cxns](http://photon-science.desy.de/research/centres_for_research/cxns)



Figure 1

View of the new CXNS building which is located in close proximity to DESY's lightsources (Photo: Marta Mayer, DESY).

# Centre for Molecular Water Science CMWS

Achieving a detailed molecular understanding of water

The Centre for Molecular Water Science (CMWS) brings together key experts from different areas of water-related sciences. The common goal of CMWS is delivering a detailed molecular understanding of the various structures, phenomena and dynamic processes in water and water interfaces that are relevant for green-energy technologies, health and environment. In a series of workshops and general meetings, the science concept has been developed by the CMWS consortium consisting of more than 140 scientists worldwide. The research of CMWS is organised in five pillars (Fig. 1) and coordinated by DESY. The key idea is a combined theoretical and multimodal experimental approach. Vital for this approach are the X-ray methods available at DESY and European XFEL for studying molecular structure and dynamics on different timescales and in various environments [1].

## Driving water research forward

A milestone was reached in May 2021 with the publication of the research programme of CMWS, the White Paper [2], authored by more than 110 scientists.

Motivated by this research agenda, several new developments aim at advancing water research at DESY. Two new CMWS laboratories were set up, offering for example Raman and Fourier-transform infrared spectroscopy (FT-IR) and are about to be further expanded with specific instrumentation. Sadia Bari, the first professorial appointment within CMWS, together with the University of Groningen, focusses on probing the dynamical local structure of isolated to solvated proteins.

To extend and further strengthen the common research activities within CMWS, an Early Science Programme (ESP) was launched by DESY in 2019 supporting PhD projects

between different CMWS partners. The programme is jointly financed by DESY and CMWS partners with equal contributions. A second call was launched in 2020 and 10 new projects started in 2021. A third round of the science programme will start in 2022 with a focus on the research agenda of the CMWS White Paper. First cooperation agreements for external CMWS hubs are prepared with the KU Leuven (Belgium) in the field of nuclear magnetic resonance spectroscopy.

## Scientific exchange

The CMWS DAYS took place in March 2021 as an all-online event with more than 275 participants. In this meeting highlights of CMWS research were presented and the final draft of the White Paper was discussed. The next CMWS DAYS are planned for March 2022.

During the summer semester 2021 the CMWS seminar started as a lunch talk series on water-related science and technology. The aim of the series is to intensify the scientific exchange within the network of CMWS and to introduce students and young scientists to the different research areas of CMWS.

Contact: *Claudia Goy, claudia.goy@desy.de*

## References

1. F. Lehmkuhler, C. Goy, R. Santra and G. Grübel, *Phys. Unserer Zeit*, 52, 6 (2021).
2. G. Gruebel, M. Schnell, C. Goy, F. Lehmkuhler and S. Bari. (Eds.), *Deutsches Elektronen Synchrotron DESY*, ISBN: 9783945931370 (2021).

## CMWS Partner Institutions

51 partner institutions from 16 countries have expressed their support by a letter of interest  
[www.cmws-hamburg.de](http://www.cmws-hamburg.de)

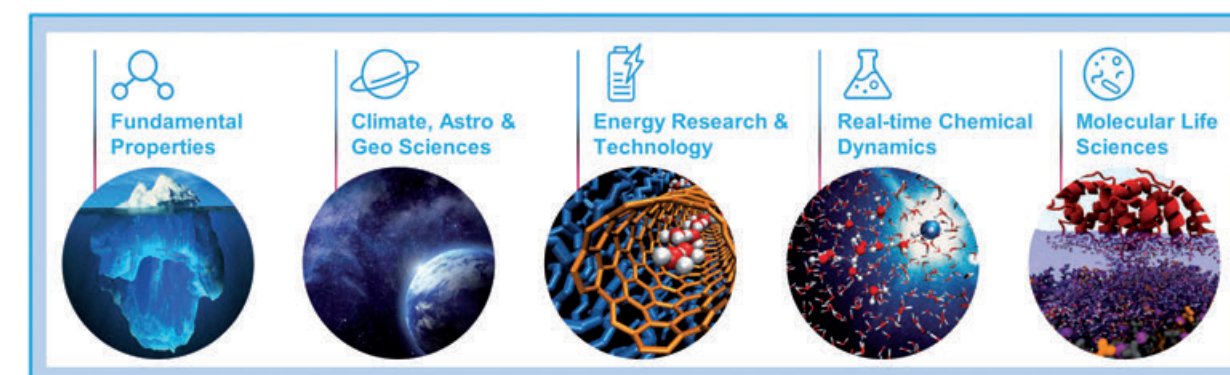
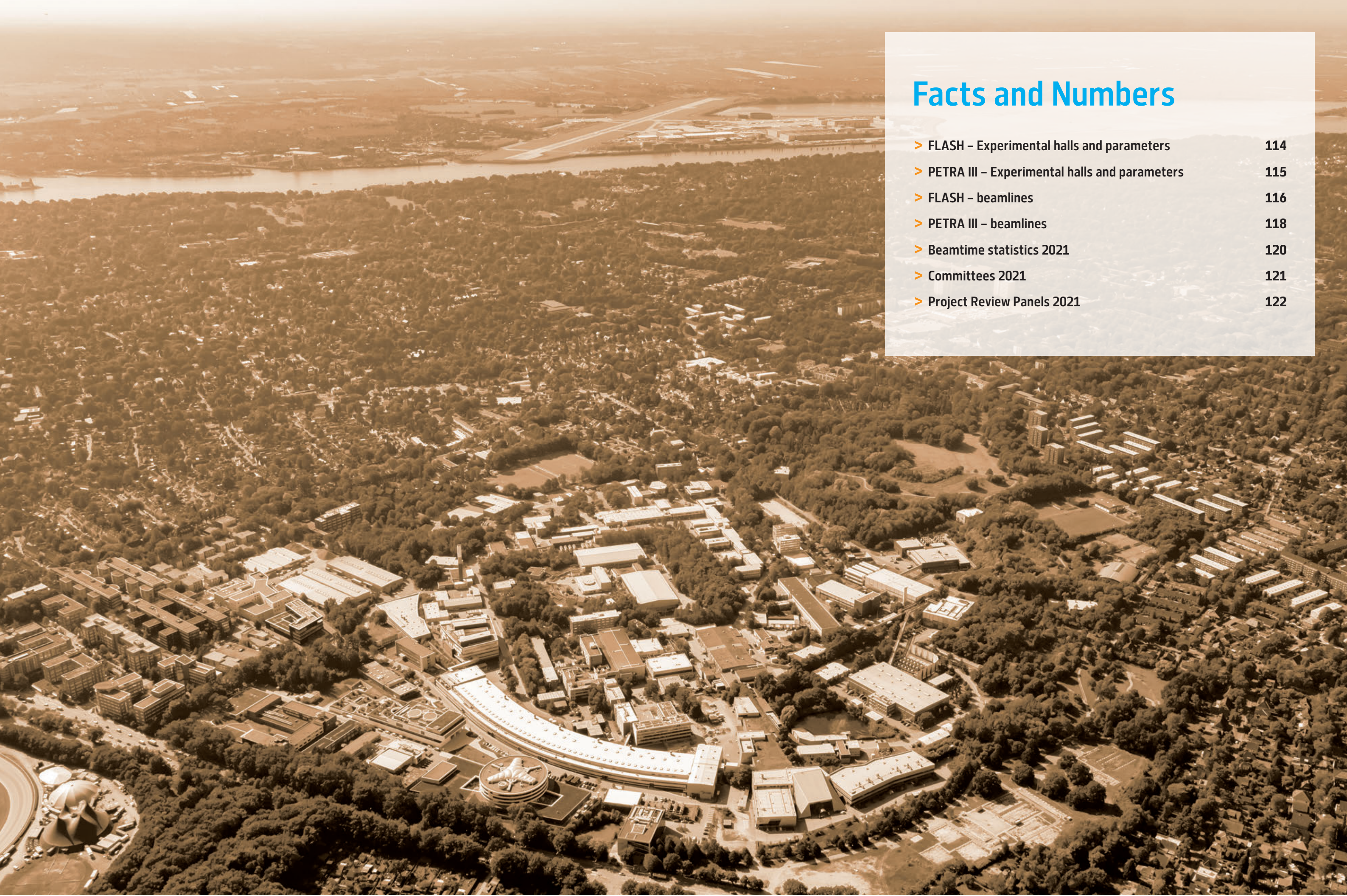


Figure 1

The five CMWS research pillars focus on different interdisciplinary aspects of molecular water research.

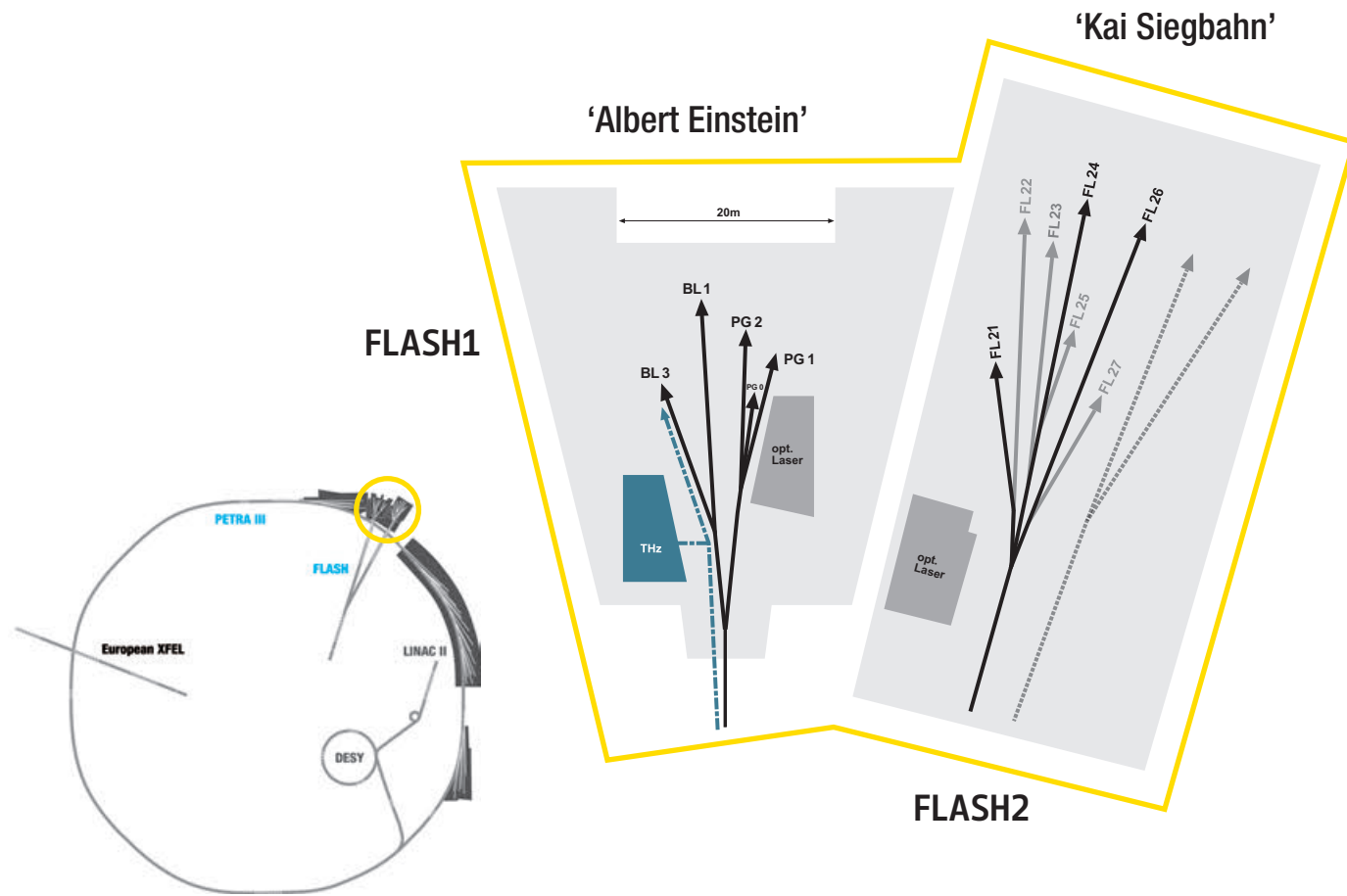


## Facts and Numbers

> FLASH – Experimental halls and parameters	114
> PETRA III – Experimental halls and parameters	115
> FLASH – beamlines	116
> PETRA III – beamlines	118
> Beamtime statistics 2021	120
> Committees 2021	121
> Project Review Panels 2021	122

# FLASH

Experimental halls and parameters



## FLASH – machine parameters

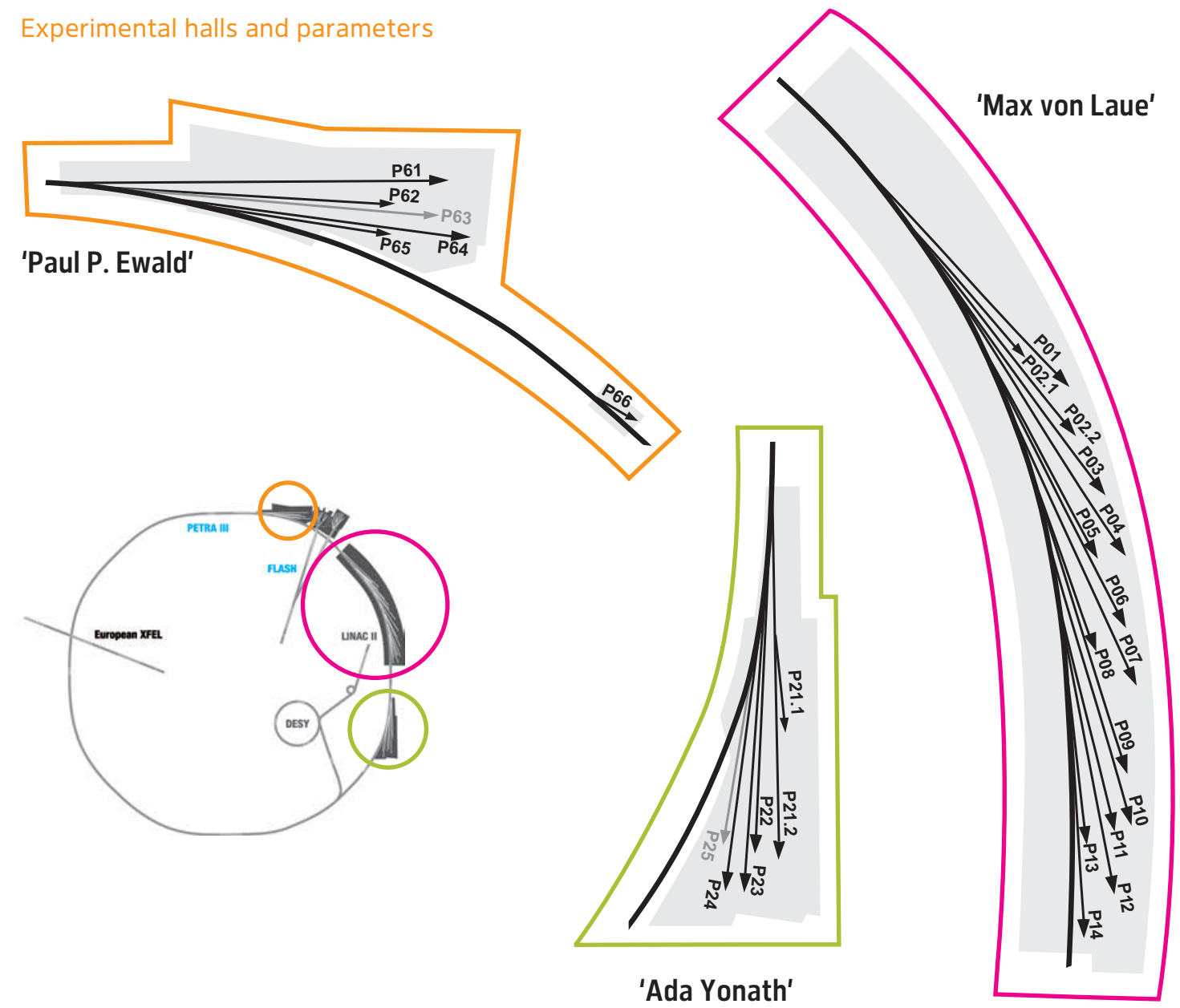
	FLASH1	FLASH2
Electron energy range	0.35–1.25 GeV	0.4–1.25 GeV
Normalised emittance at 1 nC (rms)	1.4 mm mrad	1.4 mm mrad
Energy spread	200 keV	500 keV
Electron bunch charge	0.02–1.2 nC	0.02–1 nC
Peak current	1–2.5 kA	1–2.5 kA
Electron bunches per second (to be shared between FL1 and FL2)	5000	5000

## FLASH – lasing parameters

	FLASH1	FLASH2
Photon energy fundamental	24–295 eV	14–310 eV
Wavelength fundamental	51–4.2 nm	90–4 nm
Photon pulse duration (FWHM)	30–200 fs	1–200 fs (estimated)
Peak power	1–5 GW	1–5 GW
Single photon pulse energy (average)	1–500 $\mu$ J	1–1000 $\mu$ J
Spectral width (FWHM)	0.7–2%	0.5–2%
Photons per bunch	$10^{11}$ – $10^{14}$	$10^{11}$ – $10^{14}$
Peak brilliance photons/sec/mm <sup>2</sup> /mrad <sup>2</sup> /0.1%	$10^{28}$ – $10^{31}$	$10^{28}$ – $10^{31}$

# PETRA III

Experimental halls and parameters



## PETRA III – machine parameters

Electron energy	6.08 GeV
Circumference of the storage ring	2304 m
Number of bunches	40 (timing mode) 480 (multi bunch mode)
Bunch separation	192 ns (timing mode) 16 ns (multi bunch mode)
Electron beam current	100 mA (timing mode) 120 mA (multi bunch mode)
Horizontal electron beam emittance	1.3 nrad
Vertical electron beam emittance	0.01 nrad
Electron beam energy spread (rms)	0.1%
Horizontal × vertical beam size (rms) at 5 m undulator (high $\beta$ section) and 10 keV photon energy	141 $\mu$ m × 5.2 $\mu$ m
Horizontal × vertical beam size (rms) at 5 m undulator (low $\beta$ section) and 10 keV photon energy	36 $\mu$ m × 5.7 $\mu$ m

### FLASH1 experimental hall 'Albert Einstein'

<b>BL1</b>	non-monochromatic FEL photons Kirkpatrick-Baez (KB) focusing optics, FEL focal spot of $\approx 7 \mu\text{m} \times 8 \mu\text{m}$ (FWHM) split-and-delay unit for XUV-pump-XUV-probe experiments (mirrors for 13.57 nm, -30 ps to + 650 ps delay) optional pump-probe experiments using the FLASH1 optical laser system for BL1 and BL3 4-mirror polariser for variable FEL polarisation from 30–70 eV <b>permanent end station:</b> multipurpose CAMP chamber with pnCCD detectors, electron and ion spectrometers and collinear incoupling optics for optical laser	TU Berlin
<b>BL3</b>	non-monochromatic FEL photons, spectral range: $> 4.5 \text{ nm}$ (carbon coated optics) focused to $\approx 20 \mu\text{m}$ / unfocussed beam size $\approx 5\text{--}10 \text{ mm}$ (FWHM, depending on wavelength) optional pump-probe experiments using the FLASH1 optical laser system for BL1 and BL3 4-mirror polariser for variable FEL polarisation from 30–70 eV <b>optional pump-probe experiments using THz radiation:</b> - tunable: 10–230 $\mu\text{m}$ ; up to 150 $\mu\text{J}/\text{pulse}$ ; $\approx 10\%$ bandwidth - broadband at 200 $\mu\text{m}$ ; up to 10 $\mu\text{J}/\text{pulse}$ ; $\approx 100\%$ bandwidth - synchronised and phase stable to X-ray pulses (down to 5 fs) - delivered to the experiment via vacuum beamline as: (i) ultra-high vacuum ( $\approx 10^{-8}$ mbar), shorter delay between THz and X-ray ( $\approx 4 \text{ m}$ path difference); can accommodate up to 0.3 m wide setup (ii) high vacuum ( $\approx 10^{-6}$ mbar), longer delay between THz and X-ray ( $\approx 7 \text{ m}$ path difference); can accommodate up to 2 m wide setup - UHV chamber with mounts for refocusing XUV optics to compensate for XUV/THz path delay <b>about 3 x 4 m platform for user-provided end station</b>	TU Berlin
<b>PG1</b>	high-resolution plane grating XUV monochromator (SX 700 type, $< 10^{-4}$ bandwidth, carbon coated optics): - variable combination of photon flux and resolution (from high flux to high resolution) - controlled temporal-spectral properties at moderate resolution for pump-probe experiments - high photon flux with harmonic filtering Kirkpatrick-Baez (KB) refocusing optics, FEL focal spot down to 5 $\mu\text{m}$ FWHM (vertically, monochromator exit slit size dependent) <b>permanent end station:</b> - XUV-Raman spectrometer TRIXS for high-resolution and time-resolved RIXS measurements on solid samples (15–400 K, resolving power $\approx 1700$ , time resolution 170–300 fs FWHM) - optional pump-probe experiments (RIXS; XAS + reflectivity with angular resolution) using the FLASH1 optical laser system for PG1 and PG2	
<b>PG2</b>	uses the same monochromator as PG1 50 $\mu\text{m}$ focus XUV beam splitter with variable time delay ( $\pm 6 \text{ ps}$ ) for time-resolved studies optional pump-probe experiments using FLASH1 optical laser system for PG1 and PG2 <b>about 3 x 4 m platform for user-provided end station</b>	

### FLASH1 optical / NIR laser system for pump-probe experiments for beamlines BL1 and BL3

central wavelength	810 nm
spectral bandwidth	25 nm
intra-burst repetition rate	single pulse
number of pulses per burst	1
pulse duration	$< 60 \text{ fs FWHM}$ , $< 200 \text{ ps FWHM}$ (uncompressed)
timing jitter to FEL	$< 60 \text{ fs (rms)}$
pulse energy	0–10 mJ (before coupling to chamber), 0–7 mJ (at interaction region)
polarisation	flexible
peak intensity	$> 10^{14} \text{ W/cm}^2$
time delay to FEL	-4 ns to +4 ns, 10 fs resolution, larger delays optional
energy stability	$< 10\%$ pulse-to-pulse peak (3% rms)

Harmonic generation conversion to 400 nm, 266 nm and 200 nm central wavelength are available with conversion efficiencies of  $> 30\%$  SHG,  $> 5\%$  THG

### FLASH1 optical / NIR laser system for pump-probe experiments for beamlines PG1 and PG2

central wavelength	1030 nm
spectral bandwidth	30–50 nm (pre-set for experiment)
intra-burst repetition rate	1 MHz
number of pulses per burst	1–800
pulse duration	60–100 fs FWHM
timing jitter to FEL	$< 60 \text{ fs (rms)}$
pulse energy	0–30 $\mu\text{J}$ (at interaction point at 1030 nm)
polarisation	flexible
peak intensity	$> 10^{14} \text{ W/cm}^2$
time delay to FEL	-4 ns to 4 ns, 10 fs resolution, larger delays optional
energy stability	$< 10\%$ pulse-to-pulse peak (3% rms)

Harmonic generation conversion to 515 nm, 343 nm or 257 nm central wavelength can be provided

### FLASH2 experimental hall 'Kai Siegbahn'

<b>FL24</b>	non-monochromatic FEL photons wavelength range: 4–90 nm fundamental Kirkpatrick-Baez (KB) focusing optics with variable foci down to $< 10 \mu\text{m}$ (FWHM)/unfocussed beam size $\approx 5\text{--}10 \text{ mm}$ (FWHM, depending on wavelength) optional pump-probe experiments using FLASH2 optical laser system grazing incidence split-and-delay unit with $\pm 12 \text{ ps}$ time delay <b>about 3 x 4 m platform for user-provided end station</b>	Univ. Münster
<b>FL26</b>	non-monochromatic FEL photons wavelength range: 6–90 nm fundamental optional pump-probe experiments using FLASH2 optical laser system <b>permanent end station:</b> - reaction microscope (REMI) for time-resolved AMO spectroscopy - grazing incidence delay line and refocusing optics: FEL focal spot $< 10 \mu\text{m} \times 10 \mu\text{m}$ (FWHM, depending on wavelength) - $\pm 2.7 \text{ ps}$ time delay range, 1 fs precision - grating spectrometer for online spectral distribution monitoring and for transient absorption spectroscopy	MPI-K Heidelberg

### FLASH2 optical / NIR laser system for pump-probe experiments for beamlines FL24 and FL26

central wavelength	700–900 nm (fast tuneable)
spectral bandwidth	$\sim 100 \text{ nm}$ (pre-set for experiment)
intra-burst repetition rate	100 kHz
number of pulses per burst	1–80
pulse duration	15–35 fs FWHM (compressed to $1.1 \times$ bandwidth limit), $< 500 \text{ fs FWHM}$ (uncompressed)
timing jitter to FEL	$< 60 \text{ fs (rms)}$
pulse energy	0–250 $\mu\text{J}$ (before coupling to chamber), 0–150 $\mu\text{J}$ (at interaction region)
polarisation	flexible
focus size ( $1/e^2$ diameter)	FL24: $< 100 \mu\text{m}$ , FL26: $< 50 \mu\text{m}$
peak intensity	$> 10^{14} \text{ W/cm}^2$
time delay to FEL	-4 ns to 4 ns, 10 fs resolution, larger delays optional
energy stability	$< 10\%$ pulse-to-pulse peak (3% rms)

Harmonic generation conversion to 400 nm and 266 nm central wavelength are available with conversion efficiencies of  $> 30\%$  SHG,  $> 5\%$  THG

All FLASH beamlines provide online photon diagnostics for intensity, wavelength and beam position, fast shutter, aperture and filter sets.

### Acknowledgement

We would like to acknowledge all contributions to the development and operation of FLASH and PETRA III beamlines and instruments provided within the framework of BMBF-Verbundforschung, and as part of collaborations with the Department of Science and Technology (Government of India) 'India@DESY', the Ruprecht-Haensel-Laboratory (Kiel University), the Max Planck Society and the Forschungszentrum Jülich.

### PETRA III experimental hall 'Max von Laue'

Beamline and instruments	Operated by
R — option for remote user operation M — option for mail-in service	
<b>P01</b> High Resolution Dynamics 10 m U36   2.5–80 keV	DESY
Nuclear resonant scattering	DESY
Resonant inelastic scattering	DESY   MPG
X-ray Raman scattering	DESY   MPG
<b>P02.1</b> Powder Diffraction and Total Scattering 2 m U23   60 keV	DESY
M Standard and in situ powder diffraction	DESY
M Standard and in situ total scattering	DESY
<b>P02.2</b> Extreme Conditions 2 m U23   10–60 keV	DESY
R Laser heated experiment for diamond anvil cells (DACs)	DESY
R General purpose experiment for high pressure DAC applications	DESY
<b>P03</b> Micro- and Nano-SAXS/WAXS 2 m U29   8–23 keV	DESY
Micro-beam small and wide-angle scattering	DESY
Nano-beam scattering and diffraction	DESY   Hereon   collaborators
<b>P04</b> Variable Polarisation Soft X-rays 5 m UE65   250–2800 eV	DESY
UHV diffractometer and soft X-ray spectrometer	DESY
Photon-ion spectrometer (PIPE)	DESY   collaborators
Ultra-high resolution photoelectron spectroscopy (ASPHERE)	DESY   collaborators
Soft X-ray absorption holographic imaging instrument	DESY   collaborators
Nano-focus apparatus for spatially-resolved spectroscopy	DESY   collaborators
<b>P05</b> Micro- and Nano-Imaging 2 m U29   8–50 keV	Hereon
M Micro-tomography	Hereon
Nano-tomography	Hereon
<b>P06</b> Hard X-ray Micro- and Nano-probe 2 m U32   5–100 keV	DESY
R Micro-probe	DESY
R Nano-probe	DESY
<b>P07</b> High Energy X-ray Materials Science 4 m IVU21   50–200 keV	Hereon
Surface diffraction, grazing incidence total scattering, diffraction tomogr.	DESY
Heavy-load diffractometer	Hereon
Grain mapper	Hereon
High energy tomography	Hereon
<b>P08</b> High Resolution Diffraction 2 m U29   5.4–29.4 keV	DESY
M High resolution diffractometer	DESY
Liquid surface diffractometer	DESY   collaborators
Langmuir trough in-plane diffractometer	DESY
<b>P09</b> Resonant Scattering and Diffraction 2 m U32   2.7–31 keV	DESY
Resonant X-ray diffraction at low temperatures (2 K < T < 750 K)	DESY
Resonant X-ray diffraction in high B-fields (2 K < T < 300 K; B < 14 T, B ⊥ Q)	DESY
Resonant X-ray diffraction at high pressure (4 K < T < 300 K; p < 30 GPa)	DESY
X-ray circular magnetic dichroism for powders (T > 3 K; B < 5.25 T)	DESY
X-ray resonant magnetic reflectivity (300 K; B < 0.25 T)	DESY
Open port	DESY
<b>P10</b> Coherence Applications 5 m U29   4–20 keV	DESY
R X-ray photon correlation spectroscopy (SAXS/WAXS geometry) (5–15 keV)	DESY
R Bragg coherent diffraction imaging (5–13 keV)	DESY
R GINIX — Nano-focusing setup (8 and 13.8 keV)	DESY   collaborators
<b>P11</b> High-throughput Macromolecular Crystallography 2 m U32   2.4–30 keV	DESY
R, M Macromolecular crystallography (6–26 keV)	DESY   HZI   U Lübeck
M Serial crystallography (6–26 keV)	DESY

Beamline and instruments	Operated by
R — option for remote user operation M — option for mail-in service	
<b>P12</b> Bio SAXS 2 m U29   4–20 keV	EMBL
R Small-angle and wide-angle X-ray scattering	EMBL
Time-resolved X-ray scattering	EMBL
Anomalous small-angle X-ray scattering	EMBL
<b>P13</b> Macromolecular Crystallography 2 m U29   4.5–17.5 keV	EMBL
R Macromolecular crystallography	EMBL
<b>P14</b> Macromolecular Crystallography and Imaging 2 m U29   6–20 keV	EMBL
R Macromolecular crystallography (7–27 keV)	EMBL
R Serial crystallography (7–18 keV)	EMBL
High-throughput micro-tomography (6–20 keV)	EMBL
Time-resolved serial crystallography (12.7 keV)	EMBL   U Hamburg

### PETRA III experimental hall 'Ada Yonath'

<b>P21.1</b> Swedish Materials Science Beamline side branch 2 m U29   50, 80, 100 keV	Center for X-rays in Swedish Materials Science (CeXS)   DESY
Diffuse scattering and total scattering	CeXS   DESY
<b>P21.2</b> Swedish Materials Science Beamline 4 m IVU21   40–150 keV	Center for X-rays in Swedish Materials Science (CeXS)   DESY
Multi-purpose triple-axis diffractometer	CeXS   DESY
Small-angle scattering	CeXS   DESY (commissioning)
Grain mapper	CeXS   DESY (commissioning)
<b>P22</b> Hard X-ray Photoelectron Spectroscopy 2 m U33   2.4–15 keV	DESY
R Hard X-ray photoelectron spectrometer (HAXPES)	DESY
R Ambient pressure XPS (POLARIS)	DESY   collaborators
R Hard X-ray photoemission electron microscope (HAXPEEM)	DESY   collaborators
<b>P23</b> In situ Nano-Diffraction Beamline 2 m U32   5–35 keV	DESY
XRD and secondary processes, in situ and complex environments	DESY
Tomography	DESY   KIT (operation planned 2022)
<b>P24</b> Chemical Crystallography 2 m U29   8, 15–44 keV	DESY
Single crystal diffraction in complex sample environments	DESY
Small molecule crystallography	DESY
<b>P25</b> Beamline for applied Bio-Medical Imaging, Powder Diffraction and Innovation	DESY (ITT funded) design phase

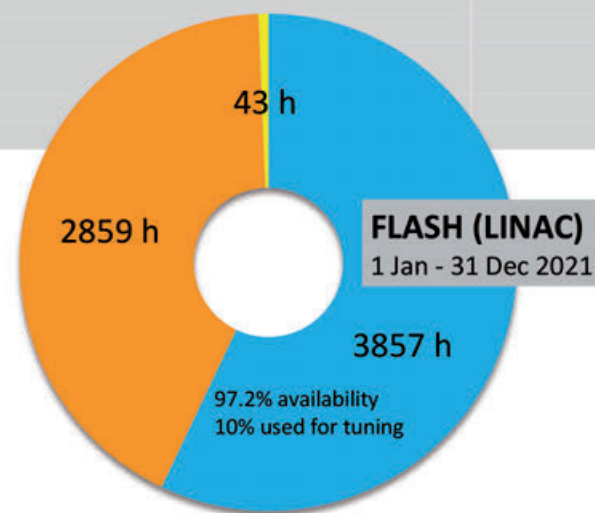
### PETRA III experimental hall 'Paul P. Ewald'

<b>P61</b> High Energy Wiggler Beamline 10 × 4 m damping wigglers   white beam btw. 30–250 keV	DESY
High energy engineering materials science	Hereon
Large volume press — extreme conditions	DESY
<b>P62</b> Anomalous Small-Angle X-ray Scattering 2 m U32   3.5–35 keV	DESY
Anomalous Small-angle X-ray scattering	DESY
SAXS tomography	DESY
<b>P63</b> t.b.d.	not yet funded
<b>P64</b> Advanced X-ray Absorption Spectroscopy 2 m U32   4–44 keV	DESY
Ex situ XAFS	DESY
High-resolution X-ray emission spectroscopy (non-resonant and resonant)	DESY
QEXAFS	DESY
<b>P65</b> Applied X-ray Absorption Spectroscopy 36 cm U32   4–44 keV	DESY
R Ex situ and in situ XAFS of bulk samples	DESY
<b>P66</b> Superlumi (between PETRA III halls 'Paul P. Ewald' and 'Max von Laue')	DESY
Bending magnet   4–40 eV	
Time-resolved luminescence spectroscopy	DESY

# Beamtime statistics 2021

FLASH				
Operation period 2021				
	User beamtime	Machine studies and user experiment preparation	Maintenance	Shutdown and commissioning
<b>FLASH (Linac)</b>				
1 Jan – 31 Dec	3857 h	2859 h	43 h	1754 h
Corona break (1 Jan – 10 Jan)				247 h
<b>FLASH1</b>				
1 Jan – 31 Dec	2559 h			
<b>FLASH2</b>				
1 Jan – 31 Dec	2015 h			

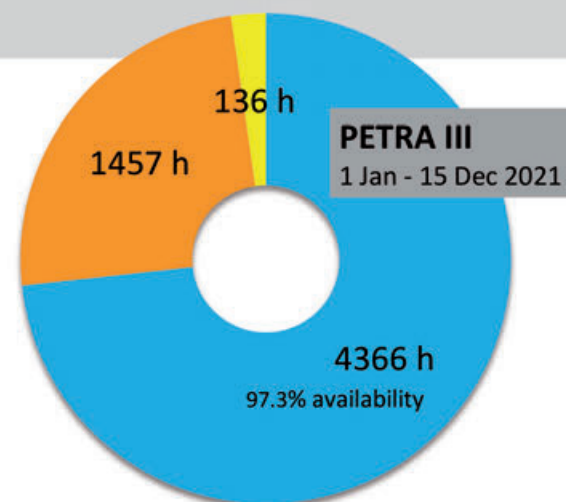
- User beamtime
- Machine studies/User experiment preparation
- Maintenance



PETRA III				
Operation period 2021				
	User beamtime	Machine studies and test runs	Maintenance	Shutdown
1 Jan – 15 Dec	4366 h	1457 h	136 h	
planned for 16 Dec – 31 Dec	273 h	7 h		
				2521 h

**run periods:**  
15 Mar – 07 Jul  
04 Aug – 22 Dec

- User beamtime
- Machine studies/Test runs
- Maintenance



# Committees 2021

## Photon Science Committee PSC — advises the DESY Photon Science management

Christian David (chair)  
Stefan Eisebitt (vice chair)  
Serena DeBeer  
Kristina Djinovic-Carugo  
Jan-Dierk Grunwaldt  
Mark Heron  
Simo Huotari  
Sarah Köster  
Jan Lüning  
Edvin Lundgren  
Arwen Pearson  
Thomas Pfeifer  
Harald Reichert  
Daniela Rupp  
Bernd Schmitt  
Thomas Schröder  
Andrea Somogyi  
Stefan Vogt  
Nele Müller (PSC secretary)

Paul Scherrer Institut, Villigen, CH  
MBI and Technische Universität Berlin, DE  
MPI-CEC, Mülheim an der Ruhr, DE  
Universität Wien, AT  
Karlsruher Institut für Technologie, Karlsruhe, DE  
Diamond Light Source Ltd, Didcot, UK  
University of Helsinki, FI  
Georg-August-Universität Göttingen, DE  
Helmholtz-Zentrum Berlin, DE  
Lund University, SE  
CUI, Universität Hamburg, DE  
MPI for Nuclear Physics, Heidelberg, DE  
ESRF, Grenoble, FR  
Eidgenössische Technische Hochschule Zürich, CH  
Paul Scherrer Institut, Villigen, CH  
Humboldt-Universität zu Berlin and IKZ, Berlin, DE  
Synchrotron SOLEIL, Saint-Aubin, FR  
Argonne National Laboratory, Lemont, US  
DESY, Hamburg, DE

## Laser Advisory Committee LAC — advises DESY and European XFEL

Jonathan Zuegel (chair)  
Miltcho Danailov  
Thomas Dekorsy  
Alan Fry  
Catherine Le Blanc  
Emma Springate  
Andreas Galler (LAC secretary)  
Nele Müller (LAC secretary)

Laboratory for Laser Energetics, Rochester, US  
Elettra-Sincrotrone, Trieste, IT  
Deutsches Zentrum für Luft- und Raumfahrt e.V., Stuttgart, DE  
SLAC, Menlo Park, US  
Ecole Polytechnique, Laboratoire LULI, FR  
STFC Rutherford Appleton Laboratory, US  
European XFEL, Schenefeld, DE  
DESY, Hamburg, DE

## DESY Photon Science User Committee DPS-UC — represents the user community

Peter Müller-Buschbaum (chair)  
Natalia Dubrovinskaia  
Markus Mezger  
Daniela Rupp  
Gregor Witte

Technische Universität München, DE  
Universität Bayreuth, DE  
MPI für Polymerforschung, Mainz, DE  
Eidgenössische Technische Hochschule Zürich, CH  
Ludwig-Maximilians-Universität München, DE

## Komitee Forschung mit Synchrotronstrahlung KFS — representative body of the German SR and FEL user community

Jan-Dierk Grunwaldt (chair)  
Sarah Köster (vice chair)  
Taisia Gorkhover  
Christian Gutt  
Birgit Kanngießer  
Dirk Lützenkirchen-Hecht  
Bridget Murphy  
Andrea Thorn

Karlsruher Institut für Technologie, Karlsruhe, DE  
Georg-August-Universität Göttingen, DE  
Universität Hamburg, DE  
Universität Siegen, DE  
Technische Universität Berlin, DE  
Bergische Universität Wuppertal, DE  
Christian-Albrechts-Universität zu Kiel, DE  
Universität Hamburg, DE

## The European Synchrotron and FEL User Organisation ESUO (Executive Board)

Cormac McGuinness (ESUO President)  
Carla Bittencourt  
Federico Boscherini  
Tom Hase  
Rainer Lechner  
Derek Logan  
Bridget Murphy  
Moniek Tromp

Trinity College Dublin, Dublin  
Université de Mons, BE  
Università di Bologna, IT  
University of Warwick, UK  
Montanuniversität Leoben, AT  
Lund University, SE  
Christian-Albrechts-Universität zu Kiel, DE  
Rijksuniversiteit Groningen, NL

For national delegates please see: <http://www.wayforlight.eu/en/users/esuo/>

# Project Review Panels 2021

## Bulk and surface diffraction

P08 | P23 | P24

Derek (Del) Atkinson  
 Michael Hanke  
 Christiane A. Helm  
 Beate Kloesgen  
 Fouad Maroun  
 Reinhard Neder  
 Beatriz Noheda  
 Oliver Oeckler  
 Maxim A. Shcherbina

Sander van Smaalen  
 Hans-Georg Steinrück  
 Chandan Upadhyay  
 Matthias Zschornak  
 Florian Bertram, Dimitri Novikov,  
 Martin Tolkiehn (PRP secretaries)

University of Durham, GB  
 Paul-Drude-Institut für Festkörperelektronik, Berlin, DE  
 Universität Greifswald, DE  
 Syddansk Universitet Odense, DK  
 Ecole Polytechnique Palaiseau, FR  
 Friedrich-Alexander-Universität Erlangen-Nürnberg, DE  
 Universiteit Groningen, NL  
 Universität Leipzig, DE  
 Enikolopov Institute of Synthetic Polymer Materials,  
 RAS Moscow, RU  
 Universität Bayreuth, DE  
 Universität Paderborn, DE  
 Indian Institute of Technology, Varanasi, IND  
 Technische Universität, Bergakademie Freiberg, DE  
 DESY, Hamburg, DE

## Coherent applications

P10

Sylvain Bohic  
 Manfred Burghammer  
 Ralf Busch  
 Gaetano Campi  
 Birgit Hankiewicz  
 Guido Meier  
 Ullrich Pietsch  
 Beatrice Ruta  
 Jesper Wallentin  
 Michael Sprung (PRP secretary)

Research Centre INSERM, Grenoble, FR  
 ESRF, Grenoble, FR  
 Universität des Saarlandes, Saarbrücken, DE  
 Consiglio Nazionale delle Ricerche, Roma, IT  
 Universität Hamburg, DE  
 MPI für Struktur und Dynamik der Materie, Hamburg, DE  
 Universität Siegen, DE  
 Université Claude Bernard, Lyon, FR  
 Lund University, SE  
 DESY, Hamburg, DE

## EXAFS

P64 | P65

Matthias Bauer  
 Dmitry Doronkin  
 Stephan Klemme  
 Dorota Koziej  
 Aleksej Kuzmin  
 Christina Roth  
 Karel Saksl  
 Claudia Schnohr  
 Kajsa Sigfridsson Clauss  
 Andrea Zitolo  
 Wolfgang Caliebe, Edmund Welter (PRP secretaries)

Universität Paderborn, DE  
 Karlsruher Institut für Technologie (KIT), Karlsruhe, DE  
 Westfälische Wilhelms-Universität, Münster, DE  
 Universität Hamburg, DE  
 University of Latvia, Riga, LV  
 Universität Bayreuth, DE  
 Slovak Academy of Sciences, Kosice, SK  
 Universität Leipzig, DE  
 MAX IV Laboratory, Lund, SE  
 Synchrotron SOLEIL, Gif-sur-Yvette, FR  
 DESY, Hamburg, DE

## Extreme conditions

P02.2 | P61 LVP

Daniel Errandonea  
 Ulrich Häussermann  
 Nadège Hilairat  
 Konstantin Litasov  
 Malcolm McMahon  
 Marco Merlini  
 Guillaume Morard  
 Carmen Sanchez-Valle  
 Chrystele Sanloup  
 Tony Withers  
 Andreas Zerr  
 Hanns-Peter Liermann, Robert Farla (PRP secretaries)

Universitat de València, ES  
 Stockholm University, Stockholm, SE  
 Université des Sciences et Techniques, Lille, FR  
 Institute for High Pressure Physics RAS, Moscow, RU  
 University of Edinburgh, GB  
 Università degli Studi di Milano Statale, Milano, IT  
 Sorbonne Université, Paris, FR  
 Westfälische Wilhelms-Universität, Münster, DE  
 Sorbonne Université, Paris, FR  
 Universität Bayreuth, DE  
 Université Paris Nord, FR  
 DESY, Hamburg, DE

## HAXPES

P22

Maria Hahlin  
 Martina Müller  
 Christian Papp  
 Christoph Rameshan  
 Anna Regoutz  
 Vladimir N. Strocov  
 Christoph Schlüter (PRP secretary)

Uppsala Universitet, SE  
 Universität Konstanz, DE  
 Friedrich-Alexander-Universität Erlangen-Nürnberg, DE  
 Technische Universität Wien, AT  
 University College London, GB  
 PSI, Villigen, CH  
 DESY, Hamburg, DE

## High energy diffraction

P07 (DESY) | P21.1 | P21.2

Frauke Alves  
 Emil Bozin  
 Olaf Borkiewicz  
 Per-Anders Carlsson  
 Magnus Colliander  
 Margit Fabian  
 Jens Gibmeier  
 Julia Herzen  
 Markus Hücker  
 Kirsten Marie Jensen  
 Simon Kimber  
 Herbert Over  
 Tobias Ritschel  
 Joachim Wollschläger  
 Ann-Christin Dippel,  
 Martin von Zimmermann,  
 Ulrich Lienert (PRP secretaries)

Georg-August-Universität, Göttingen, DE  
 Brookhaven National Laboratory, Upton, US  
 Argonne National Laboratory, Lemont, US  
 Chalmers Tekniska Högskola, Gothenborg, SE  
 Chalmers Tekniska Högskola, Gothenborg, SE  
 Centre for Energy Research, MTA, Budapest, HU  
 Karlsruher Institut für Technologie, Karlsruhe, DE  
 Technische Universität München, Garching, DE  
 Weizmann Institute of Science, Rehovot, IL  
 University of Copenhagen, DK  
 Université Bourgogne Franche-Comté, Dijon, FR  
 Justus-Liebig-Universität, Gießen, DE  
 Technische Universität Dresden, DE  
 Universität Osnabrück, DE  
 DESY, Hamburg, DE

## Imaging

P05 | P06

Matthias Alfeld  
 Martin Bech  
 Ulrike Boesenberg  
 Oliver Bunk  
 Asuncion Carmona  
 David Fenning  
 Frank Friedrich  
 Sebastian Kalbfleisch  
 Florian Meirer  
 Bert Mueller  
 Guillermo Requena  
 Jürgen Thieme  
 Katarina Vogel-Mikus  
 Ulrich Vogt  
 Benjamin Wipfler  
 Fabian Wilde, Gerald Falkenberg (PRP secretaries)

Delft University of Technology, NL  
 Lund University, SE  
 European XFEL, Schenefeld, DE  
 PSI, Villigen, CH  
 Centre d'Etudes Nucléaires de Bordeaux Gradignan, FR  
 University of California, San Diego, US  
 Universität Hamburg, DE  
 MAX IV Laboratory, Lund, SE  
 University of Utrecht, NL  
 Universität Basel, Allschwil, CH  
 RWTH Aachen, DE  
 Brookhaven National Laboratory, Upton, US  
 University of Ljubljana, SI  
 Royal Institute of Technology, Stockholm, SE  
 Zool. Forschungsmuseum Alexander Koenig, Bonn, DE  
 DESY, Hamburg, DE

## Inelastic, magnetic and resonant scattering

P01 | P09

Manuel Angst  
 Elizabeth Blackburn  
 Kristina Kvashnina  
 Catherine McCammon  
 Daniel Merkel  
 Marco Moretti  
 Valerio Scagnoli  
 Volker Schünemann  
 Joachim von Zanthier  
 Ilya Sergeev, Sonia Francoual (PRP secretaries)

Forschungszentrum Jülich GmbH, DE  
 Lund University, SE  
 Helmholtz-Zentrum Dresden-Rossendorf (HZDR), DE  
 Universität Bayreuth, DE  
 Wigner Research Centre for Physics, Budapest, HU  
 Politecnico di Milano, IT  
 ETH Zürich, CH  
 Technische Universität Kaiserslautern, DE  
 Friedrich-Alexander-Universität Erlangen-Nürnberg, DE  
 DESY, Hamburg, DE

## Materials science (Hereon)

P07 (Hereon) | P61 (Hereon)

Jeremy Epp

Guillaume Geandier  
 Astrid Haibel  
 Patrick Huber  
 Christian Krempaszky  
 Ingo Manke  
 Svea Mayer  
 Thomas Niendorf  
 Wolfgang Pantleon  
 Georg Schulz  
 Dieter Lott (PRP secretary)

Leibniz-Institut für Werkstofforientierte Technologien - IWT, Bremen, DE  
 Institut Jean Lamour, Nancy, FR  
 Beuth Hochschule für Technik, Berlin, DE  
 Technische Universität Hamburg-Harburg, DE  
 Technische Universität Muenchen, DE  
 Helmholtz Zentrum Berlin f. Materialien und Energie, DE  
 Montanuniversität, Leoben, AT  
 Universität Kassel, DE  
 Technical University of Denmark, Lyngby, DK  
 Universität Basel, CH  
 Helmholtz-Zentrum Hereon, Geesthacht, DE

# Project Review Panels 2021

## Powder diffraction

P02.1

Dorthe Bomholdt Ravnsbæk  
Robert Dinnebier  
Mads Ry Jørgensen  
Gregor Kieslich  
Simon Pauly  
Martin Sahlberg  
Anatoliy Senyshyn  
Florian Speckermann  
Claudia Weidenthaler  
Mirijam Zobel  
Martin Etter (PRP secretary)

Syddansk Universitet, Odense, DK  
MPI für Festkörperforschung, Stuttgart, DE  
Aarhus University, DK  
Technische Universität München, Garching, DE  
Leibniz-IFW, Dresden, DE  
Uppsala Universitet, SE  
Technische Universität München, Garching, DE  
Montanuniversität, Leoben, AT  
MPI fuer Kohlenforschung, Mülheim a.d. Ruhr, DE  
Universität Bayreuth, DE  
DESY, Hamburg, DE

## SAXS/WAXS/GISAXS

P03 | P62

Alexander Gerlach  
Thomas Hellweg  
Marianne Liebi  
Fredrik Lundell  
Giuseppe Portale  
Konrad Schneider  
Qi Zhong  
Stephan Roth, Sylvio Haas (PRP secretaries)

Universität Tübingen, DE  
Universität Bielefeld, DE  
Chalmers Tekniska Högskola, Gothenborg, SE  
Royal Institute of Technology, Stockholm, SE  
Universiteit Groningen, NL  
Leibniz-Institut für Polymerforschung Dresden e.V., DE  
Zhejiang Sci-Tech University, Hangzhou, CN  
DESY, Hamburg, DE

## Soft X-ray and VUV

P04 | P66

Yves Acremann  
Paola Bolognesi  
Arno Ehresmann  
Mark Golden  
Aleksandr Luštšik  
Jan-Erik Rubensson  
Emma Sokell  
Anna Vedda  
Moritz Hoesch, Aleksei Kotlov (PRP secretaries)

ETH Zürich, CH  
CNR-ISM, Istituto di Struttura della Materia, Roma, IT  
Universität Kassel, DE  
Universiteit van Amsterdam, NL  
University of Tartu, EE  
Uppsala Universitet, SE  
University College, Dublin, IE  
Università di Milano-Bicocca, Milano, IT  
DESY, Hamburg, DE

## Soft X-ray FEL experiments

FLASH

Christoph Bostedt  
Majed Chergui  
Hermann Dürr  
Irene Groot  
Marion Harmand  
Chris Jacobsen  
Claudio Masciovecchio  
Michael Meyer  
Robert Schoenlein  
Christian Schüssler-Langeheine  
Marc Simon  
Julia Stähler  
Marc Vrakking  
Martin Weinelt  
Philippe Wernet  
Elke Plönjes-Palm, Rolf Treusch (PRP secretaries)

PSI, Villigen, CH  
École Polytechnique Fédérale de Lausanne, CH  
Uppsala Universitet, SE  
Universiteit Leiden, NL  
Sorbonne Université, Paris, FR  
Argonne National Laboratory, Argonne, US  
Sincrotrone Trieste, IT  
European XFEL, Schenefeld, DE  
SLAC National Accelerator Laboratory, Menlo Park, US  
Helmholtz-Zentrum Berlin, DE  
Sorbonne Université, Paris, FR  
Humboldt-Universität zu Berlin, DE  
Max-Born-Institut Leibniz Gesellschaft, Berlin, DE  
Freie Universität Berlin, DE  
Uppsala Universitet, SE  
DESY, Hamburg, DE

## PEC: EMBL Life Science beamlines P12-P14 / PRP Bio-crystallography at P11

Savvas Savvides  
Pau Bernadó  
Kristina Djinovic-Carugo  
Gwyndaf Evans  
Robert Fischetti  
Mariusz Jaskolski  
Gergely Katona  
Annette E. Langkilde  
Javier Pérez  
Teresa Santos-Silva  
Zehra Sayers  
Joel L. Sussman  
Maria A. Vanoni  
Mark J. van Raaij  
Gregor Witte  
Christian Schroer (DESY observer)

Ghent University, BE  
CBS/CNRS, Montpellier, FR  
Universität Wien, AT  
Diamond Light Source, Didcot, GB  
Argonne National Laboratory, US  
Adam Mickiewicz University of Poznan, PL  
University of Gothenburg, SE  
University of Copenhagen, DK  
Synchrotron SOLEIL, Saint-Aubin, FR  
Universidade NOVA de Lisboa, PT  
Sabanci University, Istanbul, TR  
Weizmann Institute of Sciences, Rehovot, IL  
Università degli Studi di Milano, IT  
Centro Nacional de Biotecnología, Madrid, ES  
Ludwig-Maximilians-Universität München, DE  
DESY, Hamburg, DE



#### **Photographs and Graphics:**

Gesine Born, Berlin	Robert Gleissner, DESY	Carolin Rankin, Hamburg
Niels Breckwoldt, CFEL	Andrey Gruzinov, EMBL	Christiana Ritter, EMBL
Silvia Burastero and Creative Team/EMBL	Helmholtz-Zentrum Hereon	Isabel Romero Calvo, EMBL
CFEL	Jan Hosan, EuXFEL	Reimo Schaaf, Hamburg
Christian-Albrechts-Univ. zu Kiel	LEAPS	Schleuse 01 Werbeagentur, Berlin
CMWS	Britta Liebaug, DESY	Science Communication Lab, Kiel
CSSB	Marta Mayer, DESY	Azadeh Shamsavar, EMBL, DANDRITE
DESY	MPG	David von Stetten, EMBL
EMBL	Jörg Modrow, DESY	Universität Hamburg
European XFEL	Kerstin Pukall, Norderstedt	

#### **Acknowledgement**

We would like to thank all the authors and all those who have contributed to the realisation of this Annual Report.

## Imprint

### **Publishing and Contact:**

Deutsches Elektronen-Synchrotron DESY  
A Research Centre of the Helmholtz Association

### Hamburg location:

Notkestr. 85, 22607 Hamburg, Germany  
Tel.: +49 40 8998-0, Fax: +49 40 8998-3282  
desyinfo@desy.de

### Zeuthen location:

Platanenallee 6, 15738 Zeuthen, Germany  
Tel.: +49 33762 7-70, Fax: +49 33762 7-7413

### Photon Science at DESY

Tel.: +49 40 8998-2304, Fax: +49 40 8998-4475  
photon-science@desy.de  
photon-science.desy.de

[www.desy.de](http://www.desy.de)

ISBN 978-3-945931-39-4  
DOI: 10.3204/PUBDB-2021-05283

### **Online version:**

[photon-science.desy.de/annual\\_report](http://photon-science.desy.de/annual_report)

### **Realisation:**

Wiebke Laasch, Daniela Unger

### **Editing:**

Sadia Bari, Lars Bocklage, Günter Brenner, Thomas Keller,  
Dmytro Kutnyakhov, Wiebke Laasch, Leonard Müller,  
Nele Müller, Britta Niemann, Christoph Schlüter, Sang-Kil Son,  
Sebastian Trippel, Daniela Unger, Thomas White

**Layout:** Sabine Kuhls-Dawideit, Büro für Grafik und Design,  
Halstenbek

**Printing and image processing:** EHS Druck GmbH, Schenefeld

**Copy deadline:** December 2021

Reproduction including extracts is permitted subject  
to crediting the source.

**Deutsches Elektronen-Synchrotron DESY**  
**A Research Centre of the Helmholtz Association**

The Helmholtz Association is a community of 18 scientific-technical and biological-medical research centres. These centres have been commissioned with pursuing long-term research goals on behalf of the state and society. The Association strives to gain insights and knowledge so that it can help to preserve and improve the foundations of human life. It does this by identifying and working on the grand challenges faced by society, science and industry. Helmholtz Centres perform top-class research in strategic programmes in six core fields: Energy, Earth & Environment, Health, Aeronautics, Space and Transport, Matter, and Key Technologies.

[www.helmholtz.de](http://www.helmholtz.de)